Manufacturing Conductive Patterns on Polymeric Substrates: Development of A Microcontact Printing Process

by

Melinda Hale

B.S., Mechanical Engineering
Oklahoma State University, 2007
S.M., Mechanical Engineering
Massachusetts Institute of Technology, 2009

Submitted to the Department of Mechanical Engineering
in partial fulfillment of the requirements for the degree of

Doctor of Philosophy

at the

MASSACHUSETTS INSTITUTE OF TECHNOLOGY

June 2013

© Massachusetts Institute of Technology 2013. All rights reserved.

Author . . . .
Department of Mechanical Engineering
May 10, 2013

Certified by . . . .
David E. Hardt
Ralph E. and Eloise F. Cross Professor of Mechanical Engineering
Thesis Supervisor

Accepted by . . . .
David E. Hardt
Chairman, Department Committee on Graduate Students

Manufacturing Conductive Patterns on Polymeric Substrates: Development of A Microcontact Printing Process

by

Melinda Hale

Submitted to the Department of Mechanical Engineering
on May 10, 2013, in partial fulfillment of the
requirements for the degree of
Doctor of Philosophy

Abstract

The focus of this research was to develop a process suitable for creating very high resolution conductive patterns on polymer substrates, in a way that can be scaled to high volume manufacturing. The original motivation for this work came from the problem of manufacturing electrodes on microfluidic devices (which in volume production are commonly formed from polymers), but the findings of this work also have applications in flexible electronics, optics, surface patterning, organic micromanufacturing, and photovoltaics. After an initial exploration of various micromanufacturing processes, microcontact printing (μCP) was chosen as the most promising technique for further study.

By using μCP to directly pattern conductive inks, this work has demonstrated previously unachievable printing: feature sizes down to 5μm, using liquid inks on polymer substrates, with a process that can be scaled to high-volume production. An understanding of the mechanisms of direct liquid ink transfer was used to identify relevant process input and output factors, and then the process sensitivities of those factors were investigated with a careful design of experiments. From the empirical data, a process model was built with generalized variables. This model was then used to successfully predict behavior of other inks and other substrates, thus validating the model and showing that it is extendable for future work.

By developing an empirically verified model of ink transfer at the micron scale, this work has enabled a process for low cost, high volume microfeature patterning over large areas on polymer substrates.

Thesis Supervisor: David E. Hardt
Title: Ralph E. and Eloise F. Cross Professor of Mechanical Engineering

Acknowledgments

To my father, on his 52nd birthday.

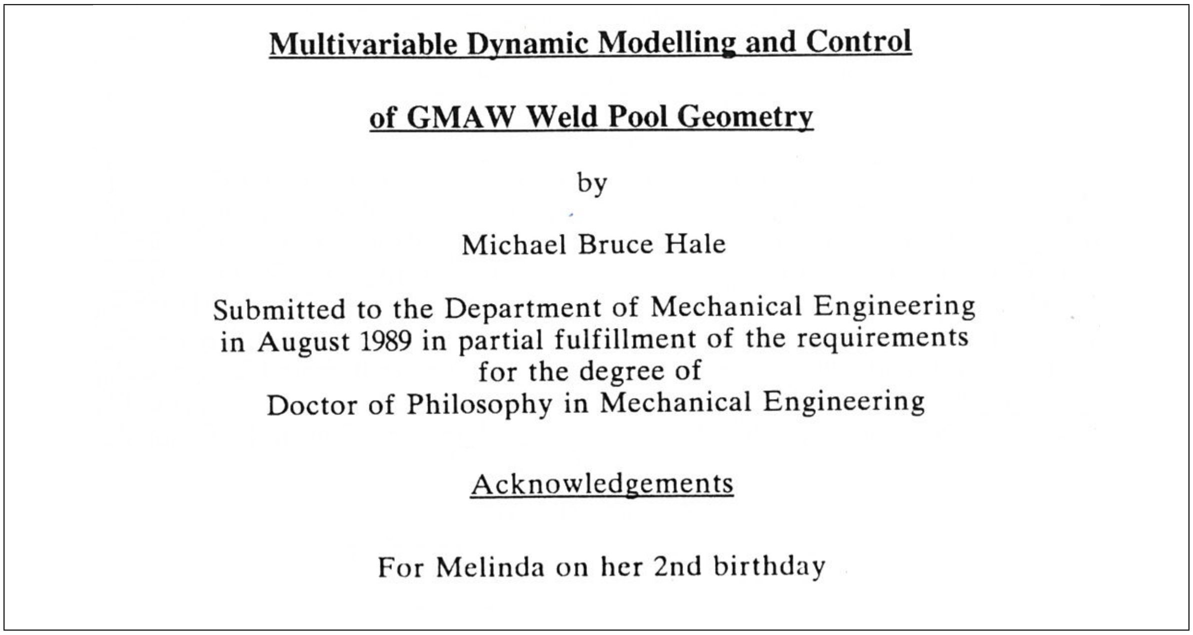

Multivariable Dynamic Modelling and Control

of GMAW Weld Pool Geometry

by

Michael Bruce Hale

Submitted to the Department of Mechanical Engineering
in August 1989 in partial fulfillment of the requirements
for the degree of
Doctor of Philosophy in Mechanical Engineering

Acknowledgements

For Melinda on her 2nd birthday

Figure 0-1: Excerpt of Mike Hale doctoral dissertation, 1989

None of this work would have been possible without funding from the Singapore-MIT Alliance, whose support is much appreciated.

I would like to thank my advisor, Professor David Hardt, for his mentorship and the opportunity to work under his direction. I would like to thank my family for their encouragement and listening ears, my labmates both in Hardt's lab and in the 35-135 office for their companionship along this journey, and the MIT staff on the administrative side as well as in the machine shop and cleanroom facilities for their dedication and support.

I have had help along the way from a variety of other students and laboratories on campus, which speaks I think to the incredibly collaborative environment at MIT. Specifically thanks goes to:

- Rachel Howden in Professor Karen Gleason's lab in the Department of Chemical Engineering for her help with initial testing of PEDOT patterning using chemical vapor deposition

- Robert Panas in Professor Martin Culpepper's Precision Compliant Systems Laboratory for his help in the MIT EML clean room to do initial testing of aluminum patterning with electron beam physical deposition
- Stephen Bathurst and Eric Lam under Professor Sang-gook Kim in the Micro & Nano Systems Laboratory, for their help with initial testing of PEDOT patterning with inkjet printing
- Joseph Sullivan in Professor Buonassisi's Photovoltaic Research Laboratory, for his help with initial testing of PEDOT patterning with screen printing
- Jean Chang in Professor Ian Hunter's BioInstrumentation Lab for her training on the gas pycometer for density testing
- Adam Paxson in Professor Kripa Varanasi's Lab for Nanoengineered Surfaces, Interfaces, & Coatings, for his training on the goniometer for surface energy testing
- Ahmed Helal in the Hatsopulos Microfluids Lab for his training on the rheometer for viscosity testing
- Joe Petrzelka, a Hardt lab alum, for his work in designing a precision positioning stage for roll-based contact lithography

Contents

1 Introduction **27**

1.1 Conductors on polymers: Motivation from the field of microfluidic devices . . 27

1.1.1 What are microfluidics? 27

1.1.2 What is the problem that needs to be solved? 28

1.1.3 Background on electrode materials 30

1.1.4 Why is it important to solve this problem? 30

1.2 Microcontact printing (μCP): Background on the process 31

1.2.1 What is the μCP process? 31

1.2.2 History of μCP 32

1.2.3 Previous work in μCP equipment 33

1.2.4 Why do we need a better μCP model? 35

1.3 Applications: Using μCP for microfluidics and beyond 35

1.4 Contributions 37

1.5 Overview of thesis 37

2 Exploration of Surface Patterning Processes in Micromanufacturing **39**

2.1 Overview of surface patterning processes in micromanufacturing 39

2.1.1 Traditional MEMS techniques overview 44

2.1.2 Inkjet printing overview 44

2.1.3 Screen printing overview 45

2.1.4 μCP overview 46

2.1.5 Other methods overview 47

2.2 Evaluation of micromanufacturing processes for conductive ink patterning . . 47

2.2.1 Initial testing with chemical vapor deposition (CVD) of PEDOT . . . 51

2.2.2 Initial testing with electron beam physical deposition of aluminum . . 52
2.2.3 Initial testing with inkjet printing of PEDOT 52
2.2.4 Initial testing with screen printing of PEDOT 55
2.2.5 Initial testing with direct μCP of PEDOT 56
2.3 Limits of resolution 59
2.4 Why μCP? 60

3 Theoretical Understanding of the μCP Liquid Ink Transfer Process 63
3.1 Overview of printing technology and terminology 64
3.2 Plasma treatment: Effect on contact angle/surface energy 65
3.3 Step 1: Coating inkpad with ink 69
3.3.1 Types of inks 69
3.3.2 Spincoating 69
3.3.3 Governing equation: wetting 70
3.4 Step 2: Transfer from inkpad to stamp 71
3.4.1 Step 2 Part 1: Is the film stable? 71
3.4.2 Step 2 Part 2: Will the film dewet at the edges or at the center? . . . 72
3.5 Step 3: Transfer from stamp to substrate 74
3.6 Step 4: Post-treatment (drying/solidifying) 75
3.7 Governing equations summary 77

4 Exploration of Microcontact Printing of PEDOT 79
4.1 What is PEDOT? 80
4.2 Why investigate PEDOT? 81
4.3 Prior PEDOT and printing work in literature 82
4.3.1 Prior work in μCP of PEDOT 82
4.3.2 Prior work in lift off of PEDOT 83
4.3.3 Prior work in other methods of printing PEDOT 83
4.3.4 Prior work in μCP of other polymers 84
4.4 Initial PEDOT experiments with microcontact printing 84
4.4.1 Effect of plasma treatment on PDMS stamp 84
4.4.2 Thickness of PEDOT ink on glass slide 84
4.4.3 Thickness of PEDOT on PDMS stamp vs. glass substrate 86

4.4.4 Need for intermediate cleaning and better transfer equipment 87
4.5 Experimental additive μCP of PEDOT 90
4.6 Experimental liftoff μCP of PEDOT 91
4.7 Investigation of surface energies 93
4.8 Conclusion: Work of adhesion shows transfer is unfavorable 98

5 Exploration of μCP of Silver Nanoparticle Ink 101
5.1 What is silver nanoparticle ink? 102
5.2 Prior work in μCP of silver ink 102
5.3 Replicating literature μCP with Ag ink 105
5.4 Investigation of silver inks 105
5.4.1 Density testing 106
5.4.2 Surface energy testing 108
5.4.3 Viscosity testing 110
5.4.4 Electrical testing 111
5.4.5 Summary of ink properties 111
5.5 Equipment and methods 114
5.5.1 Stamp making 114
5.5.2 Printing roll 114
5.5.3 Standard procedure 115
5.6 Ink volume transfer experiments 117
5.7 Design of experiments 121
5.7.1 Choice of factors 121
5.7.2 Choice of factor levels 124
5.7.3 Choice of Taguchi L18 128

6 Manufacturing Process Model for Silver Ink μCP 131
6.1 Thickness measurements 131
6.1.1 Line thickness profile 132
6.2 Geometry measurements 134
6.3 Analysis and interpretation of experimental data 136
6.3.1 Elimination of runs with anomalous thickness 136
6.3.2 Elimination of runs with anomalous coverage 137

6.3.3 Software used . . . 137
6.4 Thickness model . . . 137
6.4.1 Effect of solids loading . . . 139
6.4.2 Effect of viscosity . . . 139
6.4.3 Effect of feature size . . . 141
6.4.4 Effect of energy ratio . . . 142
6.4.5 Thickness model coefficients . . . 144
6.4.6 Note on thickness vs. pressure . . . 145
6.5 Coverage model . . . 148
6.5.1 Effect of feature size, inkpad thickness, and viscosity . . . 150
6.5.2 Effect of solids loading . . . 151
6.5.3 Coverage model coefficients . . . 153
6.5.4 Note on coverage vs. pressure . . . 153
6.6 Extension of model to other silver nanoparticle inks, other substrates, and other materials . . . 155
6.6.1 Extension of model to additional silver inks: Aldrich and MES30 . . . 157
6.6.2 Extension of model to COC polymer substrate . . . 158
6.6.3 Extension of model to gold nanoparticle ink . . . 160
6.7 Exploration of μCP of carbon nanotubes . . . 162
6.8 Importance of inking . . . 162

7 Conclusions 169
7.1 Summary . . . 169
7.2 Key contributions . . . 173
7.3 Future work . . . 174

A Detailed Methods of Micromanufacturing for Microfluidics 175
A.1 Traditional MEMS Techniques . . . 175
A.2 Other Methods . . . 177

B CLEVIOS^{TM} Material Properties 181
B.1 CLEVIOS^{TM} PH 1000 - Product Information . . . 181
B.1.1 General CLEVIOS Properties . . . 184

C Additional Details on Theory of μCP for films 187

C.1 Subtractive theory for films 187

C.1.1 Problem 1: Weakening or cracking 187

C.1.2 Problem 2: Adhesion 188

D Additional Details of PEDOT Experiments 191

D.1 Difficulty coating PDMS stamp 191

D.1.1 Difficulty with plasma settings 191

D.1.2 Difficulty with volume of ink 193

D.1.3 Difficulty adding coloring to ink 193

D.2 Initial transfers from flat stamp to slide 195

D.3 Experiment DOE with glycerol 198

E Stamping Apparatus with Flexure, Designed for Incorporation with Spincoater 201

E.1 Design of flexure for stamping apparatus 202

E.2 Design of substrate holder for stamping apparatus 202

E.3 Assembled stamping apparatus 203

F Taguchi L18 DOE for Exploring μCP of Ag ink - Detailed DOE Parameters and Results 211

F.1 Taguchi L18 DOE for exploring μCP of Ag ink - List of runs with specific parameters used 211

F.2 Taguchi L18 DOE for exploring μCP of Ag ink - Thickness and geometry coverage measurements 211

List of Figures

1-1 Steps in the direct microcontact printing process: first, coat the stamp with desired material, then bring coated stamp into contact with the substrate, finally demold the stamp leaving patterned material behind. [1] 32

1-2 Defects such as roof collapse are easily caused by poor control of the μCP process, demonstrating the need for careful machine design and process control [2] 36

2-1 Summary of methods for patterning organic electronics based on ink-jet printing techniques [3] 45

2-2 Summary of patterning for organic electronics based on screen printing and other techniques [3] 46

2-3 Summary of methods for patterning organic electronics based on μCP techniques [3] 48

2-4 CVD deposition of PEDOT onto PMMA, resulting in very high and inconsistent film resistance 52

2-5 Electron beam physical deposition of aluminum layer onto PMMA, showing successful deposition of millimeter scale features 53

2-6 Inkjet printing of PEDOT onto PMMA substrate, showing inconsistent or nonexistent film coverage 54

2-7 Inkjet printing of PEDOT onto glass substrate, showing poor film uniformity 54

2-8 Screenprinting of PEDOT onto PMMA substrate, showing successful millimeter scale feature fabrication, but potential problems with edge thickness and quality 55

2-9 μCP of PEDOT onto glass substrates, showing successful transfer but poor film quality (voids and torn areas in the flat pattern) 57

2-10 PDMS stamp used for μCP of PEDOT, after printing, showing need for cleaning method of the stamp 58

2-11 Thickness of μCP PEDOT film on glass substrates, measured with Zygo white light interferometer, showing film height of ∼65nm. a) Color map of surface height, across a scratch in film. b) Line profile across surface showing a film thickness of 62-70nm. c) Color map of surface height, across a step height in film. d) Line profile across surface showing a film thickness of 65nm. 58

3-1 Water contact angle for PMMA and COC substrates after UV/O_3 treatment, and UV/O_3 treatment followed by PVA coating, showing the effect of different plasma treatments on the surface energy of PMMA and COC. [4] 66

3-2 Comparison of surface energy changes in polymers of different chemical structure during air plasma action, showing the effect of plasma treatment on the surface energy of various polymer substrates. [5] 67

3-3 Schematic of Step 1 - Coating ink onto inkpad 71

3-4 Diagram of stamp features showing center dewetting (a-b) and edge dewetting (c-d). Under high pressure the contact point between the liquid and the edge of the stamp feature slips down the side of the feature and a) eventually breaks near the edge, creating b) a droplet in the stamp cavity. Under low pressure the contact point between the liquid and the stamp feature edge remains pinned to the side of the feature d), and eventually e) breaks in the middle of the stamp cavity as desired. [6] 73

3-5 Schematic of Step 2 Parts 1 and 2 - Film stability and ideal edge dewetting, showing the ink split from the inkpad along the feature edges, and forming a continuous coating on the stamp features 73

3-6 Schematic of Step 3 - Transfer from stamp to substrate, assuming complete transfer of a continuous film 75

3-7 Observations of coffee staining from printed nanoparticle silver ink. a) Interferometric image of a track formed from the drying of a liquid bead showing distinct ridges at the edges formed by fluid flow during drying. b) Two line profiles across the track showing variation in height across the track. [7] . . . 76

3-8 Summary of governing equations for μCP process 77

4-1 Chemical PEDOT structure 80

4-2 Effect of plasma treatment on spincoated layer of PEDOT on PDMS stamp, showing droplets in a) with no plasma, and a uniform coating in b) after plasma treatment. 85

4-3 Difference in contact angle of PEDOT on PDMS before and after plasma treatment, showing that plasma treatment lowers contact angle and allows an equal volume of ink to spread out over a larger area. 85

4-4 Zygo white light interferometer measurement of the thickness of 2000rpm 30sec spincoated PEDOT film on glass slide, showing ∼80 to 85nm film thickness. 86

4-5 Coatings of PEDOT film on PDMS stamps at different dates, showing repeatable results in getting a uniform coating. 87

4-6 Zygo white light interferometer measurement of line profiles of film thicknesses on two PDMS stamps spincoated with PEDOT at 2000rpm 30sec, showing height measurements within 5nm across a stamp, and similar height measurements between the two stamps. 88

4-7 Transferred coating of PEDOT film onto glass slide. 88

4-8 Zygo white light interferometer measurement of the thickness of transferred 2000rpm 30sec spincoated PEDOT film on glass slides, showing ∼65nm film thickness. 89

4-9 PDMS stamp used to print three consecutive glass slides, no cleaning between each experiment. 89

4-10 Glass slides with PEDOT film, showing defects caused by imprecise manual stamping. 90

4-11 Failure modes in additive stamping of PEDOT onto glass slides. a) Failure to fully cover PDMS stamp with ink leads to the PDMS stamp bonding directly to glass, and leaving clear bits of stamp attached to the substrate after demolding. b) and c) Examples of PEDOT film detaching from the PDMS stamp, but because of poor adhesion with substrate, the film forms strings and does not attach to the substrate. d) Hybrid section with some features properly attached to the substrate in flat lines, transitioning into some sections not adhered and rolled into strings. e) Addition of too much glycerol to PEDOT leads to poor film formation. f) Magnified version of d), with some sections adhered properly in flat lines, and some sections rolling into strings. 92

4-12 Example of best possible additive μCP with PEDOT. 93

4-13 Zygo white light interferometer measurements of height profiles of the 50μm lines on the example of best practice additive μCP, showing nonuniform thickness across each line. a) Color-coded height map of surface profile. b) 3D projected view of surface profile. c) Microscope image of measured surface area. d) Line profile across the surface area, showing thick buildup at edges of each feature, and nonuniform nominal heights when compared across features. 94

4-14 Failure modes in liftoff of PEDOT from glass slides. a) intended areas have been removed, but remaining pattern was also disturbed and partially lifted off during transfer, because of poor adhesion to substrate. b) entire sections of film removed instead of film breaking along feature edges. c) features removed in intended pattern, but only a very thin layer left behind. d) film does not adhere to stamp, leading to no removal of film. e) application of stamp and pressure during transfer creates a film molded into thicker and thinner regions, but not removed. f) too much glycerol additive in PEDOT leads to beads of glycerol separating from solution. 95

4-15 Additive (stamping) and subtractive (liftoff) transfer regimes, controlled by the work of adhesion (dependent on the ratio of surface energies of the stamp and substrate). 95

4-16 Surface energy comparisons of potential stamp and substrate materials, showing that PEDOT ink will only wet plasma treated glass and plasma treated PDMS. 97

4-17 Comparison of work of adhesion for liftoff and stamping methods with PEDOT, showing unfavorable surface energy ratios for both potential transfer methods. 98

4-18 Successful PEDOT μCP only over a limited areas of the substrate. a) Macro image of 1x1" substrate. b) Microscope image of 50μm line features, selected area from substrate. 99

5-1 Surface energy of Ag ink in comparison to PEDOT and typical stamp/substrate combinations, showing that because of lower surface energy Ag ink will be able to wet onto PMMA. 103

5-2 Kwak demonstration of plate-to-roll Ag ink transfer with 20μm features. [8] . 104

5-3 Takakuwa demonstration of Ag ink printing with a large area nickel mold, achieving 2μm features. [9] 104

5-4 Successful replication with benchtop process for μCP of Ag ink, showing successful transfer of 50μm lines at 50μm spacing (50% duty cycle pattern) and 100μm spacing (25% duty cycle). 106

5-5 Ink density testing data from measurements with gas pycometer, showing good correlation with expected density calculated using given solids loading. . 108

5-6 Ink surface energy testing data, showing good decoupling of energy measurements from drop volume. a) Silver nanoparticles in toluene carrier, from NanoMas b) Silver nanoparticles in cyclohexane carrier, from NanoMas c) Silver nanoparticles in xylene carrier, from NanoMas. 109

5-7 Ink viscosity testing data over a range of shear rates, showing slight effect of shear thinning. 110

5-8 Ink electrical characterization, showing an inverse exponential relationship between thickness and sheet resistance. 112

5-9 Ink electrical characteristics on PMMA and glass, plotting spincoating speed vs. thickness, showing good correlation between electrical performance on glass as compared to the polymer PMMA. 113

5-10 Printing roll equipment used in empirical testing of μCP process [10] 115

5-11 Example image of ideal results from Ag ink printing of hexagonal pattern with 5μm line width, microscope view 117

5-12 Example image of ideal results from Ag ink printing of hexagonal pattern with 5μm line width, no magnification overall slide view 118

5-13 Thickness of successive prints of CSD-66 on glass, from varying initial inkpad thicknesses, showing that each successive print has the same thickness (rather than decreasing by half each time as hypothesized). 119

5-14 Coverage of successive prints of CSD-66 on glass, showing improving feature quality with each print. 120

5-15 Coverage of successive prints of CSD-66 on glass, starting with thinner inkpad for better initial print quality, showing increasing voids with each print. . . . 121

5-16 Thickness of successive prints of CSD-66 on glass, with thinner initial inkpad for good print quality, still showing that each successive print has the same thickness (rather than decreasing by half each time as hypothesized). 122

5-17 Summary of governing equations for transfer, excerpted from Chapter 3. . . . 123

5-18 Inkpad thickness standardized around a nominal value t_o. 126

5-19 Taguchi L18 array - List of runs in design of experiments. 129

6-1 Typical μCP experiment, 5μm hex pattern, printed with CSD-66 ink onto glass, with planes of best fit in MatLab corresponding to base substrate and printed pattern. Highlighted square indicates section of print to be investigated for evidence of coffee stain effect. 133

6-2 Height map of a selected portion of 5μm hex pattern, showing that the thickest part of the print is concentrated in the centers of lines and at the corners of connecting lines. No evidence of coffee staining effect. 133

6-3 Printing defect in 5μm hex pattern, where experimental delay caused the ink to evaporate more than normal. Only corners of the pattern have transferred, indicating that the thickest ink is at the corners, where the solvent has not yet evaporated. 134

6-4 Example of MatLab Image processing for 50μm line patterns. Original microscope image shown in a), converted binary image is shown in b). Connected background areas are labeled and shown in color in c), and then the isolated printed features are shown in d) (after a cleaning for small outlying areas). The printed area coverage is calculated as the area of the printed features divided by the area of the overall image. 135

6-5 Clumping observed in runs 1, 7, 11, and 18. These runs all used MES40 ink, with known clumping tendencies, and are removed from consideration in the process model. 136

6-6 a) Poor coverage observed in Run 17, 20μm lines with CSD-66 ink. b) Observation of stamp after printing shows likely problem with the inking of the stamp. Run was treated as probable experimental error and removed from consideration in the process model. 137

6-7 Taguchi L18 Array in JMP, populated with chosen experimental parameters, ready for statistical analysis and process modeling. 138

6-8 Measured ink thickness change from annealing (drying), indicating that the dried thickness can be well correlated to the solids loading. Therefore as solids loading increases, the thickness of the final dried pattern is also expected to increase. 140

6-9 Diagram of gravure-offset printing configuration, for simulation to investigate ink transfer ratio [11] 140

6-10 Liquid transfer ratio to the upper plate (substrate) for different Capillary numbers. The direction of increasing capillary number is also the direction of increasing viscosity, showing that as viscosity increases, thickness of the transferred pattern is expected to decrease. 141

6-11 Film stability diagram, illustrating that a larger feature can support a stable thicker film, whereas for a smaller feature the same thickness creates an aspect ratio too high for stability. 141

6-12 A comparison of the calculated wavelength of the capillary wave with the pattern size as a function of the thickness of residual film. In this figure, filled symbols indicate ordering, and open symbols no ordering. To create an ordered pattern (the desirable outcome), as the pattern size decreases the residual thickness decreases. [12] 142

6-13 Liquid transfer to the upper plate (substrate) for different values of ink surface tension, showing that as surface tension increases, the thickness of the printed pattern is expected to increase. [11] 143

6-14 Thickness model effect leverage plots, showing that viscosity and solids loading have the most impact on thickness. 145

6-15 Thickness data representation - feature size plotted against thickness, differentiated by ink type and substrate. Visible trends include increasing thickness with increasing feature size, lower thickness corresponding with glass substrate, and clear differences in behavior depending on the ink used. 146

6-16 Thickness data representation with limits, with the lower limit based on a single layer of Ag particles, and a typical upper limit based on thickness printed with a flat stamp. Specific upper limit will different in each experimental case, as it is a function of ink, substrate, and inkpad thickness. 147

6-17 Thickness vs. pressure, differentiated by substrate, showing no obvious trend between thickness and pressure 148

6-18 Thickness vs. pressure, differentiated by ink, showing potential correlation between higher pressure and thinner pattern 149

6-19 a) Geometry of the mold and the dewetting film (L: feature width, h: feature height, t: ink thickness, x: length of broken strip, y: height of the mold-wetting film). b) Simplified geometrical consideration assuming that the shape of the dewetting film is part of a circle. c) Control volume of the ink before dewetting. d) Ink volume after dewetting. [8] 150

6-20 Demonstration that a constant 2μm overage in printed patterns (because of dewetted ink along edges of mold features) appears as a correlation between feature size and coverage, where coverage decreases (closer to the idea ratio of 1) with increasing feature size. 152

6-21 Comparison of lines at low and high solids loading, showing clumping at high solids loading that can lead to a coverage ratio less than 1 (therefore decreasing solids loading leads to increasing coverage). 152

6-22 Coverage model effect leverage plots, showing that viscosity and solids loading have the most impact on thickness. 154

6-23 Coverage data representation - inkpad thickness plotted against coverage, differentiated by ink viscosity and feature size. Visible trends include increasing coverage with increasing inkpad thickness and viscosity, and lower coverage corresponding with the 50μm pattern. 154

6-24 Coverage vs. pressure, differentiated by ink type, showing no obvious trend between coverage and pressure 155

6-25 Reminder of effect leverage plots for thickness and coverage, used to inform choice of new ink designed for favorable printing results. 156

6-26 Thickness results from additional silver ink on polymer substrates, showing that measured thickness lies within the 95% confidence interval of predicted thickness. 159

6-27 Coverage results from additional silver ink on polymer substrates, showing that measured coverage falls within the 95% confidence interval of predicted coverage. 159

6-28 Image of 5μm hex pattern printed on Topas (COC polymer), showing features that are wider than desired but still well defined. No other high-volume process has been able to demonstrate this resolution of electrode printing on COC substrates. 160

6-29 Thickness and coverage results of CSD-66 ink on COC, showing that measured thickness and coverage fall within the 95% confidence intervals of model predictions. Also showing that the predicted coverage is around 2, which is not ideal, and in fact the print does turn out poorly. 161

6-30 Image of 5μm hex pattern printed on PMMA with gold nanoparticle ink from Sun Chemical, showing features that very close to ideal coverage. The calculated coverage is slightly less than 1, likely due to the very fast drying of the volatile xylene solvent, leading to some gaps in the printed pattern. . . 163

6-31 Thickness and coverage results of gold nanoparticle ink on PMMA, showing that measured thickness and coverage fall within the 95% confidence intervals of model predictions. Validates the assumption that material properties of the nanoparticles themselves are not relevant to the printing model, and the ink characteristics included in the model are sufficient to capture the printing behavior of a wide variety of particle-based inks. 164

6-32 Demonstration of changing spincoating speed, thus varying inkpad thickness, and the effect on printed 50μm pattern of CNTs. Shows that there is an optimum speed, that depends on the substrate, that finds a balance between smearing the pattern and broken lines. 165

6-33 Demonstration of printed 50μm lines with CNT ink on various polymer substrates, showing successful transfer is possible. 166

6-34 Importance of inking, illustrated by defect caused by ink void on stamp. Shows that the desired pattern of 20μm squares quickly varies from rounded squares, to ideal squares, to circles, to nothing, as the ink layer thins from full thickness to a void. There is only a small range of suitable inkpad thickness for the desired pattern. 167

6-35 Alternative inking method used to print 5μm hex pattern with CSD-66 ink onto COC. First spincoating is used to create the thinnest possible inkpad on glass, then an intermediate printing step onto plasma treated glass is used to decreases stamp ink thickness, and then the final printing step deposits onto COC polymer. Dimensions of printed features are 5μm as intended, instead of 10μm as seen in the results with one step inking (where the inkpad thickness is limited by solvent evaporating during spincoating). 168

A-1 Traditional MEMS micromanufacturing technique: Hot Embossing. a) metal/polymer double layer patterned on a silicon substrate; b) contact and pressing of the silicon substrate flipped onto a polymer substrate; and c) separation of the silicon substrate from the polymer substrate. [13] 177

B-1 Clevios PH 1000 Chemical Structure 182

B-2 CLEVIOS™ PH500 (incl. 5wt% DMSO) spin curve, provided by manufacturer 183

B-3 CLEVIOS™ PH510 (incl. 5wt% DMSO) spin curve, provided by manufacturer 184

B-4 Overview of CLEVIOS family properties, provided by manufacturer 185

B-5 OLED CLEVIOS properties, provided by manufacturer 186

C-1 Modeling the μCP process with a film instead of a liquid, with cracking predicted by force minimization 189

C-2 Cracking criteria, using fracture mechanics to predict film transfer [14] 189

D-1 Uneven coating of PDMS stamp with PEDOT, even after plasma treatment at 100W for 0.3min of air plasma. 192

D-2 Manual spreading of PEDOT on plasma treated PMMA before spinning, which improves coverage, but the coating quickly beads up spontaneously when spinning stops. 192

D-3 Results of PEDOT spincoated at 2000rpm for 30 seconds onto PDMS with different treatments, to improve hydrophilicity, showing that air plasma provides the best results. 194

D-4 Difference in coverage of PEDOT on PDMS after spincoating with different initial volumes. 195

D-5 Different ink choices spincoated onto PDMS in exploration of finding a "proxy" ink to replace PEDOT, for the purpose of saving expensive ink. Food dye is not an acceptable substitute for PEDOT in spincoating behavior. 196

D-6 PEDOT transferred from PDMS to glass slide by hand, no pressure, ink remains liquid during slide removal. Resulting pattern shows liquid smear pattern. 197

D-7 PEDOT transferred from PDMS to glass slide by hand, no pressure, ink is dried prior to slide removal. Resulting pattern shows nearly complete film transfer. 197

D-8 PEDOT:Glycerol design of experiments with 50μm lines, images of macro results, showing poor overall uniformity. 199

D-9 PEDOT:Glycerol design of experiments with 50μm lines, images of micro results, choosing the best section to image from each experimental run. Shows that printing is possible for small areas, although not uniform over large areas. 200

E-1 Commercial spincoater equipment used, Model SCS6800 from Specialty Coating Systems . . . 202

E-2 Flexure design for stamping apparatus allowing motion in the vertical z-direction, tip, and tilt; constraining movement in the x, y, and θ_z directions. . 203

E-3 Spincoater with integrated flexure design. a) spincoater base with flexure assembly grounded to equipment. b) flexure assembly, with flexure attached to spacers to hold flexure at specific distance above spincoater chuck. 204

E-4 CAD model of substrate chuck, showing (from bottom to top), substrate holder with alignment ridges and sealing ring, heater, insulation block, and backing plate with kinematic coupling half-spheres. 205

E-5 Detailed drawing of 1x3" slide holder, part of substrate chuck assembly 206

E-6 Detailed drawing of 1x1" slide holder, part of substrate chuck assembly 207

E-7 Detailed drawing of heater holder, part of substrate chuck assembly 208

E-8 Fabricated stamping apparatus, with integrated flexure and independent substrate chuck. 209

E-9 Detailed view of gap between substrate holder and spincoater chuck. This is a critical assembly tolerance, as the gap must be less than the flexure range of travel. During printing the substrate holder is pressed down so that outer ring tightly contacts the outer edges of the PDMS stamp, holding alignment and maintaining seal as positive pressure is applied to the back of the stamp for "bubble transfer." 209

List of Tables

1.1 Applications and functions of conductive features in microfluidic devices, highlighting the multiple uses of electrodes for purposes including sensing, manipulation, and local heating. 29
1.2 Common material choices for microfluidic electrodes 30
1.3 Example applications of microcontact printing in literature, demonstrating the breadth of applications for this manufacturing process [15] 34

2.1 Overview of surface patterning micromanufacturing techniques, particularly for microfluidics 41
2.2 Comparison table of micromanufacturing methods for conductive ink patterning 50
2.3 Resistance of inkjet printed PEDOT films, showing high resistance under a variety of conditions 53
2.4 Minimum resolution demonstrated in literature of selected surface patterning manufacturing processes, and the likely mechanisms hindering improved resolution 60

3.1 Contact angle (θ) of water, diiodomethane and formamide on PMMA film surface before and after plasma action, showing the effect of different plasma treatment exposure times on the surface energy of PMMA. [5] 66
3.2 Changes over time to contact angle of water on PMMA and other polymers with plasma treatment [5] 68

4.1 Surface energies of potential stamp and substrate materials, and PEDOT, calculated from goniometer contact angle data. 96
4.2 Work of adhesion calculated for liftoff and stamping surface material combinations 98

5.1 Comparison of protocol for benchtop testing of μCP of Ag ink, between literature and a modified version using the equipment available. 105
5.2 Summary table of commercially available ink properties. 107
5.3 Summary of Ag nanoink properties, from testing and from manufacturer's data. 112
5.4 Input and output factors in the μCP process that are selected (from understanding of governing equations) as likely to be statistically significant to a process model 124
5.5 Ink properties of selected inks for DOE, chosen to give a good range of solids loading, viscosity, and surface tension values. 125
5.6 Calculation of minimum force for collapse of 5μm hexagonal pattern. [16] . . 127
5.7 Summary of DOE factor levels. 128

6.1 Thickness model coefficients, with the correlation direction (+ or -) showing that the coefficient signs match expected trends. 144
6.2 Coverage model coefficients, with the correlation direction (+ or -) showing that the coefficient signs match expected trends. 153
6.3 Additional silver ink properties, used to demonstrate the applicability of the process model on new inks. Aldrich ink chosen because it is widely commercially available, and MES 30 ink chosen because it has the desired characteristics for good performance, as predicted by the developed model. 157

B.1 Clevios Chemical and Physical Data, provided by manufacturer 182

D.1 PEDOT:Glycerol ink additive ratio - Design of experiments 198

F.1 L18 DOE list of runs - Specific experimental parameters 212
F.2 L18 DOE Results - Raw data of thickness and geometry coverage measurements 213

Chapter 1

Introduction

The focus of this thesis is to develop a process suitable for creating very high resolution conductors on polymer substrates, in a way that can be scaled to high volume manufacturing. The original motivation for this work came from the problem of manufacturing electrodes on microfluidic devices (which are commonly plastic), and so this chapter introduces the field of microfluidic devices and explains why the problem of creating electrodes on these devices is important and unsolved. A brief background of microcontact printing is presented here, although Chapter 2 will give more detail on why that process was chosen as a promising potential solution to pursue. Finally although the motivation for this work was in the field of microfluidics, the findings have applications far beyond that field, which are detailed at the close of the chapter along with an overview of the thesis and the major contributions.

1.1 Conductors on polymers: Motivation from the field of microfluidic devices

1.1.1 What are microfluidics?

In 1990 Manz and Widmer [17] envisioned applying miniaturization principles to biochemistry - taking standard chemical tools such as beakers, test tubes, tubing, pipettes and valves, then miniaturizing and packaging them on a small biochemical chip to do a particular job. The first attempts in the 1990s at making these biochemical chips used mostly the same methods used for computer chips: silicon tools, glass substrates, and MEMS manufacturing technology such as wet-etching and photolithography [18]. However, by early in the 2000s, there was a growing consensus that polymeric substrates had significant advantages over quartz, silicon, and glass, and were likely the future of commercial microfluidics [19, 20]. There are many ways to make microscale features in polymeric materials, such as hot embossing, injection molding, soft lithography, laser photoablation, and ultraviolet embossing [19].

Some of the oldest applications of microfluidic devices are optical waveguides and diffraction gratings in the 1970s [21]. In more recent years, the most mature applications are ink-jet printing, followed closely by lab-on-a-chip assays. Microfluidic devices now commercially exist for DNA sorting, drug-discovery applications, fertility testing, immunoassays, and other flow-through processes in chemistry [22]. Devices have been proven in research to handle jobs such as sample manipulation through mixing and T-junctions, capillary electrophoresis, miniaturized polymerase chain reaction (PCR) for DNA amplification, clinical chemistry and diagnostics, micro-reactions and containment, and cell handling [19]. However, there are many more potential applications in fields that include pharmaceuticals, biotechnology, the life sciences, defense, public health, and agriculture.

1.1.2 What is the problem that needs to be solved?

In recent years, microfluidic devices and their applications have received a lot of attention [18, 19], and much effort has gone into manufacturing microfeatures in silicon, glass, and then polymer substrates [23, 24, 21, 25]. But it does no good to only create the substrate if integration with conductive sensors, actuators, and electrical connections is ignored. Because the majority of the cost of producing microfluidic chips now lies in the back end processing, such as electrode manufacturing, bonding, and packaging, research focus is now shifting to those areas. One of the major hindrances to manufacturing fully integrated lab-on-a-chip devices is the need for a low-cost, fast, high resolution method of producing small conductive features on polymer substrates.

Conductive features (usually metal) are widely used in microfluidic devices and biological analysis [71]. The uses for metalized components are summarized in Table 1.1, and include the need for electrical pathways, sensing, manipulation of fluids and cells, and local heating. There are applications in electromagnetics (magnetically actuated pumps, mixers, and valves, particle manipulation, self assembly guidance), in biochemistry (immunoassays, hybridizing DNA and RNA, filtering biomolecules), and in cell biology (isolating cells from

Component	**Function**	**Example Applications**
Electrodes in contact with fluid	Providing current	- Electrohydrodynamic pumping system/micro pumps [29, 26] - Cell electrolysis [30, 31] - Dielectrophoresis [32, 33]
	Sensing	- Heavy metal ions [34, 35, 36, 37] - Dissolution of a membrane [38] - Temperature [39] - Droplets [40] - Chemicals and protein complexes [41, 42, 43, 44] - Surface Plasmonic Resonance (SPR) biosensing [45, 46, 32, 47, 48, 49, 50]
	Manipulation	- Electrokinetic control of fluid transport [51] - Electrokinetic separation [52]
Non-contact electrodes	Magnetic or electric field manipulation	- Alignment of asymmetric particles [53] - Cell sorting and separation [54, 55] - Fluid flow and droplet manipulation [56]
	Conductive pathways	- Interconnects between electrodes [57, 58, 59] - External connects to a power source
Resistive heaters	Heating localized areas	- PCR or other reagent reactions [60] - Microwave heating [61]
Structural Components		- Rotors, blades [26] - Piezoelectric films [62] - Microtools and wire [63, 64]
Optical Components		- Waveguides, microlenses [65] - Optofluidic microscopy [66] - Surface-enhanced Raman scattering substrate [67, 68]
Other		- Changing surface chemistry [69] - Antenna [70]

Table 1.1: Applications and functions of conductive features in microfluidic devices, highlighting the multiple uses of electrodes for purposes including sensing, manipulation, and local heating.

Material	References
titanium	[28]
gold	[65, 40, 58, 28, 33, 45, 46, 32, 42, 73, 48, 51]
silver	[45, 68]
nickel	[26, 62, 63, 30, 64]
indium oxide	[55, 35]
indium	[55, 61]
platinum	[74]
chromium	[65, 57, 40, 58, 45, 75, 50]
aluminum	[66, 76, 52, 77]
mercury	[34]
carbon nanotubes	[41]
eutectic gallium indium	[70]
zinc oxide	[62]
copper	[78, 50, 30]
iron	[30]

Table 1.2: Common material choices for microfluidic electrodes

blood, extracting DNA from cells, moving magnetotactic bacteria, measuring mechanical properties of cells) [55]. Now that the microfluidic substrate can be manufactured in a low-cost, fast, and accurate manner [72], the electrodes need to be manufactured with a similarly low-cost, fast, and accurate method.

1.1.3 Background on electrode materials

The most common conductors used currently in microfluidic devices are by far gold and chromium (followed by copper), driven by the use of traditional processes such as sputtering, evaporation, and standard lithography. Gold has the additional advantage of being strongly biocompatible, which is important in medical applications. Nickel is most often used with electroplating, indium is used when transparency is needed, and the other metals are used for convenience or if their properties make them favorable choices. See Table 1.2 for a listing of commonly used materials in microfluidic electrode manufacturing.

1.1.4 Why is it important to solve this problem?

Microfluidic technology enables cost-efficient, ultra-high-throughput assays in areas like biology and drug discovery. Many research groups and startup companies are working on microfluidic devices in health care, for point-of-care diagnostics as well as therapeutics (e.g., drug delivery) [79]. For example, Daktari in Cambridge, MA manufactures point-of-care devices to monitor HIV treatment and disease progression. Although microfluidics research has been conducted for decades in academia, the market potential is only beginning to be explored. The market for microfluidic devices is still small, but has steadily grown to $84.3 million in US Revenue in 2005[80]. The worldwide market for microfluidic devices was $128 million in 2002 [81], growing to approximately $650 million in 2007 (in just the life sciences) [82], and credible estimates of the potential market size are on the order of billions of dollars [19]. When considering barriers to the continued commercial development of this growing field, the "founding father" of the field, George Whitesides, concluded that "... crucial to many of these applications — is the development of the technology for manufacturing microfluidic devices." [83]

1.2 Microcontact printing (μCP): Background on the process

This thesis attacked the problem of making small conductors on polymers by focusing on a process called microcontact printing (μCP), and developing a process model for μCP of conductive inks at high resolution onto a variety of substrates, in particular polymer substrates. Most current processes for precise patterning of metals (such as vapor deposition, electroplating, or lithographic processes) were originally developed for MEMS systems, and have cost and capability limitations (such as requiring a vacuum, specialized equipment, high temperatures, or a clean room environment), particularly when applied to polymer substrates. The ideal patterning process would be low-cost, accurate and repeatable, robust, fast, and scalable to high volumes. Chapter 2 will give a more detailed look at how, using these criterion, μCP was chosen for further study.

1.2.1 What is the μCP process?

Microcontact printing is a subset of the micromanufacturing process called soft lithography. Soft lithography is a non-photolithographic process for microfabrication, where an elastomeric stamp with raised features is used to create patterns and structures (normally with feature sizes ranging from 30nm to 100 microns) [23, 84, 85, 86]. Microcontact printing uses the relief pattern on the surface of a stamp (nearly always a polydimethylsiloxane, or PDMS, material [87]) to form these patterns on a substrate by simple contact. See Figure 1-1. It is most often used in conjunction with catalysts for deposition or etching; for in-

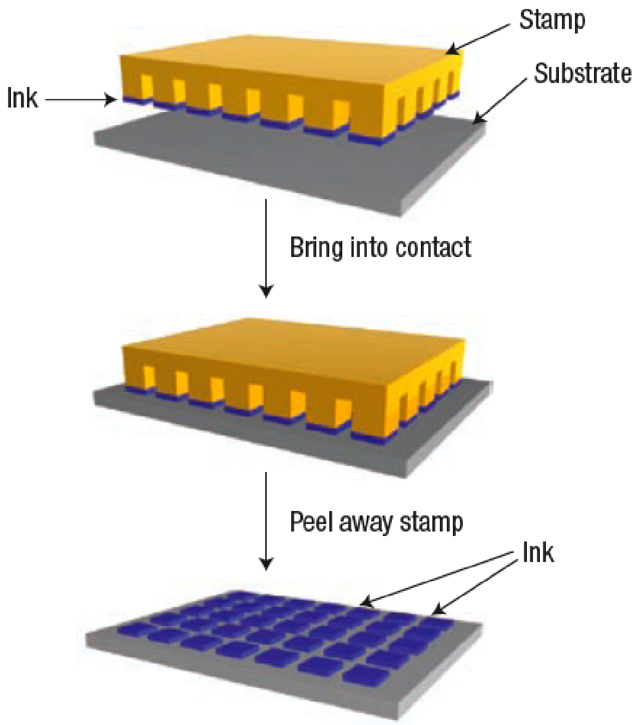

Figure 1-1: Steps in the direct microcontact printing process: first, coat the stamp with desired material, then bring coated stamp into contact with the substrate, finally demold the stamp leaving patterned material behind. [1]

stance, printing a thiol creates a self-assembled monolayer that is used to etch features in gold [88, 89, 90]. It is capable of patterning large area surfaces with spatial resolution down to the sub-micrometer range [1].

Microcontact printing a conductive ink has some advantages over other high throughput techniques such as microcontact printing of thiols or nanoimprint lithography (NIL) [91], such as lower temperatures and fewer processing steps. Printing a conductive ink directly transfers the material on the protrusions of mold to the substrate, as opposed to both NIL and μCP of a monolayer of thiols which require an additional etching step to remove unwanted material.

1.2.2 History of μCP

Microcontact printing was pioneered by the Whitesides group at Harvard [23, 89, 92]. In the original vision, microcontact printing used an elastomeric stamp to apply a self-assembling monolayer of alkenethiols [93] to gold deposited on silicon. Then the gold can be selectively etched, revealing fine patterns. This method has the advantages of being simple and low cost since a single tool can be reused to pattern many different substrates. Fabricating the elastomeric stamp from PDMS guarantees conformal contact and allows patterning non-planar substrates.

Microcontact printing was soon demonstrated to feature sizes of 30 nm [94], which was was well below the limits of photolithography when reported in 1997 and spurred research in the area from IBM [94, 95, 96, 97, 98, 99, 100, 101]. It appears that the process never became developed to the point of mainstream manufacturing in the semiconductor industry, due in part to its own difficulties with cross-layer registration, lack of compatibility with all semiconductor materials, and the industry's existing investment and continued advances in conventional lithography. [2]

In the past two decades, a variety of substrate and ink combinations have been successfully demonstrated with microcontact printing [102, 103, 104]. The simple nature, scalability, and adaptability to different materials makes microcontact printing an excellent candidate for development into a robust manufacturing process. See Table 1.3 for a listing of a wide variety of applications of μCP [15].

1.2.3 Previous work in μCP equipment

Microcontact printing has been widely demonstrated at the lab scale (for instance, a portable microcontact printing machine, manually operated, was reported by Elloumi-Hannachi [105]). However, microcontact printing at the manufacturing scale has been documented in only a handful of cases.

Cracauer et al. disclose a simple system using the stamp as a diaphragm, wherein fluid provides positive or negative pressure to control contact propagation (by ballooning the diaphragm) [106]. Kendale developed a more sophisticated three-degree of freedom printing machine that used flexural bearings to precisely adjust the pitch, roll, and height of a stamp over a wafer-scale substrate [107, 108, 109]. Chakra et. al present a microcontact machine that stamps microscope-sized slides, using a pneumatic actuator with a high accuracy linear slide[110]. Ho et. al presents a micro-stamping system for printing biosample fluids, that features a refillable stamp [111].

Each of the aforementioned machines addresses stamping of discrete rigid substrates

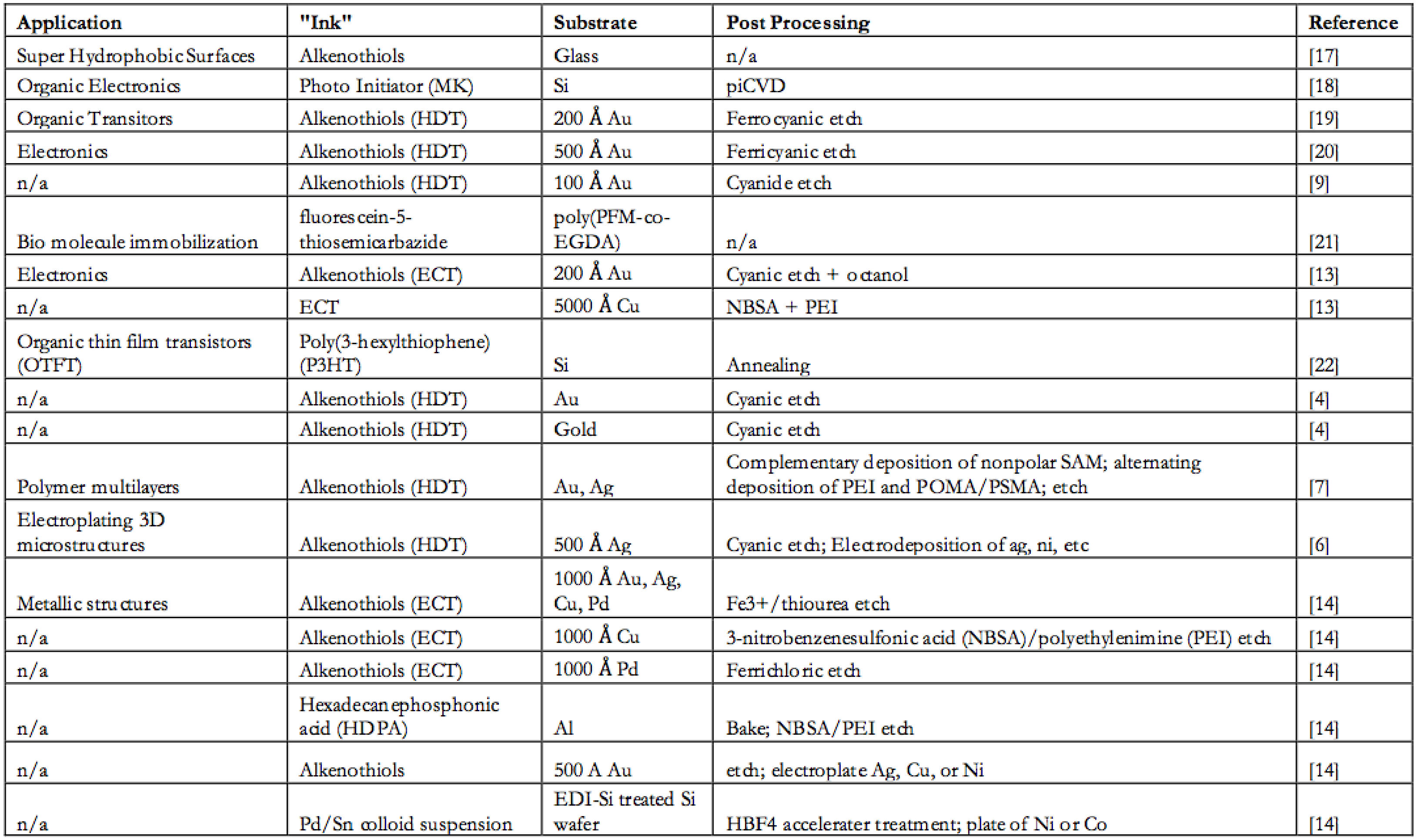

Application	"Ink"	Substrate	Post Processing	Reference
Super Hydrophobic Surfaces	Alkenothiols	Glass	n/a	[17]
Organic Electronics	Photo Initiator (MK)	Si	piCVD	[18]
Organic Transitors	Alkenothiols (HDT)	200 Å Au	Ferrocyanic etch	[19]
Electronics	Alkenothiols (HDT)	500 Å Au	Ferricyanic etch	[20]
n/a	Alkenothiols (HDT)	100 Å Au	Cyanide etch	[9]
Bio molecule immobilization	fluorescein-5-thiosemicarbazide	poly(PFM-co-EGDA)	n/a	[21]
Electronics	Alkenothiols (ECT)	200 Å Au	Cyanic etch + octanol	[13]
n/a	ECT	5000 Å Cu	NBSA + PEI	[13]
Organic thin film transistors (OTFT)	Poly(3-hexylthiophene) (P3HT)	Si	Annealing	[22]
n/a	Alkenothiols (HDT)	Au	Cyanic etch	[4]
n/a	Alkenothiols (HDT)	Gold	Cyanic etch	[4]
Polymer multilayers	Alkenothiols (HDT)	Au, Ag	Complementary deposition of nonpolar SAM; alternating deposition of PEI and POMA/PSMA; etch	[7]
Electroplating 3D microstructures	Alkenothiols (HDT)	500 Å Ag	Cyanic etch; Electrodeposition of ag, ni, etc	[6]
Metallic structures	Alkenothiols (ECT)	1000 Å Au, Ag, Cu, Pd	Fe3+/thiourea etch	[14]
n/a	Alkenothiols (ECT)	1000 Å Cu	3-nitrobenzenesulfonic acid (NBSA)/polyethylenimine (PEI) etch	[14]
n/a	Alkenothiols (ECT)	1000 Å Pd	Ferrichloric etch	[14]
n/a	Hexadecanephosphonic acid (HDPA)	Al	Bake; NBSA/PEI etch	[14]
n/a	Alkenothiols	500 A Au	etch; electroplate Ag, Cu, or Ni	[14]
n/a	Pd/Sn colloid suspension	EDI-Si treated Si wafer	HBF4 accelerater treatment; plate of Ni or Co	[14]

Table 1.3: Example applications of microcontact printing in literature, demonstrating the breadth of applications for this manufacturing process [15]

(i.e. a silicon wafer). Beyond these discrete processes, roll-based microcontact printing applications have been reported to allow continuous processing. Roll-based configurations have the advantage of inherently controlling the advance and recess of the contact zone [112]. The first was a simple experiment by Xia et al., where a stamp was mounted on a cylinder and rolled by hand over a 100 mm wafer [113]. A lack of uniformity is clearly evident in the images included in this report, indicating the need for more precise control of the process.

A roll-based configuration for printing organic transistors was proposed by Rogers et al., where the PDMS stamp is mounted to a glass roller after plasma bonding, then used to pattern a flexible substrate [114]. A series of high-speed roll-to-roll printing trials were performed at MIT, where closed loop tensioning and a compliant backup roller were used to modulate contact pressure [112, 115, 116, 117, 118, 119, 120, 121, 122] .

1.2.4 Why do we need a better μCP model?

Microcontact printing with direct inks is fundamentally a different process than printing with thiols, the most common configuration. Thiols are a monolayer, and printing becomes a binary question of transfer or no transfer. But with direct ink printing, all manner of defects can occur from poor control of the process. Too much ink leads to spreading of the pattern, while too little ink leads to drying and failure of transfer. Incompatible surface chemistries of the stamp, ink, and substrate can cause beading of the ink or incomplete coverage, and mechanical parameters such as too much pressure (as seen in Figure 1-2) can cause roof collapse [2]. Careful control of the process parameters is essential to achieve success, and become more sensitive especially as the feature sizes get smaller and the printing area grows larger. Without a robust process model, lab scale demonstrations in literature will not be able to scale to commercialization.

1.3 Applications: Using μCP for microfluidics and beyond

If a μCP process suitable for manufacturing electrodes on microfluidic chips could be developed, such a process would have wide application in other industries, because printing is the main method which allows patterning with a suitable resolution on a large area [3]. Development of this method and model has an impact in a wide variety of areas, including manufacturing microfluidic chips, organic LED displays, solar cells, and flexible electronics.

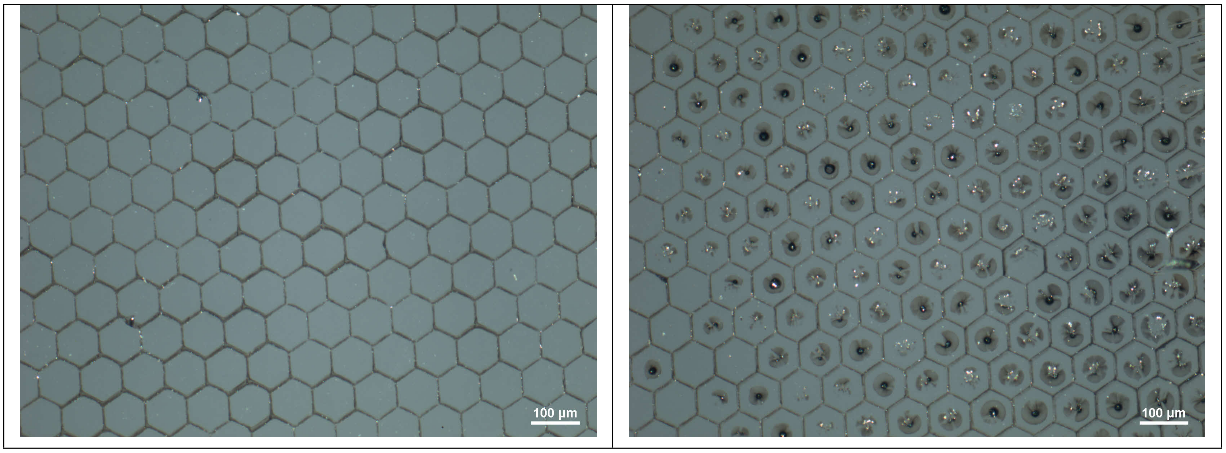

a) μCP printing of silver ink pattern with acceptable force during transfer

b) Roof collapse defect caused by excessive force during transfer

Figure 1-2: Defects such as roof collapse are easily caused by poor control of the μCP process, demonstrating the need for careful machine design and process control [2]

Photovoltaics: Small electrodes are needed in solar cell manufacturing, in particular organic solar cells and dye-sensitized solar cells [123].

Organic electronics: After the demonstration of the first organic transistor in 1986, an entirely new field of organic electronics was born [3]. Organic electronics have promising applications due to two distinct advantages: low cost over a large area, and low-temperature fabrication on a flexible substrate [124]. Organic thin-film transistors with electrodes fabricated from conductive polymers showed excellent electrical performance [1]. Commercial applications include organic LEDs [123, 125, 76].

Flexible Manufacturing: Thin substrates processed with web handling techniques require an electrode manufacturing process that can be adapted to roll-to-roll equipment. Commercial applications include RFID tags [3], electronic papers [124], and etching traces for flexible displays [71].

Optics: Commercial applications in the optics industry include diffractive optical elements and gratings, light guides [123, 99], and alignment features in LCD displays [99].

Other: Other commercial applications include photodetectors, battery elements and embedding electrical functions in packaging [123], metallic nanowires in microelectronics [99], tailoring surface energy for enhanced heat transfer [71], and catalyzing seed locations for CNT growth [71].

1.4 Contributions

The issue of integrating high resolution conductive structures into polymer devices using a low-cost, rapid, accurate manufacturing technique is important to the future of the microfluidic industry, as well as the photovoltaic, flexible printing, and organic electronics industries. This issue is also not one that has been solved - in academia, there has been work in the areas of microcontact printing but rarely with liquid inks, in the area of flexographic printing with liquid ink but not at sizes this small, and work in manufacturing conductors but not commonly on polymers. And rarely in the literature in general is the ability of the experimental method to translate into high volume industrial manufacturing considered. The expected contribution of this work is a manufacturing model of and demonstrated results from microcontact printing conductive ink onto polymer substrates. We will be able to demonstrate conductive silver patterns, with feature sizes down to 5μm, printed on polymer using a method that can be easily scaled to high volume manufacturing.

1.5 Overview of thesis

In this thesis, microcontact printing equipment is used to explore the manufacturing process model for a variety of inks on a variety of substrates, with the focus on conductive polymer ink and silver nanoparticle ink on glass, acrylic, and polyethylene terephthalate (PET) substrates. Experimental results demonstrate successful printing down to 5μm feature sizes on polymer substrates. Statistical analysis of designed experiments coupled with theoretical understanding is used to generate a process model for this manufacturing method.

This thesis was completed in the Polymer Micromanufacturing Laboratory, a division of the Laboratory for Manufacturing and Productivity. The work was completed under the direction of Professor David E. Hardt, in collaboration with the Singapore-MIT Alliance. The historic focus of this lab has been to apply process control to manufacturing processes, including sheet metal forming, welding, thermal set polymer casting and hot embossing. This thesis continues the tradition of the lab by using manufacturing equipment designed in the laboratory and applying process control to push the limits of resolution while retaining the high-volume capability of the process. This motivation for this thesis was to solve a problem with microfluidic device manufacturing, as this is funded by an overarching project with the goal of creating "a fundamental basis for the design and optimal operation of the various processes used to produce microfluidic devices" [126].

Chapter 2 explores the current state of the art in micromanufacturing processes and justifies the choice of μCP for further study, and Chapter 3 presents the theoretical understanding of the μCP process. Chapters 4 and 5 document the extensive experimentation with conductive polymer material and silver nanoparticle ink, respectively. Chapter 6 reviews the development of the process model using experimental results, and the final Chapter 7 summarizes the key contributions of the work and identifies future areas of research.

Chapter 2

Exploration of Surface Patterning Processes in Micromanufacturing

The stated goal is to create patterned conductive traces on polymer substrates, and there are multiple possible methods of accomplishing that goal. This chapter describes the decision making process that led to microcontact printing as the most promising method for further study. This chapter first gives a review of surface patterning techniques available, then uses functional requirements to narrow down the list to a handful of contenders, and then describes a series of "screening" experiments carried out with each of the contender processes to help establish viability and finally arrive at μCP as the focus for the rest of the work. A literature review of the best resolutions reported from each manufacturing process, and the mechanisms that limit those resolutions, reveals that μCP has the potential to be improved with process control.

2.1 Overview of surface patterning processes in micromanufacturing

The need for lab-on-a-chip devices to incorporate conductive features was the original motivation for a manufacturing solution. There has been some work aimed at creating integrated or hybrid platforms with electrodes and polymers [127, 128, 129, 130, 131, 37], but these papers focus more on how to integrate the chip components and less on how to integrate the manufacturing process. The lack of study in this area may be because of the incompatibility of many polymers with most semiconductor-process chemicals (e.g. solvents used in photolithography) and weak thermal endurance at typical photoresist baking temperatures [127]. Known methods of creating metal microfeatures (particularly on microfluidic devices) are given in the table below, with a more detailed look at each method following.

Table 2.1: Overview of surface patterning micromanufacturing techniques, particularly for microfluidics

	Manufacturing Method	Typical Size Range	Material	Notes	References
1	Traditional MEMS Processes				[132, 133, 27, 134, 135, 68, 42, 57, 129, 41, 40, 28, 136, 62, 53, 77, 37]
	Sputter deposition	20nm to 10μm thick	Ti, Cu, Au	Expensive, dedicated equipment. Conformal. Target isn't heated.	[38, 28, 62, 73, 77, 37, 49]
	Chemical vapor deposition	20nm-few μm thick	Many	Expensive, dedicated equipment	[62, 68]
	Evaporation	1000Å - 100nm thick	Au, Al, Cr seed layer	Thin films, non-conformal, slower rate than sputtering (1-10nm/s)	[66, 127, 50, 48, 51, 52]
	Shadow mask	20nm thick	Ag		[67]
	Tollen's reaction	30-60nm thick, $<10\mu$m wide	Ag	No clean room or vacuum for deposit, but litho needed for patterning	[137]
	Electroplating	up to 225um thick	Ni	Expensive, dedicated equipment. Possible 3D features. High thickness.	[138, 26, 64]
	Lift-off processing	50-100nm thick, 1-10um wide	Cr, Au		[65, 54]
	Hot embossing	3000Å thick	Al	Embedded in substrate	[13]

	Manufacturing Method	Typical Size Range	Material	Notes	References
	Sacrificial microchannel template	conforms to channel dimensions, ex. up to 50μm wide and 10um thick; 5μm wide by 10nm thick	Cr, Au, Cu	Direct contact. Additional step of channel fabrication. Best for continuous features with a height $>$ microns. Uses CMOS processes.	[29, 139, 58]
	Other (sol–gel, molecular beam epitaxy, pulsed laser, filtered vacuum arc, atomic layer dep.)	Varied	Cr, ZnO	Far less common, specialized cases.	[62, 75]
2	Inkjet Printing			Serial process.	[3]
3	Screen Printing	min of 100μm resolution, accuracy about 50μm	organic and inorganic		[3, 140, 44]
4	Microcontact Printing	down to 100nm	Au, Pd, conductive polymers, metal oxide, Al	High accuracy is possible, but alignment issues a challenge	[90]
5	Micromachining	100μm and larger	Cu, Al, steel	Limited by drill/mill size	[141]
6	Modifying a CD		Au, Ti	Uses a CD	[33, 43]
7	Self Assembly	5nm - 30nm thick, nano	Au, Cu, Cr	Deposit onto particles	[45, 47]
8	Laser Structuring	100nm-100um	Au, Cr, ITO	Direct laser structuring no need for a mask or add'l chemical agents. Flexible feature sizes.	[59, 46, 76, 30]

	Manufacturing Method	Typical Size Range	Material	Notes	References
9	Focused Ion Beam Milling	100-300nm	Au		[32]
10	Liquid Polymer Implantation	100um thick, various shapes	Ni, Cu iron	cast PDMS over stencil	[30]
11	Metal Ion Implantation	50nm thick	Au	Can make 3-D electrodes; implanted sticks better than sputtered	[53, 142]
12	Photoreduction from solution			Catalysts are difficult to remove	[69]
13	Flowing into polymer microchannels				
	Metal hardens	conforms to any channel dimensions 100umx100um, or nanolayer	indium and tin, indium, platinum, Ag, Cu, Au		[55, 74, 143, 69, 61]
	Metal remains liquid	150um diameter, 150x500um	mercury, eutectic gallium indium	CMOS processes still needed for auxiliary components	[34, 70]
14	Electroless deposition				
	w/ μCP	300nm thick	Ni, Ag	Resolution limited by diffusion of ink and deformation of stamp	[39]
	w/ laser	nanometer thick	Cu	Can do internal walls	[78]
	w/ multiphase laminar flow	nanometer thick	Cu	Can do internal walls	[144]

2.1.1 Traditional MEMS techniques overview

There are endless variants on ways to create microfluidic devices using polymer and metal with conventional microfabrication techniques [132]. Many of these methods of fabrication and variants are covered by Rhine et. al. [133]. Lee et. al. [129] described typical methods for making an integrated CMOS and microfluidic chip. The typical sequence looks like this:

1. Generate a pattern using lithography.
2. Use the pattern to deposit a conductive layer on a substrate.
3. Deposit one or several insulating layers on top.
4. Fabricate a fluid handling layer with one surface contoured, and second surface flat.
5. Bond the contoured surface to the insulated side of the conductive layer.

The fabrication of the microfluidic layer can be done by creating a mold pattern on a second substrate (also through photolithography), etching the substrate and then casting or molding a polymer against this master [133]. Examples of devices that use CMOS processing include detection of a neurotransmitter[41], changing the pH level in microchannels [77], low concentration ammonia sensing [57], droplet sensing [40], controlling torque on superparamegnetic beads [27, 134], detecting and analyzing trace metals [37], demixing [28], acoustic wave based sensing [62], sample processing [135], detection of protein complexes [42], counting of red blood cells [136], and surface-enhanced Raman scattering (SERS) sensing [68]. Although conventional processes are typically multi-step and time consuming, single-step optical lithographic fabrication of microfluidic channels has been demonstrated, and the fabrication process of electrodes has been simplified as much as possible [53].

The detailed descriptions of the variety of techniques listed in the micromanufacturing processes table are given in Appendix A. All involve conventional microfabrication techniques at some point in the process, and to differentiate they are listed by the method of metal deposition. Note that there is overlap with other sections (examples in other categories may also use microfab techniques), so strict classification is difficult.

2.1.2 Inkjet printing overview

Inkjet printing involves printing droplets through a nozzle in a programmed pattern onto a substrate. This method is low cost, there is a wide range of printable materials available, and

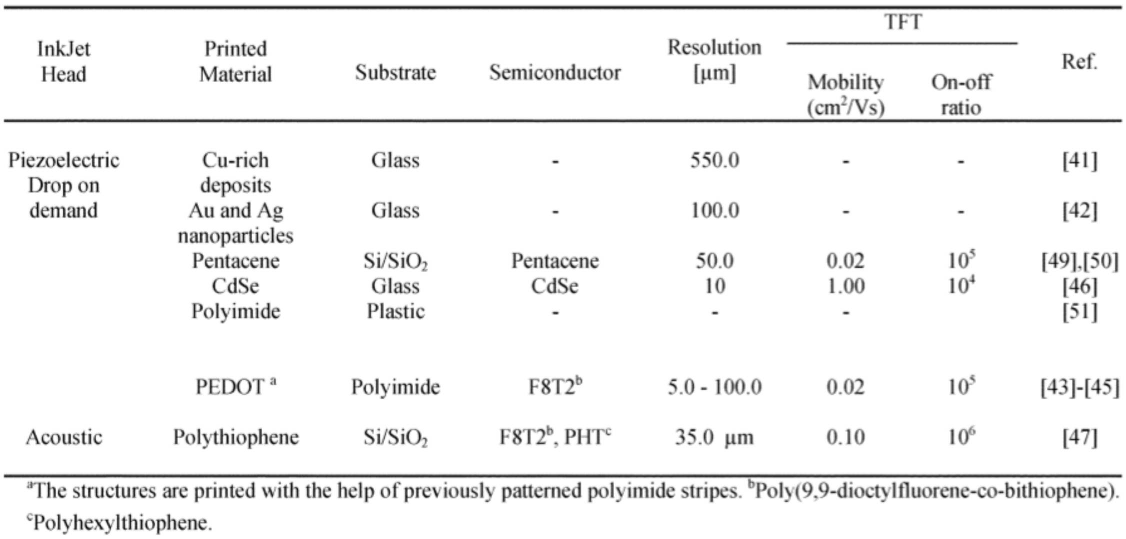

InkJet Head	Printed Material	Substrate	Semiconductor	Resolution [μm]	TFT		Ref.
					Mobility (cm^2/Vs)	On-off ratio	
Piezoelectric Drop on demand	Cu-rich deposits	Glass	-	550.0	-	-	[41]
	Au and Ag nanoparticles	Glass	-	100.0	-	-	[42]
	Pentacene	Si/SiO_2	Pentacene	50.0	0.02	10^5	[49],[50]
	CdSe	Glass	CdSe	10	1.00	10^4	[46]
	Polyimide	Plastic	-	-	-		[51]
	PEDOT ^{a}	Polyimide	F8T2^b	5.0 - 100.0	0.02	10^5	[43]-[45]
Acoustic	Polythiophene	Si/SiO_2	F8T2^b, PHT^c	35.0 μm	0.10	10^6	[47]

^{a}The structures are printed with the help of previously patterned polyimide stripes. ^{b}Poly(9,9-dioctylfluorene-co-bithiophene). ^{c}Polyhexylthiophene.

Figure 2-1: Summary of methods for patterning organic electronics based on ink-jet printing techniques [3]

it is very flexible. It has been used as a deposition tool for polymers and inorganic particles [145]. The conductivity and thermal expansion are controlled by the choice of conductive material, and the adhesion properties are dependent on surface chemistry. One potential downside of the technology is feature size - both the thickness of the layer (which if too thick may cause problems with bonding or make it unsuitable for direct contact applications) and the resolution, which is limited by the ink droplets spreading. The lateral resolution may be mitigated with process control, but the thickness of the layer is mainly controlled by surface tension and is difficult to modify. The through-put may also be a drawback to this method of manufacture, since the process is inherently slow because it involves serial droplets instead of large-area parallel processing. Parashkov [3] summarizes the uses of inkjet printing for conducting patterns nicely in Figure 2-1.

2.1.3 Screen printing overview

Screen printing is a very traditional process for large area patterning, based on squeezing a paste material through a patterned screen (either a threaded screen, or a metal stencil) onto the substrate. The advantages include a wide variety of possible materials, and low processing temperatures. It is an active subject of research, with resolutions being pushed to new limits (see Figure 2-2).

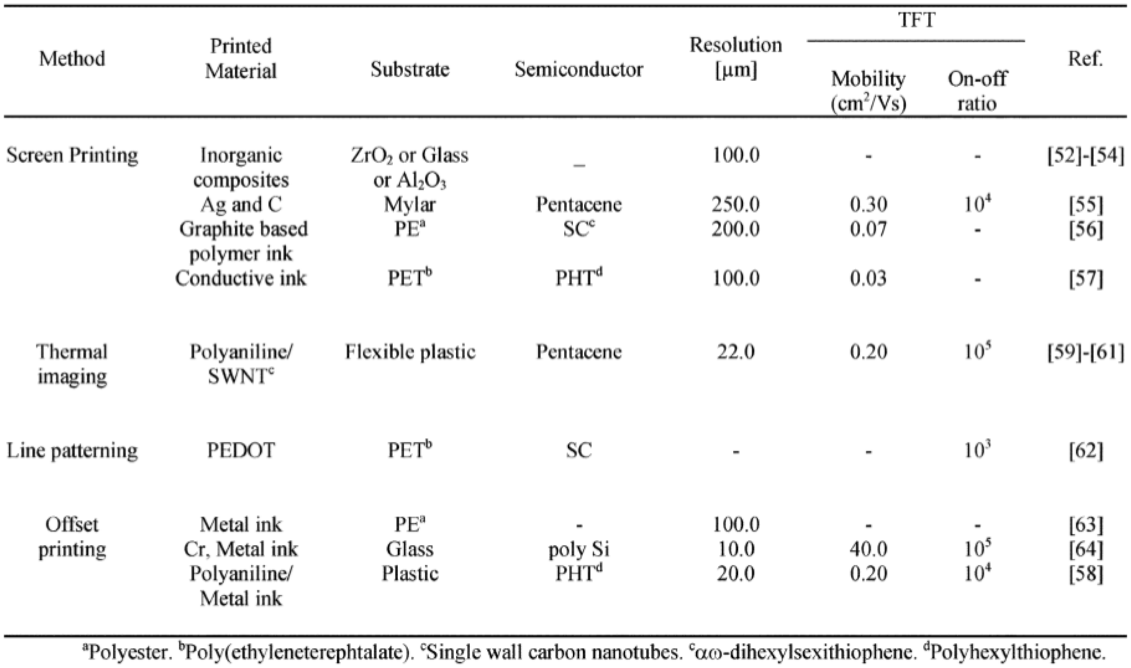

Method	Printed Material	Substrate	Semiconductor	Resolution [μm]	TFT		Ref.
					Mobility (cm^2/Vs)	On-off ratio	
Screen Printing	Inorganic composites	ZrO_2 or Glass or Al_2O_3	_	100.0	-	-	[52]-[54]
	Ag and C	Mylar	Pentacene	250.0	0.30	10^4	[55]
	Graphite based polymer ink	PE[a]	SC[c]	200.0	0.07	-	[56]
	Conductive ink	PET[b]	PHT[d]	100.0	0.03	-	[57]
Thermal imaging	Polyaniline/ SWNT[c]	Flexible plastic	Pentacene	22.0	0.20	10^5	[59]-[61]
Line patterning	PEDOT	PET[b]	SC	-	-	10^3	[62]
Offset printing	Metal ink	PE[a]	-	100.0	-	-	[63]
	Cr, Metal ink	Glass	poly Si	10.0	40.0	10^5	[64]
	Polyaniline/ Metal ink	Plastic	PHT[d]	20.0	0.20	10^4	[58]

[a]Polyester. [b]Poly(ethyleneterephtalate). [c]Single wall carbon nanotubes. [c]αω-dihexylsexithiophene. [d]Polyhexylthiophene.

Figure 2-2: Summary of patterning for organic electronics based on screen printing and other techniques [3]

2.1.4 μCP overview

There are several ways of using microcontact printing processes: 1) thiol printing for etching high-resolution patterns of noble metals [146]; 2) printing of catalysts to mediate patterned deposition of metals; and 3) direct printing of conductive inks. The most common microcontact printing methods are the first two, to print a resist and etch a metal substrate [23, 99, 147, 85], and to print a catalyst for electroplating (which is covered in the section on electroless deposition). But using direct microcontact printing instead [104, 102] is more interesting for this work. This method involves first creating a stamp with the desired features, applying a material to the stamp (through sputtering, dipping, spin coating, etc.), carefully aligning the stamp to the substrate, then transferring the material from the stamp to the substrate (either with pressure, surface tension, chemical reaction [148], or some combination thereof).

This method does not require a mask during processing, does not require rinsing or post-processing [149], is low cost (does not require any sacrificial materials or chemicals for processing, aside from the material transferred), flexible in terms of the materials available for use [102], and high-throughput (contact time on the order of seconds or less [148]).

Fabrication of devices by μCP include relatively large structures, such as arrays of metal oxide on semiconductor field-effect transistors (MOSFETs), arrays of Al/Si Schottky diodes, and electrodes for organic electronic applications [90], but μCP is also capable of high resolution patterning. The resolution of the printed features under certain conditions can be excellent (sizes down to 100nm, with edge resolution better than 15nm [148]), and the height of the film can be very thin. The conductivity, adhesion, and thermal expansion are controlled by the choice of materials for substrate and conductive features. The conductivity and adhesion can be chosen to be at least as good as semiconductor processes [150], while the thermal expansion is a possible downside of this technology.

But this thermal expansion mismatch might be mitigated by using the commercially available conductive polymer known as PEDOT, which has excellent adhesion and conductivity, instead of a metal. A paper by Li et. al demonstrates PEDOT polymer electrodes created by polymer inking and stamping.[150] The direct patterning of conducting polymers in particular is an interesting application for soft lithography.

Figure 2-3 summarizes the uses for μCP, including both monolayer applications and direct ink transfer.

2.1.5 Other methods overview

Please refer to Appendix A for more details on additional micromanufacturing processes.

2.2 Evaluation of micromanufacturing processes for conductive ink patterning

The options were evaluated using a set of functional requirements (FRs) as follows:

1. Low cost (comparable to screen printing)
2. Low temperature (less than about 125ºC, suitable for polymer processing)
3. Feature lateral resolution <10 um
4. Feature thickness <500 nm (for bonding purposes)
5. High throughput (e.g. fast rate)

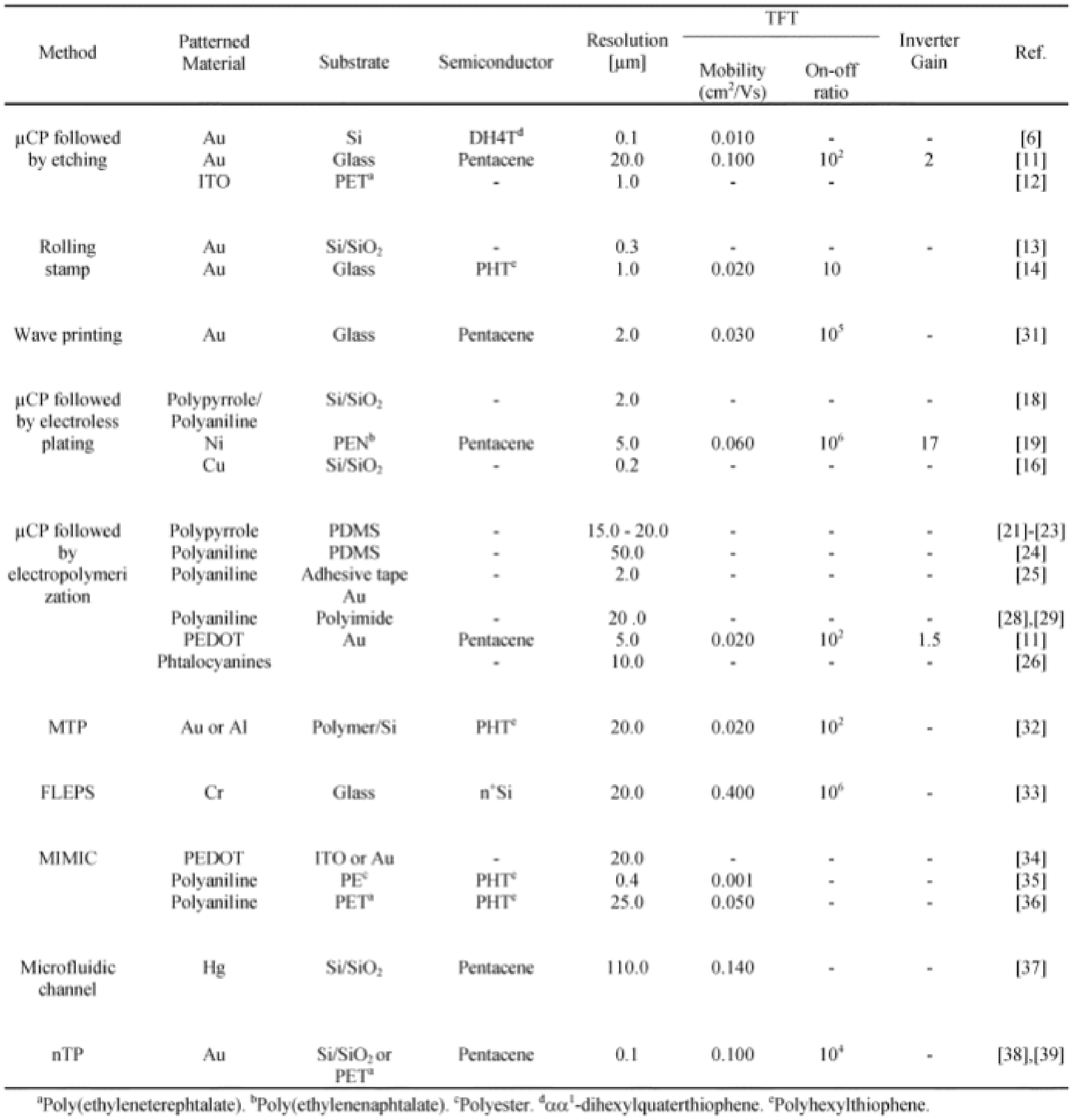

Method	Patterned Material	Substrate	Semiconductor	Resolution [μm]	TFT		Inverter Gain	Ref.
					Mobility (cm^2/Vs)	On-off ratio		
μCP followed by etching	Au	Si	DH4T^d	0.1	0.010	-	-	[6]
	Au	Glass	Pentacene	20.0	0.100	10^2	2	[11]
	ITO	PET^a	-	1.0	-	-		[12]
Rolling stamp	Au	Si/SiO$_2$	-	0.3	-	-	-	[13]
	Au	Glass	PHT^e	1.0	0.020	10		[14]
Wave printing	Au	Glass	Pentacene	2.0	0.030	10^5	-	[31]
μCP followed by electroless plating	Polypyrrole/ Polyaniline	Si/SiO$_2$	-	2.0	-	-	-	[18]
	Ni	PEN^b	Pentacene	5.0	0.060	10^6	17	[19]
	Cu	Si/SiO$_2$	-	0.2	-	-	-	[16]
μCP followed by electropolymerization	Polypyrrole	PDMS	-	15.0 - 20.0	-	-	-	[21]-[23]
	Polyaniline	PDMS	-	50.0	-	-	-	[24]
	Polyaniline	Adhesive tape Au	-	2.0	-	-	-	[25]
	Polyaniline	Polyimide	-	20 .0	-	-	-	[28],[29]
	PEDOT	Au	Pentacene	5.0	0.020	10^2	1.5	[11]
	Phtalocyanines		-	10.0	-	-	-	[26]
MTP	Au or Al	Polymer/Si	PHT^e	20.0	0.020	10^2	-	[32]
FLEPS	Cr	Glass	n$^+$Si	20.0	0.400	10^6	-	[33]
MIMIC	PEDOT	ITO or Au	-	20.0	-	-	-	[34]
	Polyaniline	PE^c	PHT^e	0.4	0.001	-	-	[35]
	Polyaniline	PET^a	PHT^e	25.0	0.050	-	-	[36]
Microfluidic channel	Hg	Si/SiO$_2$	Pentacene	110.0	0.140	-	-	[37]
nTP	Au	Si/SiO$_2$ or PET^a	Pentacene	0.1	0.100	10^4	-	[38],[39]

^{a}Poly(ethyleneterephtalate). ^{b}Poly(ethylenenaphtalate). ^{c}Polyester. $^d\alpha\alpha^1$-dihexylquaterthiophene. ^{e}Polyhexylthiophene.

Figure 2-3: Summary of methods for patterning organic electronics based on μCP techniques [3]

The manufacturing options available can be compared along those dimensions (broadly categorized by “thick” and “thin” processes for feature thickness, according to the form factor of the deposited metal). In addition, they can be separated by whether the deposited metal is in direct contact with the working fluid, and whether a mask is required for patterning. A summary table used to help in evaluation is given in Table 2.2.

Manufacturing Method	Cost	Quality	Rate	Thickness	In channel?	Mask?	Notes
Screen Printing	++	-	Parallel	Thick	No	Screen	No vacuum, variety of metals
Inkjet printing	+	-	Serial	Thin	No	None	No vacuum, variety of metals
Flowing solder into channels	+	+	Parallel	Thick	Both	Channel template	In-channel if use sacrificial template
Microcontact printing w/ etching	-	+	Parallel	Thin	Both	Stamp	Resolution limited by diffusion of ink and deformation of stamp, add'l process steps required
Electroplating	-	-	Parallel	Thick	No	Stamp	With microcontact printing of catalyst.
Hot Embossing	-	+	Parallel	Thick	No	Mask	Embedded in substrate, lots of steps involved
Micromachining	+	-	Serial	Thick	No	None	Limited by drill/mill size
Injection Molding w/ Conductive material	+	+?	Parallel	Thick	Both	Mold Set	Either co-molding or two-shot molding
Metal Ion Implantation	-	+	Parallel	Thin	Yes	Mask	Can make 3-D electrodes; implanted sticks better than sputtered
Flowing solution into channels	+	+	Parallel	Thin	Both	Channel template	Variety of metals
Electroless deposition with laser	-	++	Serial	Thin	Both	None	Can do internal walls of hollow channels
Sputter deposition	-	++	Slow	Thin	Yes	Mask	Conformal. Target doesn't get so hot. Cost is mitigated at high volumes.
Vapor deposition	-	++	Slow	Thin	Yes	Mask	Expensive, dedicated equipment. Cost is mitigated at high volumes.
Evaporation	-	++	Slow	Thin	Yes	Mask	Thin films. Non-conformal. Slower rate than sputtering (1-10nm/s)
Laser Structuring	?	+	Serial	Thin	Both	None	No chemical agent or treatments of waste chemicals. Flexible from small size to large
Focused Ion Beam Milling	-	+	Serial	Thin	Both	None	
Direct Microcontact Printing	+	+	Parallel	Thin	Yes	Stamp	High accuracy is possible, but alignment issues a challenge

Table 2.2: Comparison table of micromanufacturing methods for conductive ink patterning

Removing the methods from the Comparison Table that have an unsuitable size range, and that can only create “thick films”, leaves the promising methods of vapor deposition (CVD), evaporation, ink jet printing, microcontact printing with etching, flowing a metalized solution into pre-formed channels, screen printing, and direct microcontact printing of a conductive material. Microcontact printing followed by etching requires multiple process steps and is expensive, and limits the substrate material choice. Flowing a solution or solder into pre-formed channels is only suitable for applications that do not require direct contact with the working fluid, but most sensing applications need in-channel electrodes.

From the author’s research, the methods that seem the most promising are CVD, evaporation, ink jet printing, screen printing, and direct microcontact printing. Each of these techniques could be used with a variety of inks - either metal nanoparticles, a conductive polymer such as PEDOT, or carbon nanotubes - all of which would be conductive. PEDOT was identified as a promising material choice (discussed more in Chapter 4), for reasons including reasonable material cost, mechanical flexibility, good adhesion to polymer substrates, and low processing temperatures. Each potential manufacturing process was explored with initial experiments in the sections below, using PEDOT as the patterned material (with the exception of evaporation, for which aluminum was used as PEDOT was not available).

2.2.1 Initial testing with chemical vapor deposition (CVD) of PEDOT

To test the viability of CVD particularly with a polymer substrate, a collaborative experiment at MIT was carried out. Using an oxidative CVD process, the conductive polymer poly(3,4-ethylenedioxythiophene) (PEDOT) was polymerized from EDOT monomer, onto a poly(methyl methacrylate) (PMMA) substrate. No pattern was used for this test, simply blanket coverage. Initial tests, shown in Figure 2-4, were measured with a four-point probe to test conductivity. The films had high resistance and varying readings across each test and between tests.

Qualitatively, it was noted that the CVD process was very sensitive to variables such as the choice of oxidizing agent, the temperature of the stage and the source material, the pressure in the chamber, and the cleaning method used on the PMMA substrate prior to deposition. These variables would need to be optimized for both the mechanical properties of the film (uniformity and thickness, and perhaps adhesion) and conductivity of the PEDOT film itself. These simple initial tests did not allow thorough exploration of the tradeoffs

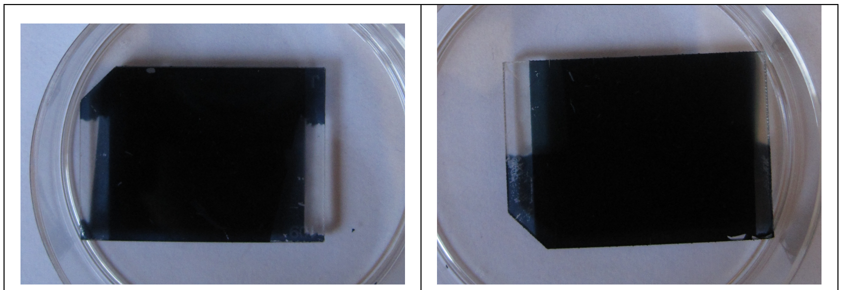

a) 45Ω resistance

b) 20-25Ω

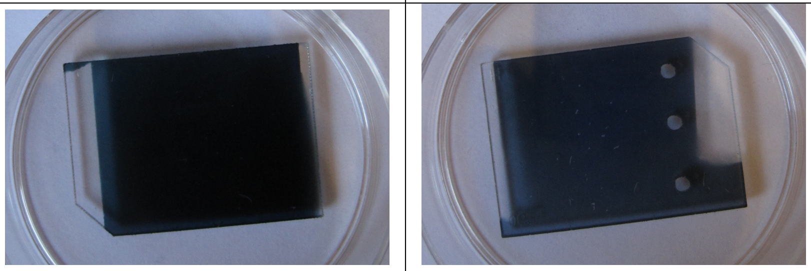

c) 25Ω

d) 125Ω

Figure 2-4: CVD deposition of PEDOT onto PMMA, resulting in very high and inconsistent film resistance

between processing parameters, so potential certainly exists for better results.

2.2.2 Initial testing with electron beam physical deposition of aluminum

Viability testing for electron beam physical deposition (E-beam lithography) applied on a polymer substrate was carried out in the MIT EML clean room facilities. A simple mask (fabricated from laser-cut acrylic) was applied to a PMMA substrate cleaned with isopropyl alcohol. Electron beam physical vapor deposition was used to deposit 800-900nm of aluminum through the mask onto the PMMA. The result is seen in Figure 2-5.

Qualitatively, the process works as expected and was successful. However the potential for improvement for this process is not as interesting, as it is a well established technology with a lot of research attention already. Also, for this work one of the key parameters is that the final chosen process be low-cost, and needing to use the clean room and expensive E-beam equipment negates some of the other advantages.

2.2.3 Initial testing with inkjet printing of PEDOT

Testing to determine validity of printing conductors onto polymers with inkjet printing with done at MIT, where an HP printer with a 45μm nozzle was used to print solutions of PEDOT

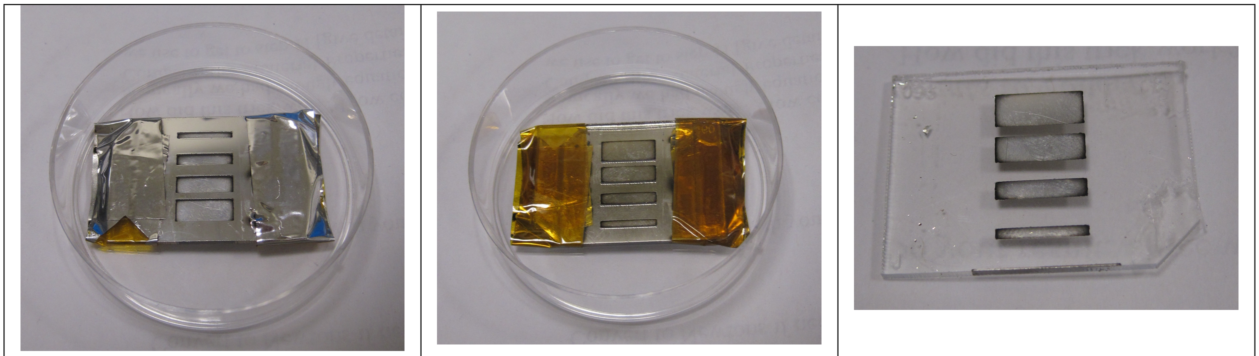

(a) Front of PMMA after deposition, before mask removal

(b) Back of PMMA after deposition, before mask removal

(c) PMMA substrate after Al deposition

Figure 2-5: Electron beam physical deposition of aluminum layer onto PMMA, showing successful deposition of millimeter scale features

Experiment	Resistance
c) 1:1 Water:PEDOT, on PMMA, 45uμm spacing, no plasma treatment, substrate 65C	150 kΩ
e) 1:1 Water:PEDOT, on PMMA, 45μm spacing, no plasma treatment, substrate 80C	120 kΩ
f) 1:1 Water:PEDOT, on PMMA, 45μm spacing, 60sec plasma treatment, substrate 65C	250 kΩ

Table 2.3: Resistance of inkjet printed PEDOT films, showing high resistance under a variety of conditions

onto PMMA. Because the viscosity of the PEDOT as provided was too high for successful drops through the nozzle, it was mixed 1:1 with water. In some cases a small amount dimethyl sulfoxide (DMSO) was added, on the recommendation of the manufacturer (H.C. Stark) to increase conductivity.

Figure 2-6 shows 10x microscope images of the results of testing under various conditions. The parameters that varied were the plasma treatment of the PMMA substrate, the ratio of water and DMSO to PEDOT material, the spacing of the droplets, and the substrate temperature. Qualitatively, a more uniform film was achieved by heating the substrate stage, and plasma treating the PMMA before deposition.

Only three of the tests on PMMA were uniform enough to achieve continuity, and these three were tested for electrical resistance with a four point probe. Table 2.3 shows that all three films had extremely high resistance, in the kilo-ohm range instead of the desired single-ohm range.

Similar testing was carried out with glass substrates, with the results shown in Figure 2-7. Even on glass (which is smoother and has more favorable surface energy than polymers) it was difficult to get a continuous film.

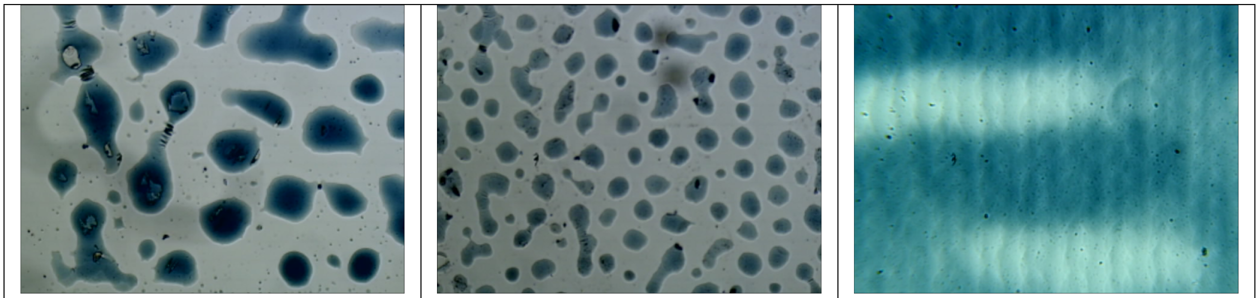

a) 1:1 Water:PEDOT, on PMMA, 45μm spacing, no plasma treatment, substrate room temp

b) 1:1 Water:PEDOT, on PMMA, 80μm spacing, no plasma treatment, substrate room temp

c) 1:1 Water:PEDOT, on PMMA, 45μm spacing, no plasma treatment, substrate 65C

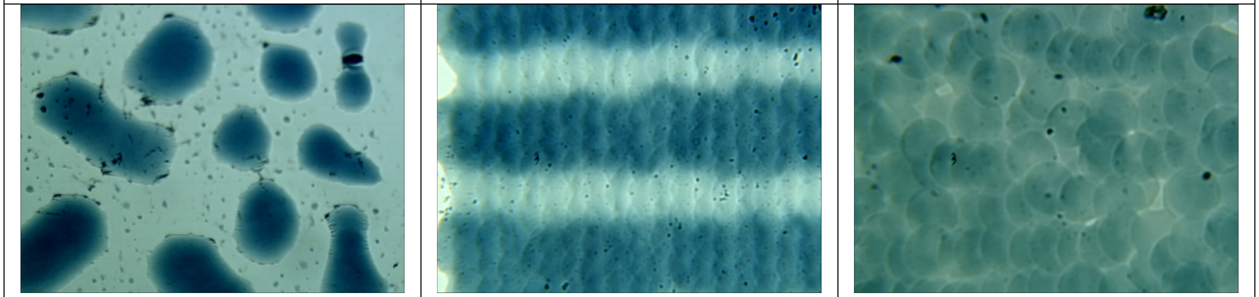

d) 5:10:15 DMSO:PEDOT:Water, on PMMA, 45μm spacing, no plasma treatment

e) 1:1 Water:PEDOT, on PMMA, 45μm spacing, no plasma treatment, substrate 80C

f) 1:1 Water:PEDOT, on PMMA, 45μm spacing, 60sec plasma treatment, substrate 65C

Figure 2-6: Inkjet printing of PEDOT onto PMMA substrate, showing inconsistent or nonexistent film coverage

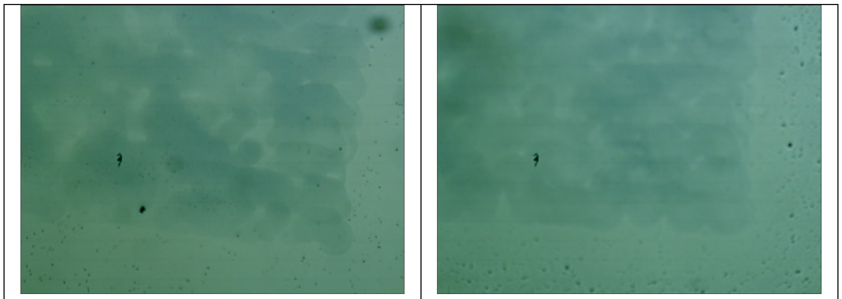

a) 1:1 Water:PEDOT, on glass, 95μm spacing, substrate room temp

b) 5:10:15 DMSO:PEDOT:Water, on glass, 80μm spacing, substrate room temp

Figure 2-7: Inkjet printing of PEDOT onto glass substrate, showing poor film uniformity

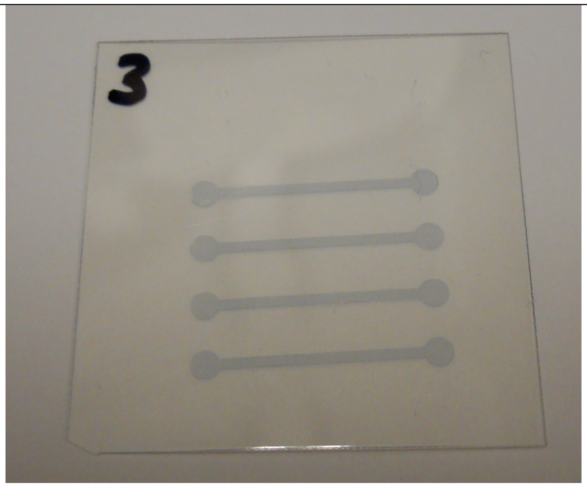

a) Screenprinted PEDOT onto PMMA substrate

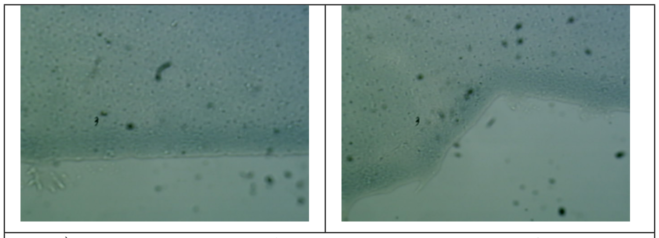

b) Edge quality of screenprinted PEDOT

Figure 2-8: Screenprinting of PEDOT onto PMMA substrate, showing successful millimeter scale feature fabrication, but potential problems with edge thickness and quality

Because of the inherent slowness of the process (each test took nearly 45 minutes to cover a 1cm by 0.5cm area), compounded with the difficulty getting a continuous film, inkjet printing does not seem to be a good candidate for further study (especially given the high throughput functional requirement).

2.2.4 Initial testing with screen printing of PEDOT

Screen printing was also evaluated as a potential process for depositing PEDOT onto polymer substrates. Screenprinting paste was acquired from Heraeus, product line Clevios SV 3. The crucial process parameter became the pressure applied during the squeegee pass, and after trial and error a successful pass is shown in Figure 2-8. A closer look at the edge quality shows extra material built up along the edges of the screen pattern, which is a common outcome.

Qualitatively it was difficult to get a film with any conductivity, and the screen clogs up easily even at relatively large thread spacing and easy dimensions of 0.5mm test lines. The process of screen printing is inherently limited at higher resolutions by the thread sizing in the screen, and for this reason it does not seem to be a promising research direction when the feature sizes need to go down to ideally less than 10 μm.

2.2.5 Initial testing with direct μCP of PEDOT

To test the viability of μCP for transferring PEDOT to a substrate, equipment in the MIT EML clean room was used. A circular flat PDMS stamp was fabricated in a standard 3" petri dish for use as stamp. The stamp was plasma treated for 30 seconds in an air plasma at 100W, and spincoated for 30seconds at 2000 rpm with PEDOT. Transfer to a plain glass side was tried in two manners: 1) pressing the slide straight down on top of the PDMS stamp, and 2) transfer in a rolling motion from the PDMS to the slide. The resulting films were cured on a hot plate at 80C for two minutes, and are shown in Figure 2-9.

In test #1, where the transfer method was to press straight down, voids can be seen from air bubbles between the stamp and slide, particularly in the center of stamp. In test #2 with a rolling motion by hand, the film is smudged in the middle on the left side from inaccuracy during rolling. This indicates a need for a better test setup if this manufacturing method is pursued.

The stamp used for the testing is shown in Figure 2-10. Instead of cleanly transferring all the ink, there is a lot of residue left behind, indicating that a stamp cleaning method will need to be developed.

Tests 1 and 2 from Figure 2-9 were measured using a Zygo NewView 5000 white light interferometer, to determine thickness of the transferred PEDOT. See Figure 2-11. It is encouraging that the film thickness is similar between two slides - initial results indicate that these PEDOT ink spincoating parameters give 65nm of PEDOT film.

From these initial tests, it seems at least possible to use soft lithography to transfer an ink such as PEDOT directly, not only monolayers. Given the other advantages of μCP (such as high throughput, low cost, and potential for excellent resolution), this seems like a promising direction to pursue.

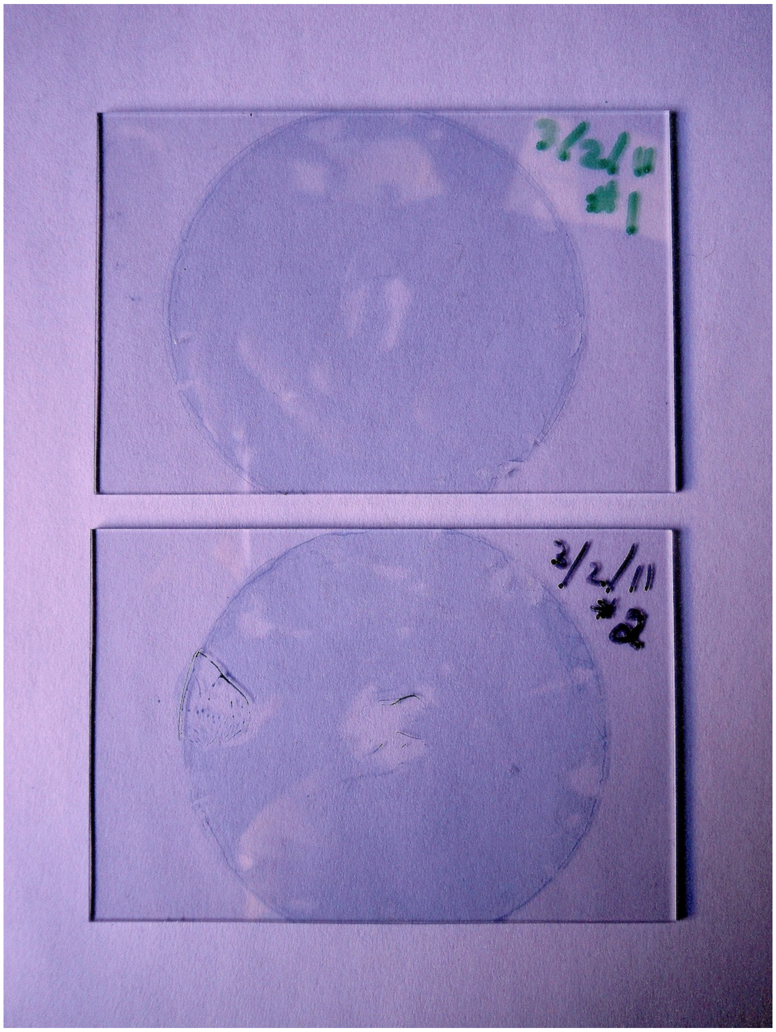

Figure 2-9: μCP of PEDOT onto glass substrates, showing successful transfer but poor film quality (voids and torn areas in the flat pattern)

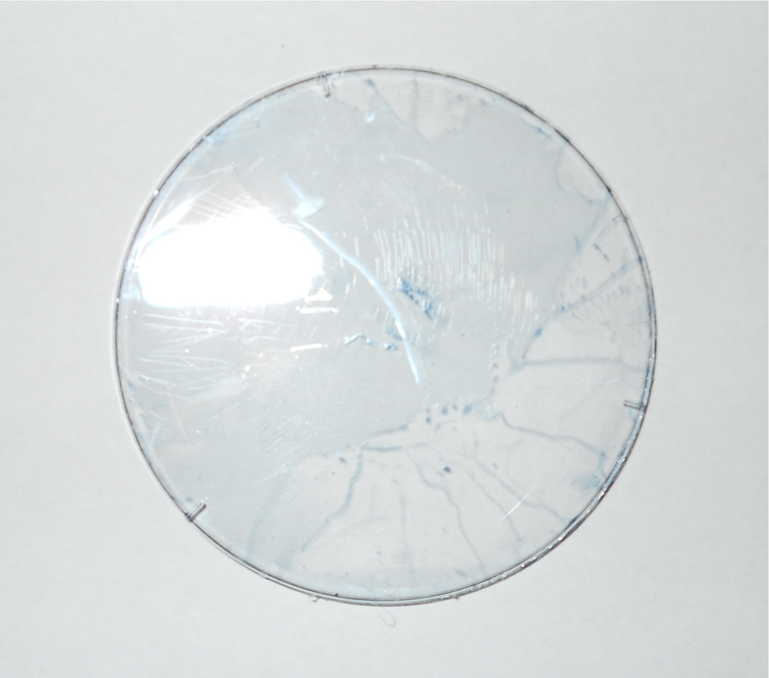

Figure 2-10: PDMS stamp used for μCP of PEDOT, after printing, showing need for cleaning method of the stamp

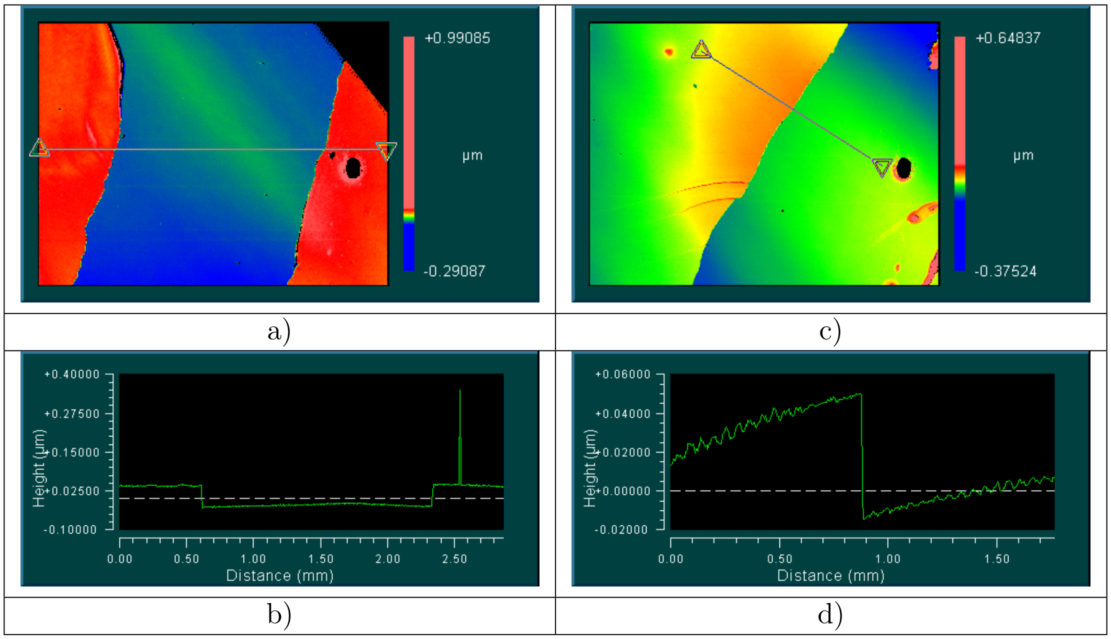

a)

c)

b)

d)

Figure 2-11: Thickness of μCP PEDOT film on glass substrates, measured with Zygo white light interferometer, showing film height of ~65nm. a) Color map of surface height, across a scratch in film. b) Line profile across surface showing a film thickness of 62-70nm. c) Color map of surface height, across a step height in film. d) Line profile across surface showing a film thickness of 65nm.

2.3 Limits of resolution

A literature review of the best resolutions reported for promising manufacturing techniques, with liquid ink, is presented in 2.4, onto polymer where possible. Particular attention was paid to the factors that limited the resolution - in other words, why isn't it better? Inkjet printing, for instance, is limited by the face that it is a serial process - arrays of nozzles can be used to raise the throughput, but arrays of nozzles introduce additional mechanical and alignment complications. Screen printing is being pushed to the very limit (esp. in Japan) down to 20μm, but it is fundamentally limited by the screen. Gravure may be limited by tool manufacture and restricted options for ink/stamp/substrate combinations.

As a note on flexography and microcontact printing - the two processes are certainly related, and indeed overlap for this thesis. Flexography is traditionally a process with a hard rubber stamp used for printing liquid ink for newspapers or graphics, and so there are few cases of flexography below 70 microns (which is the visual optical limit). Microcontact printing is traditionally a soft rubber stamp used to print a monolayer of thiols at very high resolutions. But when a soft rubber stamp is used to print liquid inks at high resolutions, the strict process definitions begin to blur and the literature is mixed in the terminology used.

When examining Table 2.4 with particular attention to the limiting factors preventing better resolution, both offset printing and μCP stand out. A scaling argument for offset printing shows that it is the tradeoff between capillary and viscous forces that governs pattern fidelity [151]. Much smaller length scales might be achieved with better process control of the gap between printing plate and substrate, because ink transfer depends only on the aspect ratio of film thickness to feature size, not the absolute feature size [151]. Therefore, we can make smaller features if we are willing to use thinner ink layers. However, thinner ink layers might degrade performance of electrodes, where the resistance is proportional to cross-sectional area.

Flexography/microcontact printing has the best chance to go down to lower resolutions. These lower resolutions are being driven by the needs of electronics manufacturing (as well as microfluidics). The things that are holding the industry back from reaching lower resolutions are tooling (which is a problem also being addressed separately [152]), machine design and control, and understanding of the process model. That means that opportunity for hitting

Process	Minimum Resolution	Limits	Ref.
Photolithography	100nm	cleanroom equipment required, areas of in^2	[151]
Inkjet Printing Ag ink	5um	slow serial process	[153, 154]
Screen Printing Ag ink	30um	thread sizing	[155]
Capillary coating Ag	12um	slow serial process	[156]
Gravure (Ag [6], PEDOT [3])	30um lines, 25um dots	pattern uniformity and tool manufacture of smaller cell size and spacing (key parameters: cell width, cell aspect ratio, and ink viscosity)	[157, 158]
Lithographic (Offset) of Ag	10's of um, (90um)	ratio of film thickness to feature size (key parameters: ink uniformity on plate, wetting angle, ink viscosity)	[151, 159]
Flexography of Ag	~20um	substrate/ink interaction (surface energy, wicking on paper)	[90, 160, 161, 162, 8]
µCP with liquid Ag ink	2um	machine design, transfer model, process control	[163, 164, 165, 166, 9]

Table 2.4: Minimum resolution demonstrated in literature of selected surface patterning manufacturing processes, and the likely mechanisms hindering improved resolution

the functional requirement of high resolution lies in understanding the process model, and that no inherent physical mechanism is preventing small feature sizes. This is encouraging, and together with the analysis and screening experiments from earlier in the chapter, points to a fruitful area for research.

2.4 Why μCP?

Direct microcontact printing is the most promising choice of manufacturing method for microfluidic devices with conductive features, as well as extended applications in other fields. It is a technique which has been applied in the field of organic LEDs, thin-film electronics, and micro-optical parts, and which is suitable for reel-to-reel production schemes [1]. It meets the stated functional requirements, initial screening experiments were encouraging, and the process has opportunity for improved performance through process control. Microcontact printing is a method where the patterns are directly transferred, which eliminates any additional solvent processing steps that may damage substrate or add expense. Some of the reasons it has not yet been explored in the intended manner - with a liquid conductive ink as the transfer material, onto a polymer, at high resolutions - include the fact that commonly the printed material is a thiol (because of its particular interaction with gold), the feature sizes are commonly larger than needed (because of the stamp deformation limits [104]), polymers have more difficult surface characteristics than glass or silicon, and the process sensitivities are not well understood. These are challenges that can be addressed during this PhD work. The microcontact printing process does have the potential to meet all functional requirements, and the technical difficulties may be solved through process control and machine design.

Chapter 3

Theoretical Understanding of the μCP Liquid Ink Transfer Process

We would like to identify the governing equations in the μCP process, at least as already available in the literature. In general, the μCP process consists of inking the stamp (also called the mold), transferring the ink from the stamp to the substrate, and then any post-treatment of the ink (annealing or drying). Although for experimentation we are using a stamp mounted to a printing roller, like an industrial roll-to-roll process would use, the experimental setup does not include an inking roll. Therefore for laboratory experiments, inking of the stamp is done by spincoating ink onto an inkpad (a glass slide, for convenience), and then rolling the stamp over the inkpad to pick up a uniform coating of ink. So for this work, the steps in the μCP process are:

1. Coating of the inkpad with ink
2. Transfer from the inkpad to the stamp
3. Transfer from the stamp to substrate
4. Post-treatment, if any, of the final printed pattern

An important note is that the surface properties of the stamp and substrate, and the surface energy of the ink, are critical parameters for each of these steps. Also, the ink is assumed to be a liquid, not a solid film (in the case of a solid, the transfer process would include concepts from fracture mechanics).

As stated in Chapter 2 when discussing limits of resolution, the strict definition of μCP begins to merge into flexography when μCP is done with a direct ink, in a roll-to-roll fashion. Because we are now borrowing concepts from the printing industry, Chapter 3 first goes over basic terminology and processes in the established printing industry.

Then, this chapter will discuss the importance of surface energy, and the use of plasma treatment to modify surface properties. Finally, governing equations for each of the four steps above will be presented. These governing equations are important because they guide the direction of research by suggesting which variables in the process are most sensitive.

3.1 Overview of printing technology and terminology

Surface patterning, or lithography, has been an active area of development since the advent of the printing press in the 1400's. During the industrial revolution of the 1800's, roll-to-roll printing presses replaced plate presses [167], resulting in unprecedented rates of production for patterned materials. Modern roll-to-roll printing presses are capable of printing flexible substrates at rates of meters per second with sub-millimeter resolution and registration between multiple colors. As in the beginning, printing at these rates is still accomplished using mechanical contact with the printing substrate, but has evolved into modern technologies like gravure, offset, and flexographic printing.

Each of these three processes - gravure, offset, and flexography - uses an impression, or backup, roller to engage a flexible substrate against a printing roller. Gravure printing uses a rigid cylinder with small engraved pockets to selectively transfer ink (housed in each pocket) to the substrate. Offset printing patterns ink on a metal roller, transfers the ink to a rubber roller, and finally to the printing substrate. Finally, flexography uses a patterned print roller with positive relief to transfer ink between an inking roll and the substrate.

Since the 1990's, flexography has overtaken the gravure and offset printing processes as the process of choice when it comes to throughput and quality of printing [167]. The term flexography was coined in the 1950's, but the process didn't reach its current state until 1972 when more advanced polymer printing plates were developed to replace molded rubber stamps.

3.2 Plasma treatment: Effect on contact angle/surface energy

Plasma treatment is a very common and very effective method of changing the surface properties of substrates, in particular of polymers. There are several types of plasma that can be used to treat surfaces, such as microwave, radio frequency, and corona discharge. But low-temperature air plasma (non-equilibrium plasma) is most frequently used with polymer films.

The interaction with plasma is thought to change the physical and chemical properties of the surfaces of polymers through several mechanisms: oxidation, degradation, cross-linking, and structural changes. For low-temperature air plasma, the mechanism with the greatest effect is the oxidation. Because the electrons in the plasma have high energy, they can break covalent bonds and trigger the creation of C=O, OH, and COOH groups during the oxidation process. The main effect of this treatment is to raise the surface energy of the polymer, and depending on the gases used, to change the surface polarity. This is desirable because a higher surface energy of the substrate improves the wettability of the ink (a liquid will bead up on a substrate if the surface energy is not high enough). Other properties that plasma treatment may change include adhesion, durability, scratch resistance, hardness, permeability, and biocompatibility.

Because the main effect of plasma treatment is to change the surface energy, the easiest way to quantify what happens after treatment is to measure the contact angle θ. (Free energy, γ_s, cannot be measured directly and is calculated from the contact angle using Young's equation [168].) Contact angle is measured by looking at the tangent angle of a droplet three-phase interface (solid-liquid-vapor).

The efficiency of the plasma treatment process depends on the types and pressures of gas used, temperature, type of polymer, and power and time of plasma action. See Table 3.1 for a comparison of the effect different exposure times will have on the contact angle of various liquids on PMMA. See Figure 3-1 for a comparison of the effect of different types of plasma on two different substrates, PMMA and COC, for different exposure times. Finally see Figure 3-2 for a comparison of the effect of plasma treatment for a variety of polymer substrates.

The other relevant factor to consider when using plasma treatment, is how long will the effect of the treatment last? Table 3.2 indicates that the effect of plasma treatment on

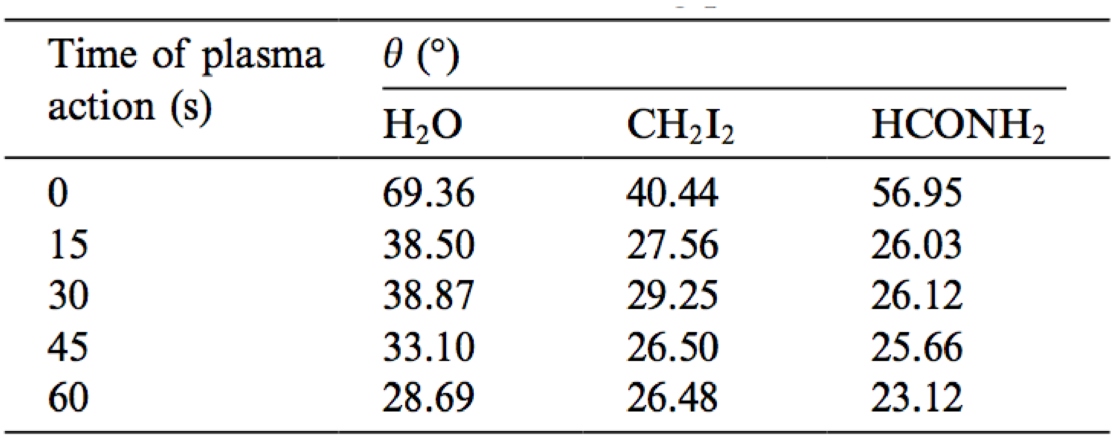

Time of plasma action (s)	θ (°)		
	H_2O	CH_2I_2	$HCONH_2$
0	69.36	40.44	56.95
15	38.50	27.56	26.03
30	38.87	29.25	26.12
45	33.10	26.50	25.66
60	28.69	26.48	23.12

Table 3.1: Contact angle (θ) of water, diiodomethane and formamide on PMMA film surface before and after plasma action, showing the effect of different plasma treatment exposure times on the surface energy of PMMA. [5]

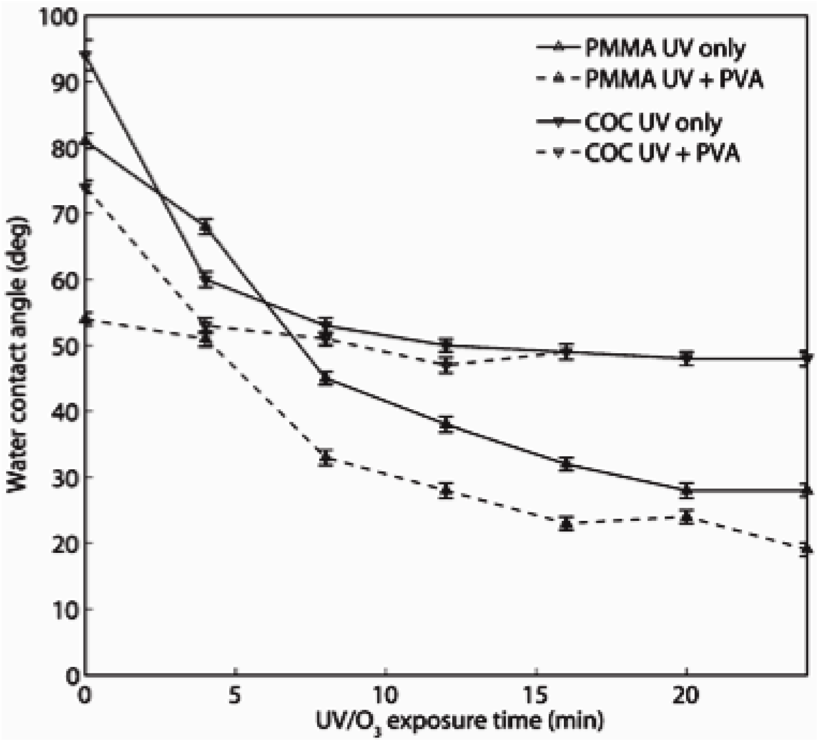

Figure 3-1: Water contact angle for PMMA and COC substrates after UV/O_3 treatment, and UV/O_3 treatment followed by PVA coating, showing the effect of different plasma treatments on the surface energy of PMMA and COC. [4]

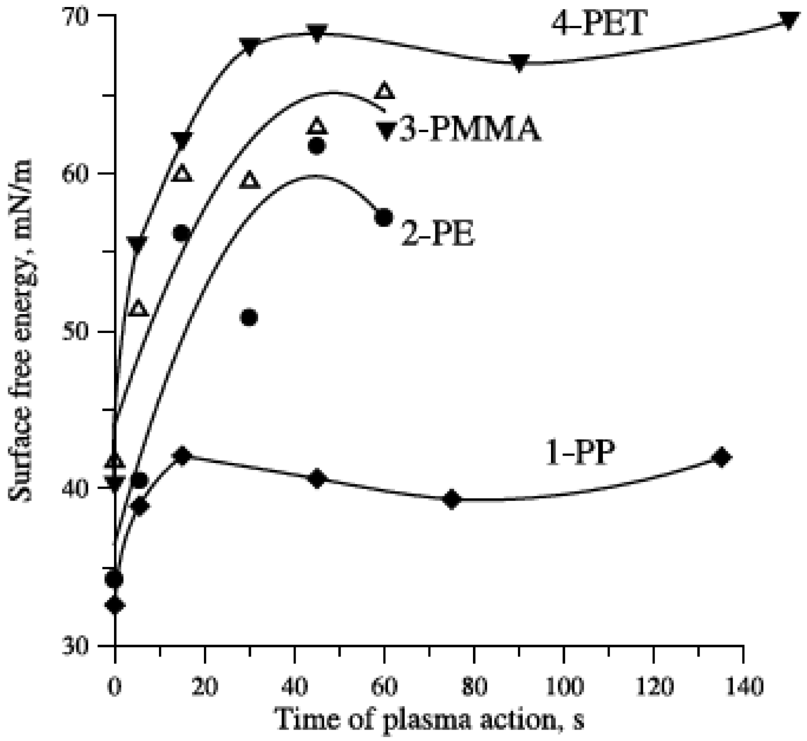

Figure 3-2: Comparison of surface energy changes in polymers of different chemical structure during air plasma action, showing the effect of plasma treatment on the surface energy of various polymer substrates. [5]

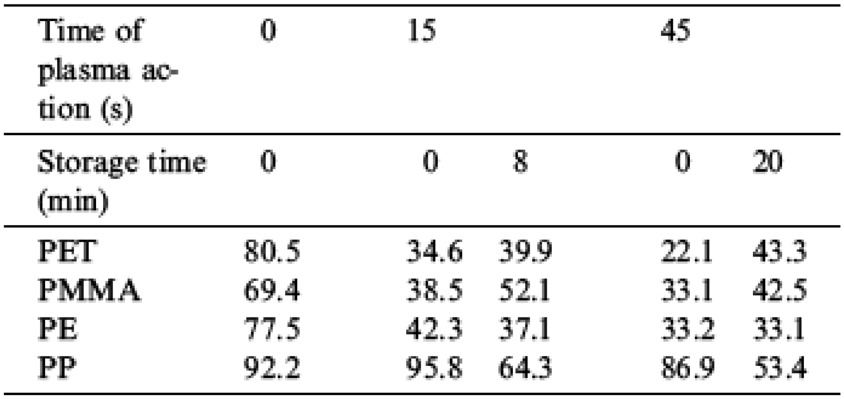

Time of plasma action (s)	0	15		45	
Storage time (min)	0	0	8	0	20
PET	80.5	34.6	39.9	22.1	43.3
PMMA	69.4	38.5	52.1	33.1	42.5
PE	77.5	42.3	37.1	33.2	33.1
PP	92.2	95.8	64.3	86.9	53.4

Table 3.2: Changes over time to contact angle of water on PMMA and other polymers with plasma treatment [5]

different polymer substrates degrades over time in storage. This would suggest that printing should be done as quickly after treatment as possible for the best results. However Tsao et. al. reports a more complicated story - PMMA and COC exposed for 4min and 24min to plasma were stored for 15 days, with no detectable change in contact angle after storage. Yet in the same paper, similar aging experiments for PDMS (the stamp/mold material) showed a degradation of 50% in ten hours of storage. [4] Without definitive conclusions from literature, and considering the hands-on experience of the author that the effect does degrade, for this work the experimental protocol will specify plasma treatment directly before printing.

All the discussion has so far been about the contact angle of water or other test liquids on substrates after plasma treatment, which is indicative of a change in surface energy of the treated substrate. Although it may be obvious, the extension of this logic is that the increased surface energy also affects the behavior of the ink on the substrate. A liquid with a given surface energy (normally called surface tension for a liquid) will "wet" onto any surface with a higher surface energy. Therefore raising the surface energy of the substrate improves the wettability of the ink.

3.3 Step 1: Coating inkpad with ink

3.3.1 Types of inks

The two main types of inks considered in this work are polymeric conductive inks, and particulate conductive inks.

Polymeric conductors [123] are liquid phase processable solutions or dispersions, capable of printing techniques, and can be used as transparent electrodes in display and solar applications or as polymeric transistors. Common polymer conductors include polyaniline, polytiophenes (including PEDOT), and polypyrrole. Solvent choice and polymer concentration are key issues in ink formulation [145]. Intrinsically conductive polymers are poorly soluble in most solvents, leading to low solid content of ink. Additives can be mixed in to mitigate this, but in general the low solid content will also lead to a low amount of conducting materials transferred during printing. This can create a high sheet resistance, and so these inks may not be ideal when high current is required. [123] Adding a small amount of glycerol may improve conductivity [145].

Particulate conductors [123] are usually silver, gold, or carbon particles with an organic binder, dispersed in a suitable solvent. The major advantage of particulate conductors over polymeric is higher conductivity. The disadvantage is that they are usually unsuitable for inkjet printing due to high viscosity, large particle size, and sedimentation. Fortunately this issue is not a concern when using μCP rather than inkjet printing. Cost can also be a disadvantage, depending on the material chosen.

3.3.2 Spincoating

In an industrial roll-to-roll printing process, coating the printing roll with ink is a well-understood problem with a variety of inking solutions available. For applications that are not roll-to-roll, the spin coating process has been used extensively as a popular conformal method of coating a substrate - either directly on the stamp, or onto an inkpad with a secondary transfer step to the stamp [150, 9, 91, 140]. An alternate method is bar coating, using a wire wound bar to spread ink over a substrate, with the thickness of the wire controlling film thickness[169]. But for this work, spin coating is the method chosen for creating a thin, uniform coating of ink.

The spin coating process can be best understood by considering the rheology, or flow behavior, of fluids on a rotating disk substrate. Initially the volumetric flow of liquid in the radial direction is assumed to vary with time, then a steady state flow regime develops quickly. At steady state, the fluid element experiences two balancing forces: the outward centrifugal force of rotation, and the viscous shear force during flow. During steady state, volumetric flow is constant and very low, so that average film thickness changes slowly. Thus the volumetric flow Q can be characterized as a plateau region during steady state, $\frac{dQ}{dt} = 0$, which is a simplifying assumption allowing a time-independent solution for thickness. [170]

Assuming time invariance, the film thickness resulting from spin coating is given as:

$$\delta = KC_v \left(\frac{\nu}{\omega^2 R^2}\right)^{1/3} \tag{3.1}$$

where δ is the film thickness, ν is the kinematic viscosity, C_v is the volume fraction of solids, ω is the angular velocity, R is the disk radius or average symmetric dimension of the sample, and K is a constant, $\left(\frac{81Q}{16\pi}\right)^{1/3}$. [170] Note that this also assumes fluid density stays constant, and there is no shear thinning. For spin coating where the fluid is non-Newtonian, or where solvent evaporation represents a substantial effect, more complicated rheological models should be used [171].

3.3.3 Governing equation: wetting

The governing equation for the ink wetting onto the inkpad (Figure 3-3) is straightforward. Based on the interplay between dispersion forces and surface tension forces, a liquid ink film can either wet or de-wet a solid surface. This behavior can be described with the equilibrium spreading coefficient, S_{eq}. [8]

$$S_{eq} = \gamma_{SV} - \gamma_{SL} - \gamma_{LV} \tag{3.2}$$

In Equation 3.2, γ_{SV} is the surface tension of the solid substrate, $\gamma_{SL}$is the solid/liquid interface tension of a droplet on the surface, and $\gamma_{LV}$is the liquid/air interface tension between the droplet and the atmosphere. This can also be written as Equation 3.3, showing a balance between the surface tension of the ink and the surface energy of the solid substrate:

$$S_{eq} = \gamma_{SV} - (\gamma_{SL} + \gamma_{LV}) \tag{3.3}$$

Figure 3-3: Schematic of Step 1 - Coating ink onto inkpad

$$S_{eq} \geq 0 \, for \, wetting \tag{3.4}$$

$S_{eq}$is positive or zero for complete wetting, while $S_{eq}$is negative for partial wetting (the ink will bead up on the substrate), as shown in Equation 3.4. [8] The thickness of the wetted ink on the inkpad is then governed by the speed and time of spincoating, and can be varied as desired.

3.4 Step 2: Transfer from inkpad to stamp

Next we would like to consider the mechanism for the stamp (mold) to pick up the ink from the inkpad, which is called dewetting. In gravure printing the ink is confined in the mold cavities, so dewetting occurs through selective mass transport to the edges of the mold (edge dewetting). For μCP, dewetting is much harder to control, because in the absence of mold confinement, ink tends to form randomly distributed droplets instead [8]. To have μCP dewetting with distinct edges, first the film must be stable, and then depending on the process parameters either edge or center dewetting may occur.

3.4.1 Step 2 Part 1: Is the film stable?

In some cases, it is desirable to have an unstable film which breaks apart into droplets, because it is possible to make nanostructures with that method that are difficult to fabricate with photolithography [12]. In our case, we would like to make sure the film stays stable and does not break apart into droplets. Film breakup is suppressed when the pattern spacing is above a certain characteristic length compared to the film thickness. (To illustrate, imagine a 1mm thick layer of ink trying to adhere stably to a 100μm protruding feature. The aspect ratio is too high - the ink would obviously from a droplet and fall off.) The characteristic length q_c for stable film is a balance of surface energy and intermolecular forces, given in Equation 3.5 [12].

$$q_c = \left(\frac{A_{eff}}{2\pi\gamma h_r^4} \right)^{1/2} \tag{3.5}$$

where $A_{eff}$is the Hamaker constant for the van der Waals interaction of the film with the surrounding media, γ is the surface tension of the ink film, and h_r is the residual thickness of the ink film on the mold. The thickness of the ink film h_r was found in Suh et. al. to be a function of the pattern size [12]. The important thing to note here is not the exact calculation of q_c, but that film stability is a function of the thickness of the inkpad film, the surface tension of the ink, and the pattern size.

3.4.2 Step 2 Part 2: Will the film dewet at the edges or at the center?

Edge dewetting is defined as the ink film breaking apart at the edges of protruding mold features, while center dewetting occurs when the ink film is squeezed out from underneath the protruding mold features, and collects in the mold cavity regions (Figure 3-4). Again, in some cases it is desirable to have center dewetting, such as when trying to create nanoparticle superlattices [6]. However in our case, we would like to ensure edge dewetting.

To model the impression process, consider Poiseuille's law in Equation 3.6, which governs the flow between parallel plates under pressure:

$$q = \frac{\Delta P h^4}{12\mu L} \tag{3.6}$$

where ΔP is the pressure gradient between the mold and the edge of the mold, q is the flow out from under the mold, h is the gap height between the mold and the substrate, μ is the dynamic viscosity of the ink, and L is is distance between the mold and the edge of the mold (see Figure 3-4 a). ΔP and h are inversely related - the higher the pressure during printing, the smaller the gap height, and the more flow q out from under the mold. The important thing to note is that edge dewetting is desirable, and getting edge dewetting as opposed to center dewetting is controlled by mainly by lowering printing pressure and by pattern spacing (which is harder to control, being specified by design of the electrode pattern to print). Lower printing pressure is also better in order to prevent stamp collapse, so the desirable trends align.

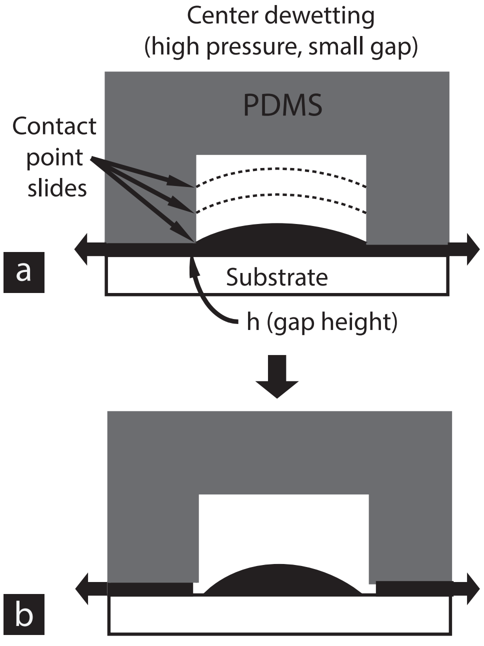
Center dewetting
(high pressure, small gap)
Edge dewetting
(low pressure, large gap)
PDMS
PDMS
Contact point slides
Contact point pinned
a
Substrate
h (gap height)
c
Substrate
h (gap height)
b
d

Figure 3-4: Diagram of stamp features showing center dewetting (a-b) and edge dewetting (c-d). Under high pressure the contact point between the liquid and the edge of the stamp feature slips down the side of the feature and a) eventually breaks near the edge, creating b) a droplet in the stamp cavity. Under low pressure the contact point between the liquid and the stamp feature edge remains pinned to the side of the feature d), and eventually e) breaks in the middle of the stamp cavity as desired. [6]

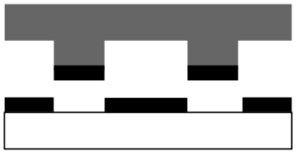

Figure 3-5: Schematic of Step 2 Parts 1 and 2 - Film stability and ideal edge dewetting, showing the ink split from the inkpad along the feature edges, and forming a continuous coating on the stamp features

3.5 Step 3: Transfer from stamp to substrate

Now that the stamp has been coated with ink, the last step is to transfer the ink from the stamp to the substrate. The mechanism for this transfer is work of adhesion. Assuming the interfluid forces are enough to keep the fluid together as a film, if the substrate is “stickier” than the stamp (called the mold, for clarity of subscripts), then the ink will transfer to the substrate. If the fluid does not stay together as a film, then some percentage of the fluid will transfer from the mold to the substrate (this is discussed more in Chapter 6).

For now we are interested in whether or not transfer will happen at all. Thermodynamic work is traditionally used to characterize the work of adhesion (W_a), as it represents a function of the surface characteristics of both the interacting surfaces [172]. The interfacial energies of any two samples can be estimated using Equation 3.7:

$$\gamma_{12} = \gamma_1 + \gamma_2 - \frac{4\gamma_1^d \gamma_2^d}{\gamma_1^d + \gamma_2^d} - \frac{4\gamma_1^p \gamma_2^p}{\gamma_1^p + \gamma_2^p} \tag{3.7}$$

where superscript d and p represent the dispersion and polar components of surface energy for surfaces 1 and 2 [172]. The surface energies of each surface (γ_1 and γ_2) can be found by combining Young’s equation for calculating surface energy from contact angle, and Owens and Wendt’s equation for the interfacial energy between a liquid and solid assuming a geometric mean combination of the dispersion and polar components [172].

Then the work of adhesion is given by Equation 3.8:

$$W_{1,2} = \gamma_1 + \gamma_2 - \gamma_{12} \tag{3.8}$$

This can also be written as:

$$W_{1,2} = \frac{4\gamma_1^d \gamma_2^d}{\gamma_1^d + \gamma_2^d} - \frac{4\gamma_1^p \gamma_2^p}{\gamma_1^p + \gamma_2^p} \tag{3.9}$$

This equation for work of adhesion is the governing equation for ink transfer in gravure printing, as well as flexography [173]. When the adhesion force at the substrate-film interface is larger than the mold-film interface, the film releases from the mold (for additive adhesion or stamping, which is the more common technique). [172] See Figure 3-6.

$$\frac{W_{sf}}{W_{mf}} > 1 \, for \, additive \, adhesion \, transfer \tag{3.10}$$

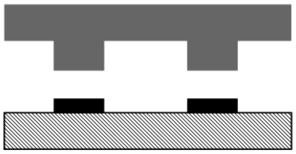

Figure 3-6: Schematic of Step 3 - Transfer from stamp to substrate, assuming complete transfer of a continuous film

There have been some methods suggested in literature to increase adhesion, for example adding an adhesive agent into the ink dispersion, or vapor coating and adhesive onto substrate prior to printing [150]. As discussed in Section 3.2, plasma treatment of the substrate surface increases surface energy which also increases adhesion.

3.6 Step 4: Post-treatment (drying/solidifying)

Most inks require post-printing annealing, usually a simple baking step at an elevated temperature. For printing on polymers (and especially microfluidics with channels formed in the polymer), we must be particularly careful that the annealing process not require a temperature approaching t_g, the glass transition temperature of the polymer.

The baking process serves several purposes [150]:

- Evaporation of the solvent component in the ink, in the case of an ink with conductive particles in a carrier (i.e. silver nanoparticle ink, not PEDOT)
- Thermally cures and anneals the film, stabilizing pattern features
- In the case where the stamp is annealed in contact with the substrate, accelerates reversion of plasma treated PDMS stamp from hydrophilic back to hydrophobic (so that ink will detach from stamp)
- In the case of an additional adhesion-promoting layer, facilitates chemical bonding between the intermediate glue layer and the substrate/ink

For polymeric inks, such as PEDOT, the annealing process is required to promote cross-linking and create conductivity. For particulate inks, annealing is required for solvent evaporation most importantly, but depending on the binder agent, also for sintering to improve conductivity. Depending on the solids loading to solvent ratio, during solute evaporation the volume change may be large. During large volume changes, the change in distribution

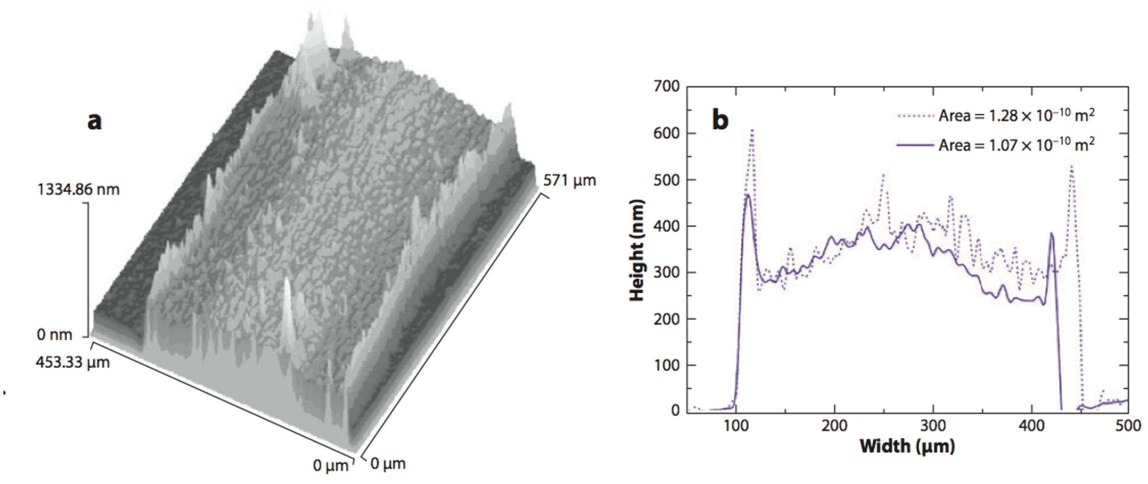

Figure 12

Figure 3-7: Observations of coffee staining from printed nanoparticle silver ink. a) Interferometric image of a track formed from the drying of a liquid bead showing distinct ridges at the edges formed by fluid flow during drying. b) Two line profiles across the track showing variation in height across the track. [7]

of particles can affect the shape of the printed pattern. A "coffee stain" effect is observed when the center of the pattern evaporates first, forcing particles to the outside edges of the features. The evaporation flux of solvent $J(r)$ proportional to radial distance r from the center of a droplet of contact radius R is given by:

$$J(r) \propto (R - r)^{-\lambda} \tag{3.11}$$

with:

$$\lambda = (\pi - 2\theta_{rec})/(2\pi - 2\theta_{rec}) \tag{3.12}$$

where θ_{rec} is the receding contact angle. [7] An example of the coffee stain effect can be seen in Figure 3-7.

Unfortunately to maintain viscosity for printing, dilute solutions of long-chain polymers or low volumes of particles in solution are desired, leading to a tradeoff with coffee stain behavior. The literature does suggest some ways to mitigate coffee staining, mainly by modifying the driving force for fluid flow during drying:

- Enhanced vapor pressure in printing environment (less rapid transport at contact line).

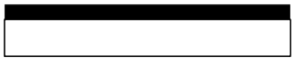	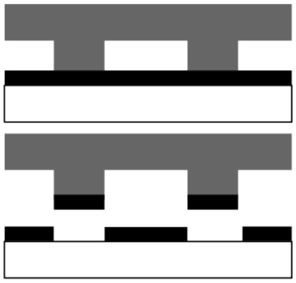	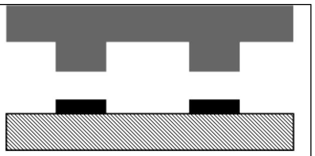
Step 1	**Step 2**	**Step 3**
$S_{eq} = \gamma_{SV} - (\gamma_{SL} + \gamma_{LV})$ $S_{eq} \geq 0\, for\, wetting$	$q_c = \left(\frac{A_{eff}}{2\pi\gamma h_r^4}\right)^{1/2}$ $q = \frac{\Delta P h^4}{12\mu L}$	$\frac{W_{sf}}{W_{mf}} > 1$ $for\, additive\, transfer$

Figure 3-8: Summary of governing equations for μCP process

This may be difficult to engineer in practice.

- Printing onto a cooled substrate. (Heat transfer through drop is faster at edge of drop, where drop is thinner, generating radial temp profile with enhanced evaporation at drop center) .

- Using a more complex solvent composition that contains fluids at different vapor pressures.

- Impeding fluid flow within the drop. (Wax droplets filled with ceramic powders, thermoreversible gel).

3.7 Governing equations summary

The reason for identifying governing equations for each step of the μCP process is to understand what factors are at work and make smart guesses as to which variables are most sensitive. Then, we can direct research effort into investigating those variables experimentally. There are many parameters which can be varied (intentionally or not) during the μCP process, including things such as printing speed, force, mechanical design of the printing equipment, substrate material, surface roughness, surface chemistry, temperature, and ink properties.

To narrow down the scope of that list, from the table of governing equations in Figure 3-8, which variables can we expect to have strong effects on the process? Step 1 and Step 3 are functions of surface energies, Step 2-1 is a function of thickness of the inkpad film, the surface tension of the ink, and the pattern size, and Step 2-2 depends on printing pressure and inkpad thickness again. (These variables are also proposed as strongly important in Kololuoma et. al. [123].) Therefore these are the variables that we can expect the process to be sensitive to, from a process modeling point of view. This understanding will drive the choice of variables and design of experiments in Chapter 6.

Chapter 4

Exploration of Microcontact Printing of PEDOT

The goal of this project is to develop a method for manufacturing conductive traces on polymer substrates. The method chosen (see Chapter 2 for discussion of manufacturing processes) is direct μCP with liquid ink (as opposed to μCP of a monolayer for etching or further deposition). Two classes of conducting inks available are conductive polymer inks, and particulate inks. Polymer conductive inks have several functional advantages over particulate inks, such as better adhesion, flexibility, and optical transparency. Polymers (an organic material) also have several manufacturing advantages over metal-based inks, such as the possibility of lower material cost compared to gold, processing under atmospheric conditions, and evaporation at relatively low temperatures. It is of great interest to find ways to directly pattern these organic polymeric materials.

Poly(3,4-ethylenedioxythiophene), shortened to PEDOT, is a conductive polymer that has received research attention as an alternative to ITO in organic electronics, particularly because of its stability, optical transparency, and good electrical properties [174]. The concept of μCP using PEDOT has been demonstrated to be feasible [9, 150], but has yet to be expanded into a manufacturing setting.

This chapter presents experimental attempts to replicate existing literature, and exploration of process parameters to achieve successful printing of PEDOT. Ultimately although some good results were obtained, the process was found to be extremely problematic and good experimental results difficult to replicate. This difficulty led to an investigation of

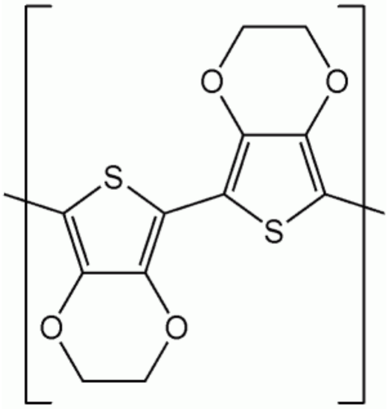

Figure 4-1: Chemical PEDOT structure

the surface energy of the stamp and substrate materials, and the surface tension of the ink used. Using the theory of work of adhesion, given the existing surface energies, both lift-off (adhesion) transfer and additive (stamping) transfer regimes were shown to be unfavorable.

Thus, theory corroborated experimental results and showed μCP of PEDOT to be a non-robust process, likely unsuitable as a high volume manufacturing process without further refinement or different substrate and ink choices, and so this direction of research was discontinued.

4.1 What is PEDOT?

PEDOT is a conjugated polymer, based on polythiophene, used as a transparent conductive polymer in industrial applications. For example, Agfa-Gevaert N.V. in Belgium uses PEDOT:PSS as an antistatic coating on photographic film [175]. The chemical structure of PEDOT is shown in Figure 4-1. Although PEDOT has good optical transparency, stability, and electrical properties, one disadvantage is the poor solubility. This disadvantage makes PEDOT traditionally hard to process in thin film form, but the addition of poly(styrenesulfonate), or PSS, addresses this problem by making the solution soluble in water. The chemical structure of PEDOT:PSS is shown in Figure 4-1.

The addition of high boiling solvents such as methylpyrrolidone, dimethyl sulfoxide (DMSO), sorbitol, or glycol can greatly improve the conductivity of the PEDOT. Conductivity of 1000S/cm or higher puts PEDOT in the range to replace ITO as an electrode material, and as the conductivity continues to improve it becomes competitive with gold electrodes. Recently, PEDOT:PSS treated with sulfuric acid was shown to achieve a conductivity of 3000S/cm [176].

Commercially available PEDOT:PSS products are sold by Heraeus under the trade name Clevios and by AGFA under the trade name Orgacon. The material used in these experiments is Clevios PH1000, with material properties shown in Appendix B.

4.2 Why investigate PEDOT?

Using PEDOT in microelectronics represents a significant manufacturing step forward from the traditional transparent conductive film, indium tin oxide (ITO), in terms of reducing material cost and for use with flexible substrates [169]. There are also functional advantages of PEDOT, such as good electrical performance and adhesion. The advantages of PEDOT (and thus the rationale for further investigation) are given below.

Electrical Performance PEDOT has good conductivity (1000 S/cm in commercially available product, 3000 S/cm demonstrated in literature [176]), and is beginning to be considered as a replacement for gold as well as ITO. In fact there is some evidence that PEDOT may have electrical characteristics superior to gold because of a lower carrier injection barrier [150].

Processing Temperatures and Pressures Organic materials in general can be processed at lower temperatures and pressures than metals, which is important when printing on polymer substrates that can't handle the environment of traditional semiconductor processes. Adding glycerol to PEDOT, (which acts as a plasticize to increase chain mobility of polymers), helps further lower the necessary processing temperatures and pressures [150].

Adhesion PEDOT may have better adhesion than gold to polymer substrates, and the thermal coefficient of expansion of PEDOT is similar to the polymer substrate, which improves cracking at the bond under elevated temperatures [150]. Here again the addition of glycerol helps adhesion by preventing the spincoated PEDOT from drying out.

Material Cost Using a polymer reduces material cost, particularly when compared to gold.

Flexibility Because of the flexibility of PEDOT and good adhesion to polymer substrates, it can be processed with roll-to-roll technology on flexible substrates [177, 174].

Optical Properties PEDOT has excellent visible light transmission, similar to ITO [150].

Stability PEDOT has good environmental and thermal stability [174].

Perhaps the strongest evidence for pursuing μCP of PEDOT is that it is a subject of ongoing current research. Section 4.3 goes over prior work in the literature with PEDOT, and the promising results obtained thus far.

4.3 Prior PEDOT and printing work in literature

4.3.1 Prior work in μCP of PEDOT

The two best examples in literature of μCP of PEDOT are reported by Li et. al. in 2006, and Takakuwa et. al. in 2010.

Li et. al report fabricating organic field-effect transistors (OTFTs) with PEDOT electrodes by "polymer inking and stamping" [150]. First PEDOT with a glycerol additive is applied by spincoating at 3000rpm for 30s onto a PDMS stamp that has been O2 plasma treated at 80W for 6-10s. The coated stamp is placed on an Si/SiO2 or flexible polymer substrate, and baked at 80°C for 2min. When the stamp is removed, the PEDOT features are left on the substrate. [150]

Takakuwa et. al. has been working in this area for several years [9, 178], and have shown that OTFTs and OLEDs can be created with conductive polymers. The process involves spincoating PEDOT:PSS aqueous solution to a thickness of 100-200nm onto a PDMS stamp treated with UV light [9]. (Note that this thickness is consistent with other work - Velten and Schuck report a 150nm spincoated layer of PEDOT, used for OLEDs [140].) In the 2007 Takakuwa paper, the substrate was Si/SiO2 coated with P3HT [178], while in 2010 an SiO2 substrate was used [9]. In either case, the coated PDMS stamp was placed on the substrate, removed, and then the substrate was annealed at 150°C after printing.

The substrate plays an important role in the process, and it is important to recognize the challenges when trying to extend work demonstrated on silicon to other materials. Not only do the printing mechanics change because of different mechanical properties, but the electrical characteristics of PEDOT can vary as well. Ceschin et. al [145] found that the sheet resistance of PEDOT changes depending on whether you deposit on polyethylene terephthalate or polyester.

Note that both of these examples report the actual transfer process as just placing the stamp on the substrate, and removing. There is no discussion of any equipment used, and although extension to flexible substrates is mentioned, neither example uses roll-to-roll techniques. This seems to be an opportunity for further contributions in machine design and testing in higher volume manufacturing.

4.3.2 Prior work in lift off of PEDOT

The concept of μCP is usually assumed to be additive - that is, the stamping process transfers material from the protruding regions of the stamp to the substrate. But the same stamp can also be used in the opposite manner, with a subtractive process called lift-off or adhesive lithography, where a film is peeled off of a coated substrate. Adhesive lithography, by definition using adhesion as the pattern-driving force, has been used for direct patterning of metals, organic and polymer semiconductors [172].

Granlund et. al. uses both additive μCP and liftoff to pattern anode lines of PEDOT:PSS, with the smallest feature being 100 μm, on substrates of glass coated with ITO or Au. Their method did not produce patterns with enough conductivity to power a diode array, however. [179] Yim et. al. similarly used liftoff from a surfactant-coated polyethersulfone (PES) substrate to fabricate OLEDs, and by using DMSO-doped PEDOT:PSS were able to achieve good conductivity [180]. Piliego et. al. [181] suggests that lift-off is a better method than additive stamping because it can leave a thicker and more uniform layer, which is preferable for lower resistance. They demonstrate down to 3μm lines fabricated with liftoff, using PEDOT with DMSO as an additive rather than glycerol, which keeps good conductivity but gives a mechanically stronger film to allow those smaller features. [181]

4.3.3 Prior work in other methods of printing PEDOT

Screen printing has been used to make gate electrodes of PEDOT:PSS, but the minimum resolution is 100 μm and the accuracy is about 50μm [140]. Oxidative chemical vapor deposition of electrically conducting PEDOT films has been demonstrated, which avoids using the water-soluble PEDOT:PSS form (PSS forms a shell around beads of PEDOT, decreasing the electrical performance) [174]. This oCVD method can also be used on flexible substrates for flexible electronic applications [177].

4.3.4 Prior work in μCP of other polymers

Bao et. al [91]uses a technique called polymer inking, which is μCP of polymer inks (PMMA and PC). A 4.5% PMMA solution in toluene is spincoated to a thickness of 100-120 nm, transferred from an Si wafer substrate at elevated temperature and pressure, then baked at 130°C for 5 min [91]. Patterns inked from PC showed large dimension shrinkage (~75%) compared to PMMA (~30%) [91]. Although these inks are not conductive, it is useful to know that other organic polymer materials have been successfully transferred with μCP.

4.4 Initial PEDOT experiments with microcontact printing

4.4.1 Effect of plasma treatment on PDMS stamp

The first experimental observation was that the PEDOT material (Clevios PH1000) would not coat a flat PDMS stamp without plasma treatment. See Figure 4-2 for two flat PDMS stamps coated with PEDOT on a spincoater at 2000rpm for 30 seconds. Example a) has no treatment, example b) was treated with air plasma for 0.3min at 100W. The PEDOT has a slight blue color, and can be seen beading up in a) and making a uniform coating in b). This is an expected result - from Section 3.2, we know that plasma treatment raises the surface energy of PDMS, allowing for better wetting.

This also tells us that the PEDOT material has a surface tension above the surface energy of untreated PDMS, and below plasma treated PDMS (see Section 3.3.3 for the governing equation of wetting, which is dependent on surface energies). The difference in contact angle can be seen intuitively in Figure 4-3, where on flat plasma treated PDMS the same volume of PEDOT ink spreads to a larger area.

Even with the knowledge that plasma treatment is necessary, it was difficult to get repeatable good coating. See Appendix D.1 for examples and investigation of difficulties with coating.

4.4.2 Thickness of PEDOT ink on glass slide

Once the procedure for getting a uniform coating on a flat PDMS stamp was established, the next step was to measure the film thickness. The governing equation for thickness during

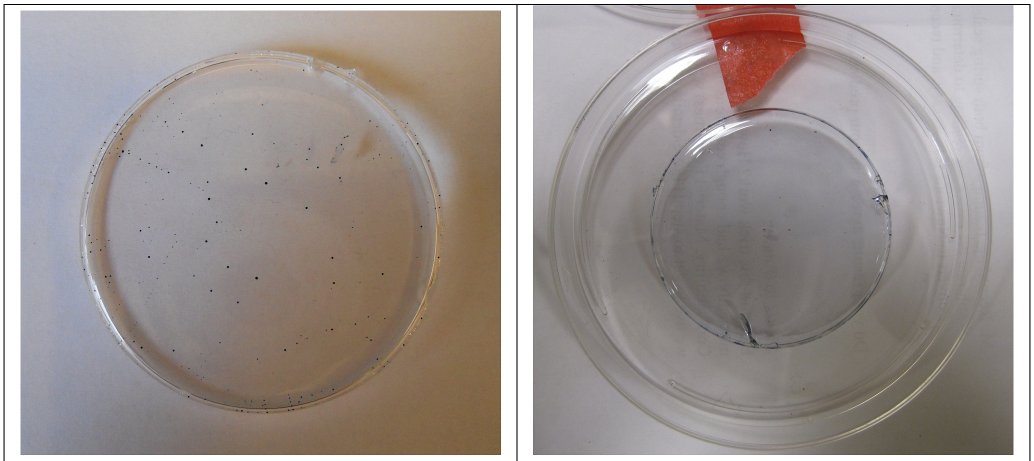

a) without plasma treatment | b) with plasma treatment

Figure 4-2: Effect of plasma treatment on spincoated layer of PEDOT on PDMS stamp, showing droplets in a) with no plasma, and a uniform coating in b) after plasma treatment.

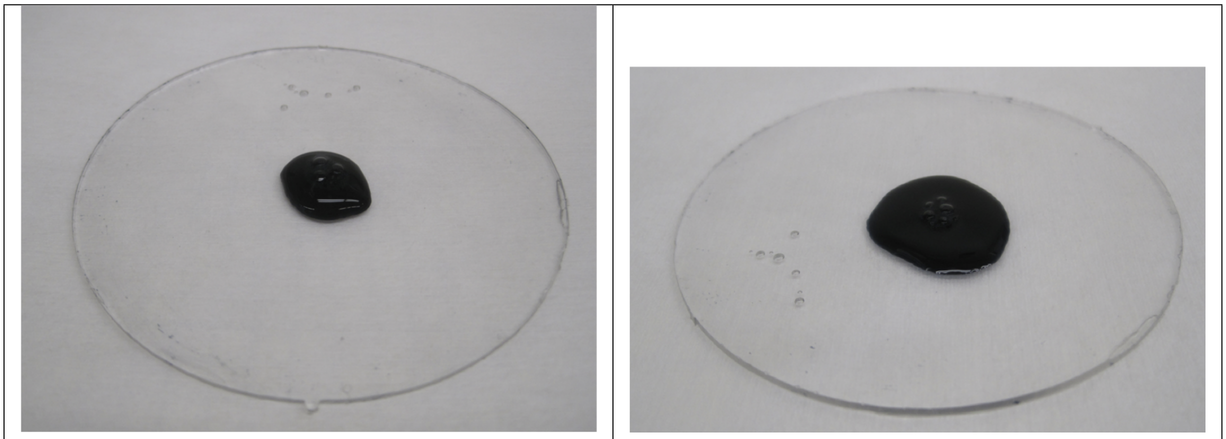

a) without plasma treatment | b) after plasma treatment

Figure 4-3: Difference in contact angle of PEDOT on PDMS before and after plasma treatment, showing that plasma treatment lowers contact angle and allows an equal volume of ink to spread out over a larger area.

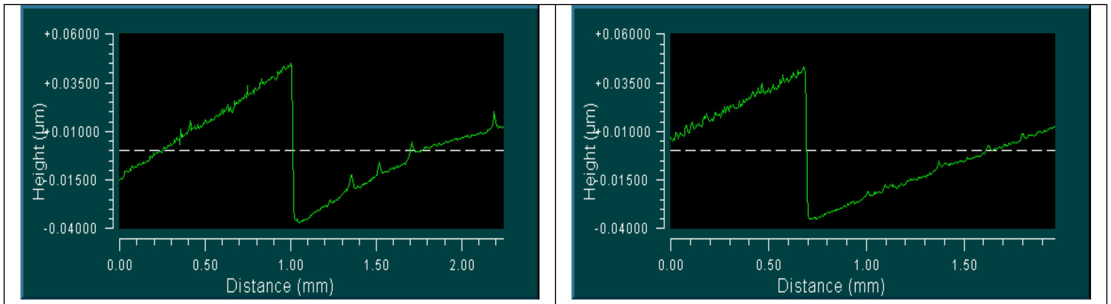

Film thickness ∼85 nm	Film thickness ∼80 nm
a) Line Profile #1	b) Line Profile #2

Figure 4-4: Zygo white light interferometer measurement of the thickness of 2000rpm 30sec spincoated PEDOT film on glass slide, showing ∼80 to 85nm film thickness.

spincoating is given in Section 3.3.2, and is inversely proportional to the angular velocity squared. Looking at the manufacturer's data, (see Figures B-2 and B-3 in Appendix B), Clevios PH 1000 is closest in viscosity and solid content to PH 510, so we expect that at a spincoating speed of 2000rpm for 30sec, the film would be ∼80nm thick (the author's spincoating equipment has no lid, and so follows the "lid open" manufacturer's curve). The manufacturer notes that for fabricating OLEDs, CLEVIOS P layers are typically 50-80 nm thick, so this film target thickness seems reasonable.

Clevios PH1000 was spincoated directly onto a plasma treated glass slide (not a PDMS stamp) at 2000rpm for 30seconds. A piece of tape was used to remove a section of the dried film from the slide, leaving a step change in height. A Zygo NewView 5000 white light interferometer was used to measure the step change, and thus the thickness of the film. Profiles from two measurements are shown in Figure 4-4, showing that the thickness is 80-85nm. This agrees well with the expected thickness of ∼80nm.

4.4.3 Thickness of PEDOT on PDMS stamp vs. glass substrate

We saw in Section 4.4.2 that the thickness of film on a glass slide with spin coating parameters of 2000rpm for 30sec was about 80nm. But what is the thickness of a PEDOT film on the PDMS stamp, and then on the glass slide after transfer? In other words, what percentage of PEDOT is transferred during printing? To investigate this, the Zygo white light interferometer was used to measure two PDMS stamps, each spincoated with PEDOT at 2000rpm for 30sec. One stamp was coated on 2/4/11, and one stamp coated on 3/9/11 (Figure 4-5). Both stamps were treated with air plasma at 100W for 0.3 min, and then after

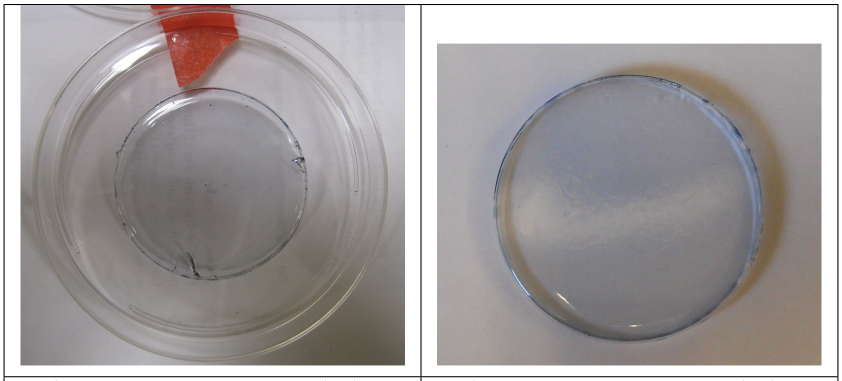

a) Stamp coated on 2/4/11

b) Stamp coated on 3/9/11

Figure 4-5: Coatings of PEDOT film on PDMS stamps at different dates, showing repeatable results in getting a uniform coating.

coating were dried on a hot plate at 60°C for 2min.

A section of PEDOT film was removed from each PDMS stamp with Scotch tape to create a step height for profile measurement. The profile measurements are shown in Figure 4-6, showing that stamp a) has an average thickness of 87.5nm across two measurements, and stamp b) has an average thickness of 72.5nm across two measurements.

Two glass slides, with PEDOT film transferred from PDMS stamps with the same specifications as above, were then measured in the same manner. The slides are shown in Figure 4-7. Figure 4-8 shows that the thickness of these films are around 65nm each. Because the film on the PDMS is thicker than the final printed pattern on the glass slide, from these initial findings it seems that there is PEDOT residue being left on the stamp (∼10-15nm of it).

4.4.4 Need for intermediate cleaning and better transfer equipment

As expected from the stamp vs. printed pattern thickness results (suggesting residue left behind), experimentally the PDMS stamp does show residue. Figure 4-9 shows a PDMS stamp after three uses, with no cleaning between each coating and printing. PEDOT can be dissolved with isopropyl alcohol or ethanol according to the manufacturer, so a rinse step should be added between experiments so that the stamp can be reused.

Experimental observation also shows the need for better printing equipment. In Figure 4-10, the printed slides show uneven contact pressure (slide #1, with only one patch transferred), slipping when the ink is thick (slide #2, with drag marks), and general smudging (slide #3). These difficulties indicate that better equipment is needed for control of the

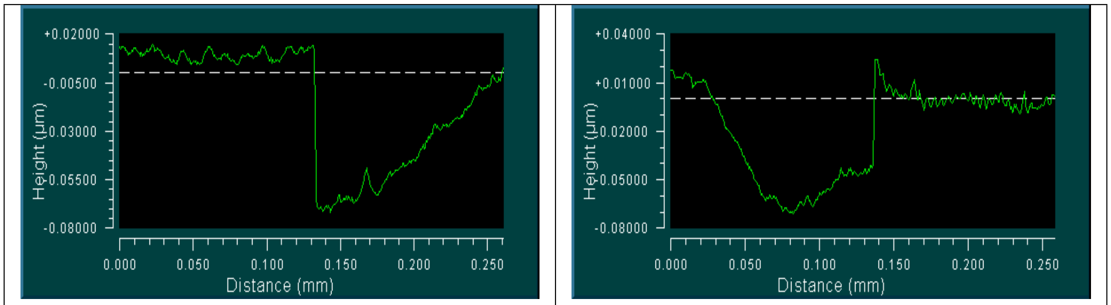

Meas #1: Film thickness ~90nm

Meas #1: Film thickness ~70nm

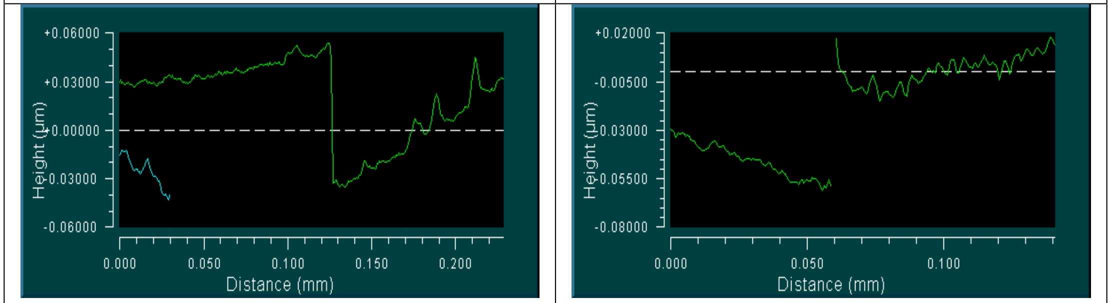

Meas #2: Film thickness ~85nm

Meas #2: Film thickness ~75nm

a) Stamp coated on 2/4/11

b) Stamp coated on 3/9/11

Figure 4-6: Zygo white light interferometer measurement of line profiles of film thicknesses on two PDMS stamps spincoated with PEDOT at 2000rpm 30sec, showing height measurements within 5nm across a stamp, and similar height measurements between the two stamps.

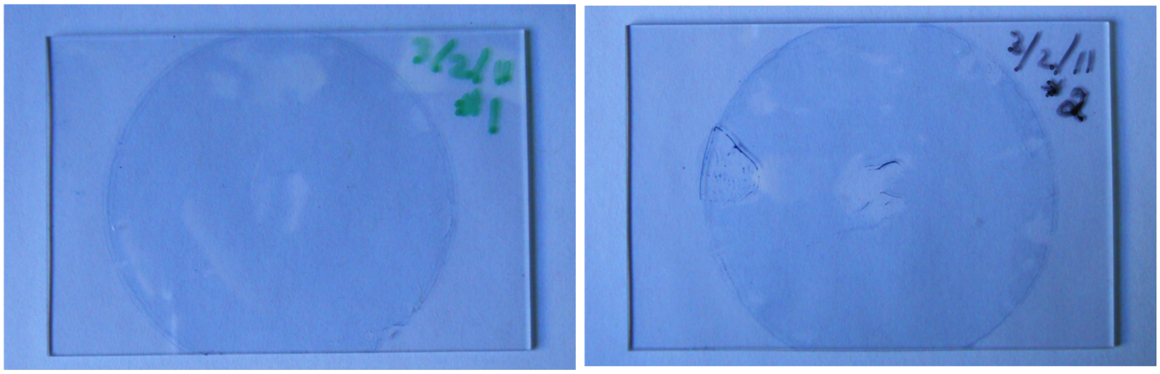

Figure 4-7: Transferred coating of PEDOT film onto glass slide.

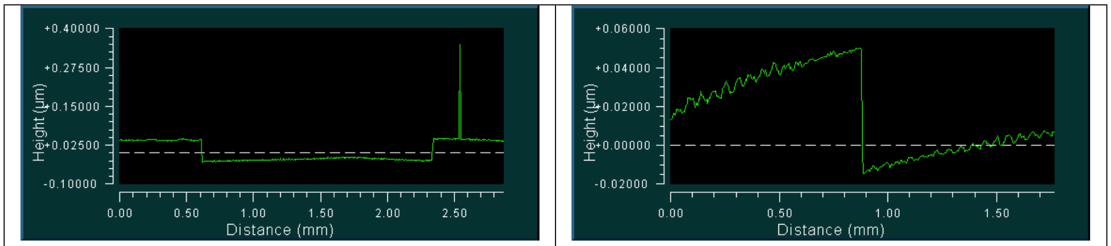

Film thickness ~62-70nm	Film thickness ~65nm
a) Line profile from slide #1	b) Line profile from slide #2

Figure 4-8: Zygo white light interferometer measurement of the thickness of transferred 2000rpm 30sec spincoated PEDOT film on glass slides, showing ~65nm film thickness.

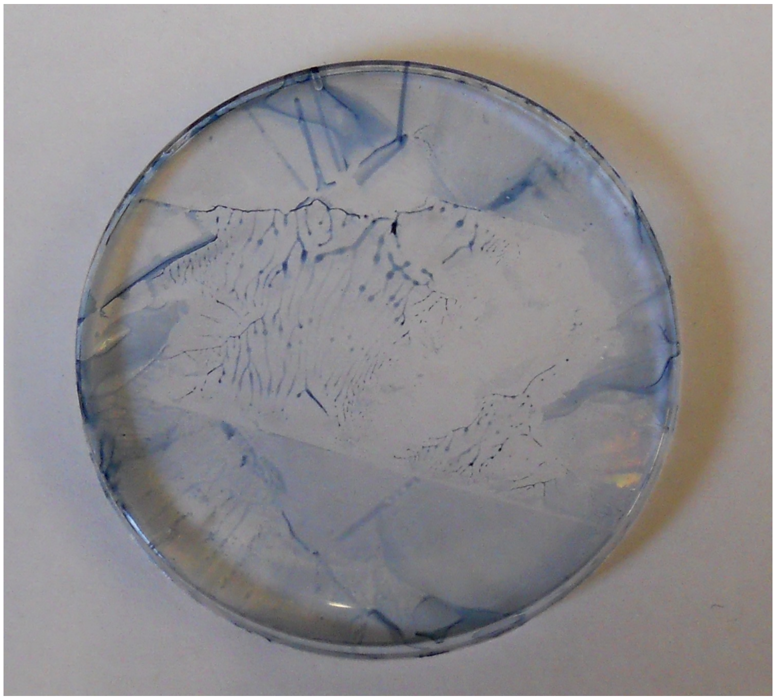

Figure 4-9: PDMS stamp used to print three consecutive glass slides, no cleaning between each experiment.

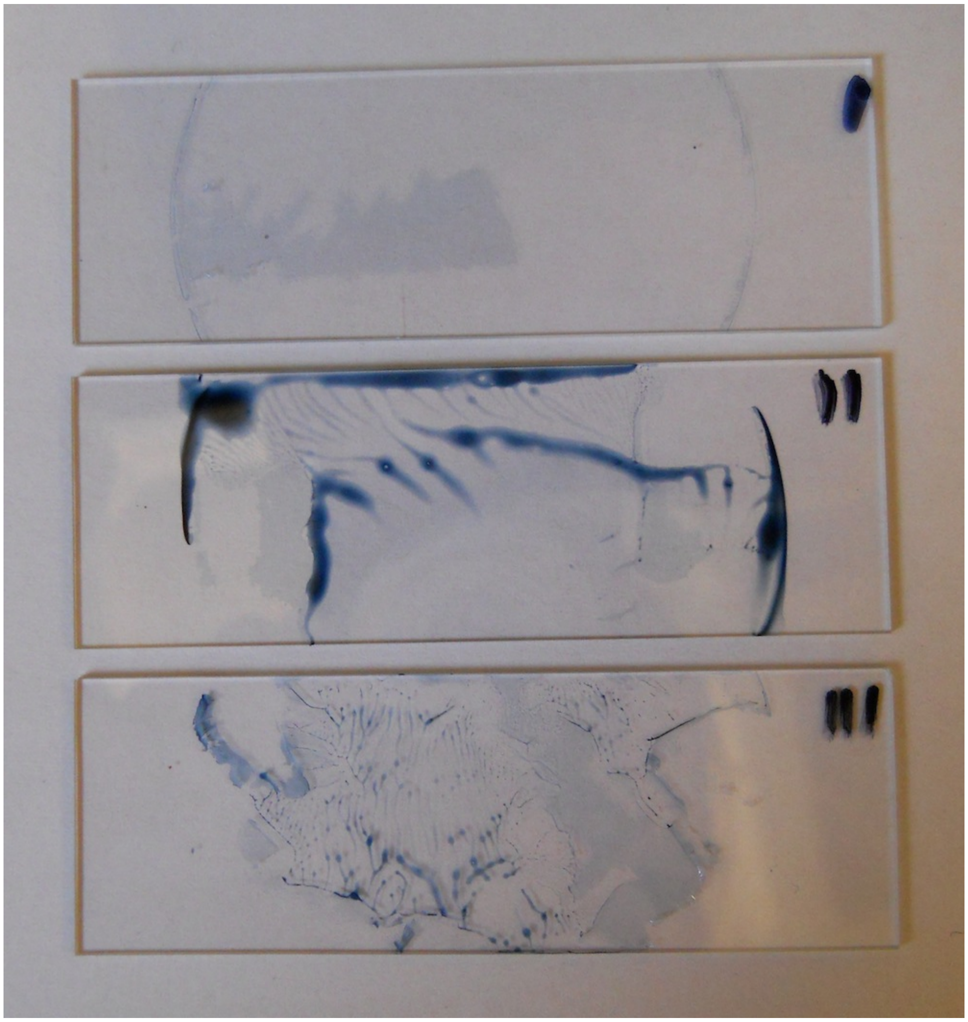

Figure 4-10: Glass slides with PEDOT film, showing defects caused by imprecise manual stamping.

transfer process - manual techniques are simply not going to be precise enough.

4.5 Experimental additive μCP of PEDOT

Using both flat stamps and a standard pattern of 50μm lines, a wide variety of settings for additive μCP transfer of PEDOT were explored. Most failed to achieve successful, repeatable transfer. Examples of failure modes are seen in Figure 4-11. The common theme of failure is that the PEDOT does not adhere to the substrate - if the PEDOT is dried first to become a film, the film peels off the substrate and curls into little strings instead of the desired lines. If the PEDOT is transferred while still wet, it produces blurry smeared lines that do not replicate the stamp features. And in some cases, if the stamp was not well coated, the

PDMS directly bonds to the glass and leaves pieces of the stamp behind.

The best results obtained are shown in Figure 4-12. For this experiment, a 4" PDMS stamp with 50μm lines was treated for 30 seconds with 125W air plasma. The stamp was spincoated with 1.5mL of Clevios PH1000 PEDOT ink, at 2000rpm for 30 seconds. A glass slide was placed on an 80°C hot plate, the stamp was placed in a rolling-down motion on top of the slide, and the stamp and slide together were left on the hot plate to dry for 10 minutes with a 200g weight on top. Then the stamp was peeled off the slide, and the transferred lines are left remaining. When measured with a profilometer, shown in Figure 4-13, there seems to be good edge replication but uneven line thickness.

At this point, with even the "best practice" parameters, most of the slide looks terrible, and only small sections have good replication. Because the failure modes seem to indicate the PEDOT material prefers to stick to the stamp, and because in the literature subtractive patterning was also demonstrated to work [179, 181, 172], at this point research inquiry shifted to using a liftoff process instead of additive stamping.

4.6 Experimental liftoff μCP of PEDOT

Subtractive patterning (peeling material off a substrate using a patterned stamp) of a film involves two problems: successful weakening or cracking of film along feature edges, and successful peeling off. If the subtractive patterning is used with a liquid, the two problems are breaking the surface tension (internal cohesion) of the ink, and creating a favorable surface energy potential between the substrate and stamp [14, 172]. Polymers pose a special challenge for subtractive patterning as opposed to metals because the fracture toughness is high, the thickness can be high (vs. monolayers or single nanometer scale thin layers), and they have much higher cohesive energy due to entangled chains (although adding glycerol reduces this). See Appendix C.1.2 for more detail on the theory of subtractive patterning.

Experimental attempts to replicate prior work in literature [179, 181] mostly failed, and good results were not repeatable. (Glycerol was used as an additive for some experiments, as noted in prior art.) Typical failure modes for liftoff transfer are shown in Figure 4-14. These include the PEDOT film not breaking along feature edges, leaving the unpatterned coating intact, the PEDOT film breaking along feature edges but also lifting up from the substrate surface, broken lines in the pattern, and droplets of unmixed or unevaporated

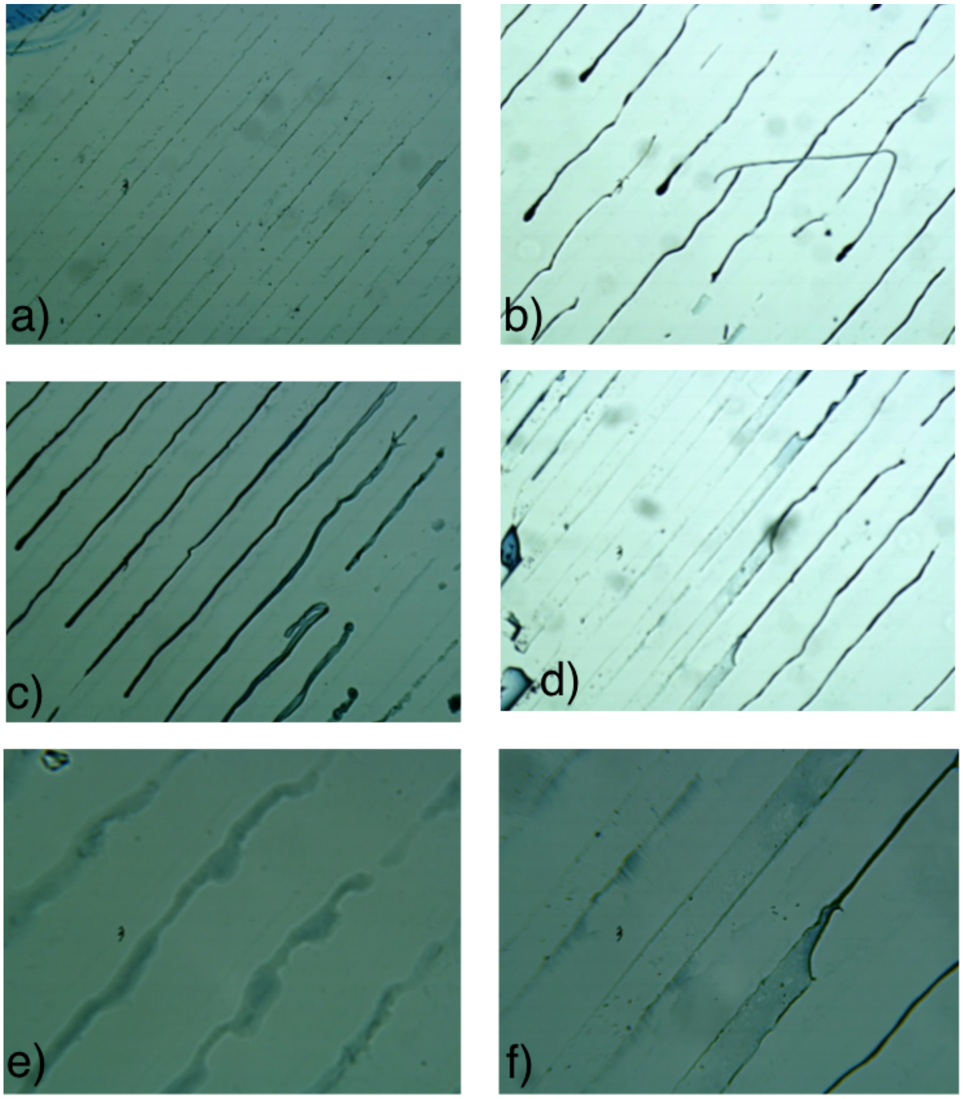

Figure 4-11: Failure modes in additive stamping of PEDOT onto glass slides. a) Failure to fully cover PDMS stamp with ink leads to the PDMS stamp bonding directly to glass, and leaving clear bits of stamp attached to the substrate after demolding. b) and c) Examples of PEDOT film detaching from the PDMS stamp, but because of poor adhesion with substrate, the film forms strings and does not attach to the substrate. d) Hybrid section with some features properly attached to the substrate in flat lines, transitioning into some sections not adhered and rolled into strings. e) Addition of too much glycerol to PEDOT leads to poor film formation. f) Magnified version of d), with some sections adhered properly in flat lines, and some sections rolling into strings.

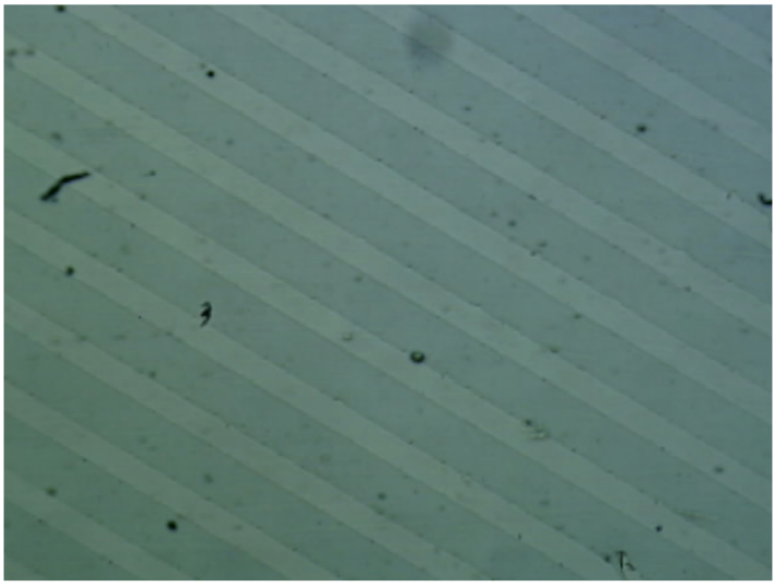

Figure 4-12: Example of best possible additive μCP with PEDOT.

glycerol additive. In some cases small strings of PEDOT were observed, similar to what was seen in the additive stamping experiments. In these cases it is hypothesized that the PEDOT film stuck to the stamp enough to be disturbed and release partially from the substrate, after which residual stresses causes curling into strings.

At this point, because experimental results were not successful, research efforts turned to better understanding the mechanisms of transfer in an effort to determine why the results were not consistent with reported literature.

4.7 Investigation of surface energies

There are two regimes of transfer between a stamp (mold) and a substrate. One is the commonly understood μCP stamping method, technically an additive lithography. The other is the opposite - liftoff or adhesive lithography, a subtractive method where the material is peeled from the substrate with a mold. These two regimes are show in Figure 4-15.

As discussed in Section 3.5, the work of adhesion between any two surfaces (1 and 2) is given by:

$$W_{1,2} = \gamma_1 + \gamma_2 - \gamma_{12} \tag{4.1}$$

or by:

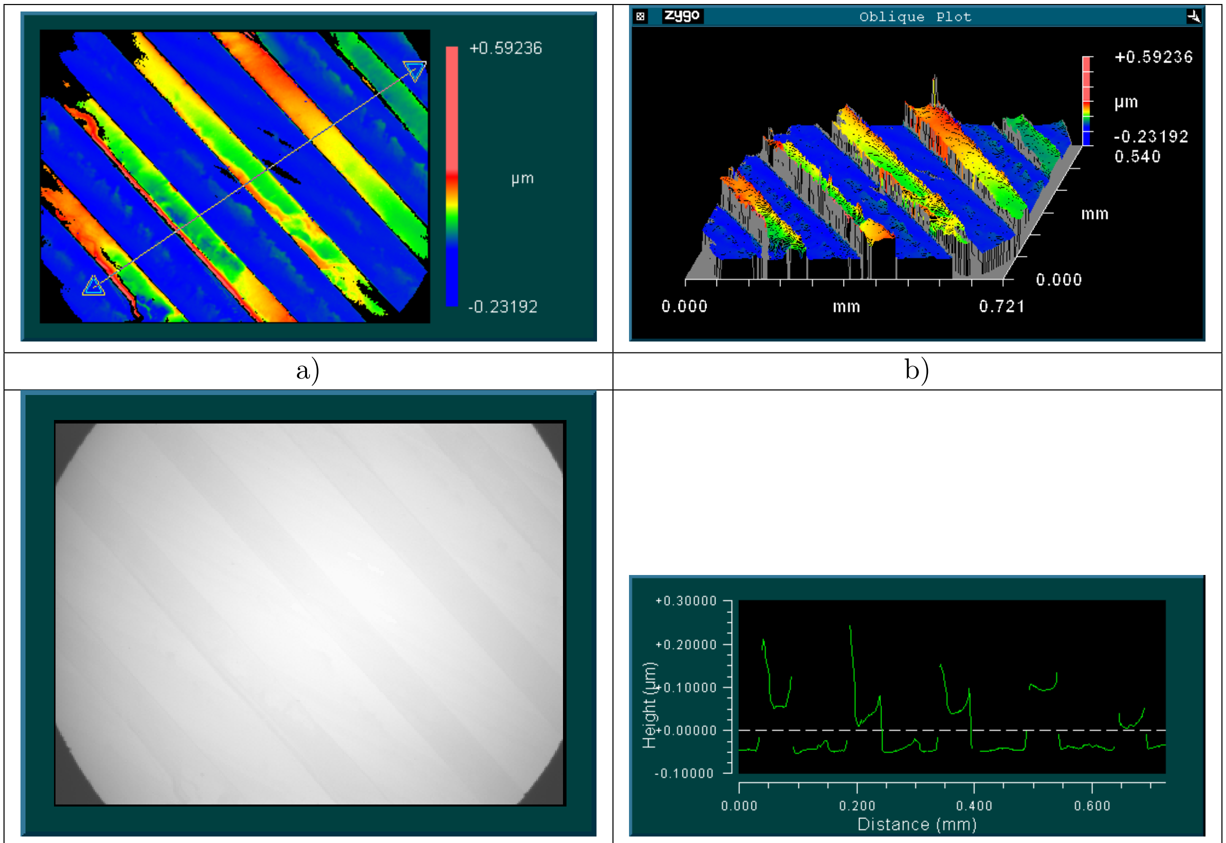

a)

b)

c)

d)

Figure 4-13: Zygo white light interferometer measurements of height profiles of the 50μm lines on the example of best practice additive μCP, showing nonuniform thickness across each line. a) Color-coded height map of surface profile. b) 3D projected view of surface profile. c) Microscope image of measured surface area. d) Line profile across the surface area, showing thick buildup at edges of each feature, and nonuniform nominal heights when compared across features.

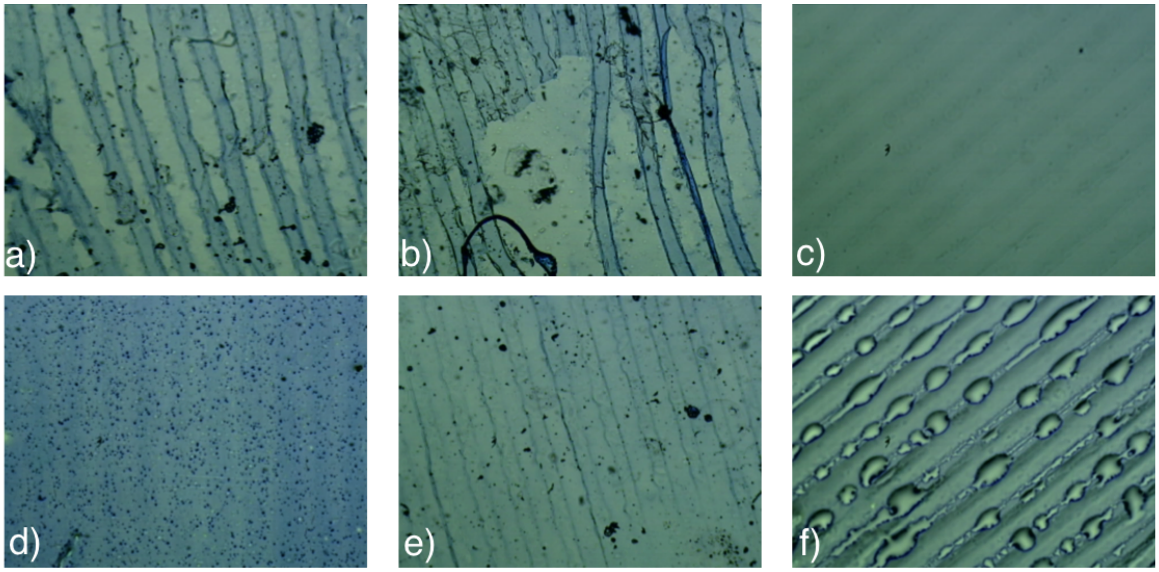

Figure 4-14: Failure modes in liftoff of PEDOT from glass slides. a) intended areas have been removed, but remaining pattern was also disturbed and partially lifted off during transfer, because of poor adhesion to substrate. b) entire sections of film removed instead of film breaking along feature edges. c) features removed in intended pattern, but only a very thin layer left behind. d) film does not adhere to stamp, leading to no removal of film. e) application of stamp and pressure during transfer creates a film molded into thicker and thinner regions, but not removed. f) too much glycerol additive in PEDOT leads to beads of glycerol separating from solution.

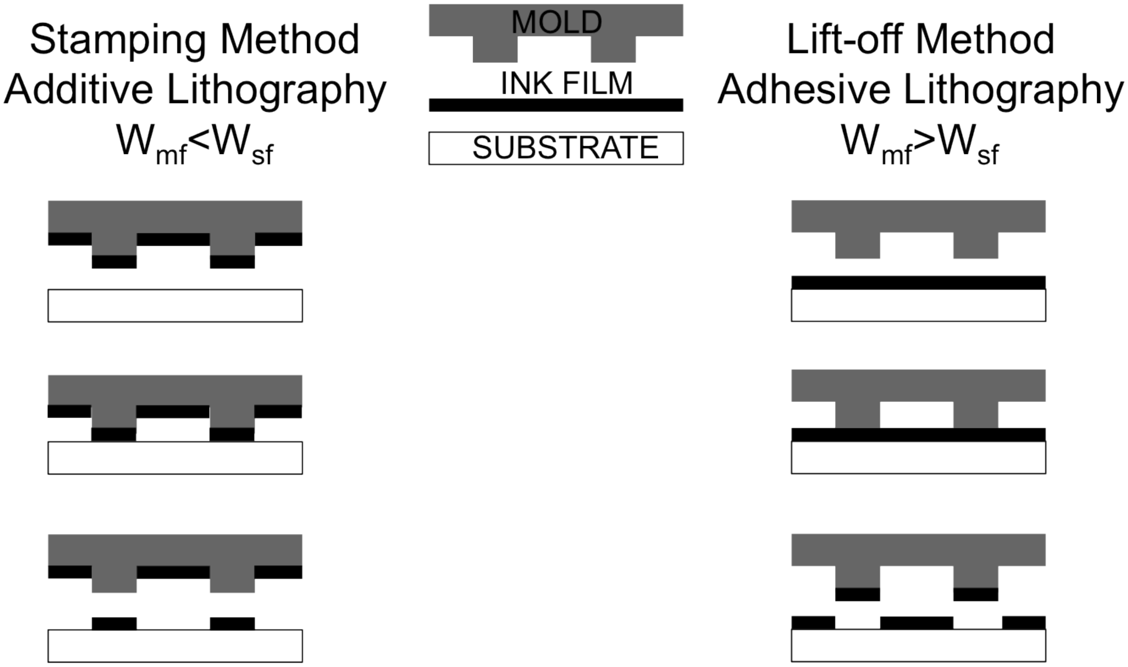
Stamping Method
Additive Lithography
$W_{mf}<W_{sf}$
MOLD
INK FILM
SUBSTRATE
Lift-off Method
Adhesive Lithography
$W_{mf}>W_{sf}$

Figure 4-15: Additive (stamping) and subtractive (liftoff) transfer regimes, controlled by the work of adhesion (dependent on the ratio of surface energies of the stamp and substrate).

Material	Surface Energy $\frac{\mathrm{mJ}}{\mathrm{m}^2}$	Dispersion Component $\frac{mJ}{m^2}$	Polar Component $\frac{mJ}{m^2}$
Glass, no plasma	69.8	24.8	45.0
Glass, plasma	Very high (100 estimated)	(36 estimated)	(64 estimated)
PMMA, no plasma	41.0	29.7	10.3
PMMA, plasma	54.6	N/A	N/A
PDMS, no plasma	19.8	19.0	0.8
PDMS, plasma	Very high (100-170 estimated)	(96 estimated)	(4 estimated)
PEDOT:PSS film	73.2	27.1	46.1

Table 4.1: Surface energies of potential stamp and substrate materials, and PEDOT, calculated from goniometer contact angle data.

$$W_{1,2} = \frac{4\gamma_1^d\gamma_2^d}{\gamma_1^d + \gamma_2^d} - \frac{4\gamma_1^p\gamma_2^p}{\gamma_1^p + \gamma_2^p} \tag{4.2}$$

where γ_d is the surface energy dispersion component, and γ_p is the surface energy polar component. If $W_{mf}$is the adhesion force at the mold-film interface, and W_{sf} is the adhesion at the substrate-film interface, then:

$$W_{mf} < W_{sf}\,\text{for stamping method} \tag{4.3}$$

$$W_{mf} > W_{sf}\,\text{for liftoff method} \tag{4.4}$$

In other words, if the stamp is “stickier,” liftoff transfer is favorable, and if the substrate is “stickier” then additive transfer is favorable.

We would like to know which of these regimes is likely to occur, given the materials used experimentally for substrate, stamp, and PEDOT ink. Using a goniometer in the MIT Lab for Nanoengineered Surfaces, Interfaces, & Coatings under Professor Kripa Varanasi, with the help of Adam Paxson, the surface contact angles of three test liquids were measured on the surfaces used experimentally. From these contact angles, the surface energies of the substrates were calculated [168]. The surface energy of PEDOT ink was determined from the contact angle of an ink droplet in air. The measured empirical data is given in Table 4.1. In cases where the contact angle was too low to be reliably measured (i.e. the ink did not from a droplet, but spread out almost completely), the surface energy is given as “very high” and a best possible estimation is provided for calculation purposes.

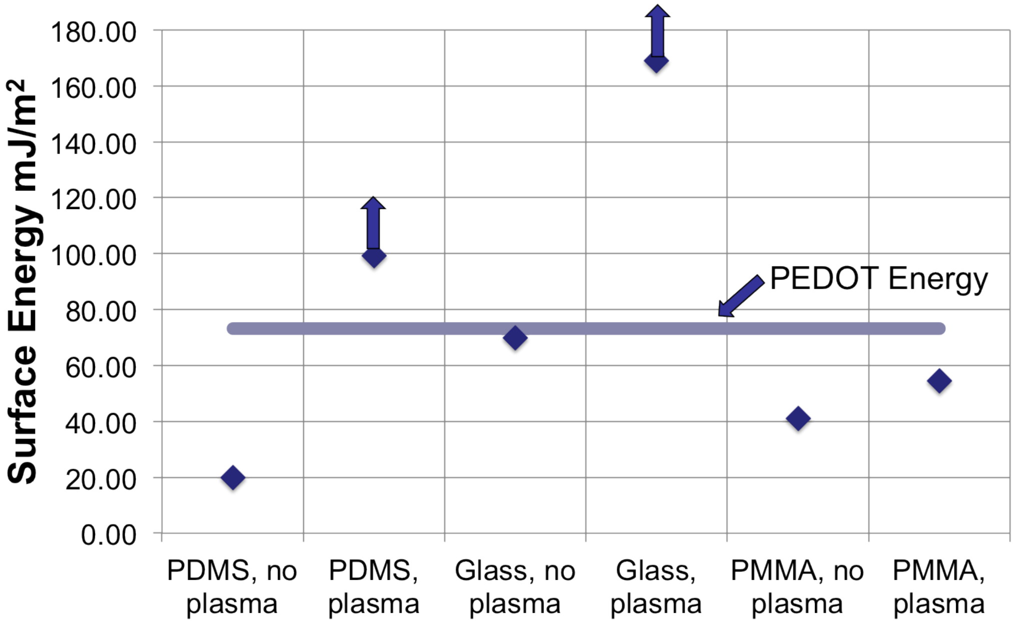

Figure 4-16: Surface energy comparisons of potential stamp and substrate materials, showing that PEDOT ink will only wet plasma treated glass and plasma treated PDMS.

The first thing this data tells us is which surfaces the PEDOT ink will wet. Recall from section 3.3.3 that a liquid will only wet a surface with higher surface energy, and will bead up otherwise. Figure 4-16 shows that only glass with plasma treatment and PDMS with plasma treatment have higher surface energy than PEDOT, so PEDOT can only be coated onto those materials. Untreated glass and PDMS, and even plasma treated PMMA, do not have high enough surface energies for the ink to wet.

This means that the potential options available for transfer are lift-off from plasma treated glass, or additive μCP from PDMS onto glass or PMMA, but not liftoff from PMMA. (Since the goal of the project is to print onto polymers, analyzing μCP onto PMMA is more interesting than onto glass.)

Now that we know the two modes of transfer available (liftoff from glass, μCP onto PMMA), the next step is to calculate the work of adhesion for each of those cases. For the liftoff case, the mold-film interface is PDMS without plasma (for maximum "stickiness") with PEDOT, and the substrate-film interface is glass with PEDOT. For the additive case, the mold-film is PDMS with plasma and PEDOT, and the substrate-film is PMMA without plasma and PEDOT. The calculated work of adhesion for each case is shown in Table 4.2.

	Surface	Energy $\frac{mJ}{m^2}$	Film	Energy $\frac{mJ}{m^2}$	$W_{1,2}$
W_{mf} (liftoff)	PDMS no plasma	19.8	PEDOT:PSS	73.2	47.8
W_{sf} (liftoff)	Glass w/ plasma	Very High	PEDOT:PSS	73.2	High (est. 169)
W_{mf} (stamping)	PDMS w/ plasma	Very High	PEDOT:PSS	73.2	High (est. 99.3)
W_{sf} (stamping)	PMMA no plasma	47.0	PEDOT:PSS	73.2	90.3

Table 4.2: Work of adhesion calculated for liftoff and stamping surface material combinations

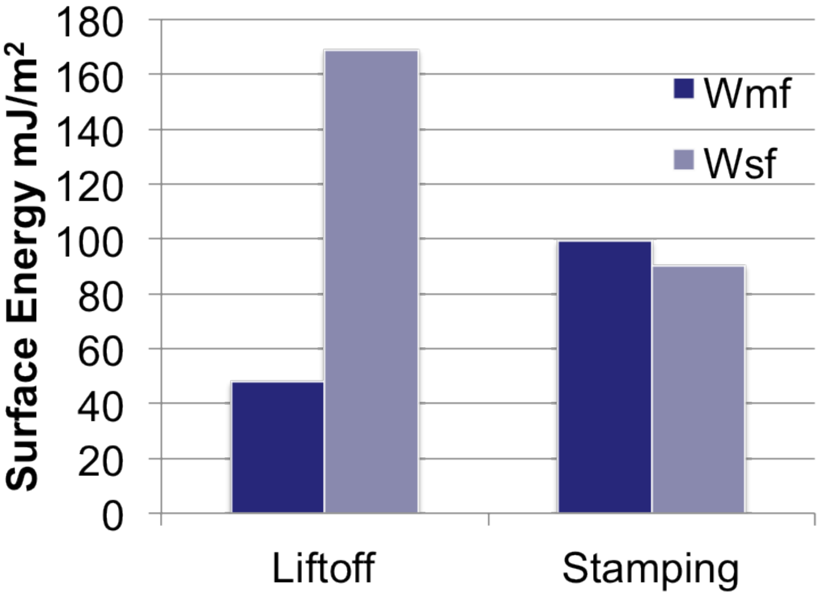

Figure 4-17: Comparison of work of adhesion for liftoff and stamping methods with PEDOT, showing unfavorable surface energy ratios for both potential transfer methods.

4.8 Conclusion: Work of adhesion shows transfer is unfavorable

The ratios of work of adhesion for each case (liftoff from glass, μCP onto PMMA) are shown graphically in Figure 4-17. This shows that for each case, the work of adhesion ratios are unfavorable. For liftoff to be successful, we want W_{mf} to be greater than W_{sf}, but the opposite is the case. For μCP to be successful, we want W_{sf} to be greater, but the opposite is the case.

However the ratio is very close for additive μCP, which helps explain why the literature reports it as possible. And indeed, experimentally we were able to get some good results with stamping. But even in cases with good results from additive μCP, the transfer may be successful at one spot but not over the whole working area. See Figure 4-18 for an example

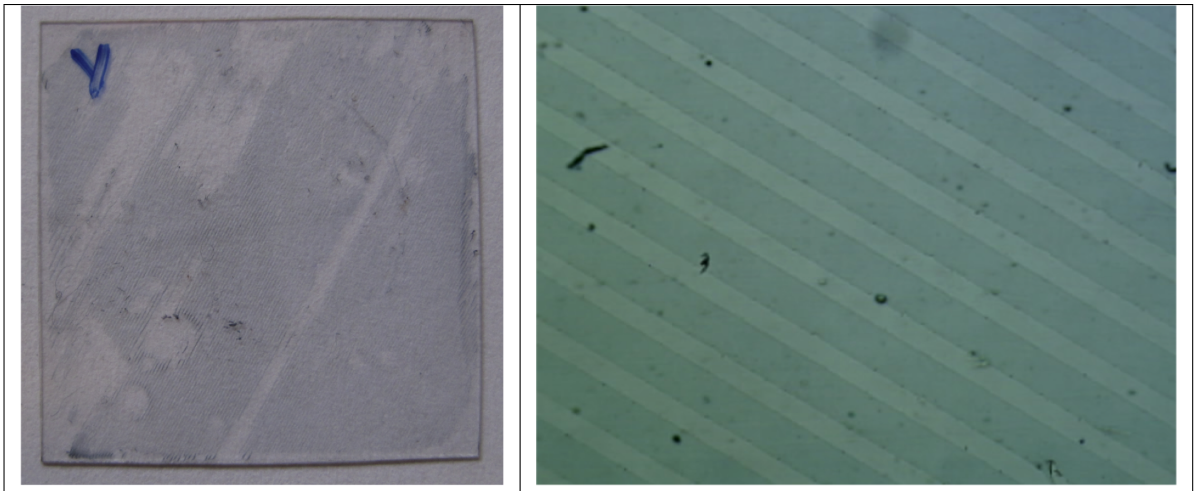

a) b)

Figure 4-18: Successful PEDOT μCP only over a limited areas of the substrate. a) Macro image of 1x1" substrate. b) Microscope image of 50μm line features, selected area from substrate.

of a 1" square glass slide printed with a stamp with 50μm lines. The entire slide is not uniform, although small sections of good lines can be isolated under a microscope.

In conclusion, PEDOT ink and polymer substrates do not have favorable surface energies to allow transfer in either the liftoff or the stamping mode. Potential further work could be done to tailor the substrate and stamp surfaces with chemical modifications, or to choose different substrate materials, or to reformulate the ink with different surface tension. But even if those items could be accomplished to make the mechanical printing process possible, PEDOT is chemically very sensitive to the additives used and the substrate properties. So optimizing for printing will create additional challenges for achieving good electrical properties. With these things in mind, the process does not seem robust, and it seems likely that other methods would be more promising for high volume manufacturing. Chapter 5 will explore using silver nanoparticle ink instead.

Chapter 5

Exploration of μCP of Silver Nanoparticle Ink

Chapter 4 discussed using μCP for patterning the conductive polymer PEDOT. Although attempts to establish a reliable and robust patterning method were unsuccessful, the key research finding was that the surface energies of the stamp, substrate, and ink are critically important. With this in mind, research effort turned to using a different material - silver nanoparticle ink, or Ag ink - with a similar μCP process. The advantages of silver ink include consistently good electrical performance and (most importantly) favorable surface tension, while possible disadvantages include high cost and potentially poor adhesion to polymer substrates.

Chapter 5 now explores using μCP with Ag ink. First, successful benchtop experiments are established, replicating reported transfer in literature. Because the properties of the inks are so important, a range of inks available commercially and by special order are characterized. (Stamp and substrate choice are of course also important, but more limited because of the functional requirements of the stamp, and the intended application of the substrate.) A brief investigation into the proportion of ink transferred from the mold to the substrate tests the hypothesis that the percentage of ink left on each surface is dependent on the ratio of surface energies. Results could not confidently confirm that hypothesis.

Then using an understanding of the mechanisms involved in directly transferring liquid inks (Chapter 3), a careful set of experiments is designed to empirically investigate the transfer process. Chapter 6 discusses the results from this DOE, determines sensitivity of the process variables, and develops a process model.

5.1 What is silver nanoparticle ink?

Metallic nanoparticle inks are often used in printed electronics, and consist of spherical crystals of metal (typically silver, but can also be gold, copper, or other materials) in a carrier. Formulations can be optimized for screenprinting (more of a paste consistency), inkjet printing, or flexography. The diameter of the particles can vary, but typical dimensions are less than 150nm, and cutting edge formulations are 10nm and smaller. Often the ink formulation will include other chemical agents for stabilizing the mixture and preventing clumping, and binders to encourage adhesion. Although metals are inherently conductive, most inks need to be sintered in order to remove the solvent carrier and to break down any organic binders which may form a shell around each nanoparticle.

In Chapter 4 on investigating PEDOT, Figure 4-16 showed the surface energy of PEDOT (also known as surface tension for a liquid) compared to the energies of the stamp and various substrates. Figure 5-1 is a copy of this earlier figure, additionally showing the surface energy of a typical Ag ink. Because the energy of this class of inks is lower than PEDOT, it opens up new possibilities of surfaces to coat (a liquid will only wet onto a higher surface energy material). Most importantly, the Ag ink is predicted to coat onto plasma treated PMMA (perhaps even non-treated PMMA, although the energies are close enough to be problematic).

5.2 Prior work in μCP of silver ink

In the literature, silver used in a printing process can either involve a liquid transfer, or a solid transfer. In metal transfer printing, a solid layer of metal is transferred from one surface to another, usually with high temperature or pressure. The transfer mechanics for this method are based on fracture mechanics, not fluid mechanics, and are not as useful to study when trying to understand liquid ink μCP [182]. For silver in a liquid transfer mode, there is some ambiguity in the literature over terminology. There are multiple reports in literature of using a rubber stamp to directly transfer liquid silver ink, whether it is called flexography [160, 161, 162, 8], soft lithography [90, 163, 162], transfer stamping [165, 166], or microcontact printing [9]. Two of these works are worth particularly highlighting. Kwak

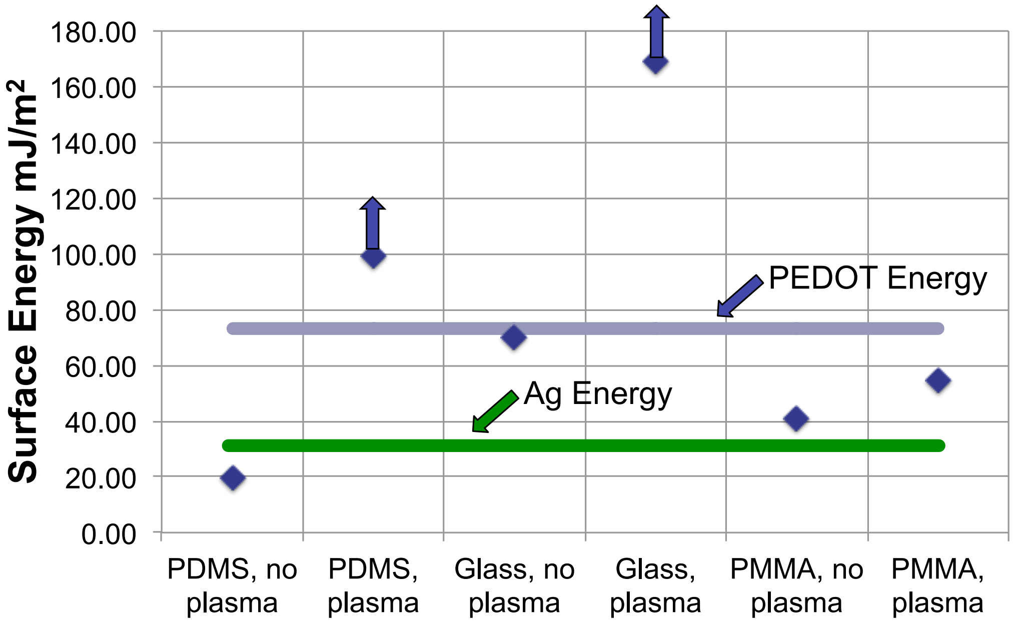

Figure 5-1: Surface energy of Ag ink in comparison to PEDOT and typical stamp/substrate combinations, showing that because of lower surface energy Ag ink will be able to wet onto PMMA.

et. al. demonstrate printing with a plate-to-roll setup similar to the equipment available in the author's lab, and use a process with materials that are obtainable and with protocols that were explained in enough detail to replicate [8]. Takakuwa et. al. demonstrate the smallest features currently reported with this method, down to 2 μm lines [9, 178].

In Figure 5-2, 20μm silver lines are shown, printed by Kwak et. al. using plate-to-roll transfer. An Si wafer is spincoated with Ag ink, and this inkpad coating is picked up with a plasma treated PDMS stamp. Then, an SU-8 coated aluminum cylinder is rolled across the PDMS, and the resulting pattern is annealed at 70°C. (Note that in this version of plate-to-roll printing, the roll is the substrate, although normally the configuration is roll-to-plate, and refers to the plate being the substrate.) [8]

Takakuwa et. al. use a PDMS plasma treated stamp (with features 2-20 μm), with Ag nanoparticle ink spin coated directly onto the stamp. The coated stamp is then placed on a substrate, removed, then the remaining pattern is annealed at 150°C. Figure 5-3 shows the final printed pattern of 2μm lines. This is the smallest feature printed in this manner that the author has been able to find. However despite impressive resolution, the process used does not use automated equipment, and it is unclear if these results would be scalable to high volumes. [9]

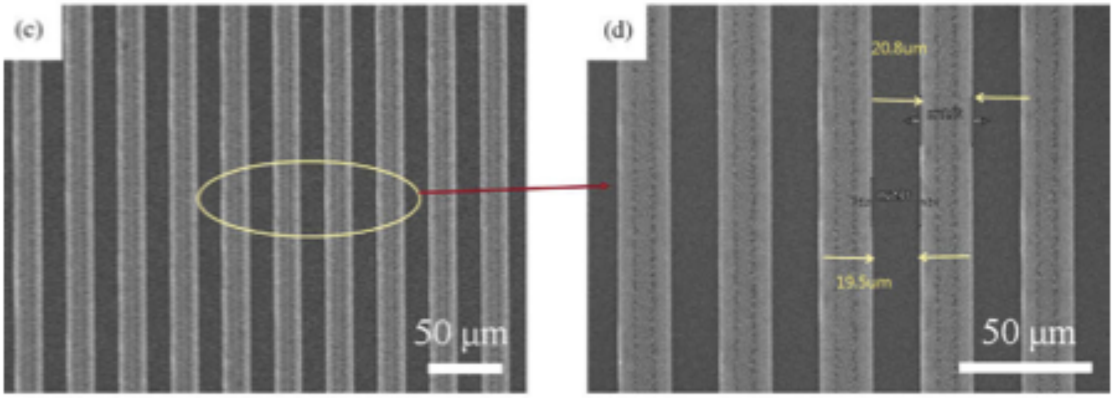
(c)
50 μm
(d)
20.8um
19.5um
50 μm

Figure 5-2: Kwak demonstration of plate-to-roll Ag ink transfer with 20μm features. [8]

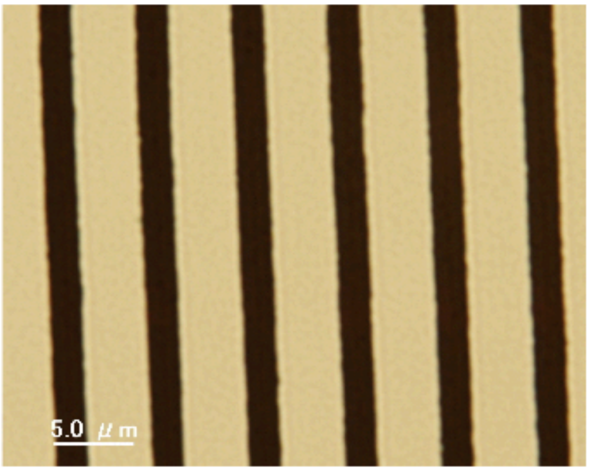

Figure 5-3: Takakuwa demonstration of Ag ink printing with a large area nickel mold, achieving 2μm features. [9]

	Kwak 2010	Hale 2012
Ink	DJ 30 ink (visc 12cps, 21.6nm particles, water solvent)	CCI-300 ink (visc. 11-15cps, 50nm particles, alcohol solvent)
Mold	PDMS mold, 20µm lines @ 40um pitch	PDMS mold, 50µm lines @ 50, 100µm pitch
Ink coating	spincoat ink onto silicon wafer, 30s at 3000 rpm, pick up with PDMS	spincoat ink onto plasma treated glass, 30s at 3000 rpm, pick up with PDMS
Substrate	SU-8 coated cylinder	PMMA, plasma treated
Stamping	multiple cycles	one cycle
Anneal	70C for 1 min after each cycle	100C for 30min

Table 5.1: Comparison of protocol for benchtop testing of μCP of Ag ink, between literature and a modified version using the equipment available.

5.3 Replicating literature μCP with Ag ink

Although literature may report that μCP of Ag ink is possible, it is important to test empirically (PEDOT transfer was reported possible, as well, but was not robust). To establish the feasibility of this method, the protocol in Kwak 2010 [8] was taken as a general guideline, and replaced with materials and equipment already available in the author's lab. Table 5.1 compares the parameters reported in literature to the parameters used for lightning empiricism testing. A glass slide was plasma treated with air plasma at 250Watts for 30 seconds, and then spincoating with CCI-300 ink (Cabot Corporation) at 3000rpm for 30 seconds. A PDMS stamp with 50μm lines at two spacings (50μm, for a 50% duty cycle pattern, and 100μm for a 25% duty cycle pattern) was placed by hand onto the glass slide and then removed. Then the coated stamp was placed onto a plasma treated PMMA substrate, removed, and annealed at 100ºC for 30 minutes. Figure 5-2 shows the results that are to be replicated, and Figure 5-4 shows the results of this successful printing protocol, (50 μm lines at different pitches, or different pattern duty cycles). It is encouraging to obtain successful transfer, especially since the materials and process used had not been optimized.

5.4 Investigation of silver inks

With this initial testing showing transfer is at least possible, the next step was to more thoroughly investigate the inks available. The work with PEDOT showed that surface energy is especially important, and because spincoating will be used, viscosity is another

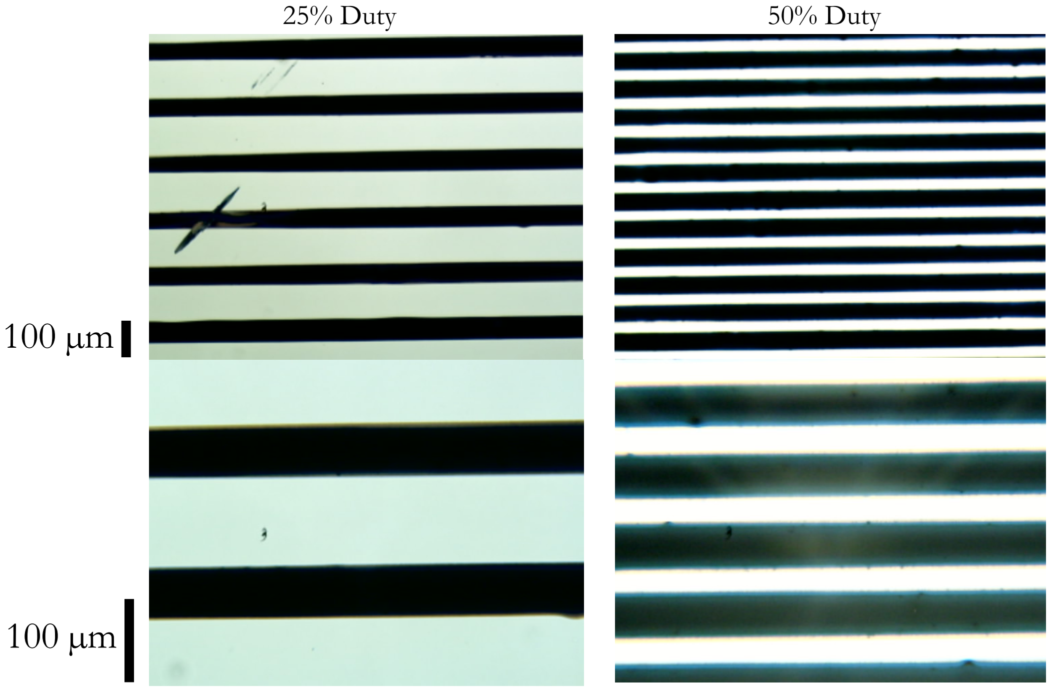

Figure 5-4: Successful replication with benchtop process for μCP of Ag ink, showing successful transfer of 50μm lines at 50μm spacing (50% duty cycle pattern) and 100μm spacing (25% duty cycle).

obvious parameter of importance. Table 5.2 lists the properties of a range of commercially available inks [161, 8]. Although a number of inks formulated for screenprinting were also identified, these are unsuitable for μCP because they are too viscous.

A range of inks were purchased, and then tested to determine all properties (for cases where properties were not specified by the manufacturer, or were unknown because of custom formulations).

5.4.1 Density testing

Density was tested by measuring the mass of a sample of ink, and the precise volume with a Micromeritics AccuPyc 1340 gas pycometer. The densities of Ag inks measured in this manner were plotted against the predicted density given the weight % of silver and the density of the carrier (Figure 5-5, where the labels along the X axis are the solvent carriers of the different Ag inks). The discrepancy in predicted and actual density of the toluene ink is likely due to measurement error - toluene is such a volatile solvent that it was difficult to accurately get a volume measurement before it evaporated.

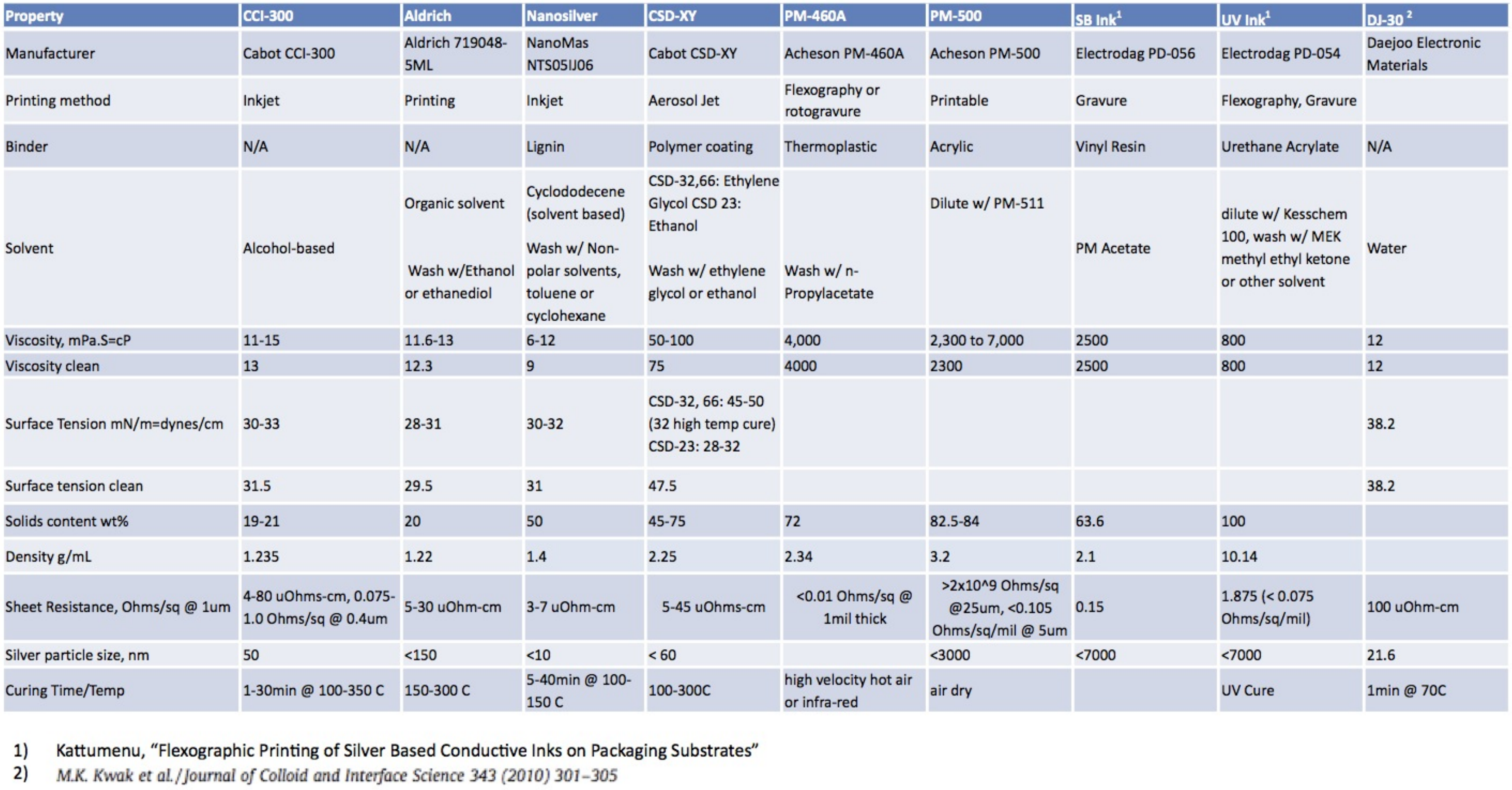

Property	CCI-300	Aldrich	Nanosilver	CSD-XY	PM-460A	PM-500	SB Ink[1]	UV Ink[1]	DJ-30 [2]
Manufacturer	Cabot CCI-300	Aldrich 719048-5ML	NanoMas NTS05IJ06	Cabot CSD-XY	Acheson PM-460A	Acheson PM-500	Electrodag PD-056	Electrodag PD-054	Daejoo Electronic Materials
Printing method	Inkjet	Printing	Inkjet	Aerosol Jet	Flexography or rotogravure	Printable	Gravure	Flexography, Gravure	
Binder	N/A	N/A	Lignin	Polymer coating	Thermoplastic	Acrylic	Vinyl Resin	Urethane Acrylate	N/A
Solvent	Alcohol-based	Organic solvent Wash w/Ethanol or ethanediol	Cyclododecene (solvent based) Wash w/ Non-polar solvents, toluene or cyclohexane	CSD-32,66: Ethylene Glycol CSD 23: Ethanol Wash w/ ethylene glycol or ethanol	Wash w/ n-Propylacetate	Dilute w/ PM-511	PM Acetate	dilute w/ Kesschem 100, wash w/ MEK methyl ethyl ketone or other solvent	Water
Viscosity, mPa.S=cP	11-15	11.6-13	6-12	50-100	4,000	2,300 to 7,000	2500	800	12
Viscosity clean	13	12.3	9	75	4000	2300	2500	800	12
Surface Tension mN/m=dynes/cm	30-33	28-31	30-32	CSD-32, 66: 45-50 (32 high temp cure) CSD-23: 28-32					38.2
Surface tension clean	31.5	29.5	31	47.5					38.2
Solids content wt%	19-21	20	50	45-75	72	82.5-84	63.6	100	
Density g/mL	1.235	1.22	1.4	2.25	2.34	3.2	2.1	10.14	
Sheet Resistance, Ohms/sq @ 1um	4-80 uOhms-cm, 0.075-1.0 Ohms/sq @ 0.4um	5-30 uOhm-cm	3-7 uOhm-cm	5-45 uOhms-cm	<0.01 Ohms/sq @ 1mil thick	>2x10^9 Ohms/sq @25um, <0.105 Ohms/sq/mil @ 5um	0.15	1.875 (< 0.075 Ohms/sq/mil)	100 uOhm-cm
Silver particle size, nm	50	<150	<10	< 60		<3000	<7000	<7000	21.6
Curing Time/Temp	1-30min @ 100-350 C	150-300 C	5-40min @ 100-150 C	100-300C	high velocity hot air or infra-red	air dry		UV Cure	1min @ 70C

1) Kattumenu, "Flexographic Printing of Silver Based Conductive Inks on Packaging Substrates"
2) *M.K. Kwak et al. / Journal of Colloid and Interface Science 343 (2010) 301–305*

Table 5.2: Summary table of commercially available ink properties.

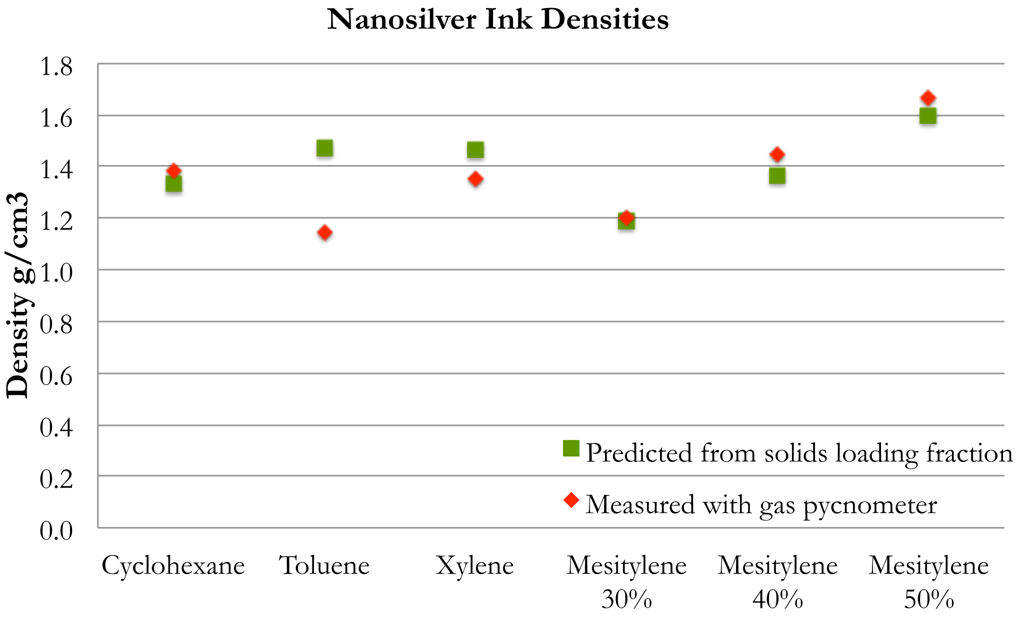

Figure 5-5: Ink density testing data from measurements with gas pycometer, showing good correlation with expected density calculated using given solids loading.

Because density and solids loading are so well correlated, they are considered dependent variables and it will not be necessary to use both of these parameters in a process model. Solids loading is chosen as the independent variable, because the inks used are all particulate-based inks. But, if non-particulate inks were to be used in the future (such as carbon nanotubes), the solids loading parameter could be replaced with a density parameter - it would just be necessary to know how much of the ink evaporates during annealing, to obtain an accurate thickness model.

5.4.2 Surface energy testing

Surface tensions of various Ag inks were tested with a Ramé-Hart Model 590 Advanced goniometer. A goniometer creates a droplet of ink in front of a camera, and the associated software calculates the energy from the geometry (i.e. contact angle) of the droplet. During a test the drop volume is varied, and an ideal measurement series will report an energy independent of the drop volume. Selected samples of collected surface energy vs. drop volume data over time is shown in Figure 5-6. Final surface energy numbers for each ink are calculated by taking an average energy over a stable region of measurements.

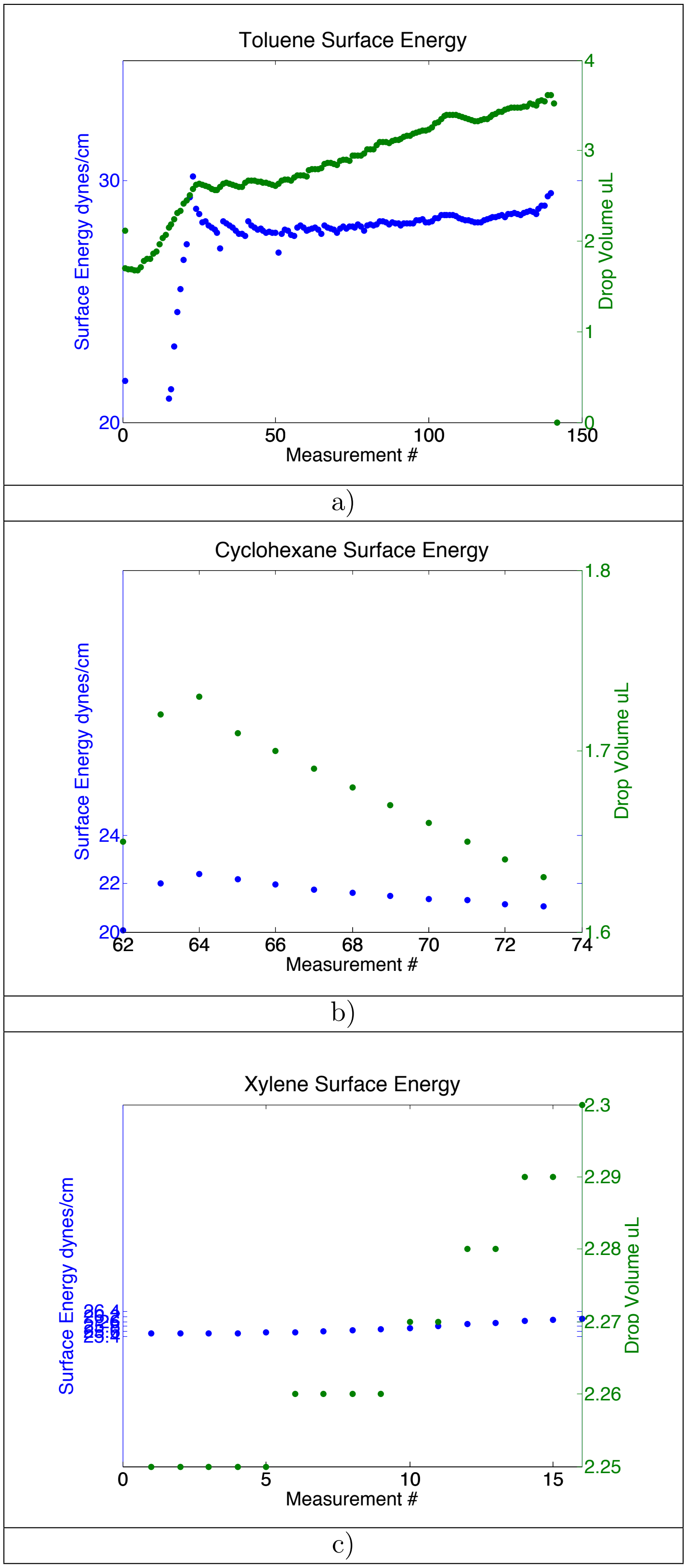

a)

b)

c)

Figure 5-6: Ink surface energy testing data, showing good decoupling of energy measurements from drop volume. a) Silver nanoparticles in toluene carrier, from NanoMas b) Silver nanoparticles in cyclohexane carrier, from NanoMas c) Silver nanoparticles in xylene carrier, from NanoMas.

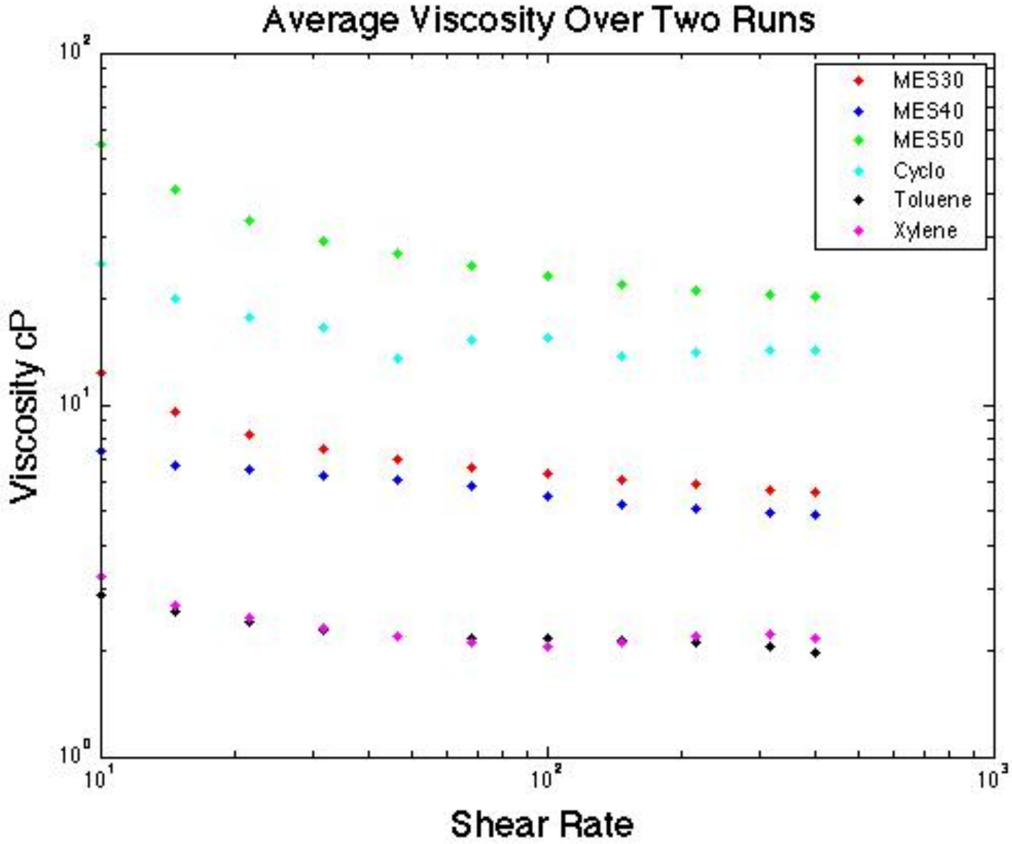

Figure 5-7: Ink viscosity testing data over a range of shear rates, showing slight effect of shear thinning.

5.4.3 Viscosity testing

Viscosity was measured with a ARG2 stress controlled rheometer from TA instruments. The quantitative viscosity of each ink was of interest, and also any shear thinning effects observed. Shear thinning would be a sign that the rate of printing might be a factor in the process. Figure 5-7 shows the measured viscosity for a variety of inks tested (averaged over two runs, one stepping from low shear rate to high, the second going backwards from high shear rate to low). There is some shear thinning, but it is not dramatic. It is a safe assumption that over the range of printing rates achievable with the equipment available, shear thinning will not be a large contributing factor. The final viscosity values tabulated for each ink are an average over the stable range of shear rates (i.e., not including the very first two points at low shear rates, which can have high measurement error).

5.4.4 Electrical testing

As well as determining physical ink characteristics that may affect printing, it is also important to look at the electrical characteristics, which are important to the function of the printed pattern. To characterize the resistivity (or, conversely, the conductivity) of each ink, a flat coating on plasma treated glass was produced by spincoating. Inks were filtered with a 25μm syringe filter to eliminate any clumping. Each flat coating was then measured for thickness with a Zygo white light interferometer (a scratch or Scotch tape removal creates a step height for measurement), and for resistance with a standard (student-built) four point probe with thin-film probe tips. Figure 5-8 shows the thickness vs. sheet resistance curves for a variety of Ag inks. Each resistance point plotted is the average of four sheet resistance measurements on the sample.

As expected, the relationship is a negative exponential - as the ink layer grows thinner, the resistance goes up. This illustrates a tradeoff between good electrical performance (better with a thicker layer) and good bonding behavior (better with a thinner layer). It also illustrates that above a certain threshold thickness, the electrical performance does not vary much (i.e., there is a wide range of thicknesses that give good electrical results, which allows the printing process to be more robust).

There should not be any significant effect of the substrate material on the coating behavior of the ink as long as the ink is wetting well, but to check this assumption, some inks were also tested on plasma treated PMMA. Figure 5-9 shows that there is negligible difference in coatings on PMMA as compared to glass. Discrepancies are likely due to experimental variation (the surface of PMMA is not as uniform as glass, and can lead to differences in spincoating behavior).

5.4.5 Summary of ink properties

In summary, Table 5.3 reports the characteristics of all inks purchased, using the manufacturer's reported data when known, and measured data where properties were unknown. With this data now available, experiments to investigate process sensitivities can be carried out.

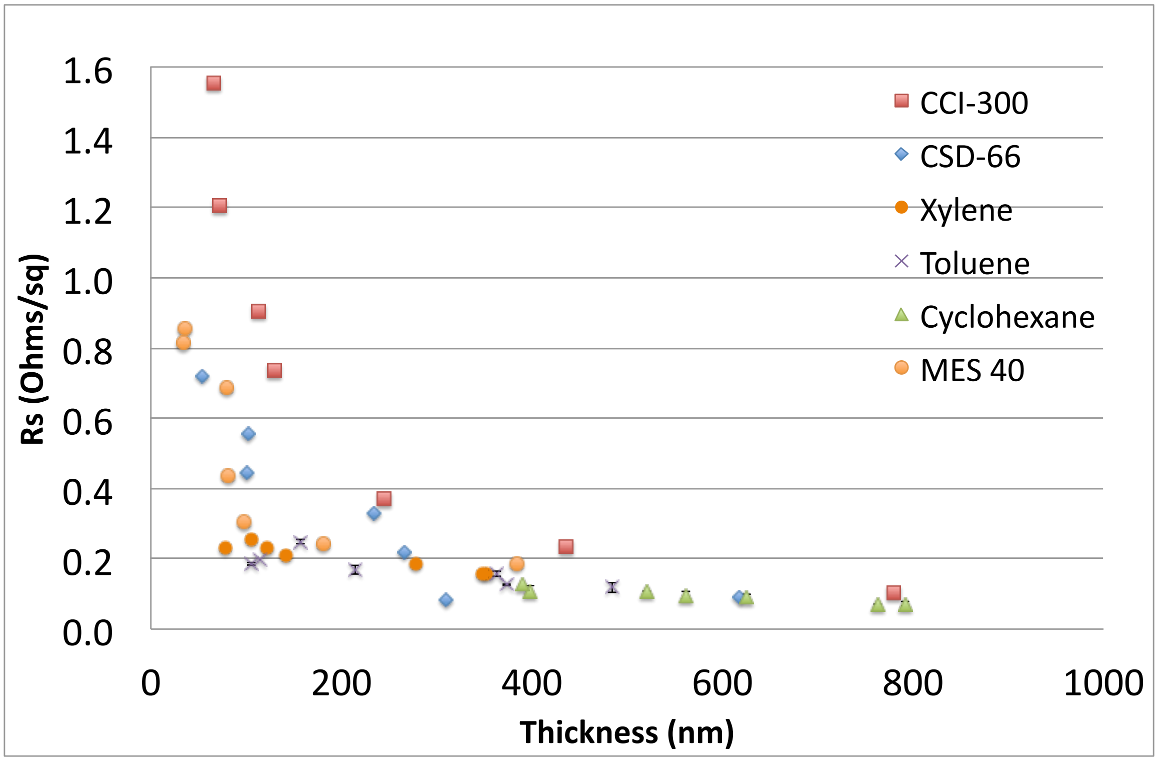

Figure 5-8: Ink electrical characterization, showing an inverse exponential relationship between thickness and sheet resistance.

	CCI-300	Aldrich	CSD-66	Cyclohexane	Toluene	Xylene	MES 30	MES 40	MES 50
Viscosity (cP)	13.0	12.3	75.0	14.4*	2.1*	2.2*	6.2*	5.4*	22.6*
Solids loading (wt%)	20	20	60	45	45	45	30	40	50
Density (g/cm^3)	1.24	1.22	2.25	1.38*	1.14*	1.35*	1.20*	1.44*	1.67*
Surface tension (mN/m)	31.5	29.5	47.5*	21.5*	28.2*	25.7*	26.5*	27.5	26.9*

*Measured data

Table 5.3: Summary of Ag nanoink properties, from testing and from manufacturer's data.

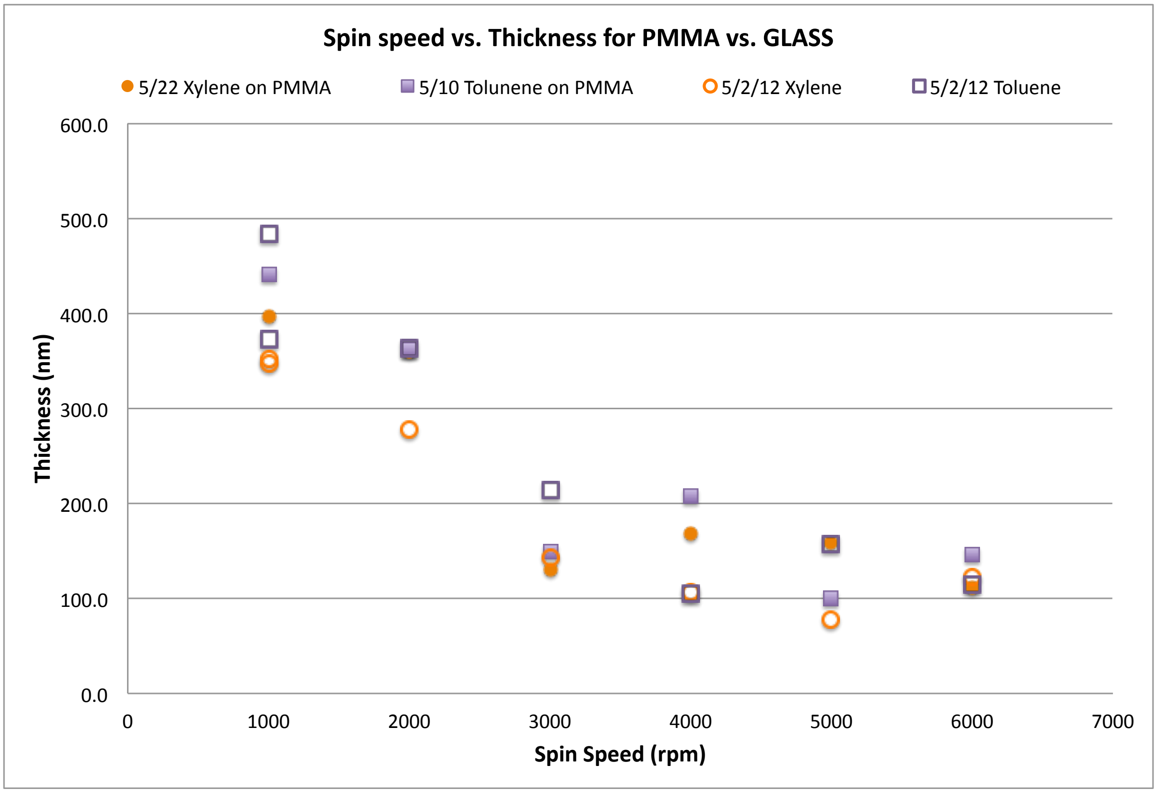

Figure 5-9: Ink electrical characteristics on PMMA and glass, plotting spincoating speed vs. thickness, showing good correlation between electrical performance on glass as compared to the polymer PMMA.

5.5 Equipment and methods

The μCP process consists of coating a stamp with ink, and transferring that ink to a substrate. This section will describe how the stamp is made, how it is coated with ink, and the equipment used for the transfer.

5.5.1 Stamp making

A 4" silicon wafer was coated with SU8 polymer resist, and exposed through a chrome mask with the desired pattern. The particular formulation of SU8 from the SU8 series was chosen based on the data sheet recommendations for the thickness of the layer desired (for any given pattern the aspect ratio was kept roughly at 1).

Then Sylgard 184 PDMS (Dow Corning) in a ratio of 10:1 base to curing agent is cast against the patterned wafer. A aluminum clam shell mold, designed by Joe Petrzelka, holds the wafer with a spacer above an aluminium backplate. Casting PDMS in this mold creates a more uniform stamp (with thickness determined by the spacer) than simply pouring the PDMS over the wafer in a petri dish, as is more common. The stamp is then cured at 60°C for 4 hours, and demolded from the wafer.

There is new work directed at making cylindrical stamps, but the technique was not yet available at the time of the author's experiments [152].

5.5.2 Printing roll

The printing equipment used was designed by Joe Petrzelka as a precision positioning stage for roll-based contact lithography [10]. Flexural and air bearings driven by non-contact voice coil actuators allow precise control of both position and force of the roll. The control scheme used for this equipment is critically important for achieving high resolution. Using force control allows the machine to adapt to variations in the roller, stamp, and substrate, instead of position control where even a few microns of error can be enough to cause stamp collapse.

Figure 5-10 shows the printing roll, which is mounted above a linear stage fitted with a vacuum chuck for holding substrates. It is this linear stage that moves under the roll. The rolling direction is not active - the roller passively turns, driven by the motion of the substrate.

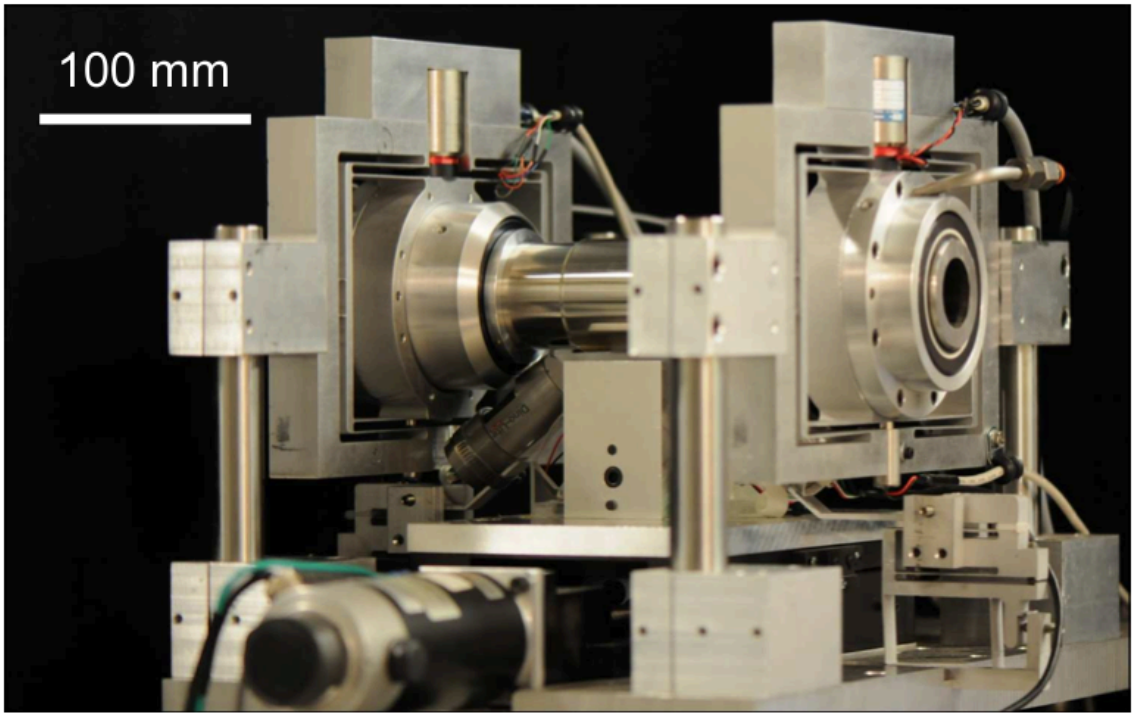

Figure 5-10: Printing roll equipment used in empirical testing of μCP process [10]

5.5.3 Standard procedure

In a typical experiment, the procedure is as follows:

- Turn on power to printing roll, let warm up for at least 30 minutes. Be sure to turn on air as well as electrical power before trying to print, although not necessary for warm up.

- Set the print roll to position control, at position -0.0015m with 0 tilt. Hit Set Calibration Point, and then Calibrate.

- Wash the PDMS stamp and desired substrate in isopropyl alcohol, dry with towel or air stream.

- Plasma treat the PDMS stamp, substrate, and one glass slide at ~250W for 30 seconds.

- Apply the PDMS stamp to the print roll, starting from the center and pressing outward to avoid trapped air pockets. A fresh stamp that has been plasma treated will be sticky enough to adhere. (Stamps last roughly six weeks before drying out and losing adhesion even with plasma treatment.)

- Change the printing roll mode to force control, set at desired force (-3.0N is a good starting point), roll applied stamp over a clean glass slide. Check that the roller is making good contact, hit Set Calibration Point. Roll off the slide into empty air, hit Calibrate.
- Place the plasma treated glass slide on spincoating chuck, place ~0.5mL of ink in the center (through a syringe filter if clumping is an issue), spincoat at desired parameters (6000 rpm for 30s is a good place to start for inks that do not dry out, 800rpm for 10s is a good starting point for volatile inks.)
- Place coated slide (i.e. the inkpad) on the vacuum chuck on the linear stage. Hit vacuum switch with foot to secure inkpad. Make sure roller is in force control, and roll the stamp over the inkpad.
- Release vacuum switch, remove inkpad, swap in the plasma treated substrate (tweezers help). Hit vacuum switch again once substrate is in place.
- Roll the opposite direction back over the substrate. Watch the forces reported at each end of the roller, displayed in software. If force indicated goes below 0 or above the maximum 25, then the roller has not made good contact, and has "tipped" off the side of the substrate. In this case a failed print will be visible under the microscope, but not always by eye (thus the reason to watch the forces).
- Anneal the printed substrate in an oven at the manufacturer's recommended temperature, or a temperature below T_g of the polymer, whichever is lower. Generally, 150°F for 20 minutes is a good starting point. Most inks in the author's experience will change color (usually yellow to gray) and indicate the solvent has been removed.

The specific experimental parameters used depend on the ink, pattern, and substrate, but an example of an ideal resulting pattern is shown in Figure 5-11. This particular experiment used a PDMS stamp with a 5μm hex pattern and Ag ink with 40% loading in a Mesitylene carrier (NanoMas). The inkpad used was a glass slide was plasma treated in air plasma for 30 seconds at 250W, then spincoated with the ink at 800rpm for 4 seconds. The PDMS stamp was plasma treated with the same parameters as the inkpad, applied to the printing roll, and rolled over the inkpad under force control at 3N. The inkpad was replaced with a clean plasma treated slide, and printed with the coated stamp (also at 3N). The macroview

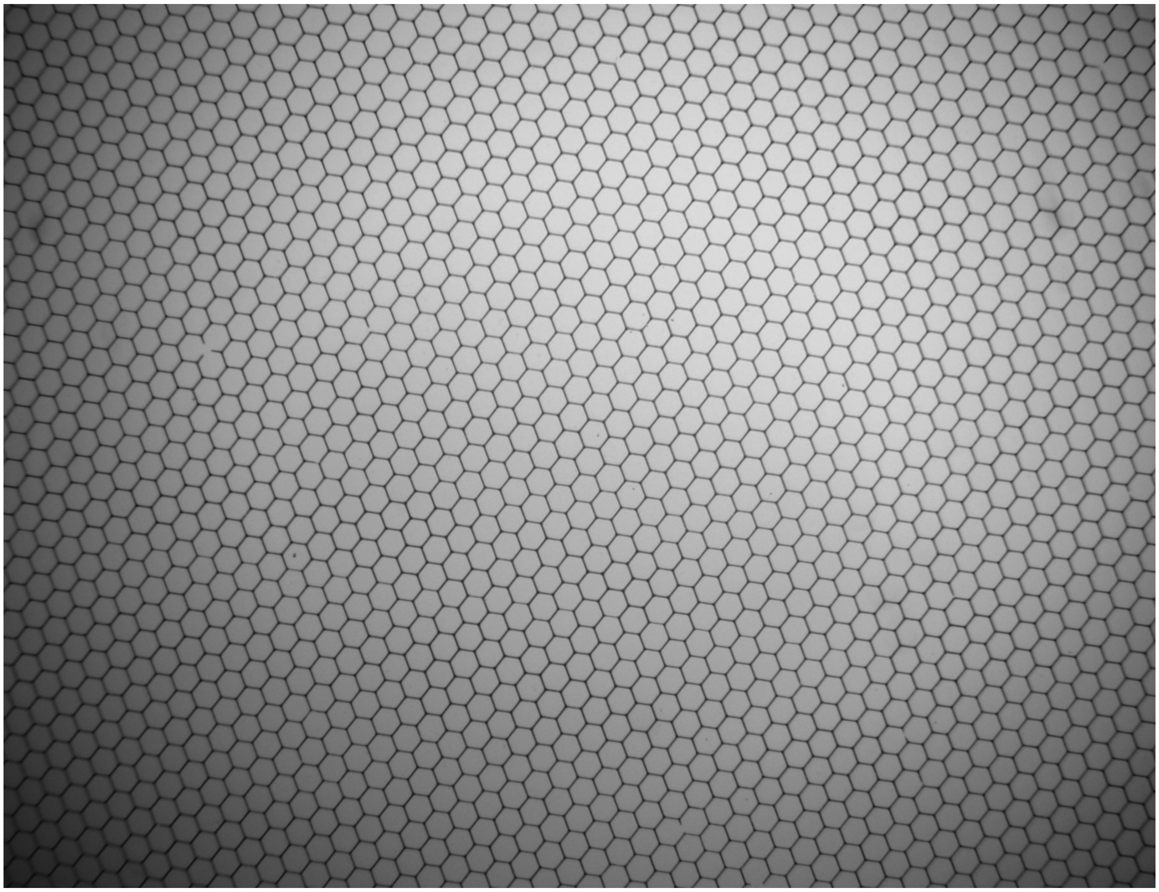

Figure 5-11: Example image of ideal results from Ag ink printing of hexagonal pattern with 5μm line width, microscope view

of an ideal print, for the 5μm hex pattern at least, is hardly even visible (see Figure 5-12 , which shows the overall slide for the same experiment as shown in Figure 5-11).

5.6 Ink volume transfer experiments

Once a reliable protocol for good pattern transfer was established, it was of interest to investigate how much of the ink is transferred during each print. A simple inspection of the stamp shows that ink residue is left behind, so it is not 100% transfer. A short discussion of this topic in Kwak 2010 [8] suggests that the percentage of ink transferred depends on the ratio of the surface energies of the two materials, however the concept is not well explained or tested. In another paper [151], there is an investigation into "the transfer and volume partition of liquid droplets in the mm size range from one unpatterned solid surface to another for varying rates of plate separation. The fastest separation rates showed that

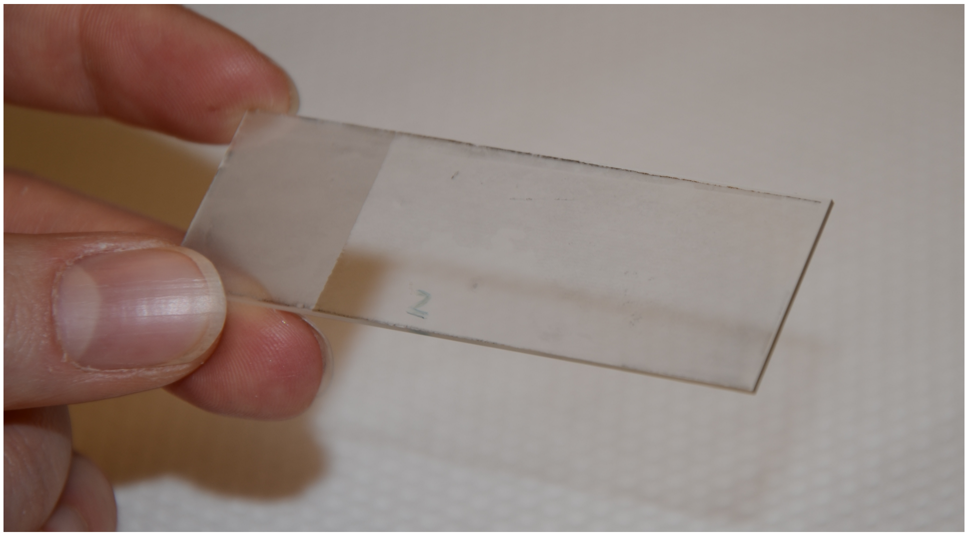

Figure 5-12: Example image of ideal results from Ag ink printing of hexagonal pattern with 5μm line width, no magnification overall slide view

the liquid volume was equally partitioned among the two surfaces. For slow separation rates, ...volume partition was completely determined by the receding contact angles on the respective surfaces. In the limit of small Bond number, the partition ratio was independent of the liquid volume used." This would suggest that printing rate plays a role, and that at slow rates the energy ratio hypothesis may be correct, and at faster rates, the ink splits in a manner independent of the surface energies.

To investigate the ink splitting behavior, a series of experiments was carried out where a PDMS stamp was inked once, and then printed onto a series of substrates. Each print was measured with a Zygo white light interferometer to determine thickness. If the ink transfer ratio is determined by the ratio of surface energies (plasma treated PDMS and plasma treated glass being roughly equal), then the thickness of each successive print should be halved.

Protocol

Ink: CSD-66

Stamp: PDMS plasma treated 5μm hex pattern

Inkpad Coating: 6000 and 7000 rpm for 10 sec (no re-inking between printing)

Printing Force: -5N

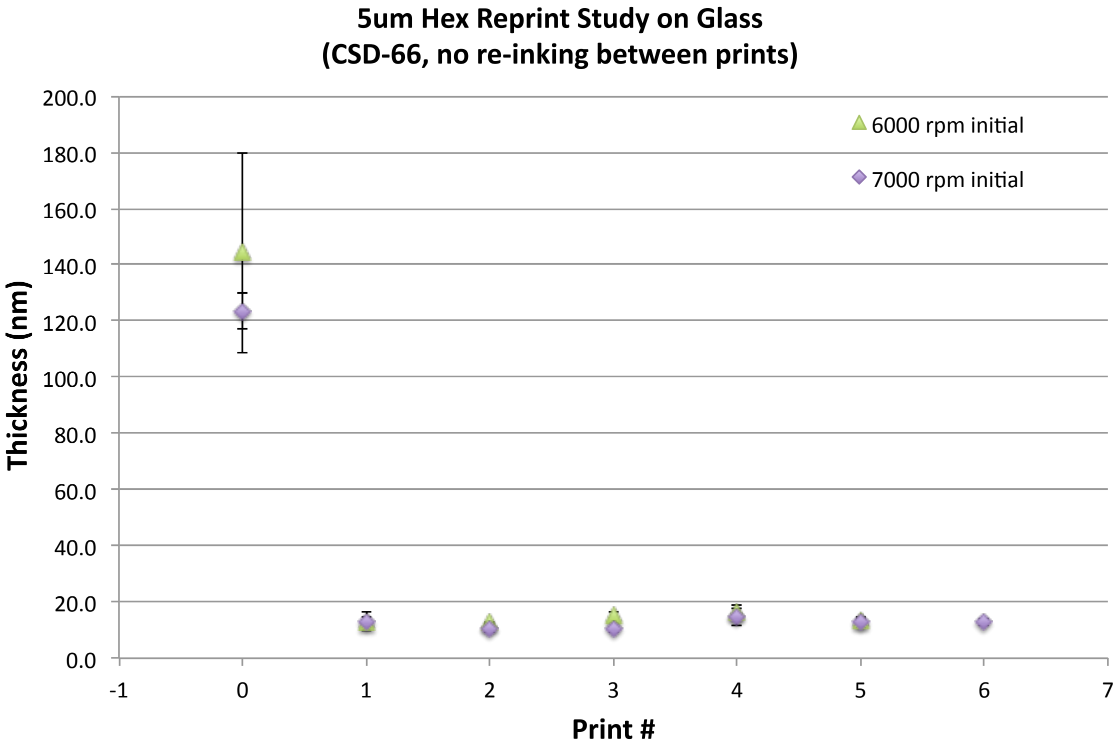

Figure 5-13: Thickness of successive prints of CSD-66 on glass, from varying initial inkpad thicknesses, showing that each successive print has the same thickness (rather than decreasing by half each time as hypothesized).

Substrate: Glass

Output: Thickness of ink, measured with Zygo interferometer

Hypothesis: Thickness will decrease by half each re-printing

The measured thickness of the successive prints is shown in Figure 5-13. Each point is the average of three thickness measurements from each print, although the uniformity is such that the errors bars are barely visible. The thickness of each print is staying constant - not supporting the hypothesis that it will decrease by half after each print. Also, the thickness seems to be the same for the inkpad coated at 6000rpm and 7000rpm. This suggests that another mechanism is at work, independent of the initial inkpad thickness or the ratio of surface energies.

Looking at the geometry of the printed pattern (or the coverage) in addition to the thickness is helpful. Figure 5-14 shows a top view of each successive print. The red and blue colors are assigned by software to demarcate two planes of best fit at differing heights - in

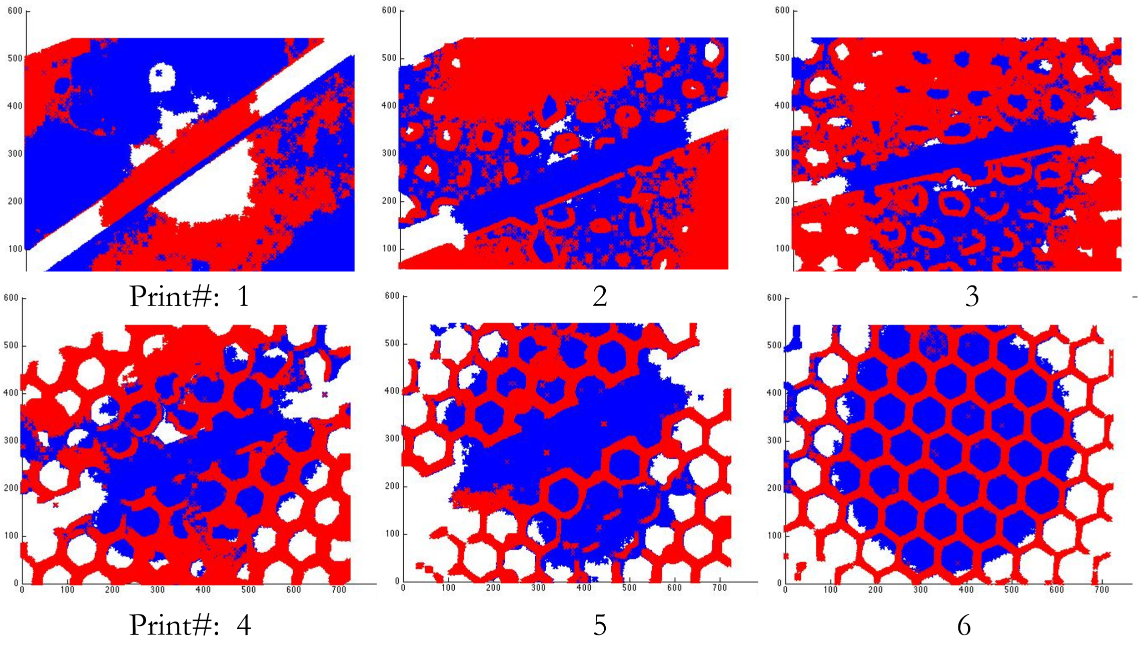

Figure 5-14: Coverage of successive prints of CSD-66 on glass, showing improving feature quality with each print.

an ideal print, the base plane would be the substrate in one color, and the printed pattern would be the other color. (The horizontal scratches evident in some prints are intentional, to create a known step height location to measure the substrate.) Figure 5-14 shows that the first few prints were a mess - the inkpad was so thick that the pattern smeared everywhere. Successive prints, as the inkpad thickness lost volume (no re-inking), showed better pattern replication.

If the print thickness is not decreasing, but the print quality is increasing, what happens if the inkpad starts out thinner, so that the print quality is good from the very first print? Would the thickness then follow a halving rule? To test this, an additional set of experiments was carried out, with a thinner starting inkpad. The coverage from this set of experiments (using spincoating of 7000rpm for 30 seconds, not 7000 rpm for 10 seconds) is shown in Figure 5-15.

Clearly the print quality is better here. Instead of the print quality increasing with each print, the first print looks slightly smeared, subsequent prints are nearly ideal, and then gaps start appearing where no ink is transferred at all. This seems to indicate that instead of the thickness decreasing by half, the ink simply does not transfer below a certain threshold. This does make physical sense, because the printed patterns are about 20nm

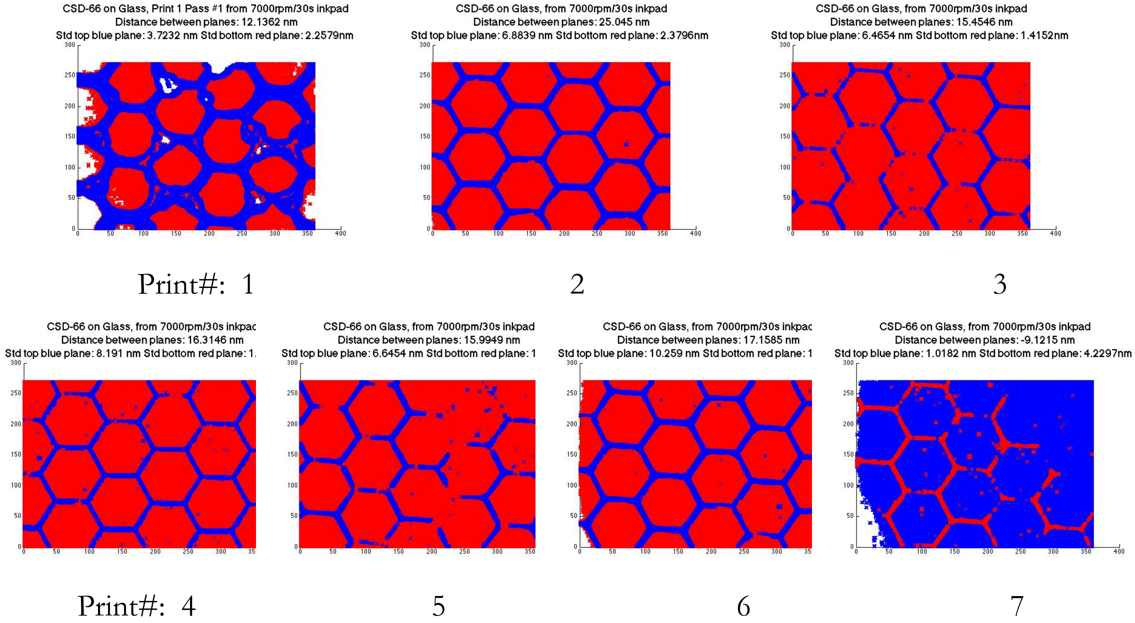

Figure 5-15: Coverage of successive prints of CSD-66 on glass, starting with thinner inkpad for better initial print quality, showing increasing voids with each print.

thick but the particle diameter is only 10nm, so you can't get much thinner before nothing is left to transfer.

Figure 5-16 shows the thickness of this set of experimental prints, plotted with the prior experiments. There is no significant difference, so the hypothesis that the print quality was interfering with transfer behavior is not supported. It looks like a similar amount of ink is transferred every print, until the ink runs out and then nothing is transferred. Additional runs of reprints exploring plasma treatment of the glass vs. plain glass also showed no significant difference in reprint thickness, as did trying PMMA instead of glass.

5.7 Design of experiments

5.7.1 Choice of factors

When designing a set of experiments to investigate the process sensitivities of a manufacturing method, there are many possible factors to consider. For μCP, possible process inputs might include:

Substrate properties: Surface chemistry (plasma or chemical treatment), surface roughness, substrate temperature

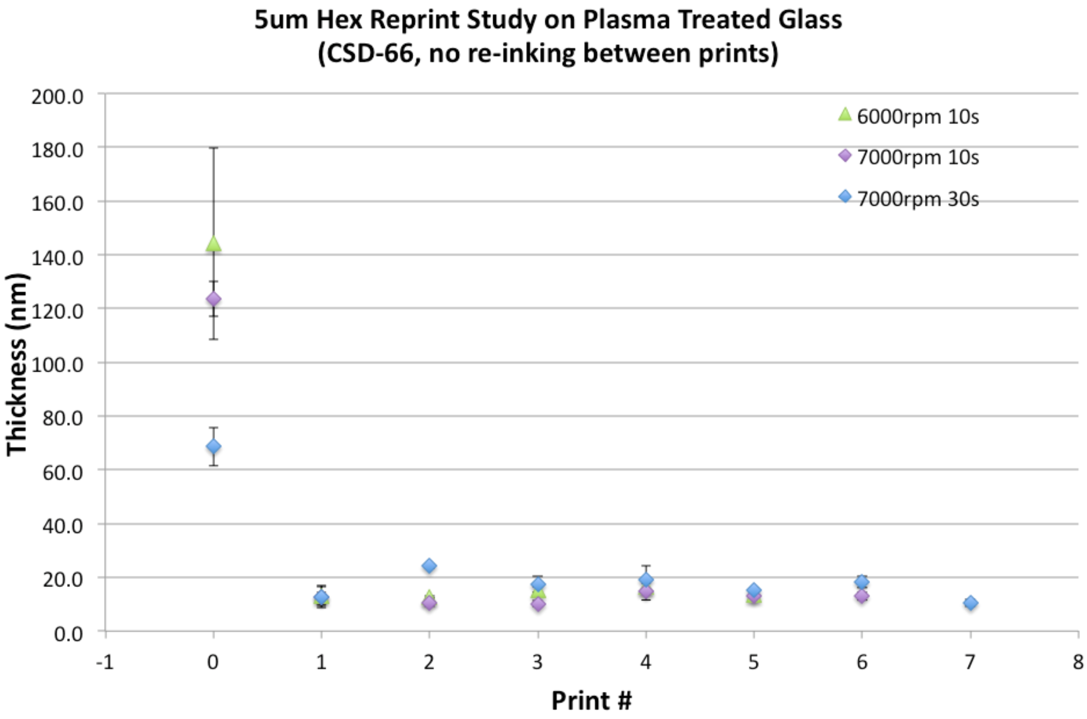

Figure 5-16: Thickness of successive prints of CSD-66 on glass, with thinner initial inkpad for good print quality, still showing that each successive print has the same thickness (rather than decreasing by half each time as hypothesized).

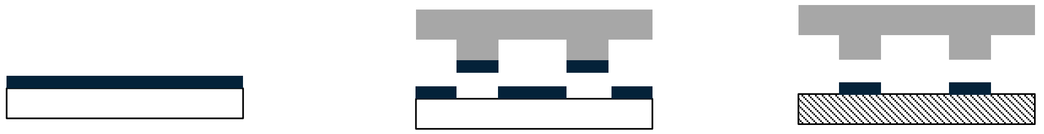

Step 1: Coating Inkpad	Step 2: Inkpad to Mold	Step 3: Mold to Substrate
Surface Energy $S_{eq}=\gamma_{SV}-(\gamma_{SL}+\gamma_{LV})$	Film Stability & Dewetting $q_c=\left(\frac{A_{\text{eff}}}{2\pi\gamma h_r^4}\right)^{1/2}$ $q=\frac{\Delta P h^4}{12\mu L}$	Work of Adhesion $W_{mf}<W_{sf}$

Figure 5-17: Summary of governing equations for transfer, excerpted from Chapter 3.

Stamp properties: Feature size, aspect ratio of stamp, stiffness of PDMS stamp, surface treatment of the stamp (plasma or chemical treatment)

Ink properties: Viscosity, chemical additives, density, solids loading, volatility

Machine inputs: Spin parameters such as time and speed, printing force, printing rate, cleaning procedure between stamps

Post-processing: Annealing temperature, annealing time

As well as many potential process inputs, there are also several process outputs that might be of interest:

Physical properties: Feature dimensions, feature thickness, adhesion

Electrical properties: Resistivity, defect rate (i.e. holes in transferred pattern)

Manufacturing concerns: Cost, rate, quality of feature dimensions and thickness (i.e. variation)

To narrow down the list of potential process parameters to the ones which are likely relevant, it is useful to recall the discussion of transfer theory from Chapter 3. Figure 5-17 shows a summary of the governing equations for each step of the transfer process. Both Step 1 (coating the inkpad) and Step 3 (transfer from stamp to substrate) depend highly on the surface energies of the ink, stamp, and substrate. Because PDMS is the accepted standard for stamp making material in soft lithography literature, the stamp material will not be varied, and will not be a factor in the model - but the substrate and ink can certainly vary. In Step

Input Parameters	
Ink Density	
Ink Solids Loading	
Ink Viscosity	
Ink Surface Tension	
Inkpad Thickness	
Feature Size	**Output**
Substrate surface energy	Pattern Thickness
Printing force	Pattern Geometry

Table 5.4: Input and output factors in the μCP process that are selected (from understanding of governing equations) as likely to be statistically significant to a process model

2, the film stability depends on the feature size and the inkpad thickness, so those should be included, and dewetting depends partly on printing force. The ink viscosity will affect spincoating behavior, and the density and solids loading may influence the final thickness of the pattern (more solids mean a thicker pattern left behind after solvent evaporates).

With these informed choices for inputs, what potential outputs are of most interest? The thickness of the pattern directly affects the functional requirement of conductivity, and the pattern geometry is also critical to determining whether the stamp features were accurately replicated. Electrical properties are of course important, but unlike PEDOT where the chemical structure and the physical handing of the ink can change the resistance of the material, the inherent conductivity of silver is not affected during printing. (It may be somewhat dependent on annealing, but that part of the process is not within the scope of this investigation.) Therefore the electrical properties can be reasonably correlated to the cross sectional area of the printed pattern, which can be determined from the thickness and geometry anyway.

Table 5.4 summarizes the factors chosen for further study.

5.7.2 Choice of factor levels

Not all factors can be varied independently - the ink density, solids loading, viscosity, and surface tension cannot be tuned within the ink. What can be varied is the ink chosen, and then the results can be correlated to the properties of those inks. Similarly, the substrate energy is difficult to tune for a given material, but different materials can be specified. So,

	MES 40	CCI-300	CSD-66
Viscosity (cP)	5.4*	13.0	75.0
Solids loading (wt%)	40	20	60
Density (g/cm^3)	1.44*	1.24	2.25
Surface tension (mN/m)	27.5	31.5	47.5*

*Measured data

Table 5.5: Ink properties of selected inks for DOE, chosen to give a good range of solids loading, viscosity, and surface tension values.

the five factors for a DOE become ink, inkpad thickness, feature size, substrate, and force.

Inks

From the broad range of inks characterized in Section 5.4, three were chosen to give a good range of viscosity, density, and surface tension. (Also, practical constraints such as drying time eliminate some choices, where experimental procedure cannot be completed before volatile solvents evaporate.) The three inks chosen are CCI-300 (Cabot Corporation), CSD-66 (Cabot Corporation, or Sun Chemical), and MES 40 (40% solids loading in Mesitylene, by request from NanoMas). See Table 5.5 for a summary of the properties of these inks.

Inkpad Thickness

Because each ink has a different viscosity, the spincoating behavior is different, and the same spincoating speed and time will produce an inkpad layer of differing thicknesses. To standardize the inkpad thickness variable, a nominal thickness t_o was chosen (from experience of what seems to work well), and then the spincoating parameters to produce t_o as well as thicknesses 75% of t_o and 125% of t_o were determined for each ink. Figure 5-18 shows that the inkpad thicknesses of the CSD-66 ink and the CCI-300 ink were able to be closely matched. However the MES 40 ink has additional constraints - spincoating any slower than shown does not adequately spread the ink over the inkpad slide, and spincoating any faster than shown causes the solvent to evaporate. For these reasons, the thickness of the MES40 ink does vary from 75% to 125% of a nominal thickness that works well, but does not match the thickness of the other two inks.

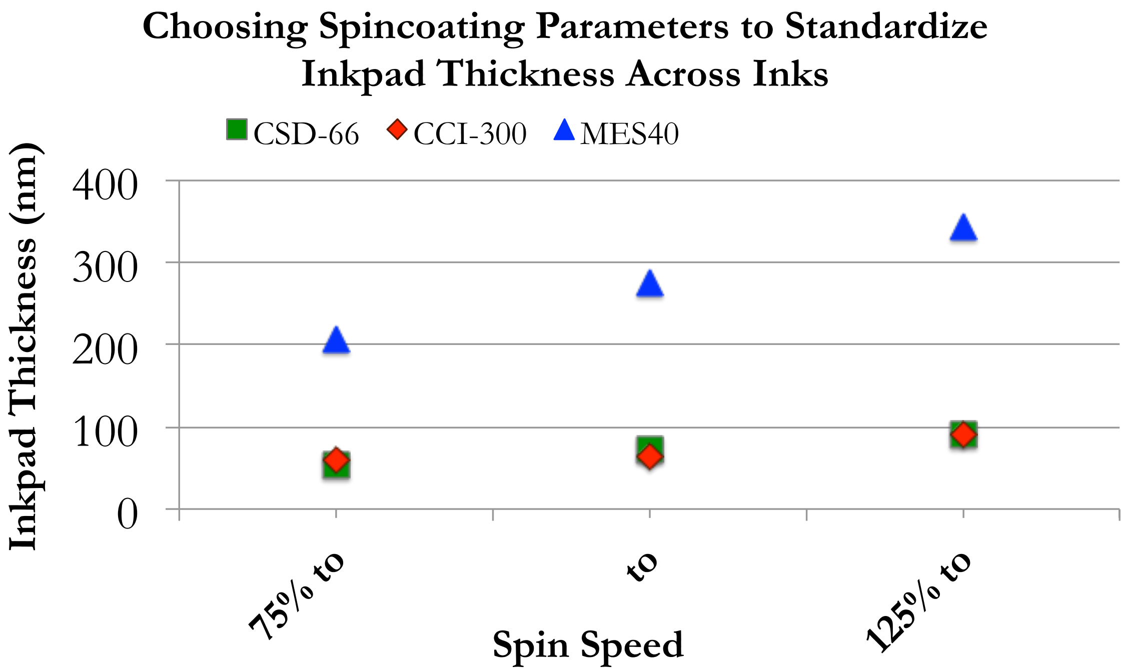

Figure 5-18: Inkpad thickness standardized around a nominal value t_o.

Feature Size

Standard flexography is capable of reproducing features down to 70 μm, which is near the limit of the naked eye. For printing applications like newspapers and magazines, this is sufficient. But because the goal of this work is to push the limits of resolution, the largest pattern is chosen as 50μm lines, the middle pattern is chosen as 20 μm lines, and the smallest pattern is chosen to be 5μm hexagons. The hexagonal pattern was chosen based on other examples in literature, as a pattern desirable in industry for printing conductive grids on solar cells. In addition, it is a good test of printing capability, because printing corners poses a challenge over straight lines, and printing a continuous pattern is more desirable than printing square dots (which also have corners, but no electrical continuity).

Substrate

Glass was chosen as a substrate because it has favorable surface energy. PMMA was chosen because it is common in microfluidics, which is the industry that provided the motivation for this work. Polyethylene terephthalate (PET) was chosen as the third substrate, because

$K_I = K\rvert_{A\to 0, A/P\to 0} = \frac{2\pi}{3}\frac{AP}{(P+1)^2}\left[-\log\cos\left(\frac{\pi}{2}\frac{P}{P+1}\right)\right]^{-1}$	$S_c = \pi/4 \cdot K$
a) Dimensionless Stiffness K	b) Dimensionless Collapse Pressure S_c

Table 5.6: Calculation of minimum force for collapse of 5μm hexagonal pattern. [16]

it is the most common substrate for printing flexible electronics, as observed at the August 2012 FlexTech workshop ("Printing Electronics: Ink/Substrate Interactions").

Force

The limit on force is going to be the collapse of the most sensitive stamp pattern. Of the 50μm lines, 20μm lines, and 5μm hex pattern, the most sensitive is the hex. If the pressure is too high, the first defect mode is roof collapse, where the centers of the hexagons droop down and touch the substrate. The force at which this occurs can be calculated as follows: first, find the dimensionless stiffness (in this case the features are very short and far apart, A<<1, A <<P), with the equation shown in Table 5.6 a [16]. (For the 5μm hex pattern, A and P are about 1 and 15, respectively). Then the collapse displacement X_c can be found, from which the dimensionless collapse pressure $S_c = K * X_c$. For roof collapse, the lower bound on dimensionless collapse pressure S_c is as shown in Table 5.6 b, and turns out to be about 0.75K.

Then dimensional collapse pressure σ_c is S_c times the elastic modulus E_o, about 1.5 to 2 MPa for PDMS. With these calculations, the roof collapse force for the 5μm hex pattern across a 75mm slide is f_c=7.5N, which becomes the upper limit on force. The lower limit on force is the capability of the printing roll. While not an exact limit, by practical experience at forces less than ∼1N, the stamp does not always make good contact.

To stay well away from both limits, the forces in the DOE are chosen to be:

1/2f_c=3.75N

1/3f_c=2.5N

Summary

In summary, for the five factors in this DOE, the levels chosen for each factor are given in Table 5.7.

Factor	Low Level	Medium Level	High Level
A Ink	MES 40	CCI-300	CSD-66
B Inkpad Thickness	75% t_o	t_o	125% t_o
C Feature Size	5um	20um	50um
D Substrate	PET	PMMA	Glass
E Force	-	2.5N	3.75N

Table 5.7: Summary of DOE factor levels.

5.7.3 Choice of Taguchi L18

With four three-level factors, and one two level-factor, the Taguchi L18 orthogonal array was chosen as the model for design of experiments. The Taguchi L18 array serves as an excellent screening DOE to narrow down a list of multiple inputs to a more manageable range. It can handle two levels for factor 1 and three levels for factors 2 – 7 (although in our case, we only have five total factors, not seven). With this many factors, 18 runs does not allow testing every possible combination, but compared to the more traditional "fractional factorial" design the L18 is far more powerful and orthogonal (balanced). [183] This design however only allows testing for linear main effects, not interactions or second order effects.

The DOE table of runs, filled in with the choice of factor levels from the preceding section, is given in Table 5-19. Chapter 6 will go over the results and analysis of these experimental runs.

	Force	Substrate	Feature Size	Inkpad Thickness	Ink
Run	A	B	C	D	E
1	2.5N	PET	5μm	75%t_o	MES 40
2	2.5N	PET	20μm	t_o	CCI-300
3	2.5N	PET	50μm	125%t_o	CSD-66
4	2.5N	PMMA	5μm	75%t_o	CCI-300
5	2.5N	PMMA	20μm	t_o	CSD-66
6	2.5N	PMMA	50μm	125%t_o	MES 40
7	2.5N	Glass	5μm	t_o	MES 40
8	2.5N	Glass	20μm	125%t_o	CCI-300
9	2.5N	Glass	50μm	75%t_o	CSD-66
10	3.75N	PET	5μm	125%t_o	CSD-66
11	3.75N	PET	20μm	75%t_o	MES 40
12	3.75N	PET	50μm	t_o	CCI-300
13	3.75N	PMMA	5μm	t_o	CSD-66
14	3.75N	PMMA	20μm	125%t_o	MES 40
15	3.75N	PMMA	50μm	75%t_o	CCI-300
16	3.75N	Glass	5μm	125%t_o	CCI-300
17	3.75N	Glass	20μm	75%t_o	CSD-66
18	3.75N	Glass	50μm	t_o	MES 40

Figure 5-19: Taguchi L18 array - List of runs in design of experiments.

Chapter 6

Manufacturing Process Model for Silver Ink μCP

Chapter 5 discussed the characterization of a range of Ag inks, the standard experimental procedure used for printing, and the design of a set of experiments to explore the μCP process. Chapter 6 now discusses the results of the completed DOE, and the development of a process model from the data collected (informed by an understanding of the physical mechanisms at work). This process model is able to predict printing behavior of other inks (based on their known properties), and of other substrates (based on their surface energy). This shows that the model developed is applicable to more general situations, and can be used and extended by other researchers. A short exploration of printing carbon nanotubes (CNTs) is also described. Although the properties of the CNT paste are outside the current prediction capabilities of the model, the same trends are observed as with Ag ink, and the model could be extended by incorporating a viscosity term dependent on shear rate.

Finally, the end of this chapter proposes future work that is now of interest, enabled by the contributions of this thesis. Chapter 7 will summarize the conclusions and contributions of the entire work.

6.1 Thickness measurements

One of the two output metrics of the DOE to investigate Ag ink μCP is the thickness of the printed pattern. To determine thickness of an experimental run (an experimental run consisting of one printed sample - no replicates), four areas on the sample were measured with a white light interferometer (Zygo). Using MatLab, each of the four areas was analyzed by fitting two planes of best fit to the data - one plane corresponding to the base substrate, and one plane fitted to the printed features (a typical example is shown in Figure 6-1). The difference between the height of the two planes was taken as the thickness of the print for that area. The four areas taken from each sample were averaged to provide an overall average thickness for that experimental run.

6.1.1 Line thickness profile

The "coffee stain" effect had been noted from literature review as a potential problem in liquid ink transfers. The evaporating solvent in a deposited solution can in some cases force the particles in solution to the outside of the wetted liquid area, leaving a "coffee stain" or ring of particles at the edges of the desired pattern. To determine if this was happening in the μCP process, the Zygo white light interferometer was used to interrogate the thickness profile of a printed pattern. Figure 6-1 highlights a typical μCP result for further investigation of coffee stain effect.

Figure 6-2 shows a selected portion of the data from Figure 6-1, with the 3D data points from the Zygo colored by z-height, rather than by planes of best fit. This shows that the thickest portions of the printed hex pattern are at the centers of the lines, and particularly thick at the corners of connecting lines. This is the opposite behavior of coffee staining, which would have the thickest portion of the print at the edges of the lines.

Figure 6-3 is an example of a printing defect, but it gives additional evidence that the thickest portion of the ink is at the corners of the printed pattern. In this case, the ink was almost too dry to transfer (the experiment was delayed due to an error in the software, and the ink dried while the author fixed the equipment). The only places where the ink remained wet was at the corners of the hexagonal pattern, where the ink was thickest and the solvent had not yet fully evaporated. The print therefore shows only the corners have transferred.

From the Zygo data showing the ink height profile, and experimental evidence, we can conclude that coffee staining is not a problem within the experimental parameters tested.

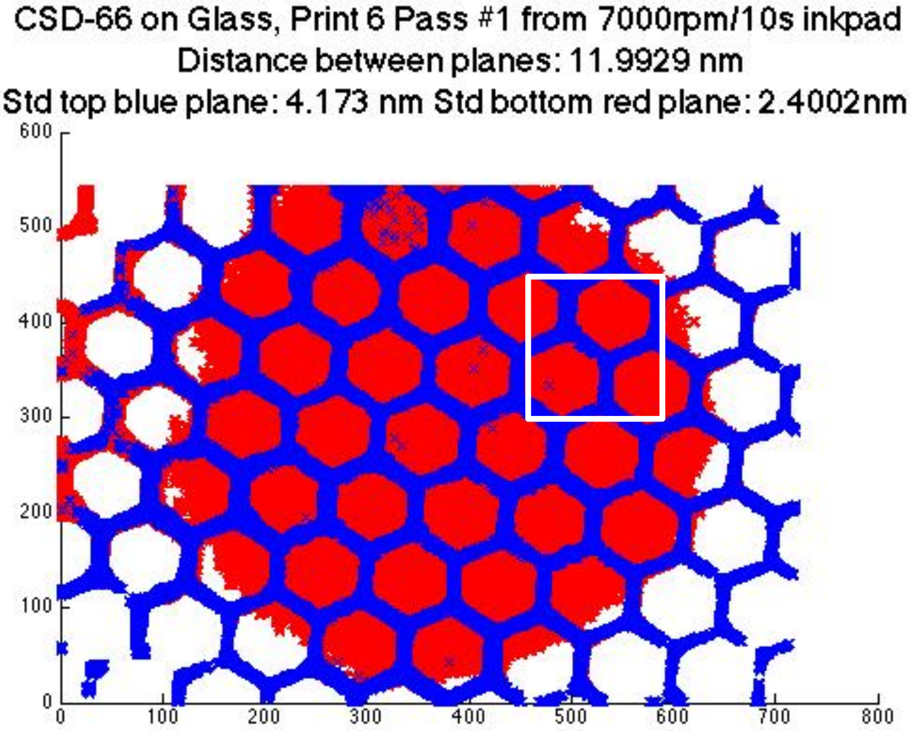

Figure 6-1: Typical μCP experiment, 5μm hex pattern, printed with CSD-66 ink onto glass, with planes of best fit in MatLab corresponding to base substrate and printed pattern. Highlighted square indicates section of print to be investigated for evidence of coffee stain effect.

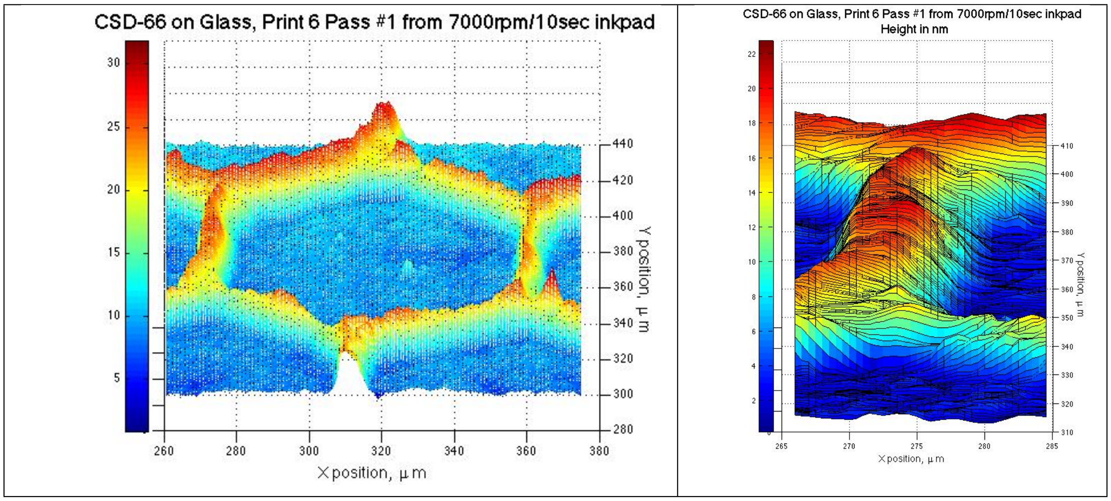

Figure 6-2: Height map of a selected portion of 5μm hex pattern, showing that the thickest part of the print is concentrated in the centers of lines and at the corners of connecting lines. No evidence of coffee staining effect.

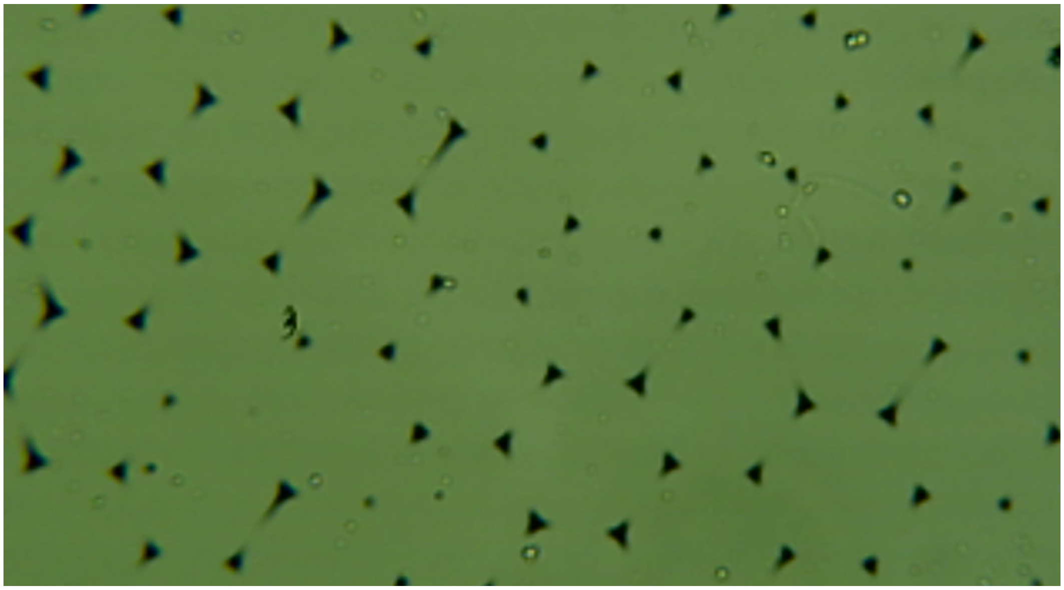

Figure 6-3: Printing defect in 5μm hex pattern, where experimental delay caused the ink to evaporate more than normal. Only corners of the pattern have transferred, indicating that the thickest ink is at the corners, where the solvent has not yet evaporated.

6.2 Geometry measurements

The second of two output metrics of the DOE to investigate Ag ink μCP is the geometry of the printed pattern. There are many metrics that could be used to represent the accuracy of the geometry of the pattern, including things like edge roughness and defect rate (holes in the pattern). But for a screening experiment where the goal is to determine mainly how well the printed pattern matches the stamp, the metric chosen is the coverage ratio. The coverage ratio is defined as the ratio of the printed area coverage to the stamp area coverage. This can also be thought of as the actual coverage divided by the ideal coverage.

The stamp area coverage is a constant determined for each pattern (50μm lines, 20μm lines, and 5μm hexagons) by MatLab image analysis of an area of the PDMS stamp with that pattern. Image processing is able to determine the area covered by the protruding pattern features, which when divided by the area of the overall image gives a percentage coverage. (For instance, regular 50μm lines with 50μm spacing between lines would give a coverage of 0.5, or 50%.)

The printed area coverage is determined in the same manner. Figure 6-4 shows the steps in the image processing. First the microscope image of the printed pattern (Figure 6-4 a) is converted to binary colors using a threshold value to define the line between black and white

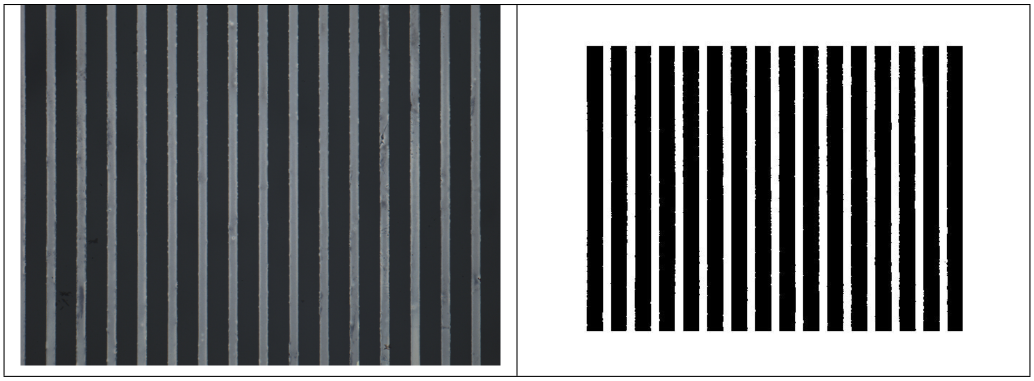

a) Typical original image of printed 50μm line pattern

b) Image converted to binary black and white

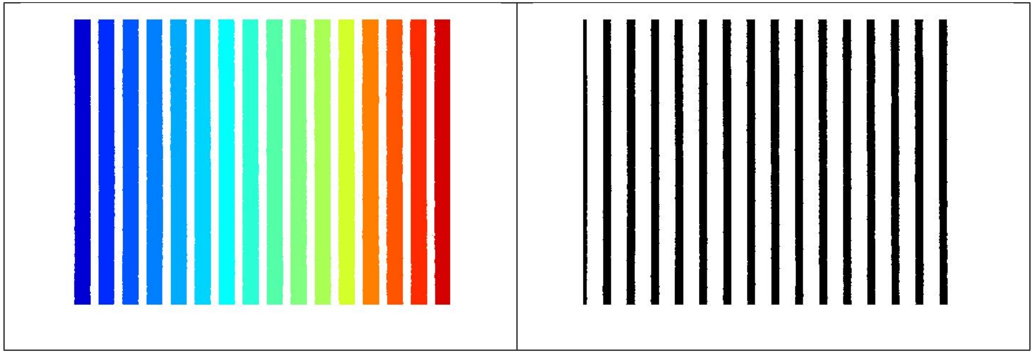

c) Image with connected areas in the background labeled and identified in color

d) Image of isolated printed features, with areas smaller than a given pixel area removed (dust specks and optical anomalies)

Figure 6-4: Example of MatLab Image processing for 50μm line patterns. Original microscope image shown in a), converted binary image is shown in b). Connected background areas are labeled and shown in color in c), and then the isolated printed features are shown in d) (after a cleaning for small outlying areas). The printed area coverage is calculated as the area of the printed features divided by the area of the overall image.

(Figure 6-4 b). Then, the software identifies connected areas of the black background area, and labels each connected background area block with a color (Figure 6-4 c). Connected background areas are then removed, along with areas smaller than a given pixel threshold (a cleaning steps for dust and optical anomalies). The remaining area is divided by the image area to give the printed area coverage (Figure 6-4 d).

The coverage metric, then, is the ratio of the printed coverage to the stamp coverage.

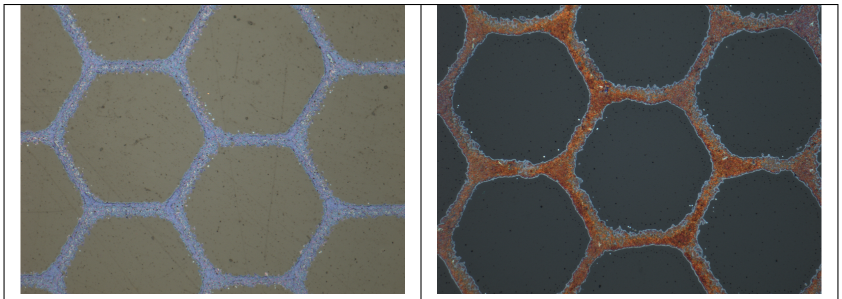

a) Run 1, 5μm hex | b) Run 7, 5μm hex

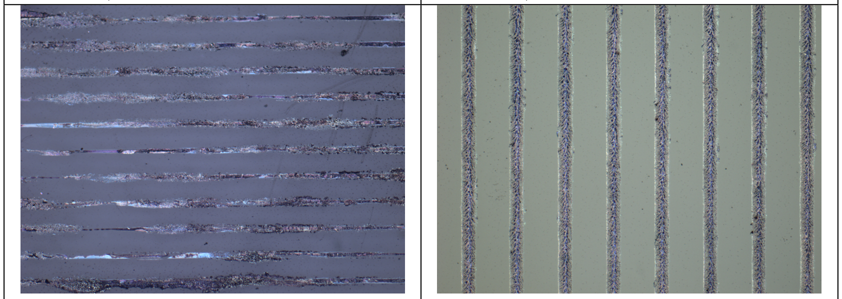

c) Run 11, 20μm lines | d) Run 18, 50μm lines

Figure 6-5: Clumping observed in runs 1, 7, 11, and 18. These runs all used MES40 ink, with known clumping tendencies, and are removed from consideration in the process model.

6.3 Analysis and interpretation of experimental data

All 18 experimental runs from the DOE described in Section 5.7 were analyzed as described above, resulting in thickness and coverage measurements from each run. It was expected that some runs would be so poor as to be regarded as failures, and not used in developing a process model. (In fact this is necessary, otherwise the limits of the process have not been tested). This was indeed the case, and the runs eliminated as outliers are shown below.

6.3.1 Elimination of runs with anomalous thickness

Most thickness measurements fell in the 25-60nm range. But for the MES 40 ink, in some runs results of 450nm and higher were observed. The provider of this ink has indicated that clumping can be a problem (especially since the MES40 ink was made upon request, and was not optimized for performance), and even though the ink was dispensed through a filter, visual inspection of these very thick prints indicates that clumping has occurred. This physical clumping mechanism removes these runs from consideration in a process model - as seen in Figure 6-5, the runs removed are Run 1, Run 7, Run 11, Run 18.

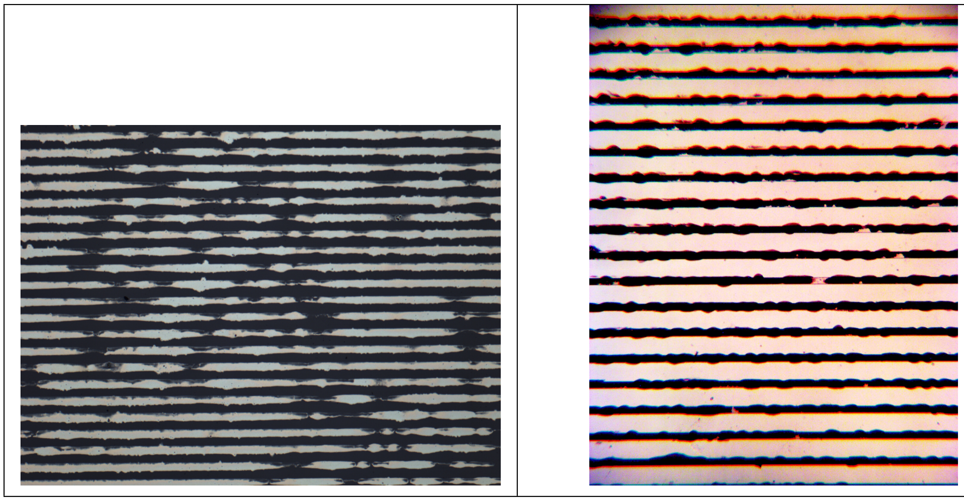

a) Run 17, 20μm lines

b) Run 17, stamp observed after printing to have uneven inking

Figure 6-6: a) Poor coverage observed in Run 17, 20μm lines with CSD-66 ink. b) Observation of stamp after printing shows likely problem with the inking of the stamp. Run was treated as probable experimental error and removed from consideration in the process model.

6.3.2 Elimination of runs with anomalous coverage

Upon observation, Run 17 had very poor coverage, which was not expected given the experimental parameters (CSD-66 ink, on glass). Inspection of the stamp post-printing shows uneven coverage of the stamp, likely due to problems with inking. (See Figure 6-6). Since the problem was not assumed to be associated with the transfer process, this run was not included in the process model.

6.3.3 Software used

As mentioned before, image processing for coverage was done in MatLab. Thickness data was measured with a Zygo and analyzed in MatLab. Statistical analysis and plotting of the results from the DOE was done in JMP 10. A Taguchi L18 matrix was set up and populated with the chosen experimental parameters, shown in Figure 6-7.

6.4 Thickness model

In this section we will discuss the anticipated effect of the various DOE parameters on the thickness, what the process model for thickness is, and whether it matches expectations. It

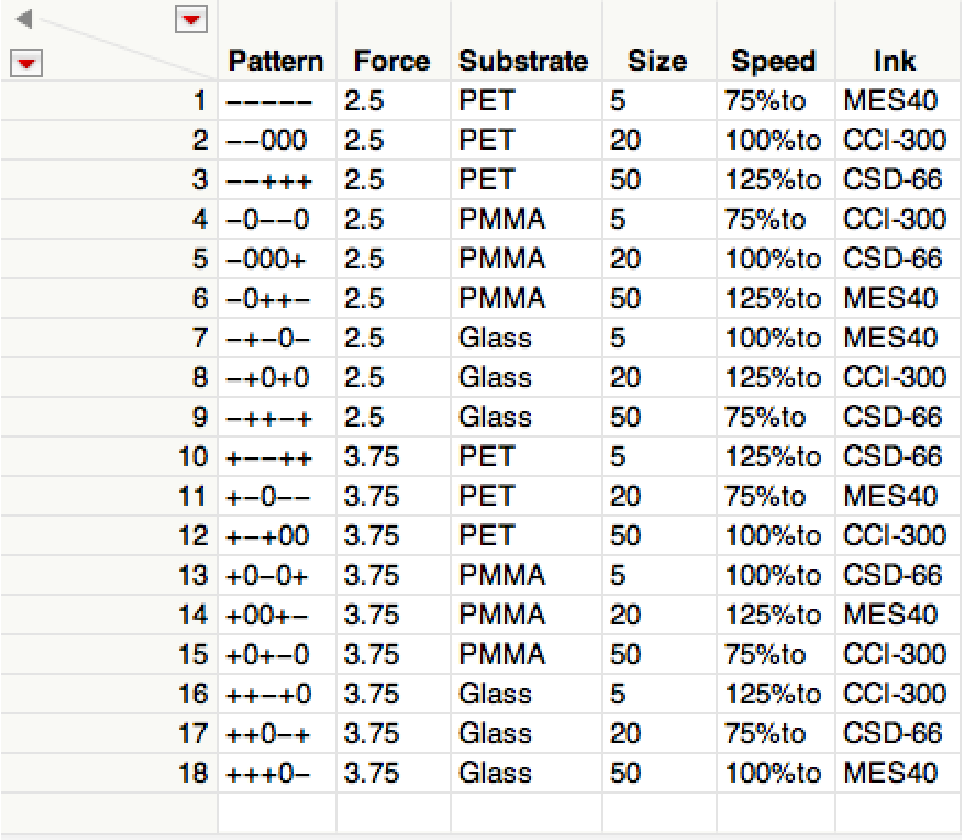

	Pattern	Force	Substrate	Size	Speed	Ink
1	−−−−−	2.5	PET	5	75%to	MES40
2	−−000	2.5	PET	20	100%to	CCI-300
3	−−+++	2.5	PET	50	125%to	CSD-66
4	−0−−0	2.5	PMMA	5	75%to	CCI-300
5	−000+	2.5	PMMA	20	100%to	CSD-66
6	−0++−	2.5	PMMA	50	125%to	MES40
7	−+−0−	2.5	Glass	5	100%to	MES40
8	−+0+0	2.5	Glass	20	125%to	CCI-300
9	−++−+	2.5	Glass	50	75%to	CSD-66
10	+−−++	3.75	PET	5	125%to	CSD-66
11	+−0−−	3.75	PET	20	75%to	MES40
12	+−+00	3.75	PET	50	100%to	CCI-300
13	+0−0+	3.75	PMMA	5	100%to	CSD-66
14	+00+−	3.75	PMMA	20	125%to	MES40
15	+0+−0	3.75	PMMA	50	75%to	CCI-300
16	++−+0	3.75	Glass	5	125%to	CCI-300
17	++0−+	3.75	Glass	20	75%to	CSD-66
18	+++0−	3.75	Glass	50	100%to	MES40

Figure 6-7: Taguchi L18 Array in JMP, populated with chosen experimental parameters, ready for statistical analysis and process modeling.

is important to note that with all thickness measurements, the reported number is the dry thickness, not the wet thickness.

6.4.1 Effect of solids loading

Figure 6-8 shows the change in thickness of a printed ink from wet to dry. This was accomplished by bringing the printed wet pattern as quickly as possible to the Zygo for measurement, then annealing the pattern, and remeasuring. The measured dry thickness is compared to the predicted dry thickness, calculated from the known solids weight % in the ink formulation. (The weight % of silver can be converted into a volume %, and assuming all of the solvent is removed, that is the portion left behind when dry.) There is a significant change in thickness during drying, and this thickness is well correlated to the predicted dry thickness. The “predicted annealed” line assumed 60% solids loading, according to the manufacturer. The actual measurements are slightly thinner than the predicted, which can be explained if for example the manufacturer was slightly off and the true solids loading was 57%. (Or, some ink evaporated during transfer to the Zygo, and the wet thickness was inaccurate.)

This means that as the ink solids loading percentage increases, we can expect the thickness of the printed pattern to increase as well, simply because of the additional material in the ink that will be left behind when the solvent evaporates.

6.4.2 Effect of viscosity

To understand the effect of ink viscosity on the final printed thickness, we turn to Ahemd et. al. who explore the ink transfer between two separating plates in gravure-offset printing [11, 184]. Although in gravure-offset printing the ink is patterned onto a flat roller (not a stamp with raised features), the assumption is that the transfer mechanics will follow the same trends.

Figure 6-9 shows the diagram of ink between two plates. Note that in this setup [11], the substrate is the top plate, and the mold is the bottom plate. The contact angles of the substrate and mold are α and β, respectively, the gap height is g and the velocity of pull-apart is $\underline{U}$.

Figure 6-10 shows that as capillary number increases, the ratio of ink transferred to the upper plate decreases. Capillary number is proportional to viscosity and velocity, and

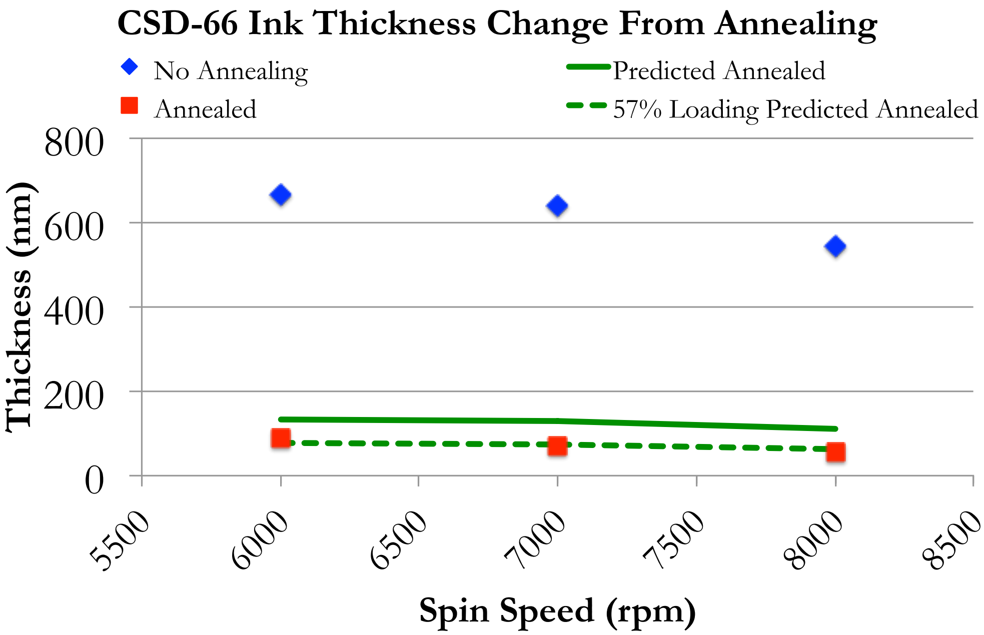

Figure 6-8: Measured ink thickness change from annealing (drying), indicating that the dried thickness can be well correlated to the solids loading. Therefore as solids loading increases, the thickness of the final dried pattern is also expected to increase.

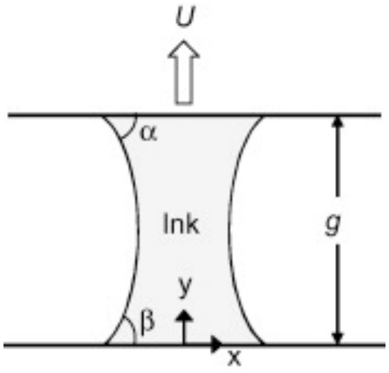

Figure 6-9: Diagram of gravure-offset printing configuration, for simulation to investigate ink transfer ratio [11]

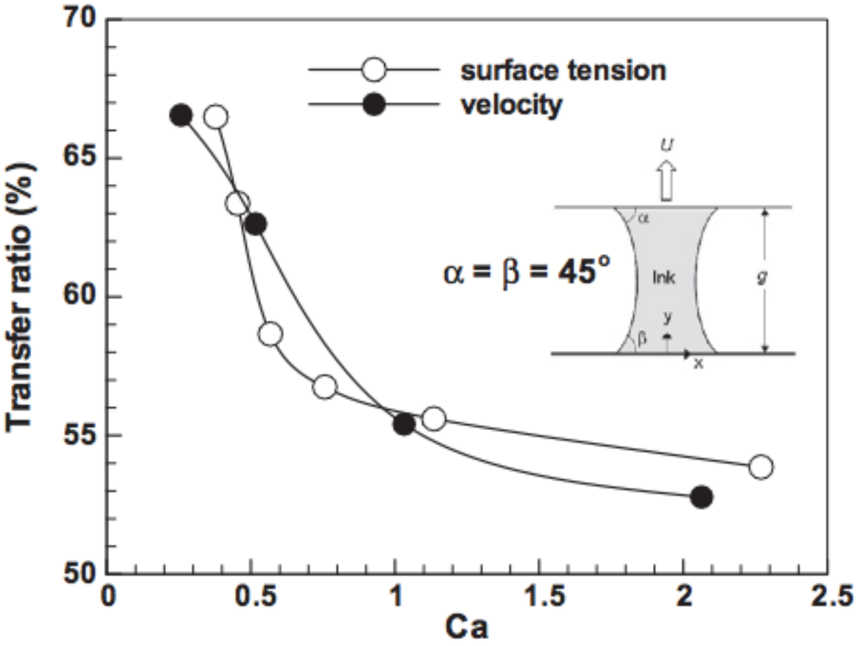

Figure 6-10: Liquid transfer ratio to the upper plate (substrate) for different Capillary numbers. The direction of increasing capillary number is also the direction of increasing viscosity, showing that as viscosity increases, thickness of the transferred pattern is expected to decrease.

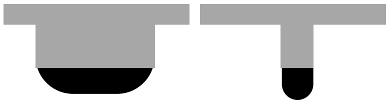

Figure 6-11: Film stability diagram, illustrating that a larger feature can support a stable thicker film, whereas for a smaller feature the same thickness creates an aspect ratio too high for stability.

inversely proportional to the surface tension of the liquid. So increases capillary number correlates to increasing viscosity, and the thickness of the printed pattern is expected to decrease as the viscosity goes up.

6.4.3 Effect of feature size

Recalling from Chapter 3, the amount of ink that the mold can pick up from the inkpad is limited partly by the stability of the ink film. Intuitively it can be understood that for a very tiny feature, the aspect ratio of the ink collected on the tip of the feature cannot be too high, or the ink will simply bead up and fall off. However a larger feature may be able to maintain the same thickness in a stable manner (see Figure 6-11 for a simple illustration).

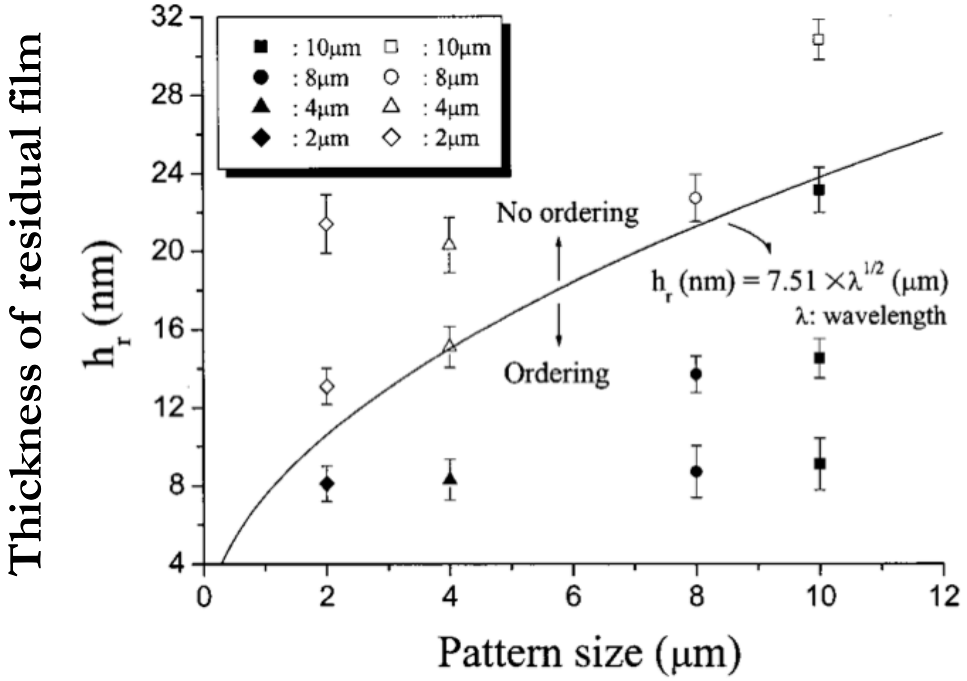

Figure 6-12: A comparison of the calculated wavelength of the capillary wave with the pattern size as a function of the thickness of residual film. In this figure, filled symbols indicate ordering, and open symbols no ordering. To create an ordered pattern (the desirable outcome), as the pattern size decreases the residual thickness decreases. [12]

The limit of this film stability is calculated using capillary wave theory, as given in Suh et. al. [12]. Figure 6-12 shows that in order to create a stable, ordered film (that does not bead up or break apart into droplets), the thickness of the residual film (the thickness of the remaining printed layer) depends on the feature size. A larger feature size is needed to support a thicker film, and for this reason we expect that as the feature size decreases, thickness will decrease as well.

6.4.4 Effect of energy ratio

Again consulting Ahmed et. al. for simulation of ink transfer ratio in a printing configuration, we can see from Figure 6-13 that as the surface tension of an ink increases, the transfer % to the substrate increases. In our process model, we have used the ratio of ink surface tension to substrate energy as the non-dimensional variable of choice. Increasing ink surface tension then corresponds to an increasing ink/substrate energy ratio. Therefore, we expect that as the energy ratio increases, the thickness of the pattern will also increase.

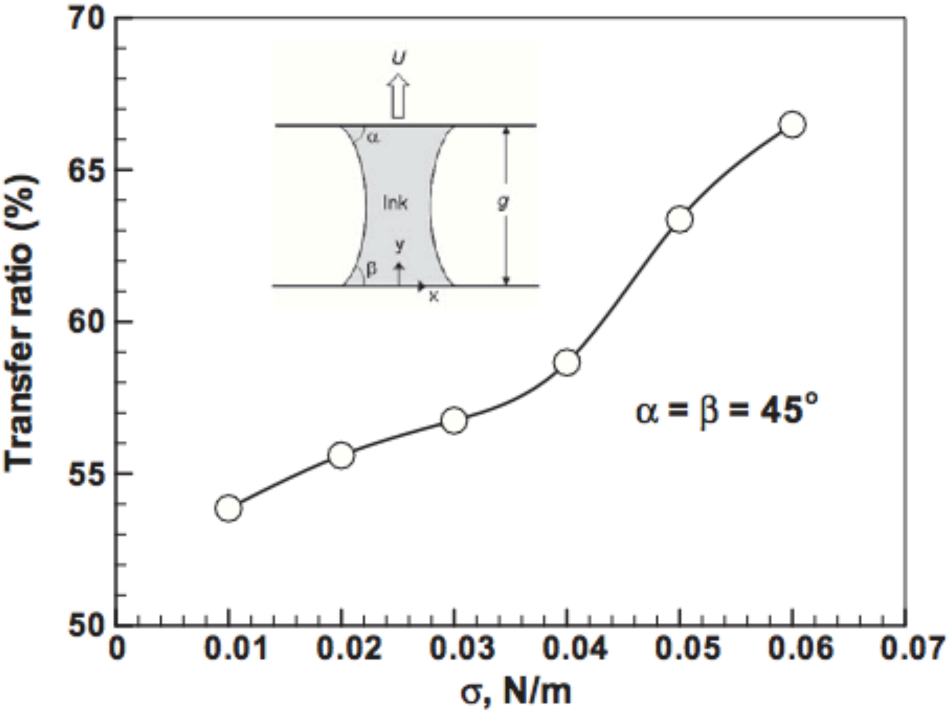

Figure 6-13: Liquid transfer to the upper plate (substrate) for different values of ink surface tension, showing that as surface tension increases, the thickness of the printed pattern is expected to increase. [11]

β_0		-8.3		
β_1	+	1.0	X_1	Solids Loading (wt%)
β_2	-	-0.63	X_2	Viscosity (cP)
β_3	+	0.26	X_3	Feature Size (μm)
β_4	+	20	X_4	Energy Ratio

Table 6.1: Thickness model coefficients, with the correlation direction (+ or -) showing that the coefficient signs match expected trends.

6.4.5 Thickness model coefficients

Finally, with an understanding of the expected effects of the process variables, the process model can be developed and compared to expected trends. The Taguchi L18 design does not give enough information to confidently determine second order effects or interactions, but we can develop a linear multivariate model with the form in Equation 6.1:

$$Y = \beta_o + \beta_1 X_1 + \beta_2 X_2 + \beta_3 X_3 + \beta_4 X_4 \tag{6.1}$$

Four factors were found to be statistically relevant (solids loading, viscosity, feature size, and energy ratio). Inkpad thickness and printing force were not found to be statistically significant in the ranges tested. The coefficients for these four factors in the model are given in Table 6.1.

The effect leverage plots for these factors on thickness are shown in Figure 6-14, showing that feature size and energy ratio have limited impact on the thickness (and in fact, the 95% confidence interval includes zero, so additional testing may be necessary), but that viscosity and solids loading have a clear and definitive effect on thickness.

There are many ways to represent the thickness data points measured, but a particularly useful representation is shown in Figure 6-15. Here feature size is plotted against thickness, separated by the type of ink. From this display we can see that each ink has a separate behavior (remember, as viscosity increases, thickness decreases), and that within each ink type, increasing feature size shows increasing thickness. The colors of the points correspond

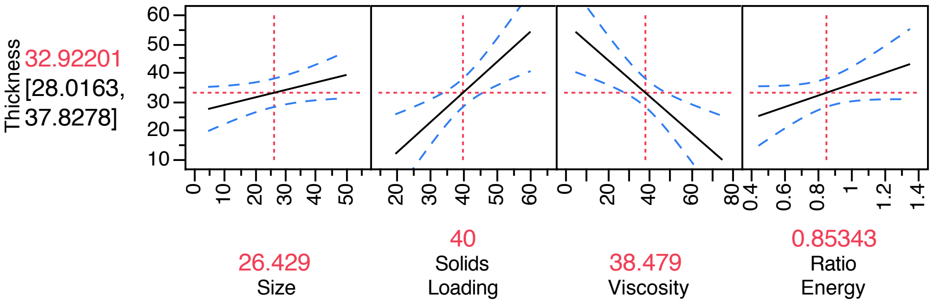

Figure 6-14: Thickness model effect leverage plots, showing that viscosity and solids loading have the most impact on thickness.

to the substrate. Although PMMA and PET have similar surface energies, making it hard to visually tell the difference, what is clear is that the glass substrate always has a lower thickness (decreasing ratio of energy correlates with decreasing thickness).

It is important to note that although the intercept term for the thickness model is -8.3nm, that number does not make physical sense. That leads to the question - what limits do make physical sense? The lower limit on thickness is intuitively the diameter of the particles, as there cannot be a layer less than one particle thick. That sets a lower bound at 10nm.

The upper limit on thickness may either be the thickness of the inkpad (cannot transfer more than the stamp has picked up), or it may be the thickness of a flat stamp (thickness increases as feature size increases, and a flat stamp is the limit as feature size grows to infinity). We know from Figure 5-18 (designing the inkpad thickness) that the inkpad thickness is around 75-100nm for CCI-300 and CSD-66. Additional testing was carried out using CSD-66 ink, with a flat stamp, on PMMA, with varying inkpad thicknesses. When using the nominal inkpad thickness t_o, the average thickness of several replicates of flat stamping was 60nm. Because this is less than the inkpad thickness, this then becomes the upper limit on thickness. The upper and lower limits on thickness are plotted on Figure 6-16, and as expected the measurements all fall between these two.

6.4.6 Note on thickness vs. pressure

It was consciously decided that the variable to change in the DOE would be force, but an alternate choice of variable could be pressure. Force was not demonstrated to cause any effect to thickness (or coverage, for that matter), at least over the range tested, but it is possible

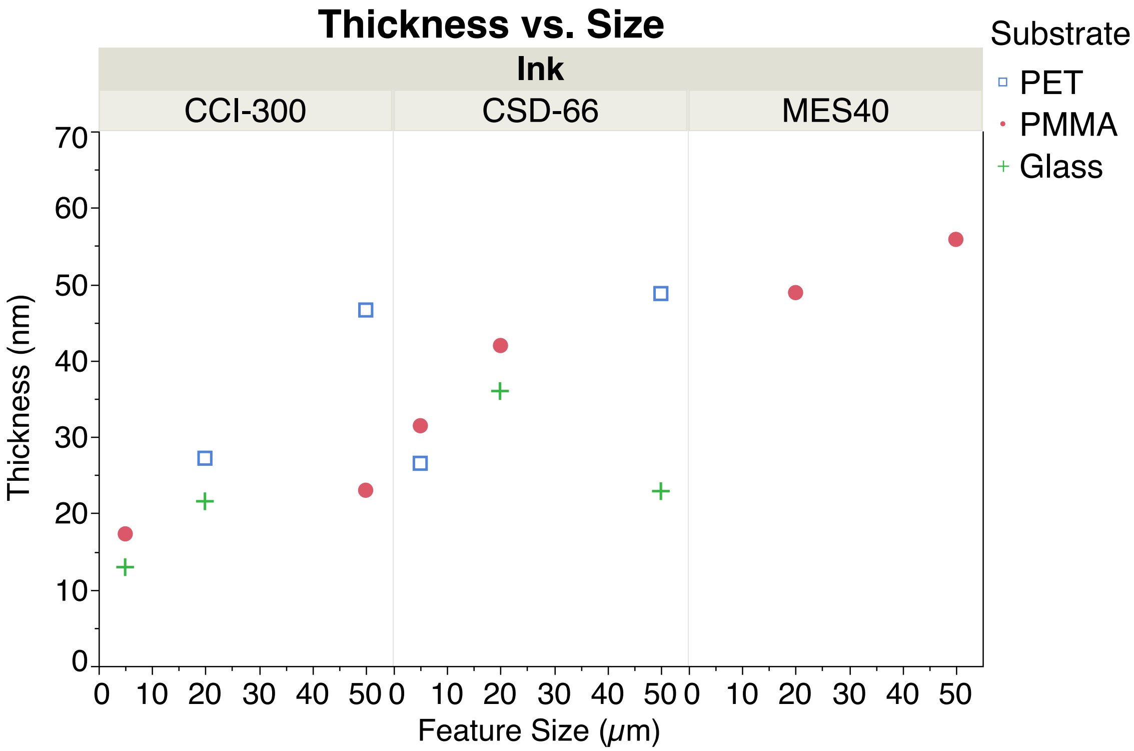

Figure 6-15: Thickness data representation - feature size plotted against thickness, differentiated by ink type and substrate. Visible trends include increasing thickness with increasing feature size, lower thickness corresponding with glass substrate, and clear differences in behavior depending on the ink used.

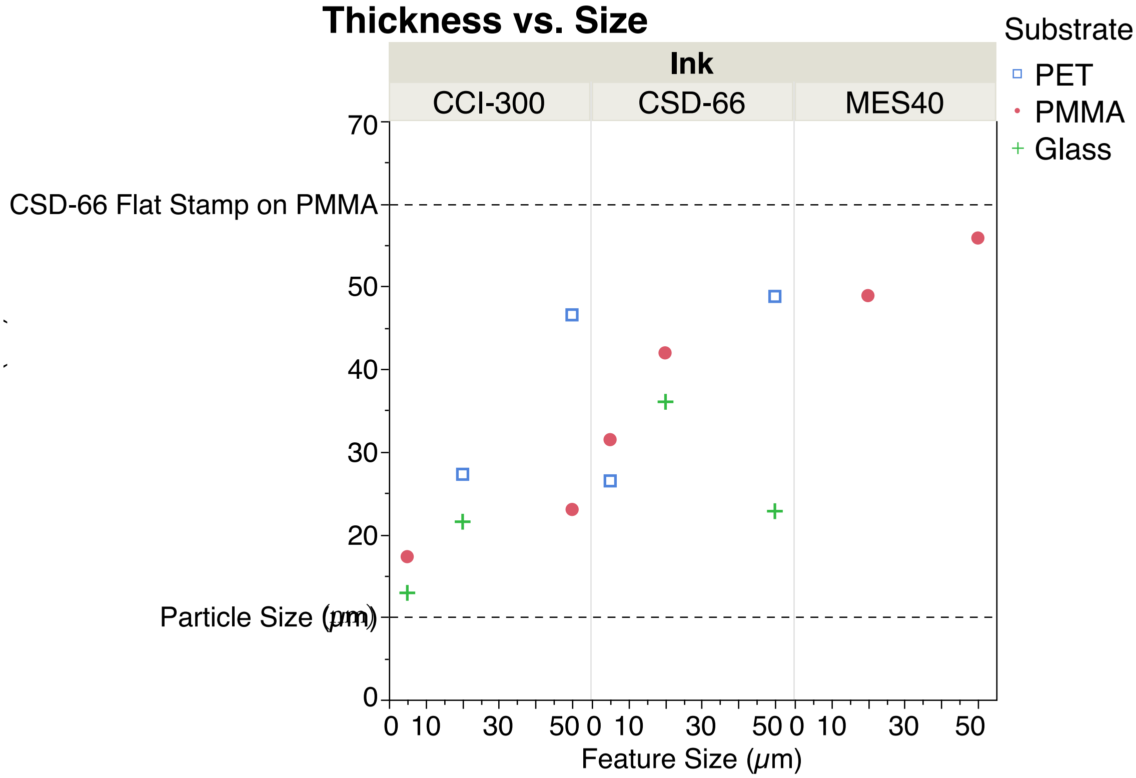

Figure 6-16: Thickness data representation with limits, with the lower limit based on a single layer of Ag particles, and a typical upper limit based on thickness printed with a flat stamp. Specific upper limit will different in each experimental case, as it is a function of ink, substrate, and inkpad thickness.

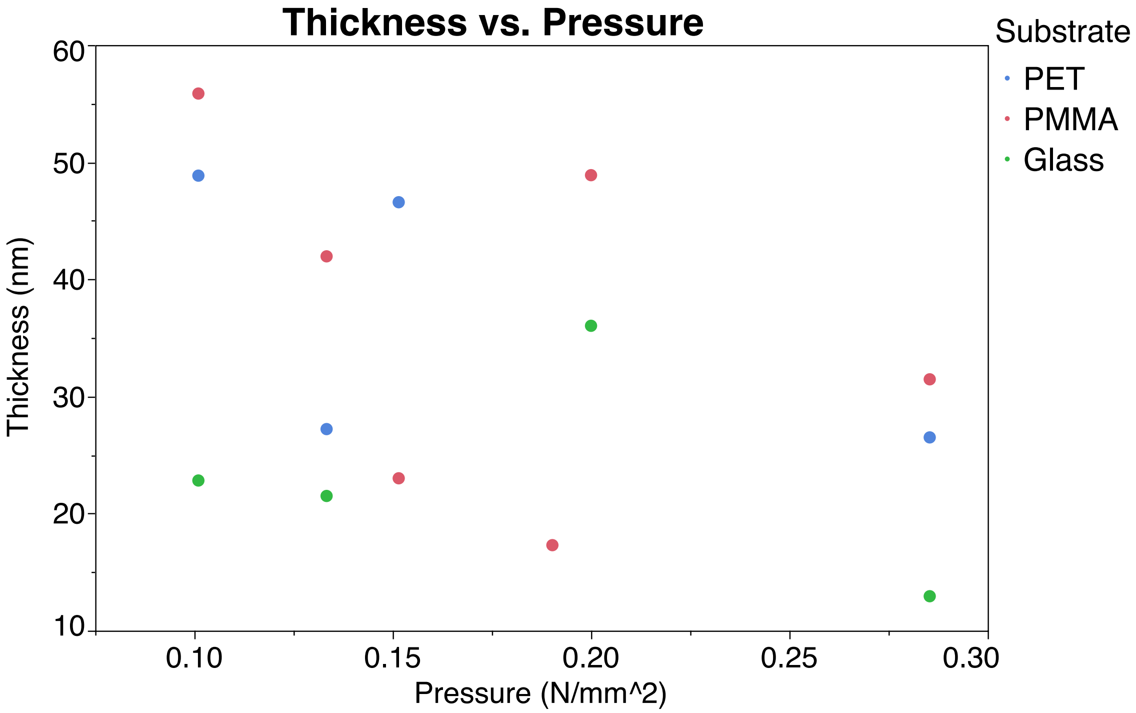

Figure 6-17: Thickness vs. pressure, differentiated by substrate, showing no obvious trend between thickness and pressure

that pressure might be a significant variable, or that force could become significant when tested over a larger range. Because force was varied over two settings for three patterns, there is data available for six different pressure settings. When pressure is plotted vs. thickness, and different substrates shown in different colors, there is no obvious trend observable (Figure 6-17).

But when pressure is plotted vs. thickness, differentiated by ink (seen in Figure 6-18), there is some evidence that increasing pressure leads to decreasing thickness. This would be an intuitively reasonable effect (higher pressure squeezes the ink layer thinner). There are not enough data points, however, to determine statistical validity. Additional testing would be needed, and this would be an interesting variable to pursue further.

6.5 Coverage model

In this section we will discuss the anticipated effect of the various DOE parameters on the coverage, what the process model for coverage is, and whether it matches expectations.

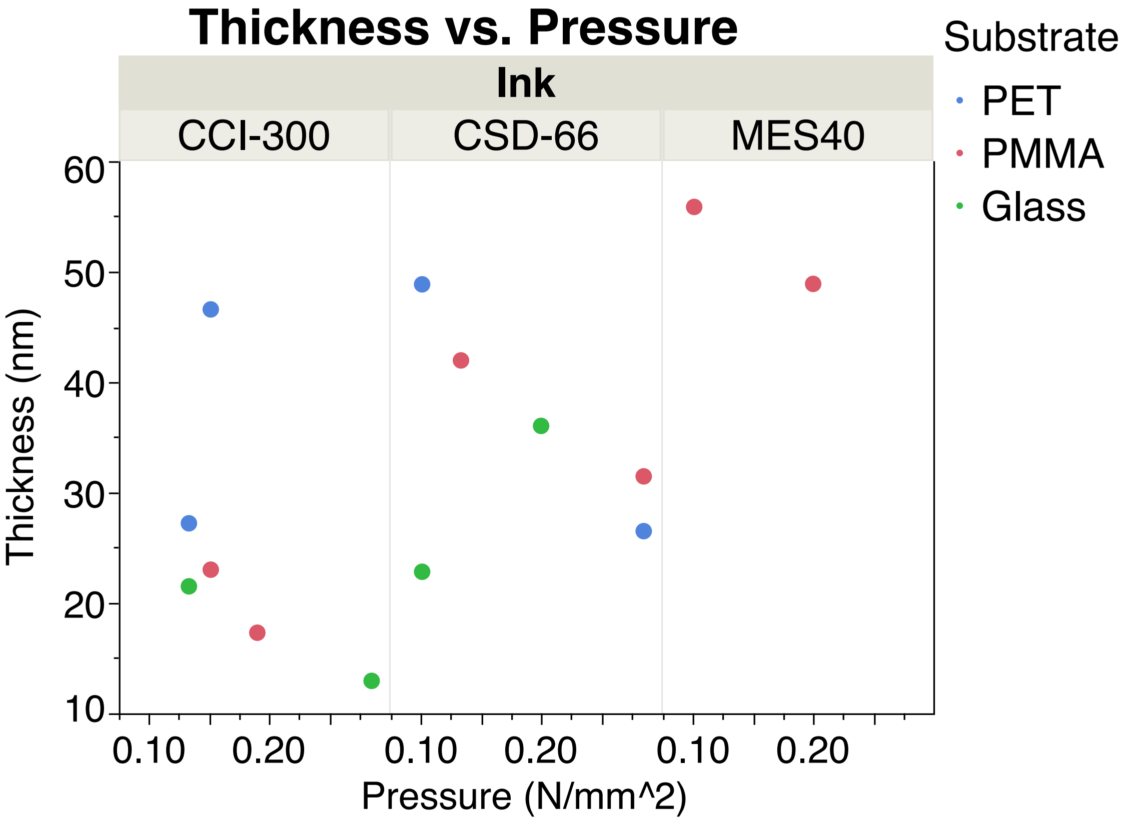

Figure 6-18: Thickness vs. pressure, differentiated by ink, showing potential correlation between higher pressure and thinner pattern

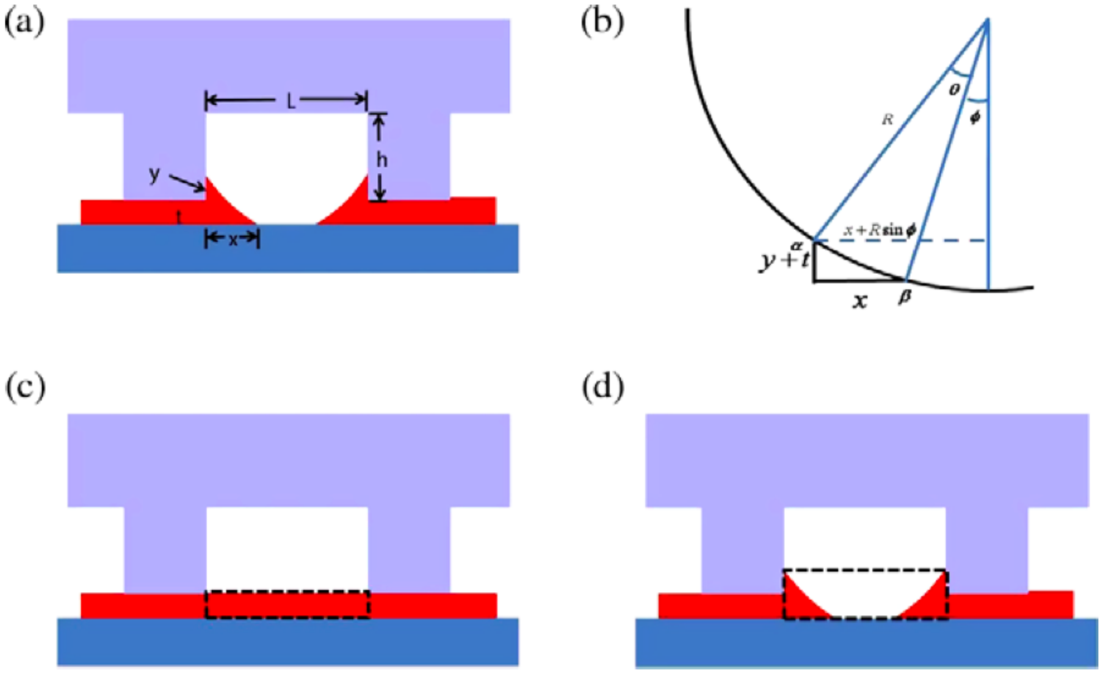

Figure 6-19: a) Geometry of the mold and the dewetting film (L: feature width, h: feature height, t: ink thickness, x: length of broken strip, y: height of the mold-wetting film). b) Simplified geometrical consideration assuming that the shape of the dewetting film is part of a circle. c) Control volume of the ink before dewetting. d) Ink volume after dewetting. [8]

6.5.1 Effect of feature size, inkpad thickness, and viscosity

The effect of feature size, inkpad thickness, and viscosity are all tied together into the physical mechanism of the ink climbing up the walls of the protruding features of the mold. Figure 6-19 a) shows the geometry of the ink dewetting configuration. Under the conditions of dewetting, the film is trying to achieve the minimum free energy by mass transport. Assuming the shape of the meniscus is part of a uniformly curved circle at the time of breakup (Figure 6-19 b), the total free energy can be calculated by incorporating contribution from surface free energies (mJ/m^2) at all interfaces. The equation for this is given in [8], but the important finding is that the minimum free energy occurs at the maximum radius of curvature R.

The maximum curvature R can be found from mass conservation. As can been seen in Figure 6-19 c) and d), the total mass must be conserved between the initial volume of ink ($V_i = L * t * b$), and the final volume ($V_f = \{(y+t)x - R^2(\theta - sin\theta)\}b$).

Inkpad thickness then influences the final coverage in that the thicker the inkpad, the higher the initial volume of ink, and the higher the ink will wet the sides of the mold in order to conserve mass in the final volume of ink. This ink carried by the sides of the features is transferred to the substrate and creates a printed pattern wider than the desired dimensions, increasing the coverage (not necessarily a good thing - the ideal coverage ratio is 1).

Although viscosity is not a term in the purely geometric consideration of mass conservation above, it is physically reasonable to assume that as the viscosity of the ink increases, the amount of ink that can be stably collected at the edges of the mold will increase. Then coverage would increase as viscosity increases, and more ink would be unintentionally added over the edges of the desired pattern dimensions. (This suggests that lower viscosity would be better for printing, so that there would be less ink wetting up the sides of the mold).

The effect of feature size on coverage is again simply a geometric argument. If the ink is wetting up the sides of the mold, controlled by the inkpad thickness and the ink viscosity, then the amount of ink wetting up the sides is not dependent on the feature size. As seen in Figure 6-20, if a 20μm line pattern and a 50μm line pattern both have an unintentional and constant 2μm amount of ink printed outside the desired patten edges, the effect will be more noticeable for the 20μm pattern. In other words, because of the way the coverage metric is defined, a constant offset will show up as coverage decreasing with increasing feature size.

6.5.2 Effect of solids loading

In Section 6.1.1, it was shown that the thickest parts of the printed pattern were concentrated along feature centerlines. And in Section 6.4.1, it was shown that a higher solids loading directly correlates to a thicker pattern. Therefore it is not a surprise that particularly for higher solids loading inks, the printed pattern can display thick concentrations of ink along feature centerlines. The effect of this phenomenon on coverage is that lower solids loading inks tend to conform better to the stamp dimensions, while higher solids loading inks can clump toward the center of the features and create a coverage ratio less than 1 (i.e. decreasing solids loading leads to increasing coverage). Figure 6-21 compares a low solids loading ink in a), with a higher solids loading ink in b), demonstrating the clumping towards the center of the features.

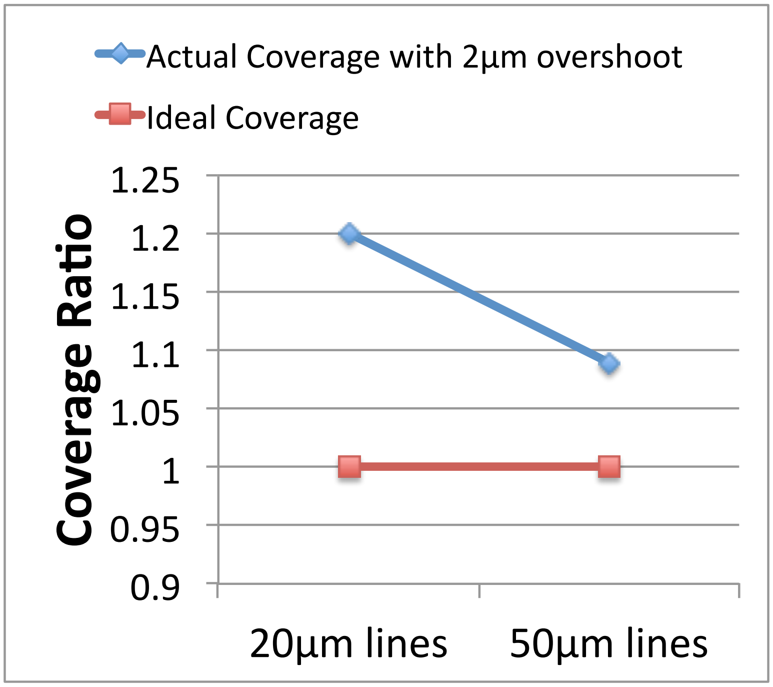

Figure 6-20: Demonstration that a constant 2μm overage in printed patterns (because of dewetted ink along edges of mold features) appears as a correlation between feature size and coverage, where coverage decreases (closer to the idea ratio of 1) with increasing feature size.

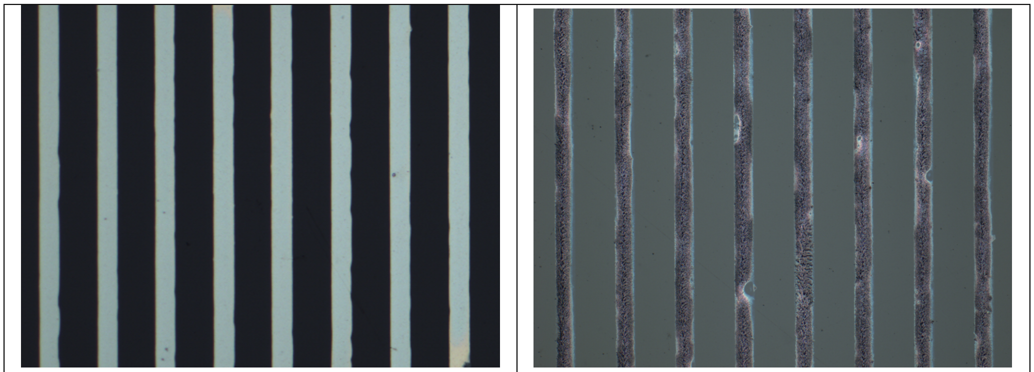

a) Printed pattern with a low solids loading ink

b) Printed pattern with a higher solids loading ink, showing clumping behavior towards the center of the features.

Figure 6-21: Comparison of lines at low and high solids loading, showing clumping at high solids loading that can lead to a coverage ratio less than 1 (therefore decreasing solids loading leads to increasing coverage).

β_0		150		
β_1	-	-2.8	X_1	Solids Loading (wt%)
β_2	+	1.5	X_2	Viscosity (cP)
β_3	-	-1.0	X_3	Feature Size (µm)
β_4	+	0.72	X_4	Inkpad Thickness (%nominal)

Table 6.2: Coverage model coefficients, with the correlation direction (+ or -) showing that the coefficient signs match expected trends.

6.5.3 Coverage model coefficients

As with thickness, the process model for coverage follows the model form:

$$Y = \beta_o + \beta_1 X_1 + \beta_2 X_2 + \beta_3 X_3 + \beta_4 X_4 \tag{6.2}$$

Again, four factors were found to be statistically significant: solids loading, viscosity, feature size, and inkpad thickness. The model coefficients are given in Table 6.2. The effect leverage plots for these factors on coverage are shown in Figure 6-22, showing that feature size and inkpad thickness have limited impact on the coverage (and in fact, the 95% confidence interval includes zero, so additional testing may be necessary), but that viscosity and solids loading have a clear and definitive effect on coverage. Because for coverage there is a desired value (1), this target can be used to create desirability functions (seen below the effect leverage plots in Figure 6-22.

Again there are many ways to graph the coverage data from the L18 DOE, but a particularly useful representation is shown in Figure 6-23. Here inkpad thickness (as a % of the nominal thickness) is plotted against coverage ratio, sorted by ink viscosity. This shows that for a given ink, as the inkpad thickness goes up, the coverage goes up. Also that as viscosity goes up, coverage goes up. And although it is not as obvious between feature sizes 5μm and 20μm, the 50μm features always have less coverage.

6.5.4 Note on coverage vs. pressure

As discussed for the process model for thickness, the variable chosen for the DOE was printing force, not printing pressure. But because two forces were used on three different patterns, a total of six different pressures occurred over the experimental runs. Pressure vs.

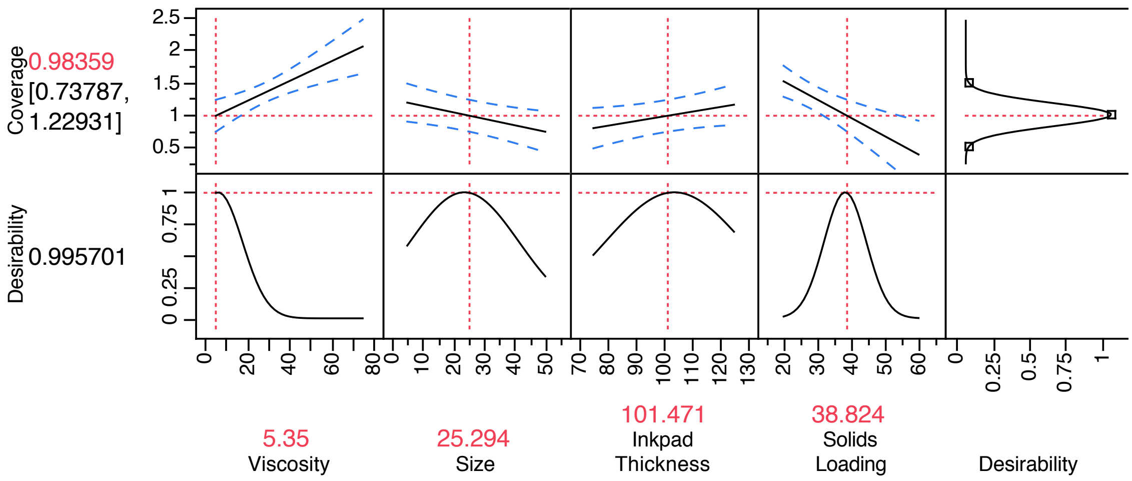

Figure 6-22: Coverage model effect leverage plots, showing that viscosity and solids loading have the most impact on thickness.

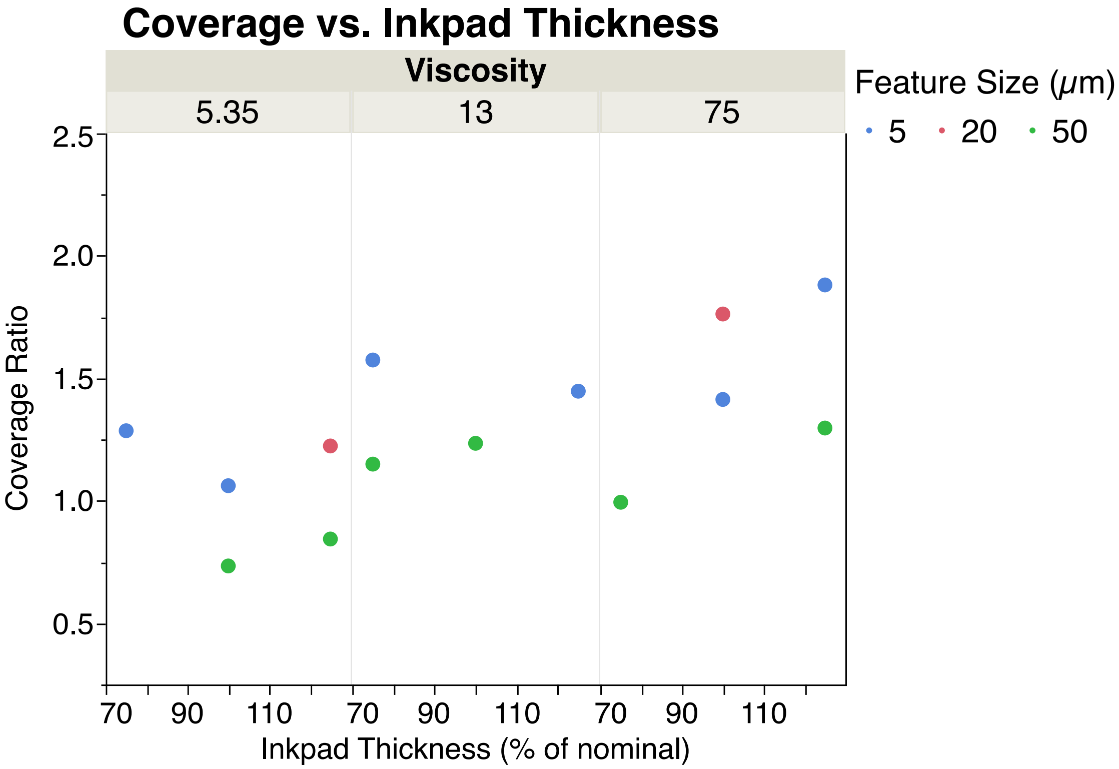

Figure 6-23: Coverage data representation - inkpad thickness plotted against coverage, differentiated by ink viscosity and feature size. Visible trends include increasing coverage with increasing inkpad thickness and viscosity, and lower coverage corresponding with the 50μm pattern.

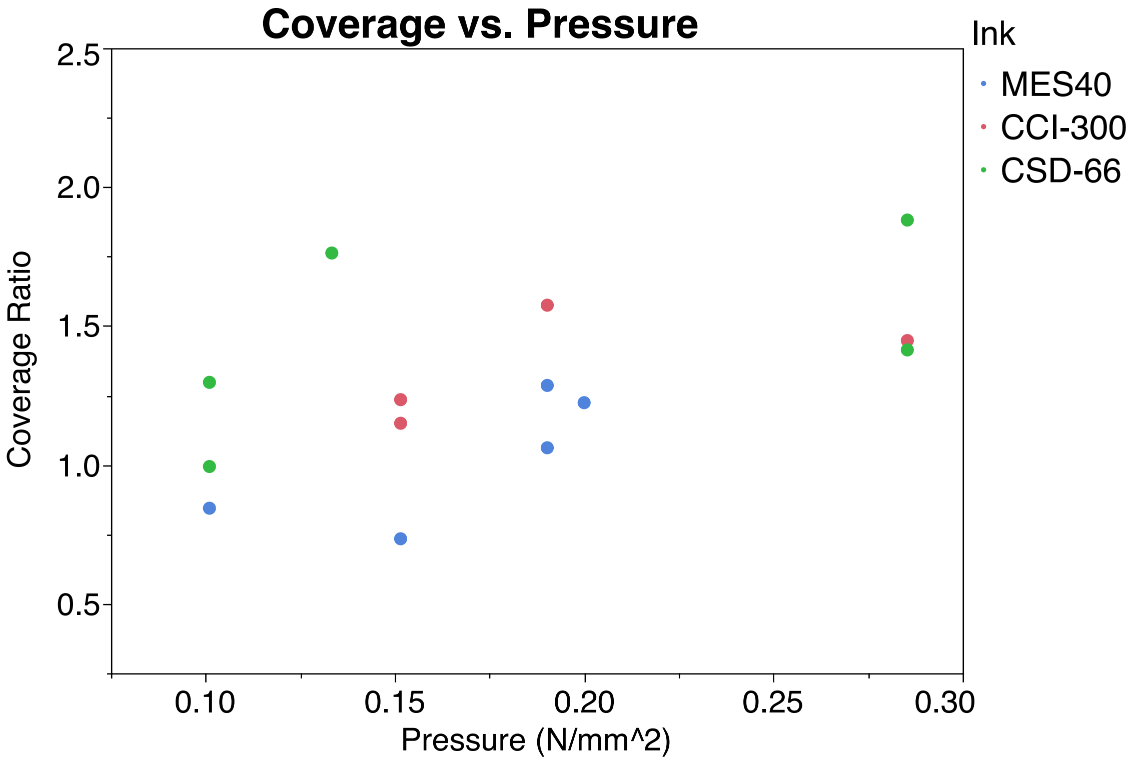

Figure 6-24: Coverage vs. pressure, differentiated by ink type, showing no obvious trend between coverage and pressure

coverage is plotted in Figure 6-24, differentiated by ink type. There is no obvious correlation from the data available.

6.6 Extension of model to other silver nanoparticle inks, other substrates, and other materials

Now that a model has been developed for thickness and coverage, in order to be useful it must be proven to be applicable to other situations. The model parameters were specifically chosen to be general (viscosity and solids loading instead of a specific ink, or substrate surface energy instead of a particular material) so that the model would be generally applicable. To test this, the model will first be used to predict behavior of two new silver inks.

One ink is chosen because it is widely commercially available - Aldrich silver nanoparticle ink. This is important practical factor, and availability is a real concern, illustrated particularly in that two of the three inks used for the DOE (CCI-300 and CSD-66) are no longer commercially produced. The second ink will be chosen for advantageous properties. As a

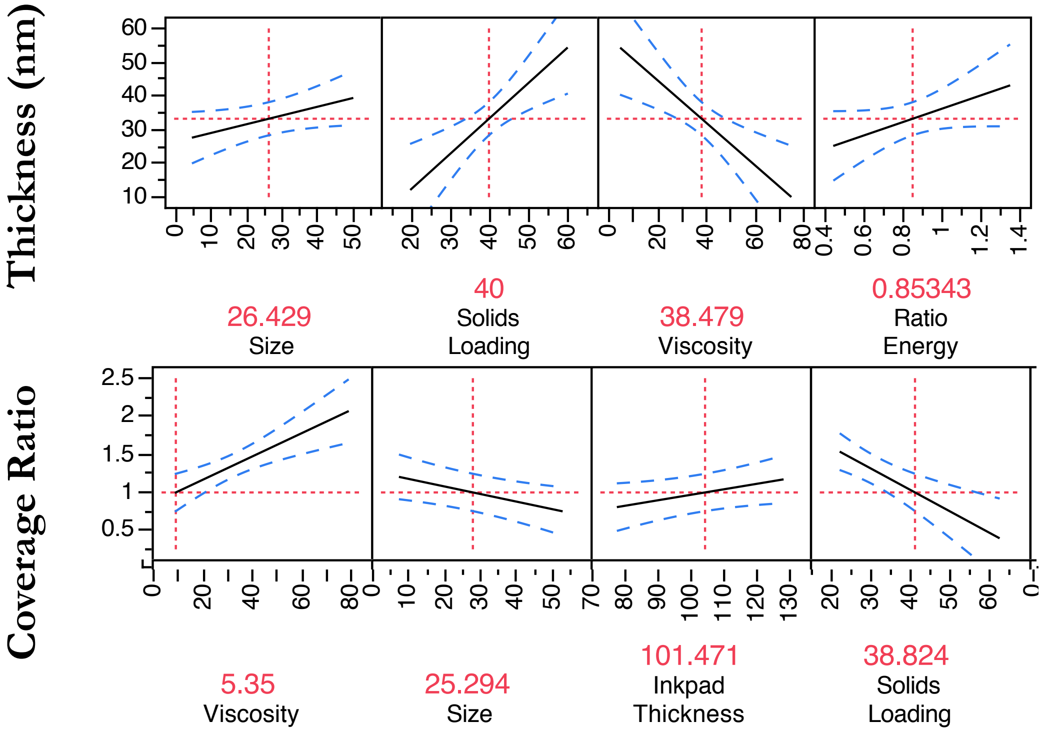

Figure 6-25: Reminder of effect leverage plots for thickness and coverage, used to inform choice of new ink designed for favorable printing results.

reminder, Figure 6-25 shows the effects of model factors on both thickness and coverage.

For both new inks, the 5μm pattern will be used, as it is the hardest pattern to replicate and therefore the most desirable to demonstrate. The substrates used will be PMMA and PET, because for microfluidics the substrates are polymers.

Then the model will be used for a new substrate - COC - on the recommendation of Holger Becker from ChipShop, a microfluidic job shop. Finally the model will be used to predict the behavior of gold ink, to validate the assumption that particle-based ink behavior can be described without any knowledge of the material properties of the particle.

For each case, the measured average thickness and coverage is compared to the model's predicted mean thickness and coverage, with 95% confidence intervals. A hypothesis test is carried out for each case; the one-sample t-test tests if a sample comes from a normal distribution with unknown variance and a specified mean, against the alternative that it does not have that mean. All distributions are assumed normal.

	MES 40	CCI-300	CSD-66	Aldrich	MES 30
Viscosity (cP)	5.4	13.0	75.0	12.3	6.2
Solids loading (wt%)	40	20	60	20	30
Density (g/cm$^{3)}$	1.44	1.24	2.25	1.22	1.20
Surface tension (mN/m)	27.5	31.5	47.5	29.5	26.48

Table 6.3: Additional silver ink properties, used to demonstrate the applicability of the process model on new inks. Aldrich ink chosen because it is widely commercially available, and MES 30 ink chosen because it has the desired characteristics for good performance, as predicted by the developed model.

6.6.1 Extension of model to additional silver inks: Aldrich and MES30

To design the printing parameters for two new inks, the first step is to identify the properties of the inks. Table 6.3 lists the characteristics of the inks as compared to the three inks used in the DOE.

For the first ink from Aldrich, we want want the coverage = 1, so consulting the effect leverage plots in Figure 6-25, the desired properties would be low viscosity and solids loading of 40. But the ink comes with a solids loading 20, and the pattern chosen is the 5μm size, which may make coverage too high. Therefore to compensate for those effects, the inkpad thickness should be decreased to lower the coverage toward 1. (This means using spincoating parameters of 9000rpm for 30 sec.) With these given ink characteristics and chosen printing parameters, the process model predicts 1.6 coverage (160%). Looking at the thickness performance with the Aldrich ink, the solids loading and viscosity effects will counteract each other, and the energy ratio and size (5μm) suggest low thickness. The thickness model predicts 25nm thickness of the printed pattern.

To choose an ink with desirable properties, we look at the desirability function for coverage. The desired coverage = 1, and to get that the ink should have low viscosity, and a solids loading of about 30. The chosen ink is MES30, from NanoMas, which is a 30% solids loading ink in Mesitylene carrier, with a very low viscosity. The coverage model predicts 1.25 coverage (125%). For thickness performance, again the energy ratio and size (5μm) suggest low thickness, but a higher solids loading and lower viscosity compared to the Aldrich ink suggest a slightly higher thickness. The thickness model predicts 33nm thickness for the MES30 ink.

Three experiments were carried out, all with the 5μm pattern and 2.5N force: Aldrich ink on PMMA, MES30 ink on PMMA, and MES30 ink on PET. The results of these experiments are plotted in Figures 6-26 and 6-27, for thickness and coverage respectively. In all cases, the measured thickness and coverage falls within the 95% confidence interval predicted by the process model developed in this chapter. The MES30 on PET experiment had a higher variation in measured thickness than PMMA, and this was likely due to the surface roughness of the PET.

Each experiment was measured at five points with a Zygo profilometer, and analyzed for thickness. For hypothesis testing, the null hypothesis is that the measured mean thickness from each experiment comes from a normal distribution with mean equal to the predicted mean, against the alternative that the mean is not the predicted value. The t-test for the thickness of Aldrich on PMMA, and MES30 on PMMA, does not reject the null hypothesis at the 1% significance level (meaning that we can be 99% confident that the measured mean is equal to the thickness model's predicted mean). The t-test for the thickness of MES30 on PET does not reject the null hypothesis at the 5% significance level (the higher variation in the thickness measured on PET only allows us to reach a 95% confidence level).

For Aldrich on PMMA and MES 30 ink on PMMA, two coverage measurements were made on each experiment. A hypothesis test for the coverage mean does not reject the null hypothesis at a significance level of 1%, i.e. we can be 99% confident that the measured coverage mean is the same as the coverage model's predicted mean. For MES 30 ink on PET, only one coverage measurement was made, so a statistical t-test is not possible. But because the coverage measurement falls within the 95% confidence interval predicted by the coverage model, the behavior of the ink seems to be well captured.

6.6.2 Extension of model to COC polymer substrate

In addition to demonstrating the applicability of the process model for other inks, it is also desirable to apply the model to other substrates. Another common choice of substrate in microfluidics is cyclic olefin copolymer (COC). A commercially available COC, trade name Topas, was printed with a 5μm pattern. The printed pattern is shown in Figure 6-28, and the measured thickness and coverage are shown in comparison with the model predictions in

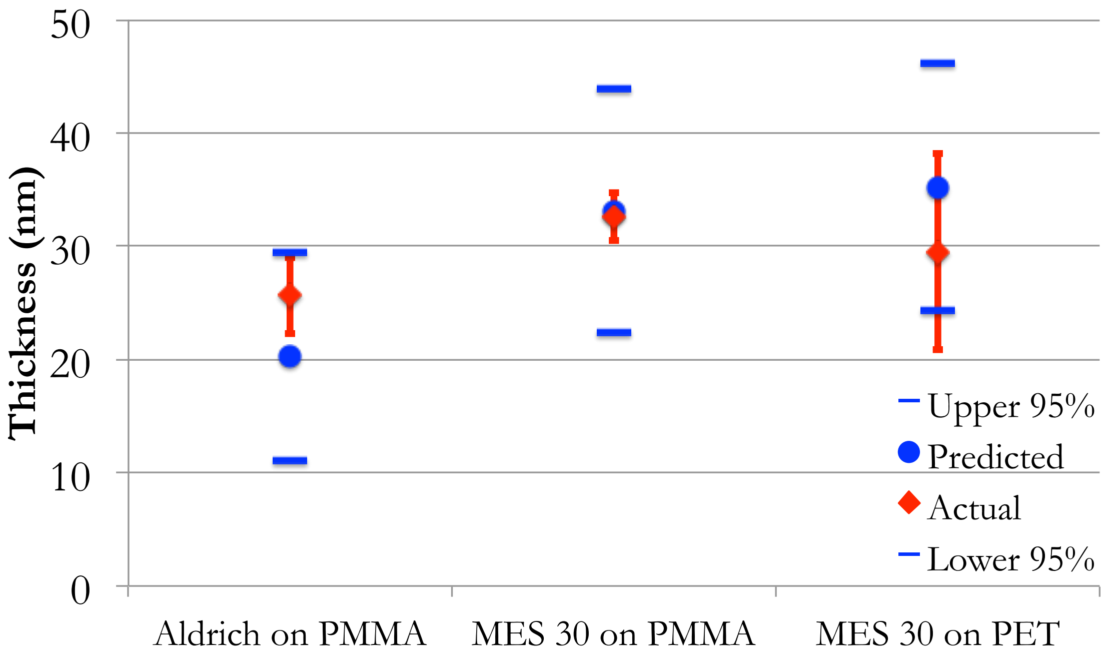

Figure 6-26: Thickness results from additional silver ink on polymer substrates, showing that measured thickness lies within the 95% confidence interval of predicted thickness.

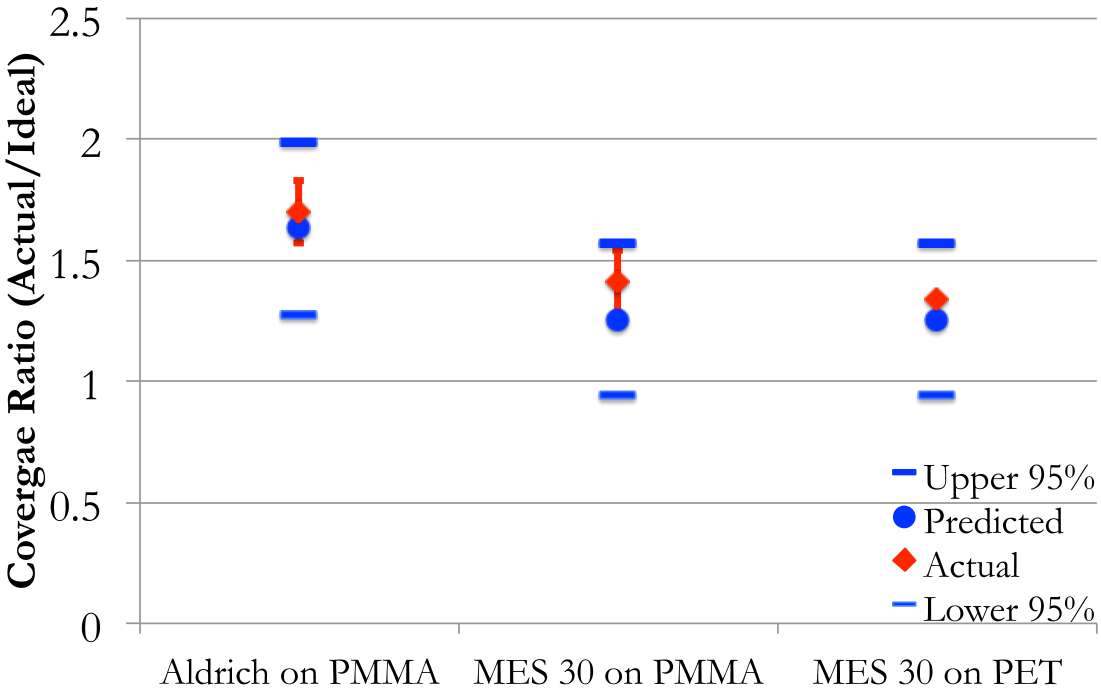

Figure 6-27: Coverage results from additional silver ink on polymer substrates, showing that measured coverage falls within the 95% confidence interval of predicted coverage.

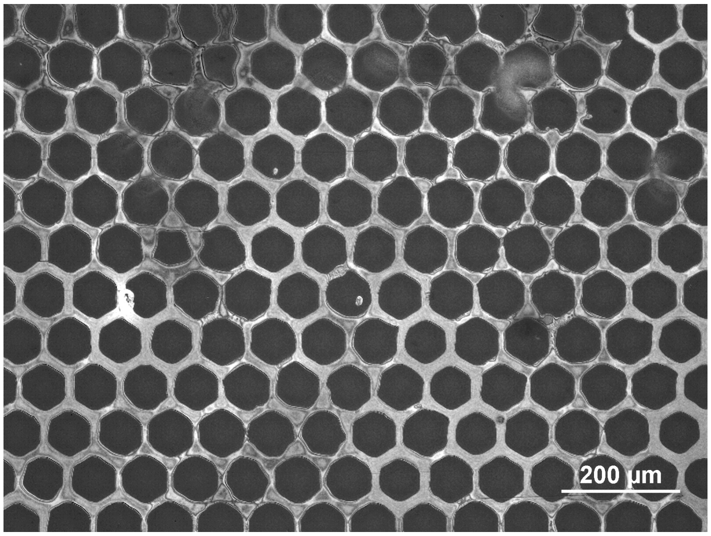

Figure 6-28: Image of 5μm hex pattern printed on Topas (COC polymer), showing features that are wider than desired but still well defined. No other high-volume process has been able to demonstrate this resolution of electrode printing on COC substrates.

Figure 6-29. A t-test on the measured thickness mean as compared to the mean predicted by the thickness model does not reject the null hypothesis (that both means are equal) at a significance level of 1%. This assumes all distributions are normal. Only one coverage measurement was taken, so a hypothesis test could not be performed, but the measured value lies within the 95% confidence interval predicted by the coverage model.

Although the print is not as ideal as results on PMMA or PET (and, in fact, the coverage model predicts that the print will not be all that good), to get better results the inkpad would need to be thinner, and with the available inking technique a layer any thinner would dry out and prevent transfer. Alternatively, an ink with different properties could be custom formulated.

It is worth noting that features of this size have never been demonstrated before with μCP on COC. An industry expert stated in conversation to the author in April 2013 that the best technology currently available for microfluidic electrode patterning (not even limited to μCP, but by any process) could not even create 50μm features on COC.

6.6.3 Extension of model to gold nanoparticle ink

An assumption made in the beginning of experimental design was that the exact material of the nanoparticle ink was not relevant to the printing process itself. Therefore the ink

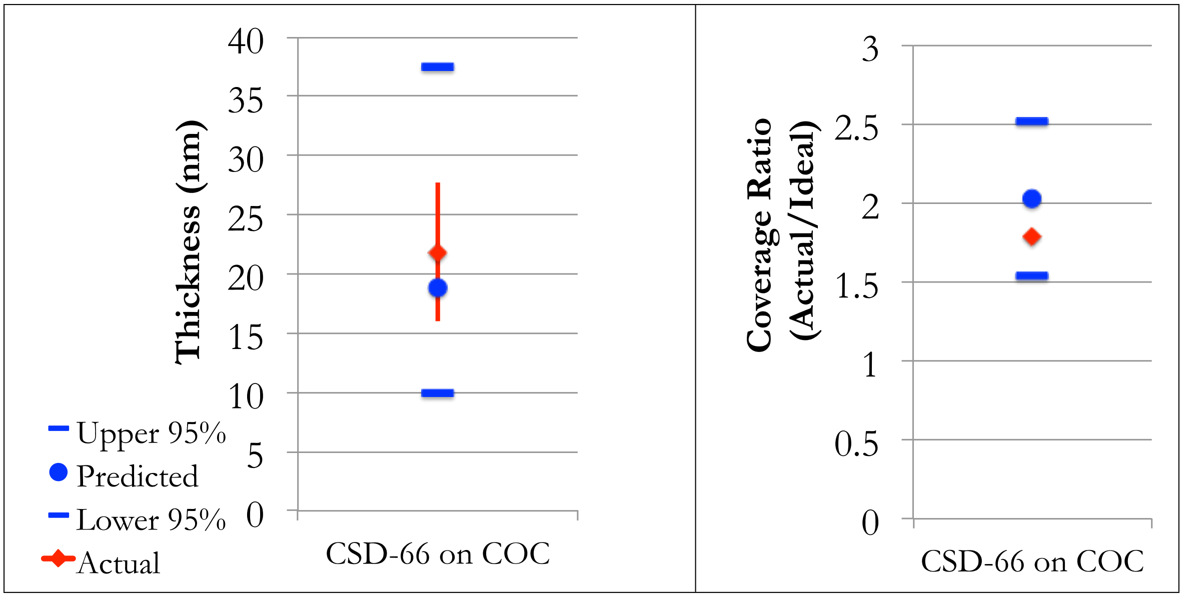

Figure 6-29: Thickness and coverage results of CSD-66 ink on COC, showing that measured thickness and coverage fall within the 95% confidence intervals of model predictions. Also showing that the predicted coverage is around 2, which is not ideal, and in fact the print does turn out poorly.

parameters explored included viscosity, surface tension, and solids loading, but nothing in the developed model is dependent on silver being the material used. To test the assumption that viscosity, surface tension, and solids loading can sufficiently describe the behavior of an ink, a gold nanoparticle ink was tested (UTDAu25 from Sun Chemical). This ink has a viscosity of 1.5cP, solids loading of 25%, and a surface tension of 27 mN/m. The solvent is xylene.

A PMMA substrate was printed with the 5μm pattern in gold ink. The printed pattern is shown in Figure 6-30, and the measured thickness and coverage are shown in comparison with the model predictions in Figure 6-31. A t-test on the measured thickness mean as compared to the mean predicted by the thickness model does not reject the null hypothesis (that both means are equal) at a significance level of 1%, assuming all distributions are normal. This means we can be 99% confident that the measured mean thickness comes from a distribution with the same mean as predicted by the thickness model. Only one coverage measurement was taken, so a hypothesis test could not be performed, but the measured value lies within the 95% confidence interval predicted by the coverage model. This excellent correlation of experimental results with model predictions validates the assumption that the material properties of the nanoparticles themselves are not relevant to this printing model. (Although it may make a difference to the overall electrical performance of the printed pattern.)

6.7 Exploration of μCP of carbon nanotubes

So the process model developed in this chapter has been shown applicable to different silver nanoparticle inks, and different substrates. But what about an ink that is not a silver nanoparticle ink? Another class of inks that would be desirable to print is carbon nanotubes, or CNTs. These are desirable because they do not require drying or sintering, and so the polymer substrate is not put through any heat cycle. (This allows polymers with low glass transition temperatures to be used, and speeds up the cycle time by eliminating the annealing step).

In collaboration with Chasm Technologies, formulations of CNT inks were tested with a variety of polymer substrates. Unfortunately the process model is not directly applicable to this case, because the CNT ink formulation used is a jelly consistency under normal conditions, and relies on shear thinning to spread and create coatings. However the model could be extended to include shear thinning, by identifying the viscosity at the spin speeds and printing rates used.

Although the model cannot directly be extended to CNTs, the broad trends still apply. For instance, from the process model we know that if the coverage is too high, the inkpad thickness can be decreased. This knowledge allowed suitable inkpad coating parameters to be quickly dialed in. Figure 6-32 shows the effect of changing the spincoating speed (which changes the inkpad thickness). Too thin of an inkpad thickness means the stamp does not transfer continuous features (due to either ink drying out or lack of material on the stamp), while an inkpad that is too thick smears the pattern.

With the appropriate inkpad spincoating parameters identified for each material, successful printing of 50μm lines is demonstrated for polycarbonate (PC), polyethylene naphthalate (PEN), polyimide (PI), and polyethylene terephthalate (PET, type st_505). See Figure 6-33.

6.8 Importance of inking

One of the unanticipated findings of the experimentation in this chapter was the importance of inking to the printing process. Investigation of the transfer portion of the printing process

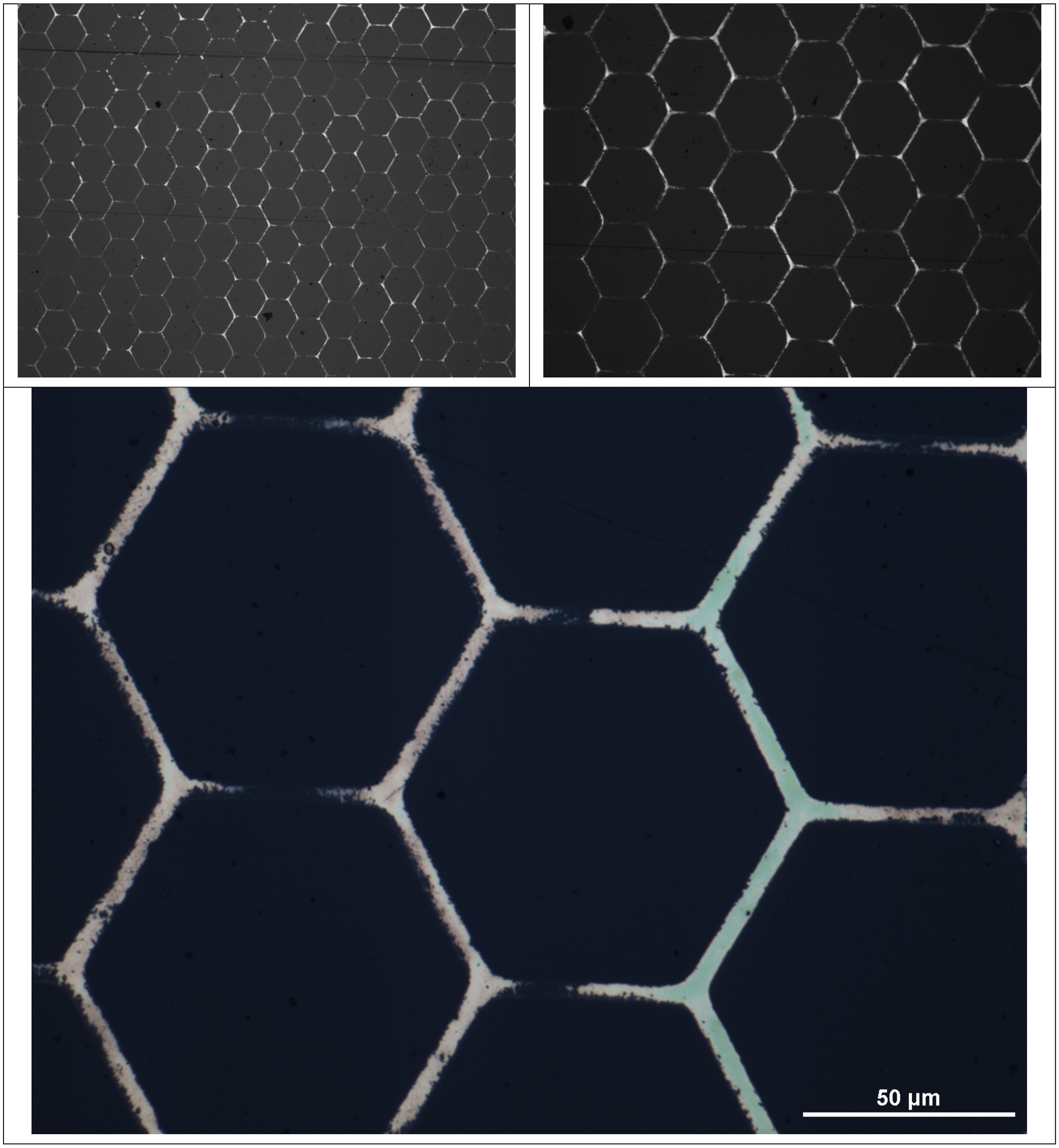

Figure 6-30: Image of 5μm hex pattern printed on PMMA with gold nanoparticle ink from Sun Chemical, showing features that very close to ideal coverage. The calculated coverage is slightly less than 1, likely due to the very fast drying of the volatile xylene solvent, leading to some gaps in the printed pattern.

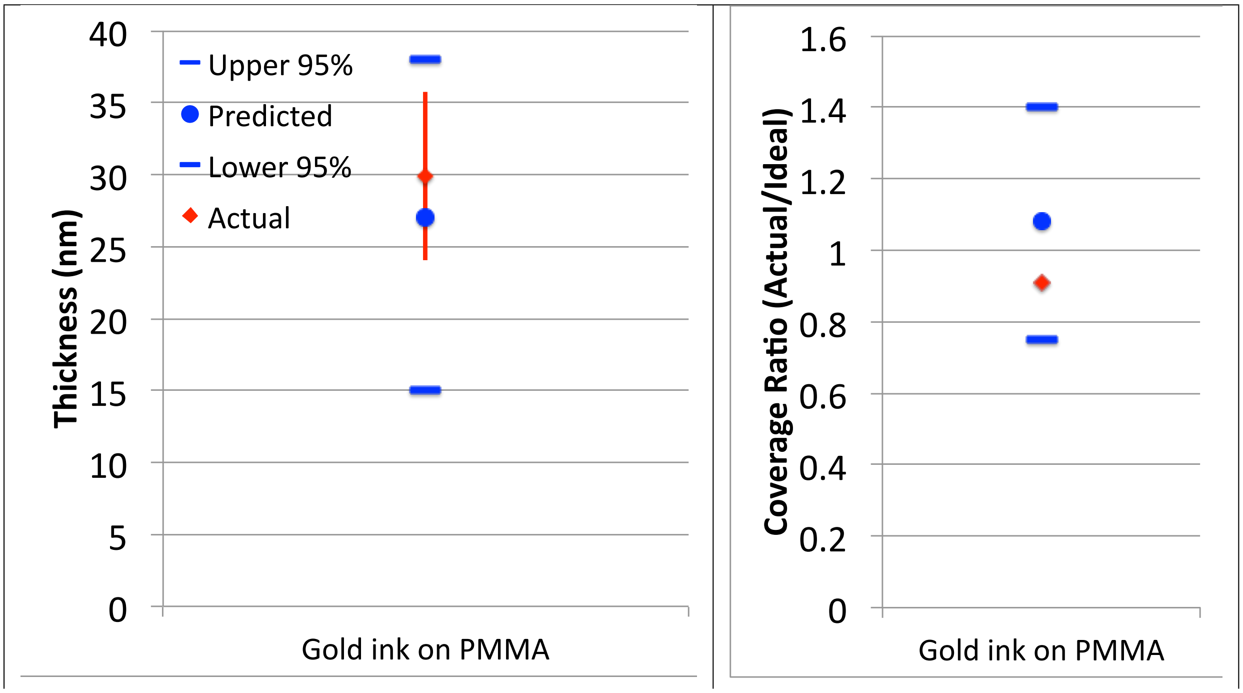

Figure 6-31: Thickness and coverage results of gold nanoparticle ink on PMMA, showing that measured thickness and coverage fall within the 95% confidence intervals of model predictions. Validates the assumption that material properties of the nanoparticles themselves are not relevant to the printing model, and the ink characteristics included in the model are sufficient to capture the printing behavior of a wide variety of particle-based inks.

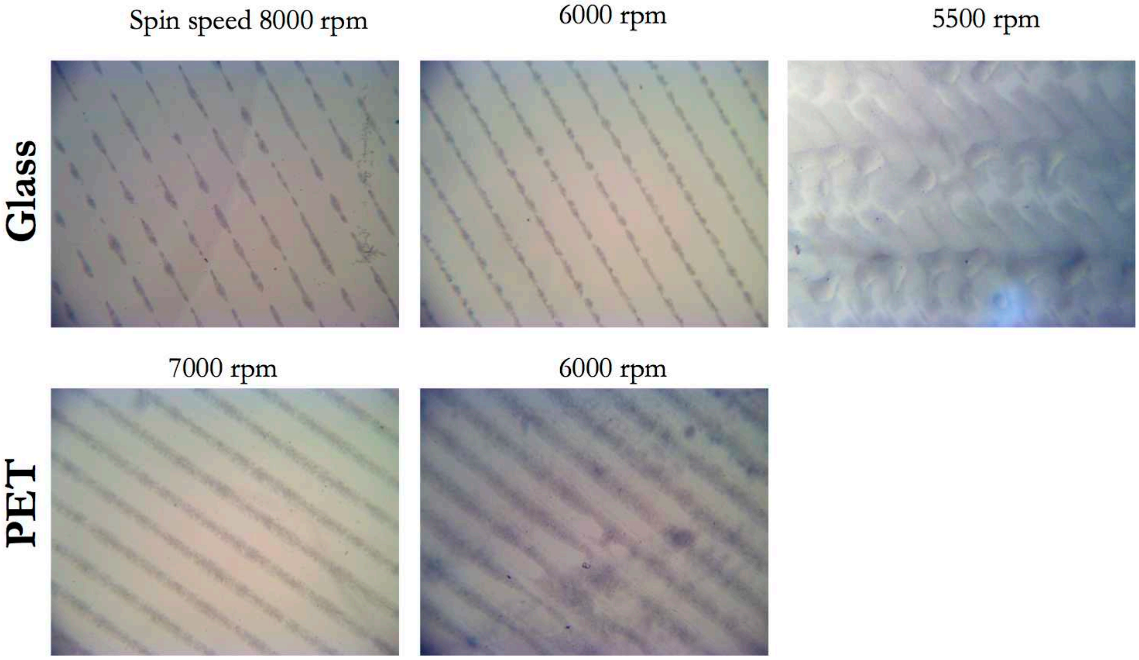

Figure 6-32: Demonstration of changing spincoating speed, thus varying inkpad thickness, and the effect on printed 50μm pattern of CNTs. Shows that there is an optimum speed, that depends on the substrate, that finds a balance between smearing the pattern and broken lines.

relies on having consistent inking of the stamp. Spincoating a glass slide with ink for use as an inkpad is wasteful, the spinning dries out the ink if the solvent is volatile, and the time it takes to transfer the inkpad from the spincoater to the printing equipment also allows time for the solvent to evaporate. In industry there are solutions available for roller ink coating, that would alleviate these issues related to spincoating.

The inkpad thickness parameter used in the design of experiments is based on a nominal thickness for each ink, which is varied +/- 25%. Because of the tendency of the volatile inks to dry out while spincoating, the same nominal thickness could not be chosen for all inks. If an alternate inking technique was developed, this model parameter could be standardized, instead of needing to be based on empirical testing of what inkpad thicknesses seem to give good results, bounded by what is possible with spincoating.

There are also additional inking issues related to stamp application on the roller. If any air gets trapped between the stamp and the roller, this raised air pocket creates a local high pressure area that can prevent good ink coating from the inkpad, collapse the stamp, and cause a coffee staining effect.

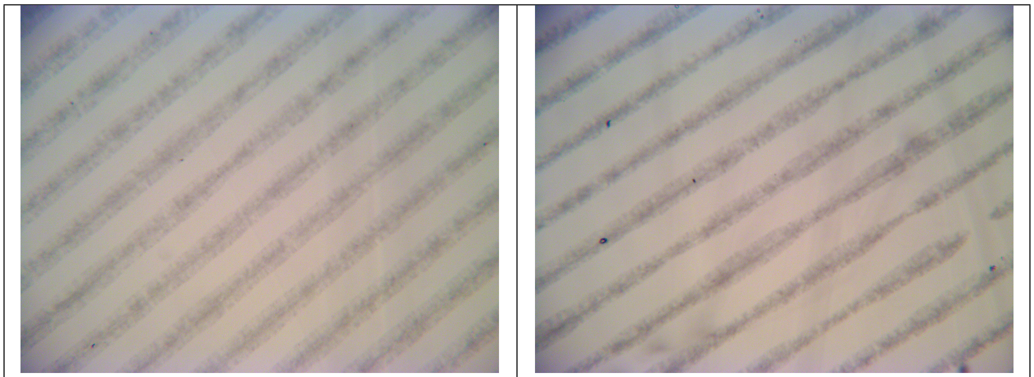

a) PC

b) PEN

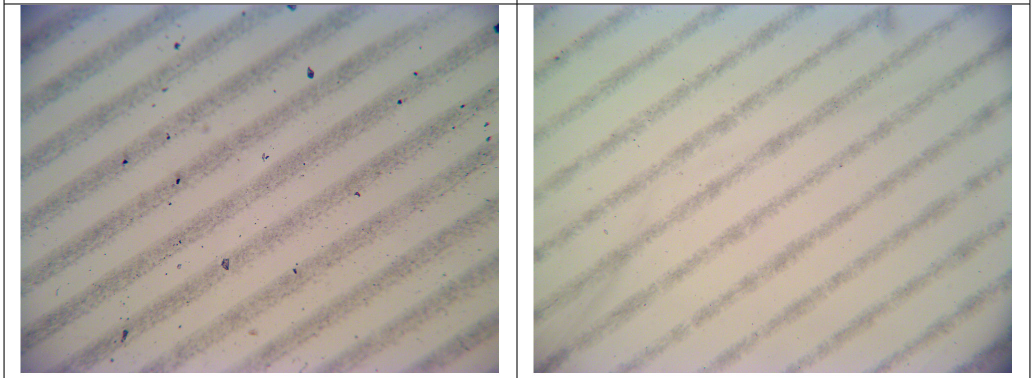

c) PI

d) PET_st505

Figure 6-33: Demonstration of printed 50μm lines with CNT ink on various polymer substrates, showing successful transfer is possible.

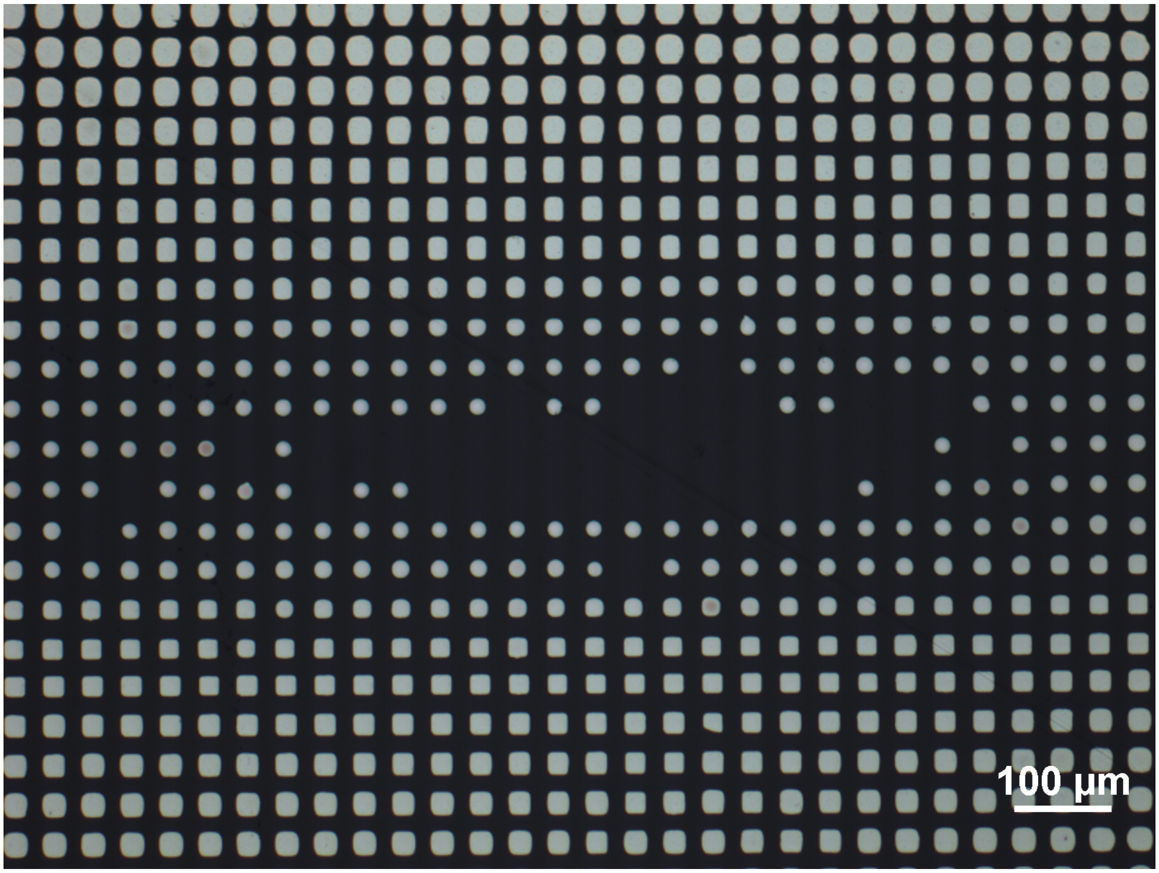

Figure 6-34: Importance of inking, illustrated by defect caused by ink void on stamp. Shows that the desired pattern of 20μm squares quickly varies from rounded squares, to ideal squares, to circles, to nothing, as the ink layer thins from full thickness to a void. There is only a small range of suitable inkpad thickness for the desired pattern.

To illustrate the sensitivity of the ink layer, Figure 6-34 shows a serendipitous case where the stamp was not properly coated, and one area had no ink at all. The desired pattern was 20μm squares, and the inkpad thickness used was actually too thick for ideal coverage. In the printed pattern, the pattern can be seen to vary from rounded squares (at the top and bottom, where the inkpad was too thick), to ideal squares (as the inkpad layer thinned to an ideal thickness), to circles (as there was not enough volume of ink to cover the stamp features), to nothing at all where there was no ink. There is only a small range (perhaps two rows of squares) where the inkpad thickness was appropriate for the desired pattern.

The experimentation in this chapter was limited by the inking technique. In some cases, such as printing on COC polymer in Section 6.6.2, to get better printing results the inkpad needed to be thinner. However increasing the spincoat speed in order to get a thinner layer would dry out the inkpad, creating an artificial limit to inkpad thickness.

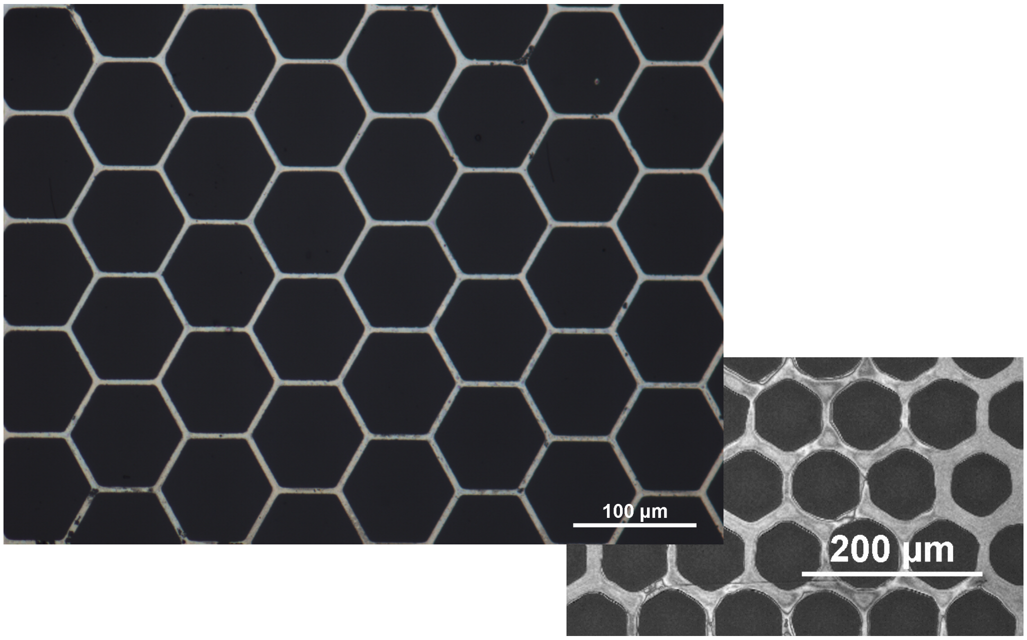

Figure 6-35: Alternative inking method used to print 5μm hex pattern with CSD-66 ink onto COC. First spincoating is used to create the thinnest possible inkpad on glass, then an intermediate printing step onto plasma treated glass is used to decreases stamp ink thickness, and then the final printing step deposits onto COC polymer. Dimensions of printed features are 5μm as intended, instead of 10μm as seen in the results with one step inking (where the inkpad thickness is limited by solvent evaporating during spincoating).

To circumvent this, an alternate inking technique was tried. First the thinnest inkpad possible was created on glass with spincoating. The PDMS stamp was used to pick up this layer, and then the PDMS stamp was printed onto a clean plasma treated glass substrate. This intermediate printing step decreased the thickness of the ink on the stamp. Then, the same stamp was used to print onto COC with no re-inking. This technique yielded the results seen in Figure 6-35. The print here is much closer to the ideal 5μm dimensions than the best possible results with the thicker inkpad (shown behind).

This is strong evidence that future work should investigate other methods of inking as an alternative to spincoating.

Chapter 7

Conclusions

7.1 Summary

The focus of this thesis was to develop a process suitable for creating very high resolution conductors on polymer substrates, in a way that could be scaled to high volume manufacturing. The original motivation for this work came from the problem of manufacturing electrodes at low cost on microfluidic devices (which are commonly polymers), a problem that is both important and unsolved. However the findings of this work have applications far beyond that field into flexible electronics, photovoltaics, optics, and organic micromanufacturing.

There are multiple potential methods for creating patterned conductive traces on polymer substrates. A review of surface patterning techniques available identified the processes currently in use and their capabilities, then desired functional requirements were used to narrow down the list to a handful of contenders. Finally a series of screening experiments were carried out to establish the viability of each of the contender processes. In addition, a literature review of the best resolutions reported from each surface patterning process (and the mechanisms limiting those resolutions) revealed that microcontact printing (μCP) had the potential to be improved with process control. This identified opportunity for improvement, along with successful initial screening experiments, pointed to direct μCP with liquid ink as the most promising method for further study.

It should be noted that the strict definition of μCP begins to merge into flexography when μCP is done with a direct ink in a roll-to-roll fashion. This is a consideration in favor of exploring μCP, because it means that any understanding gained in this work may be applied to the current flexography industry.

In general, the μCP process consists of inking the stamp (also called the mold), transferring the ink from the stamp to the substrate, and then any post-treatment of the ink (annealing or drying). For experimentation the stamp was mounted to a printing roller, as it would be in an industrial roll-to-roll process, but the experimental setup did not include an inking roll. For laboratory experiments, inking of the stamp was done by spincoating ink onto an inkpad (a glass slide, for convenience), then rolling the stamp over the inkpad to pick up a uniform coating of ink. The steps in the μCP process then are:

1. Coating of the inkpad with ink
2. Transfer from the inkpad to the stamp
3. Transfer from the stamp to substrate
4. Post-treatment, if any, of the final printed pattern

An inspection of the governing equations for each of these steps in the μCP process revealed that the surface properties of the stamp and substrate, and the surface energy of the ink, are critical parameters for each of these steps. (Assuming the ink is transferred in a liquid state, not as a solid film, in which case the transfer process would include concepts from fracture mechanics).

Two classes of conducting inks available are conductive polymer inks, and particulate inks. Polymer conductive inks have several functional advantages over particulate inks, such as better adhesion, flexibility, and optical transparency. Polymers (an organic material) also have several manufacturing advantages over metal-based inks, such as the possibility of lower material cost compared to gold, ability to process under atmospheric conditions, and evaporation at relatively low temperatures.

Poly(3,4-ethylenedioxythiophene), shortened to PEDOT, is a conductive polymer that has received research attention as an alternative to indium tin oxide (ITO) in organic electronics, particularly because of its stability, optical transparency, and good electrical properties [174]. The concept of μCP using PEDOT has been demonstrated to be feasible [9, 150], but has yet to be expanded into a manufacturing setting.

Experimental attempts were made to replicate existing literature showing μCP of PEDOT, and a variety of process parameters were explored in trying to achieve successful printing. Ultimately although some good results were obtained, the process was found to be extremely problematic and good experimental results difficult to replicate. In particular, a common failure mode observed with stamping transfer was that the PEDOT film would fail to adhere well to the substrate, and would curl up into “strings” instead of the desired line features. Or, conversely, the PEDOT film would fail to adhere well to the stamp during liftoff, and the disturbed features would detach in random strips (sometimes again curling into strings).

This difficulty led to an investigation of the surface energy of the stamp and substrate materials, and the surface tension of the ink used. Using the theory of work of adhesion, given the existing surface energies, both lift-off (adhesion) transfer and additive (stamping) transfer regimes were shown to be unfavorable. Thus, theory corroborated experimental results and showed μCP of PEDOT to be a non-robust process, likely unsuitable as a high volume manufacturing process without further refinement or different substrate and ink choices. Therefore this direction of research was discontinued.

Research effort turned to using a different material - silver nanoparticle ink, or Ag ink - with a similar μCP process. The advantages of silver ink include (most importantly) favorable surface tension, as well as consistently good electrical performance, while possible disadvantages include high cost and potentially poor adhesion to polymer substrates.

First, successful benchtop experiments with silver nanoparticle ink were established, replicating reported transfer in literature. Because the properties of the ink are so important, a range of silver nanoparticle inks available commercially and by special order were characterized. (Stamp and substrate choice are of course also important, but more limited because of the functional requirements of the stamp and the intended application of the substrate.) A brief investigation into the proportion of ink transferred from the stamp to the substrate tested the hypothesis that the percentage of ink left on each surface is dependent on the ratio of surface energies. Results could not confidently confirm that hypothesis.

Then using an understanding of the mechanisms involved in directly transferring liquid inks, a set of variables were chosen that were hypothesized to be important to the manufacturing process. To empirically investigate the transfer process, a careful design of experiments (DOE) was planned and executed to confirm relevant variables through experimentation, and to determine the process sensitivity to these variables. From the empirical data, a process model was built with generalized variables. The variables that were shown to be statistically relevant to the process output of thickness were solids loading, viscosity, feature size, and the energy ratio of ink to substrate. The variables that were statistically significant in the process model for coverage (a metric chosen to characterize the geometry of the features printed) were solids loading, viscosity, feature size, and inkpad thickness. Three out of the four variables in each output model are common factors, but the energy ratio is relevant only to the printed thickness, and the inkpad thickness is relevant only to the coverage of the printed pattern. This suggests that these factors in particular can be used as tuning parameters in an industrial process, to influence these two process outputs independently.

This process model was able to predict printing behavior of other silver inks (based on their known properties), and of other substrates (based on their surface energy), with confidence levels of 95% or higher for all cases. This validates the model and shows that the model developed is applicable to more general situations, and can be used and extended by other researchers. The results from gold ink testing validates the assumption that the material properties of the ink particles are not statistically relevant to the printing process (although the electrical properties of the printed pattern would certainly be affected by the conductance of the material chosen).

If this process model is to be extended to inks that exhibit shear thinning behavior (non-Newtonian fluids), then the model would need to include a printing rate term. The ink viscosity would then be a function of the printing rate (i.e. shear rate). A short exploration of printing carbon nanotubes (CNTs) was described in this work, which were in a formulation that was highly non-Newtonian. The CNT ink was a jelly consistency at rest, but fluid at the printing rates tested (the exact relationship is unknown, the ink is proprietary). Although the properties of the CNT paste are outside the current prediction capabilities of the model, the same trends are observed as with silver ink, giving confidence that the process model developed here would be relevant if extended by incorporating a viscosity term dependent on shear rate.

If this process model is to be extended to non-particulate inks, then the solids loading term can be replaced with a density term. For particulate inks, the solids loading and the density are linearly correlated and dependent, so both terms were not needed in the model. Because the solids loading has a direct effect on the final printed thickness, due to the solvent evaporation during annealing, solids loading was chosen as the more intuitive factor for the model. But, as long as the thickness change during annealing of any non-particulate ink is characterized, density can be substituted with solids loading.

7.2 Key contributions

The three pieces necessary to enable μCP of electrodes at high resolution on polymers are: i) printing equipment capable of controlling the process at high resolutions (less than $\sim 70\mu m$), ii) a stamp manufacturing process that produces cylindrical stamps with high resolution features, and iii) development of a method and process model for the printing process. This work focused on this last piece, the development of a process model for μCP of conductive patterns on polymer substrates.

This process model has been developed using an understanding of the mechanisms of direct liquid ink transfer to identify relevant process input and output factors, and then investigating the process sensitivities of those factors with a carefully designed DOE. This process model is important because it was the missing piece that will now enable scaling a benchtop process to a commercial process. In literature, μCP with silver ink has been reported at a small scale, using transfer accomplished with manual techniques, and rarely at resolutions below 20μm. But in order to have the largest impact possible, any electrode patterning technique developed must be adaptable to current industrial processes. Because this work uses a printing roll for transfer (specially designed for precise control of printing pressure), the contributions of this work can be applied to any industrial roll-to-roll equipment that is retrofitted with a similar printing roll.

This work has been able to demonstrate previously unachievable printing: pattern features down to 5μm, using liquid inks on polymer substrates, with a process that will scale to high-volume production. This process model has been shown to have extensible results for future applications, and these contributions have received interest at industry conferences and sparked ongoing collaborations with local industry.

It now becomes possible to use μCP for low temperature non-cleanroom fabrication of conductors on polymers, and more generally for low cost microfeature patterning over large areas. This has an immediate impact in the field of microfluidics, with applications in flexible electronics, optics, surface patterning, and photovoltaics.

7.3 Future work

The most critical piece of future work is to improve the inking step. Ink choice and process parameters are currently limited by the drying time of the ink, and the spincoating process is wasteful. The technique for stamp application to the roller also needs to be improved, as the uniformity of the pattern is limited by air bubbles caught between the stamp and roller (some work has already begun in this area [152]).

The design of experiments presented in this work has served its purpose as a screening experiment, but a finer granularity DOE focused on the most sensitive model factors could improve the model (especially if better inking and stamp application were available).

Additional factors may also be needed in the model, such as a rate-dependent viscosity term to deal with shear thinning, and/or a surface roughness term. If non-particulate inks are used, the solids loading term could be substituted with a density term (as long as the drying behavior of the ink with regards to thickness is known).

Finally, the process and model developed in this work can now be applied on roll-to-roll equipment, and extended to high volume production. Work along these lines has in fact already begun, in the same lab where this work was completed.

Appendix A

Detailed Methods of Micromanufacturing for Microfluidics

A.1 Traditional MEMS Techniques

Sputter deposition: Sputter deposition is a common method of metal deposition, used to make systems for trace metal analysis [37], acoustic wave based sensors[62], biosensing [73, 49], and systems for demixing [28]. Sputter deposition is a physical vapor deposition process that involves ejecting material from a target source onto the substrate, creating a layer that can then be patterned by etching or other techniques. [38]

Chemical vapor deposition: Chemical vapor deposition (CVD) is another common method of conventional metal deposition, used for example to make acoustic wave based sensors [62] and surface-enhanced Raman scattering (SERS) substrates [68]. The substrate is exposed to chemically reactive precursors, which react or decompose onto the substrate surface to deposit the intended material. There are many variants of CVD, depending on the operating pressure during the reaction process, the physical characteristics of the vapor, and whether plasma is used to assist.

Evaporation: Evaporation is used to make very thin films - particularly used in lensless imaging and optofluidic microscopy [66]. A heated source material evaporates under vacuum, and travels directly to the target substrate and deposits there as it condenses. It has been demonstrated that evaporation (Lee. et. al. used 1000Å gold) can be used with cyclicn olefin copolymer (COC) as a substrate without an adhesion layer, instead of glass or silicon with an adhesive step. [127] Evaporation is commonly used in many applications, including biosensing [50, 48] and electrokinetic control of fluid transport [51, 52].

Shadow mask deposition: Shadow mask deposition is like spray painting through a mask, as opposed to sputtering which coats the entire surface and is then patterned. For instance, Liu et. al. deposited silver on PDMS nanowells using a shadow mask, in conjunction with an electron beam evaporator. [67]

Tollen's reaction deposition: Silver is deposited on a glass substrate using chemical reaction between a silver solution and glucose solution droppered onto a slide (which does not use a clean room or a vacuum), then standard lithographic techniques are used to micropattern the silver film. [137]

Electroplating: Electroplating uses a current passing through a solution containing dissolved metal cations to create a charge that deposits a continuous metal coating on a target electrode. Metal (commonly nickel) can be deposited by electroplating, then patterned by photolithography. Electroplating has the capability to make very thick components, suitable for microtools (magnetically actuated), robot-on-a-chip [64], and micromixers and micropumps. [138].There are some options to get 3-D components using electroplating [53, 142], for instance making 3D electromagnets surrounding a microfluidic chamber by electroplating copper wires around a nickel-iron core [185, 55].

Lift-off processing: Lift-off processing can be used to pattern a deposited layer (be it from sputtering, ebeam, or other method) [54] as opposed to a shadow mask. A photoresist or other sacrificial material is first laid down on the substrate and patterned. Then the desired material is deposited through this stencil, and finally the stencil is removed. Lift-off is an additive process, as opposed to etching which is subtractive. [65]

Hot embossing: Metal can be embedded in polymer substrate by using conventional IC fabrication on a silicon substrate, then transferring the pattern to a polymer substrate by hot embossing. See Figure A-1. [13]

Sacrificial microchannel template: Using a sacrificial template enables manufacturing electrodes in direct contact with the fluid. The sacrificial template can be PDMS cast,

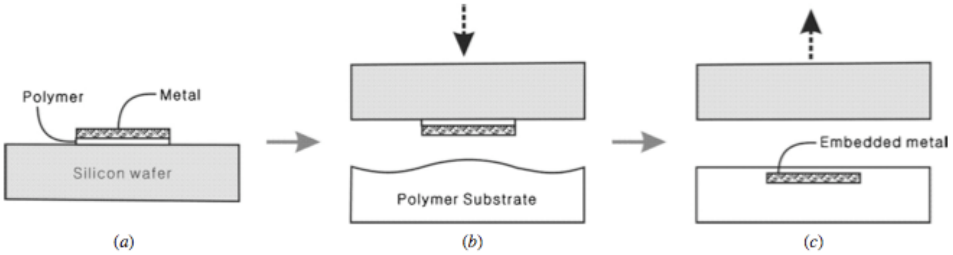

Figure A-1: Traditional MEMS micromanufacturing technique: Hot Embossing. a) metal/polymer double layer patterned on a silicon substrate; b) contact and pressing of the silicon substrate flipped onto a polymer substrate; and c) separation of the silicon substrate from the polymer substrate. [13]

or hot embossed [139]. The template can be "sacrificed" after use by peeling off after deposition (if using PDMS [137]), or decomposed by heating (if using PNB chemisty [29, 139]) , or etched away [58, 139]. Making nanochannels with integrated metal electrodes by rapidly etching a sacrificial layer. Couple a chromium sacrificial layer with gold electrodes, which 10-fold increases etch rate. Electrodes are 3 microns wide, 5 microns long, put in a 50nm high channel (so has to be less than 50nm), 1 microns separated. See.

Other: Many different methods have been reported for the deposition of ZnO films (used in acoustic wave based sensors), including sol–gel processes, metal-organic chemical vapour deposition, molecular beam epitaxy, pulsed laser deposition, filtered vacuum arc deposition and atomic layer deposition. [62] Wang et. al. report using a maskless system to deposit, pattern SU-8, cast PDMS, and lift-off Cr features. The system is well capable of printing 60 μm thick resist at a resolution as small as a single pixel (less than 13 µm) with an aspect ratio about 5:1. [75]

A.2 Other Methods

Micromachining: Suzuki et. al. micromachine copper wires in silicon to move superparamagnetic beads in a microchannel [141]. In general micromachining is difficult to extend to small features (less than 20μm or so), because of physical limitations of drill sizing and stiffness of the cutting machine and tool.

Modifying a CD: A laser printed mask of the desired electrode pattern is heat-transferred from non-sticking paper onto the CD-R (previously ‘‘peeled’’ with HNO3). In a subtractive process, the exposed gold is removed with a iodide/iodine solution; after removal of the toner mask, revealing the gold electrode(s), a new printed mask with the microchannels is heat-transferred on the base plane and a flat cap is heat-sealed on top of the channels. [33] Can also cap with Scotch tape, in good engineering tradition [43].

Self Assembly: Self-assembly is used when making nano structures for biosensing on the LSPR principle (Localized Surface Plasmonic Resonance). A reagent containing polystyrene nano-spheres is dropped onto a quartz plate, then the spheres arrange themselves into a regular compact two-dimensional array. Then, vaporized heavy metal (Au, Ag, Cr) deposits not only on the surface of spheres, but also onto the surface of quartz through the gaps between spheres. [45] Or, modified silica nanoparticles (100 nm in diameter) can form esters with acid in a gold substrate, producing of a slightly random nanoparticles monolayer. Later deposition of gold layer completes the fabrication process of the gold-capped nanoparticle structure. [47]

Laser Structuring: Laser micromachining as a manufacturing technique has emerged from the development of micro- and nano-technologies over the past two decades. While laser micromachining is still considered a new process in many areas of microengineering, it has become an established manufacturing method in niche application areas such as inkjet printer nozzle drilling and flat panel display patterning. By controlling the number of laser pulses, and hence the total incident radiation, precise machining depths can be achieved while minimal thermal distortion occurs at the edge of the exposed region. [59]Lasers can ablate nanoholes in deposited gold, [46], or can directly pattern a metal cathode [76]. Laser microfabrication can make microelectrodes by demetalizing a thin film (less than one micron) from a substrate. [59]A fiber laser can also be used to cut out various shapes from metal sheets (100um thick) [30]. The average wavelength of the fiber laser is 1um, and it has a cutting resolution of 30um. The main advantage of laser structuring is that it can make the channels, optical components, microelectrodes, and I/O ports, all with one tool.

Focused Ion Beam Milling: A focused ion beam is used to make a nanohole array for SPR biosensing, but this process is limited with respect to cavity aspect ratio. [32]

Conductive Polymer: If PDMS is cast with metal powders, the resulting material is conductive [186]. Johnson et. al. modeled ionic polymer-metal composites [187], Kim et. al. developed a melt-processable conductive polymer [188] and described manufacturing techniques using these ionic polymers [189]. Shahinpoor et. al. combined these ideas, and put conductive powder into a polymer ionic network [190].

Liquid polymer implantation: Various shapes of metal polymers were cut out of metal sheets using a fiber laser, and then that shape was embedded in the bottom layer of PDMS, and coated with PDMS to prevent contact with the cells. This technique is only useful for 2-D patterns, and limited by resolution of the laser. [30]

Metal ion implantation: It is possible to make 3-D electrodes within a fluidic channel by ion implementation. Low energy metal ions are implanted into a PDMS part through an angled metal shadow mask. [53, 142]

Photoreduction from solution: Korchev in 2004 and Baldacchini in 2005 demonstrate that metals can be reduced from solution, but the catalysts needed for this are difficult to remove after the metal has been deposited [69].

Flowing into polymer microchannels:

Metal hardens: Microelectrodes can be made several ways by flowing metal into channels. First, we could inject molten solder into microfluidic channels (silanized to be wettable) that hardens upon cooling, conforming to the fluidic channel. The channels provide a mold, so no additional alignment is required, but direct contact with the fluid is not possible. [55] Secondly, we could use wire that is melted with soldering iron. [74] Instead of coating the channels to change the hydrophobicity, you can also just place the substrate on a hot plate, insert a solder wire into the inlet holes, and let capillary action (or vacuum) fill the channels as the solder melts [61]. A slightly different approach is to pattern electrical contacts via clean room methods, form microfluidic channels in SU-8 interconnecting the electrical contacts, use those SU-8 channels to deliver a solution to the electrical contacts on the substrate, allow the solution to dry leaving a residue that forms a part of each TFT device, then can flow a protective layer of polymer through the channels to seal up the residue. [143] Similarly, (used to change the surface chemistry) you can write metal nanoparticle films inside sealed channels by using UV light to reduce Ag, Cu, or Au from an aqueous solution. [69]

Metal remains liquid: Mercury can be used as a sensing element - either a mercury droplet directed by an external heater then sealed in with epoxy[34], or deformable, mechanically tuneable antennas made by injecting a liquid metal alloy (eutectic gallium indium) into PDMS channels. [70]

Electroless deposition:

With μCP: Metallic features can be patterned using microcontact printing where electroless silver is the substrate. [39] The metallization can be directed by either selective deactivation of a catalytic substrate or selective activation of a nonreactive surface. Catalysts typically used for the deposition of copper include mixed Sn/Pd colloids, surface-bound palladium(II) species, or palladium colloids. Limitations of this technique include size limits determined by the size of the metal mask used in the photolithographic process, and that it is applicable only to planar surfaces [39]. A technique to reduce the size of features (down to 500nm line size) is to shrink the substrate after microcontact printing of the catalyst [191].

With Laser: Selective metallization in a fabricated microreactor can be accomplished by immersing photostructurable glass in an electroless Cu plating solution. The substrate is moved on a CNC stage with respect to a focused fs laser, so that metal ions in the plating solution are reduced, and metal atoms precipitate out at the laser focused regions. This allows selective metallization of internal walls of hollow microstructures. [78]

With Multiphase Laminar Flow: Flowing solutions of different densities through channels allows electroplating on the inner surfaces of walls [144].

Appendix B

CLEVIOS$^{\text{TM}}$ Material Properties

The material used in Chapter 4 during exploration of μCP of PEDOT is specifically CLEVIOS$^{\text{TM}}$ PH 1000. This appendix provides additional product information.

B.1 CLEVIOS$^{\text{TM}}$ PH 1000 - Product Information

Chemical name: Poly(3,4-ethylenedioxythiophene) poly(styrenesulfonate), abbreviation PEDOT/PSS or PEDOT:PSS. CLEVIOS™ PH 1000 is an aqueous dispersion of the intrinsically conductive polymer PEDT/PSS [poly(3,4-ethylenedioxythiophene) poly(styrene sulfonate)]. CLEVIOS™ PH 1000 is tailored to a high conductivity and forms conductive coatings, and displays the following properties:

- Conductivity over 900 S/cm after the addition of 5% Dimethylsulfoxide, measured at a dried film
- High transmission in the visible spectrum
- Transparent, colourless to bluish coatings
- Good resistance to hydrolysis
- Good photo stability and good thermal stability
- High absorption in the range of 900 to 2000 nm
- No absorption maximum in the visible spectrum up to 800 nm
- Storage at 5°C is recommended.

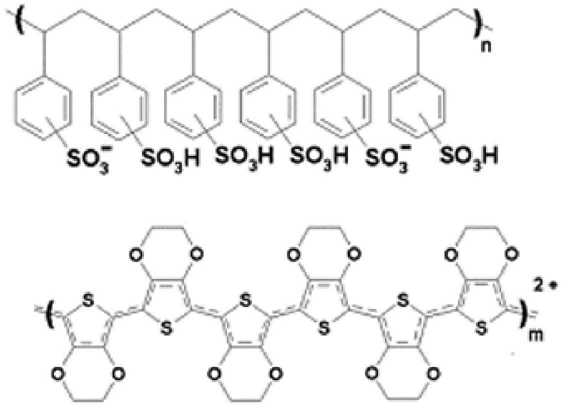

Figure B-1: Clevios PH 1000 Chemical Structure

Form	liquid
Odor	odorless
Color	Dark Blue
Conductivity	min. 900 S/cm (after addition of 5% Dimethylsulfoxide)
Solid content	1.0 to 1.3%
Viscosity	max. 50 mPa-s
pH Value	1.5 to 2.5 at 20°C
Density	1 g/cm^3 at 20°C
PEDOT:PSS ratio	1:2.5 (by weight)
Boiling Point	approx. 100°C

Table B.1: Clevios Chemical and Physical Data, provided by manufacturer

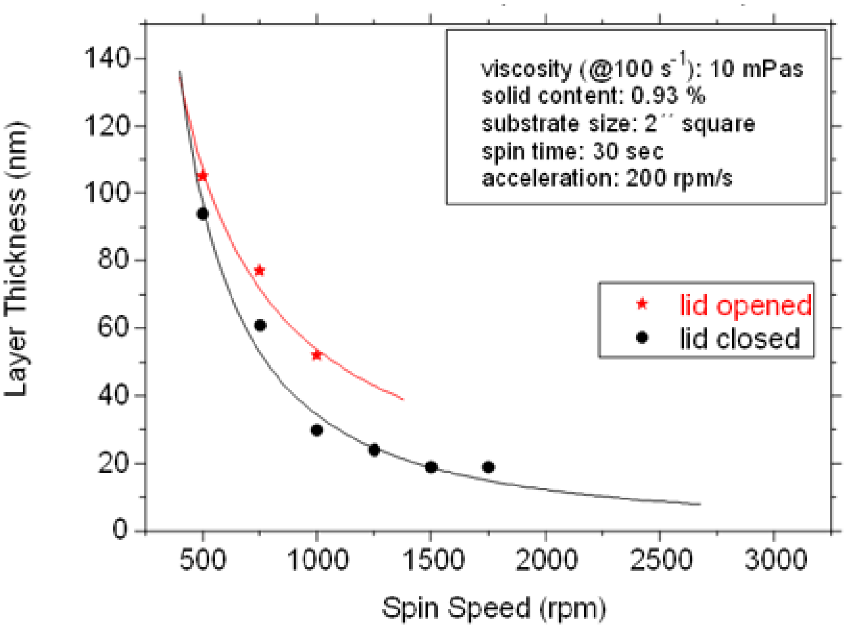

Figure B-2: CLEVIOS™ PH500 (incl. 5wt% DMSO) spin curve, provided by manufacturer

The thickness of the CLEVIOS™ P layer after spin-coating onto ITO is determined by several parameters: spin speed, acceleration, spin time, design of the spin-coater, substrate size, and quality of the pre-conditioning of the substrate surface. The pre-conditioning of the ITO glass strongly affects the ability to uniformly disperse CLEVIOS P onto the substrate surface. Therefore, no general rule can be given to determine at what spin speeds specific layer thicknesses will result.

However Figures B-2 and B-3 give empirically derived spin curves for two grades of PEDOT from Clevios. The spin-curves were obtained on cleaned and ozonized glass substrates of size 5.0 x 5.0 cm^2 . For spin-coating a Carl Süss Spin-Coater RC8 with 3´´gyrset-lid was employed. About 1-2 ml of CLEVIOS™ dispersion was deposited onto the substrate by using a Pasteur pipette (Hilgenberg). The polymer dispersion was distributed manually across the entire substrate surface prior to spin-coating. After spin-coating layers of CLEVIOS™ PH500 and CLEVIOS™ PH510 including 5% DMSO on glass are dried for 15min on a hot plate set to 130°C. After spin-coating, the CLEVIOS™ P layer is dried for 5 minutes at 100 °C to 200 °C on a hot-plate with a Petri dish covering the substrate during drying in order to allow some air exchange while keeping the temperature at a constant level.

In general, the layer-thickness was found to be homogeneous across the substrate, with a somewhat increased thickness at the edges of the substrate.

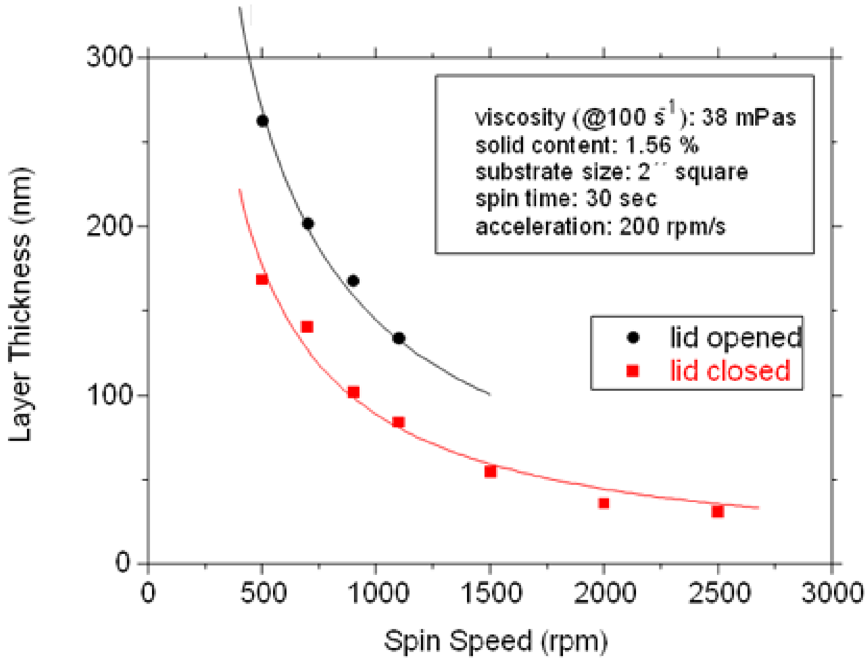

Figure B-3: CLEVIOS™ PH510 (incl. 5wt% DMSO) spin curve, provided by manufacturer

B.1.1 General CLEVIOS Properties

General properties of the whole family of Clevios products are given Tables B.4 and B.5, for future reference in case a different PEDOT formulation is desired.

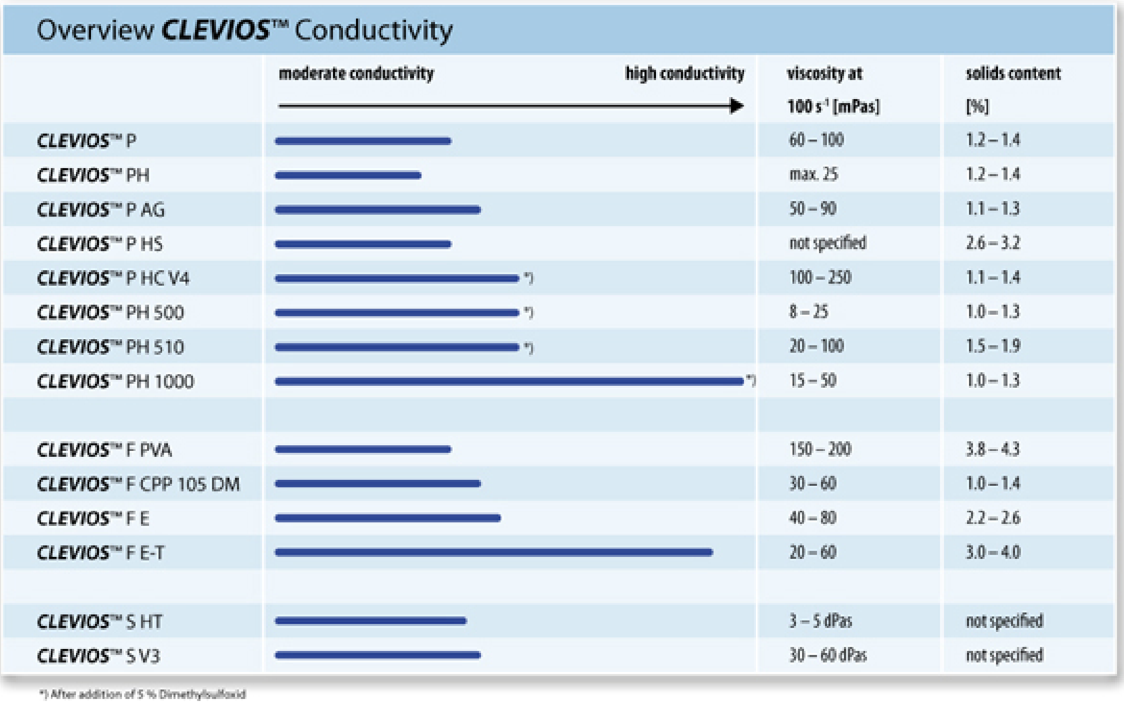

Overview *CLEVIOS*™ Conductivity

	moderate conductivity → high conductivity	viscosity at 100 s^{-1} [mPas]	solids content [%]
CLEVIOS™ P		60 – 100	1.2 – 1.4
CLEVIOS™ PH		max. 25	1.2 – 1.4
CLEVIOS™ P AG		50 – 90	1.1 – 1.3
CLEVIOS™ P HS		not specified	2.6 – 3.2
CLEVIOS™ P HC V4	*)	100 – 250	1.1 – 1.4
CLEVIOS™ PH 500	*)	8 – 25	1.0 – 1.3
CLEVIOS™ PH 510	*)	20 – 100	1.5 – 1.9
CLEVIOS™ PH 1000	*)	15 – 50	1.0 – 1.3
CLEVIOS™ F PVA		150 – 200	3.8 – 4.3
CLEVIOS™ F CPP 105 DM		30 – 60	1.0 – 1.4
CLEVIOS™ F E		40 – 80	2.2 – 2.6
CLEVIOS™ F E-T		20 – 60	3.0 – 4.0
CLEVIOS™ S HT		3 – 5 dPas	not specified
CLEVIOS™ S V3		30 – 60 dPas	not specified

*) After addition of 5 % Dimethylsulfoxid

Figure B-4: Overview of CLEVIOS family properties, provided by manufacturer

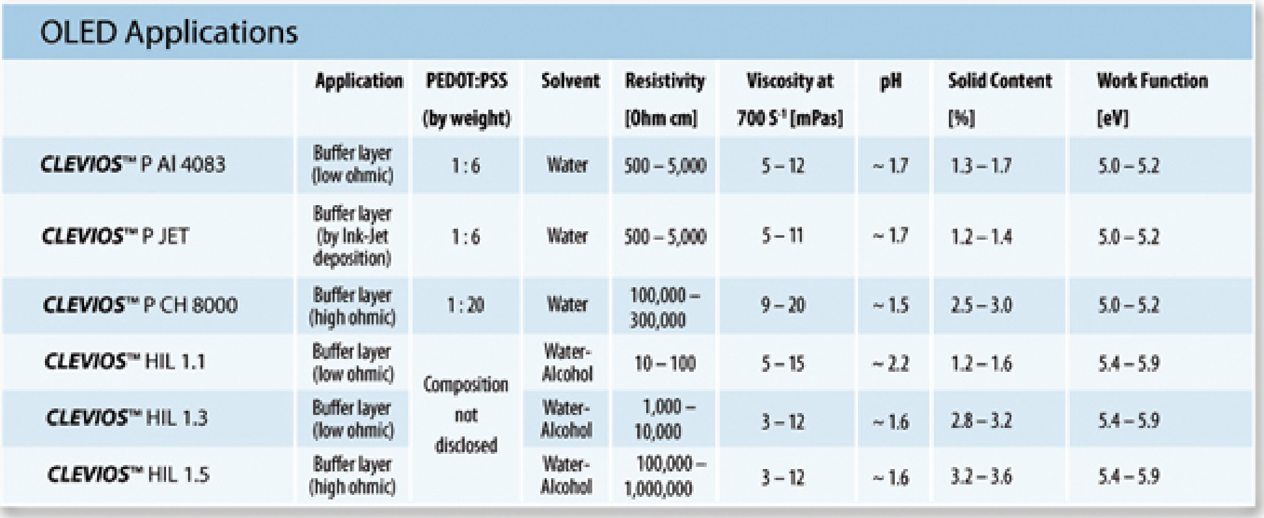

OLED Applications

	Application	PEDOT:PSS (by weight)	Solvent	Resistivity [Ohm cm]	Viscosity at $700\ S^{-1}$ [mPas]	pH	Solid Content [%]	Work Function [eV]
CLEVIOS™ P AI 4083	Buffer layer (low ohmic)	1 : 6	Water	500 – 5,000	5 – 12	~ 1.7	1.3 – 1.7	5.0 – 5.2
CLEVIOS™ P JET	Buffer layer (by Ink-Jet deposition)	1 : 6	Water	500 – 5,000	5 – 11	~ 1.7	1.2 – 1.4	5.0 – 5.2
CLEVIOS™ P CH 8000	Buffer layer (high ohmic)	1 : 20	Water	100,000 – 300,000	9 – 20	~ 1.5	2.5 – 3.0	5.0 – 5.2
CLEVIOS™ HIL 1.1	Buffer layer (low ohmic)	Composition not disclosed	Water-Alcohol	10 – 100	5 – 15	~ 2.2	1.2 – 1.6	5.4 – 5.9
CLEVIOS™ HIL 1.3	Buffer layer (low ohmic)		Water-Alcohol	1,000 – 10,000	3 – 12	~ 1.6	2.8 – 3.2	5.4 – 5.9
CLEVIOS™ HIL 1.5	Buffer layer (high ohmic)		Water-Alcohol	100,000 – 1,000,000	3 – 12	~ 1.6	3.2 – 3.6	5.4 – 5.9

Figure B-5: OLED CLEVIOS properties, provided by manufacturer

Appendix C

Additional Details on Theory of μCP for films

The theory presented in the main thesis body deals with transfer for a liquid. But for PEDOT in particular, it can be desirable to anneal the polymer before transfer to create a film. This is a different transfer regime, and this alternative approach is discussed here.

C.1 Subtractive theory for films

All subtractive methods involve two problems: successful weakening or cracking of film along edges, and successful peeling off. Polymer semiconductors pose a special challenge because i) the fracture toughness is high (esp. vs. metals), so it is not as easy to just use adhesion force, ii) thickness is high (vs. monolayers or nanometer scale thin layers), and iii) polymers have much higher cohesive energy due to entangled chains (although glycerol reduces this).

C.1.1 Problem 1: Weakening or cracking

In order to weaken or crack the film along feature edges, it is necessary to apply relatively high pressure to weaken film at edge of protruding features. This is used for processes such as cold-welding, detachment patterning, and hot lift-off. For cold-welding (normally used with metal films), the high pressure is on the order of 100-300MPa. For hot lift-off (used with polymers or metals), both pressure and temperature are involved. Hot lift-off consists of: applying pressure to mold onto film for short time, which locally fractures film along edges; reduce pressure, raise temperature (enhanced adhesion between mold and film); cool to room temperature, remove pressure; demold, i.e. liftoff. If there is pressure but no heating, there is not good enough adhesion to peel off film. If there is heating but no pressure, the pattern fidelity is poor and the printed geometry doesn't follow the feature edges. [172]

Cracking can be produced by using an elastic back plane to creating pressure points. For instance, using a flat PDMS substrate and epoxy mold can assist in cracking, because under pressure the elastic deformation of PDMS around the protruding edges of the mold is larger than the plastic deformation in the polymer film between the protrusions. Elastic deformation of PDMS substrate gives rise to deformation in the polymer film, which elongates the polymer film at the edge of the pattern and reduces the thickness of the film. It is the polymer film (stiff compared to the PDMS) that endures most of the external pressure, thus it is possible to cut the polymer film into regular structures. [172]

C.1.2 Problem 2: Adhesion

Weakening and cracking variable definitions: [14]

F : Peel Force normal to the stamp/mold interface, where the stamp is peeled in direction parallel to edges of features

$G_{substrate-film}$: Fracture energy (or energy release rate) per unit crack area required to demold substrate and film

$G_{film-mold}$: Fracture energy per unit crack area between film and mold

$G_{film-film}$: Fracture energy associated with tearing the film itself

W_a : Work of adhesion

W_{mf} : Work of adhesion between mold and film

W_{sf} : Work of adhesion between substrate and film

There are two criteria for whether a film will crack along feature edges and transfer from mold to substrate:

Criteria 1: $W_{mf} > W_{sf}$

This means that the adhesion strength between mold and film is greater than the adhesion between substrate and film, for liftoff, or vice-versa for stamping.

Criteria 2: $|W_{mf} - W_{sf}| > G_{film-film}$

This means that the difference in adhesion strength of two interfaces should exceed the cohesion strength of the film [14].

The actual force involved in peeling may be orders of magnitude higher than predicted

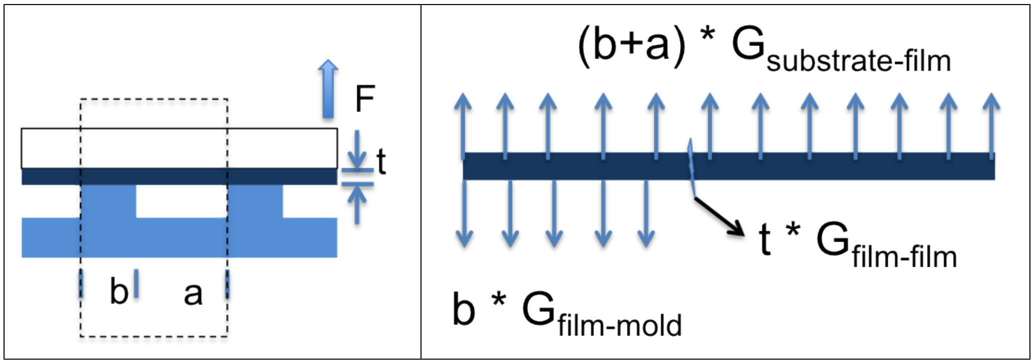

Figure C-1: Modeling the μCP process with a film instead of a liquid, with cracking predicted by force minimization

$$\frac{F}{N} = \begin{cases} b^*G_{\text{film-mold}} & \text{No Transfer to mold} \\ b^*G_{\text{substrate-film}} + t^*G_{\text{film-film}} & \text{Lift-off} \\ (b+a)^*G_{\text{substrate-film}} & \text{Blanket Transfer to mold} \end{cases}$$

Figure C-2: Cracking criteria, using fracture mechanics to predict film transfer [14]

by W_a, because of irreversible energy dissipated at the surface and in the bulk of materials. The actual force is a function of interfacial geometry, peeling velocity, and temperature. [14]

Thinking about the problem of film transfer from a fracture mechanics perspective, there are three possible outcomes - either the film stays stuck to the mold and does not transfer at all, the film cracks along feature edges and the pattern transfers to substrate, or the film does not crack along edges and the entire film transfers to the substrate. To determine which of these outcomes will occur, the goal is to minimize the total peel force on unit segment of film at crack propagation plane. Figure C-1 shows a diagram of the process to model, with repeating line patterns of width b and spacing a.

The process with the smallest peel force is most likely to occur. The criteria under which each outcome will occur are given in Figure C-2.

Fracture energy G is described by [14]:

$G = G_o * [1 + f(v, T)]$

where G_o is critical fracture energy below which no fracture occurs, and $[1 + f(v, T)]$ is amount of energy expended in irreversible processes. While the irreversible energy term is close to 1 for interfaces of most elastic materials (i.e. $G_{film-substrate}$ or $G_{film-fim}$), it rapidly increases with increasing v or decreasing T for interfaces of viscoelastic materials such as PDMS (i.e. $G_{mold-film}$).

Therefore rapid peeling at reduced temperatures increases $G_{mold-film}$, without significantly influencing other terms, making a value associated with Case 2 and 3 smaller than Case 1, so that lift-off or blanket transfer to PDMS mold is favored. Slow peeling at high temperatures decreases $G_{mold-film}$, so that no transfer to mold is favored (which is the failure mode most commonly observed by the author).

Appendix D

Additional Details of PEDOT Experiments

D.1 Difficulty coating PDMS stamp

The first necessary step in doing μCP is to coat the ink onto the PDMS stamp (or, onto an inkpad, and then onto the PDMS stamp). If the ink is unable to uniformly coat the stamp, every other effort is wasted - so PDMS spincoating was the first exploration.

D.1.1 Difficulty with plasma settings

Spincoating PEDOT directly onto untreated PDMS does not work at all - the PDMS is naturally hydrophobic and the ink flies right off. From the literature, it was clear that some sort of treatment to improve hydrophilicity would be needed, and the most common method is to plasma treat the PDMS. Initial testing in the MIT cleanroom used O2 plasma at 100W for 0.3min, and was able to get a good coating of PEDOT ink with spincoating parameters of 2000rpm for 30 seconds.

Then experiments moved to the 35-029 Hardt lab, where an air plasma chamber was available. Using the same 100W, 0.3min settings produced uneven coating, as seen in Figure D-1. The manufacturer of PEDOT recommended using a Q-tip or spreader to manually distribute the ink over the stamp before turning on the spincoating. As seen in Figure D-2, this manual step does produce good coverage initially, but within a few seconds the resulting film soon begins to bead up.

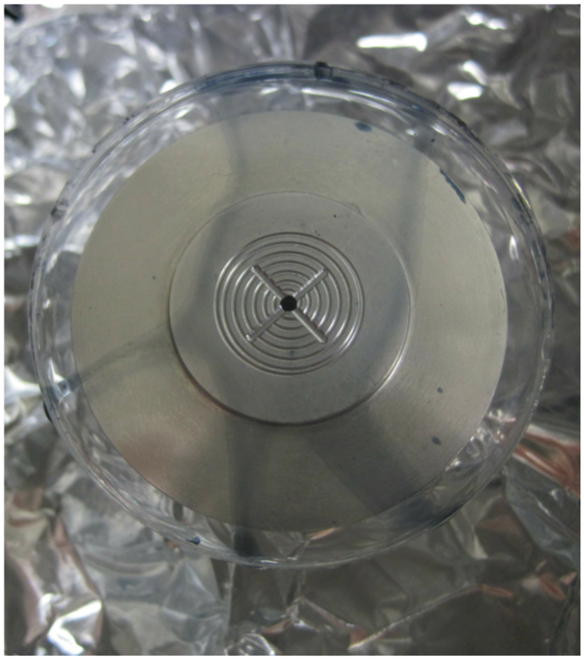

Figure D-1: Uneven coating of PDMS stamp with PEDOT, even after plasma treatment at 100W for 0.3min of air plasma.

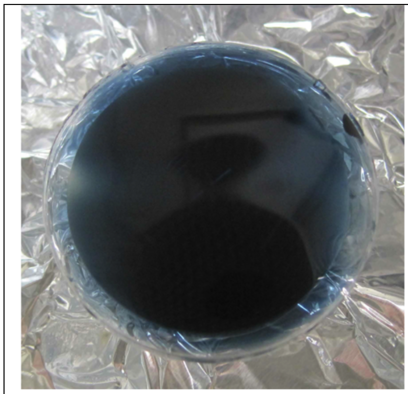	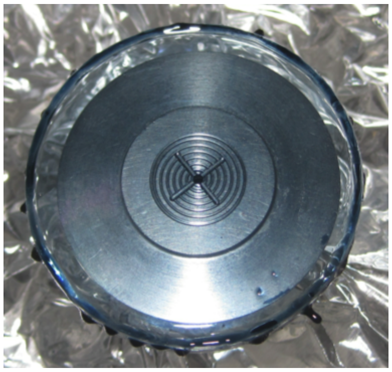	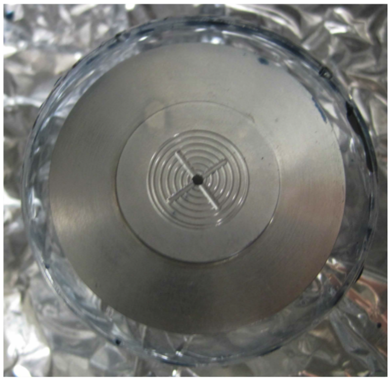
a) manual spreading of PEDOT prior to spinning	b) immediately after spinning	c) quickly beading up after spinning

Figure D-2: Manual spreading of PEDOT on plasma treated PMMA before spinning, which improves coverage, but the coating quickly beads up spontaneously when spinning stops.

Why is this occurring? In pursuit of this question, spin parameters were varied, the ink was varied (water as well as PEDOT and water:PEDOT mixtures were tried), and the substrate was varied (PDMS, glass, and PMMA were all tried). A PDMS stamp with features was also tried instead of a flat stamp. Because none of these parameters yielded a good uniform coating of PEDOT, the conclusion was that it was the type of plasma used (air, instead of O2). But because O2 plasma is not available in the experimental lab, several alternative treatments were tested.

Figure D-3 shows the results of spincoating PEDOT ink at 2000rpm for 30 seconds on PDMS with a) no treatment, b) handheld corona treatment with polyethyleneimine (PEI) coating, c) air plasma at 250W for 30 seconds, and d) handheld corona alone. The PEI coating is supposed to make PDMS hydrophilic for at least five days, as opposed to 15-30min with plasma. This screening experiment indicates that the air plasma at 250W is the only treatment which raises the surface energy of PDMS enough to wet completely with PEDOT ink.

It is also useful to note that a short ramp-up step (0.5-2 seconds or so) at the beginning of spincoating helps to distribute the ink.

D.1.2 Difficulty with volume of ink

It is also important to put enough ink on the PDMS stamp. Although it seems wasteful, failure to provide a generous abundance of ink leads to voids in the coating (see Figure D-4).

D.1.3 Difficulty adding coloring to ink

While doing all these tests to establish a good coating protocol, a lot of ink was being wasted. To avoid this expense, alternate inks were tried, to see if a “proxy” PEDOT could be identified. Although it seems obvious now at the end of the thesis, at the beginning it was not clear how sensitive processes such as spincoating would be to ink properties. Figure D-5 shows the results when spincoating a) blue food dye, b) green food dye in water, c) 1:1 green and blue food dye, and d) PEDOT ink as a control.

Of these, the only successful coating was the PEDOT control ink. For this reason, it was concluded that there is no simple “proxy” PEDOT, and it was better to just continue all necessary tests with PEDOT.

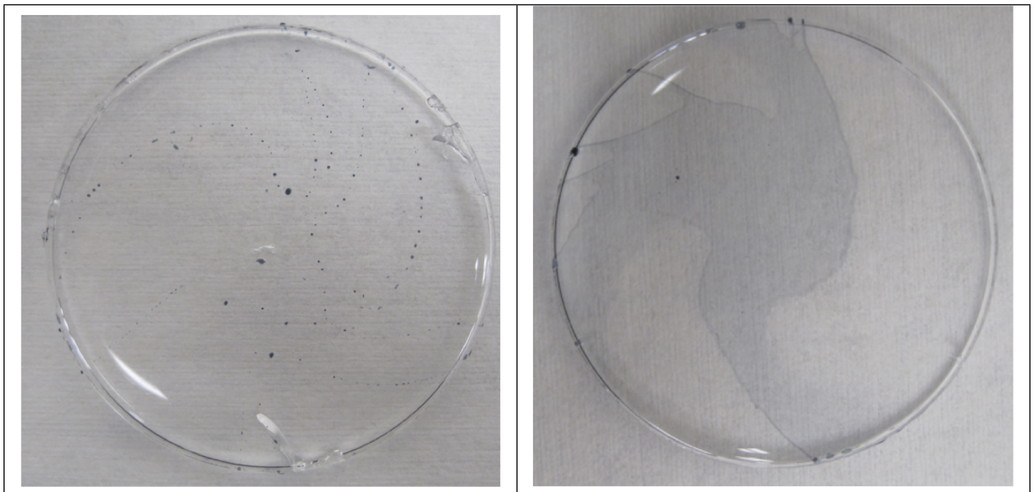

a) no treatment

b) Corona + PEI

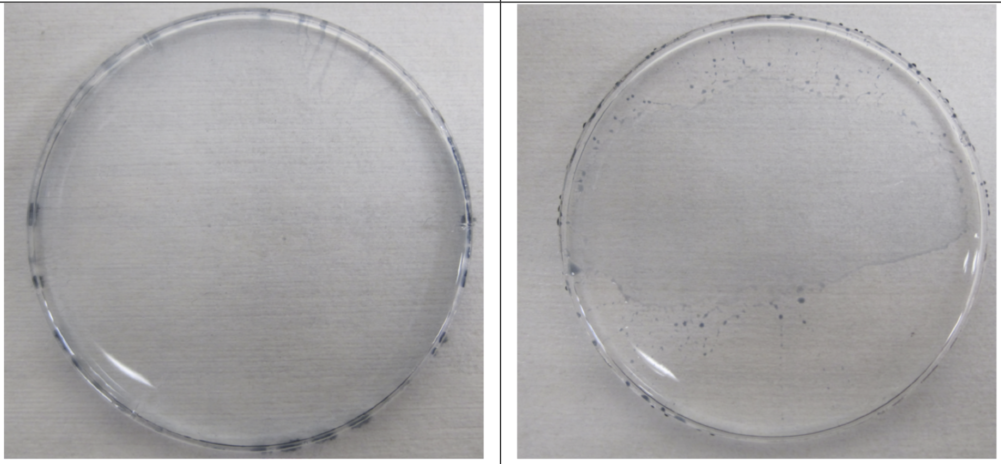

c) Air plasma at 250W for 30 seconds

d) Corona

Figure D-3: Results of PEDOT spincoated at 2000rpm for 30 seconds onto PDMS with different treatments, to improve hydrophilicity, showing that air plasma provides the best results.

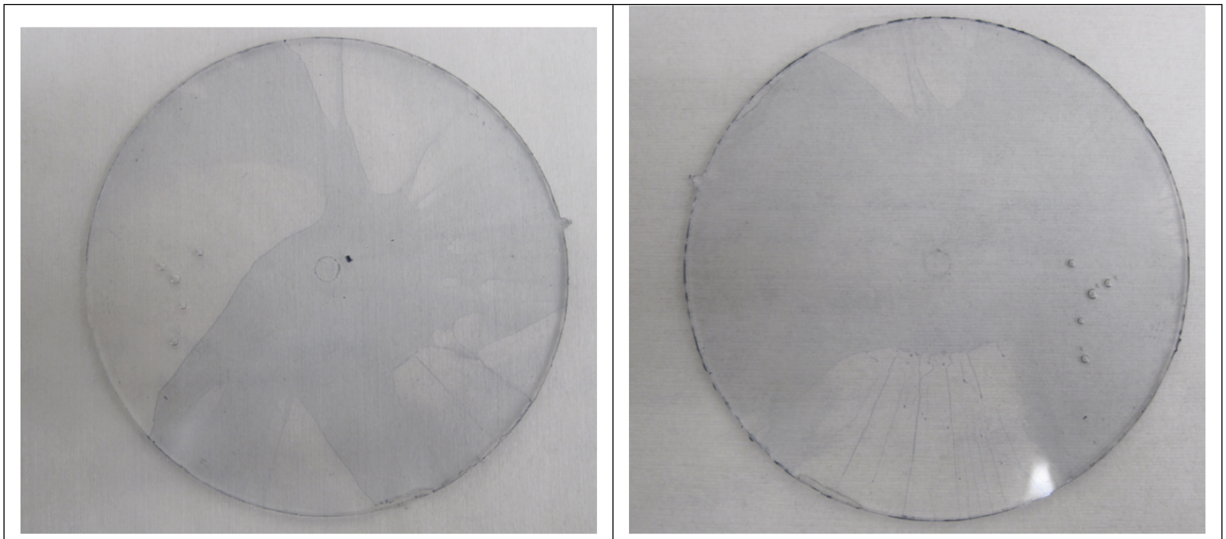

a) with small volume, <0.5mL

b) with larger volume, at least 1mL

Figure D-4: Difference in coverage of PEDOT on PDMS after spincoating with different initial volumes.

D.2 Initial transfers from flat stamp to slide

Once a procedure for simple coating of a PDMS stamp with PEDOT was established, the next step was to transfer that coating to a substrate. To start with the most simple case, a flat PDMS stamp with PEDOT was used to stamp onto a glass slide (glass being more favorable that a polymer for printing).

A flat PDMS stamp was plasma treated as spincoated at 2000rpm for 30 seconds, then placed by hand onto a glass slide, with no pressure other than gravity. If the ink remained liquid, then a smeared pattern would appear after the slide was removed (see Figure D-7). Therefore it was decided that the slide and PDMS stamp needed to be dried while still in contact. This was accomplished by placing stamp and slide together on a hot plate at 80°C (setting of the hot plate, not necessarily the temperature of the slide or stamp).

Figure D-7 shows the results of transfer with the PEDOT dried to a film. For this experiment, a 4" PDMS stamp was treated for 30 seconds with 125W air plasma. The stamp was spincoated with 1.5mL of Clevios PH1000 PEDOT ink, at 2000rpm for 30 seconds. A glass slide was placed on an 80°C hot plate, the stamp was placed in a rolling-down motion on top of the slide, and the stamp and slide together were left on the hot plate to dry for 20 minutes (Figure D-7 a). Then the stamp was peeled off the slide (Figure D-7 b), and the film transferred nearly completely (only a few small voids where the film tore).

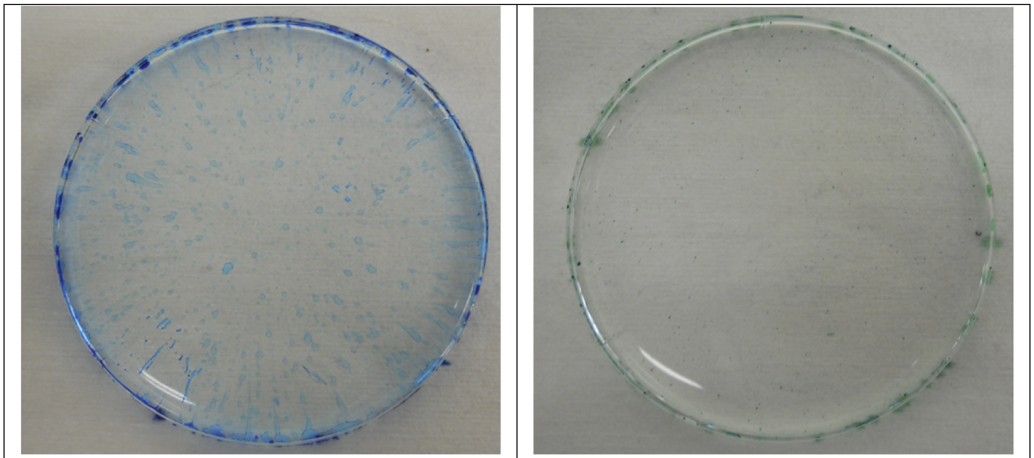

a) blue food dye

b) ∼1:1 green food dye:water

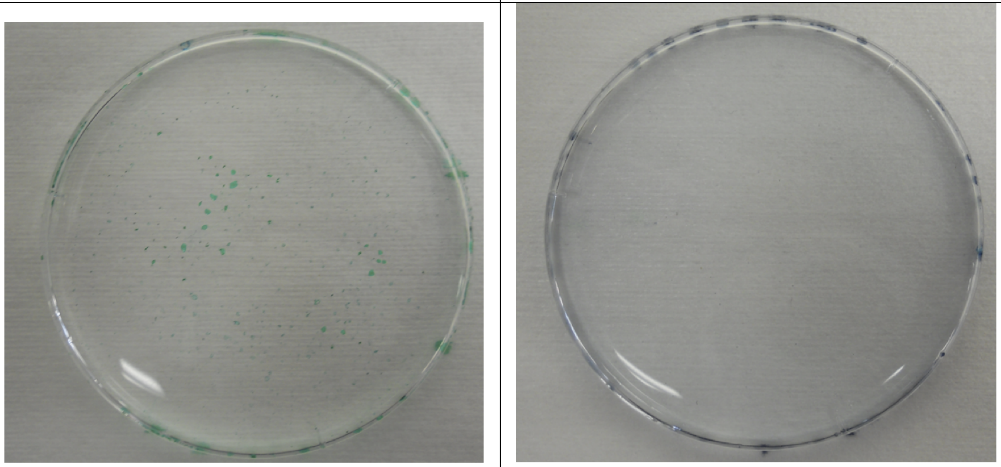

c) 1:1 green and blue food dye

d) PEDOT, as control

Figure D-5: Different ink choices spincoated onto PDMS in exploration of finding a "proxy" ink to replace PEDOT, for the purpose of saving expensive ink. Food dye is not an acceptable substitute for PEDOT in spincoating behavior.

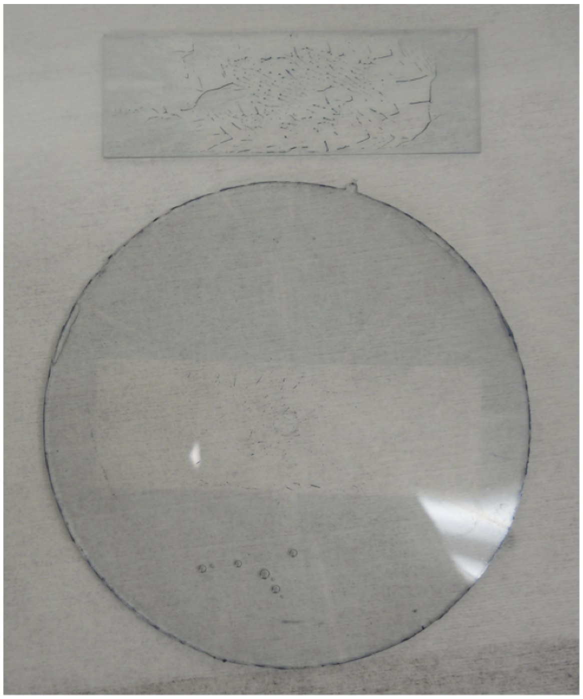

Figure D-6: PEDOT transferred from PDMS to glass slide by hand, no pressure, ink remains liquid during slide removal. Resulting pattern shows liquid smear pattern.

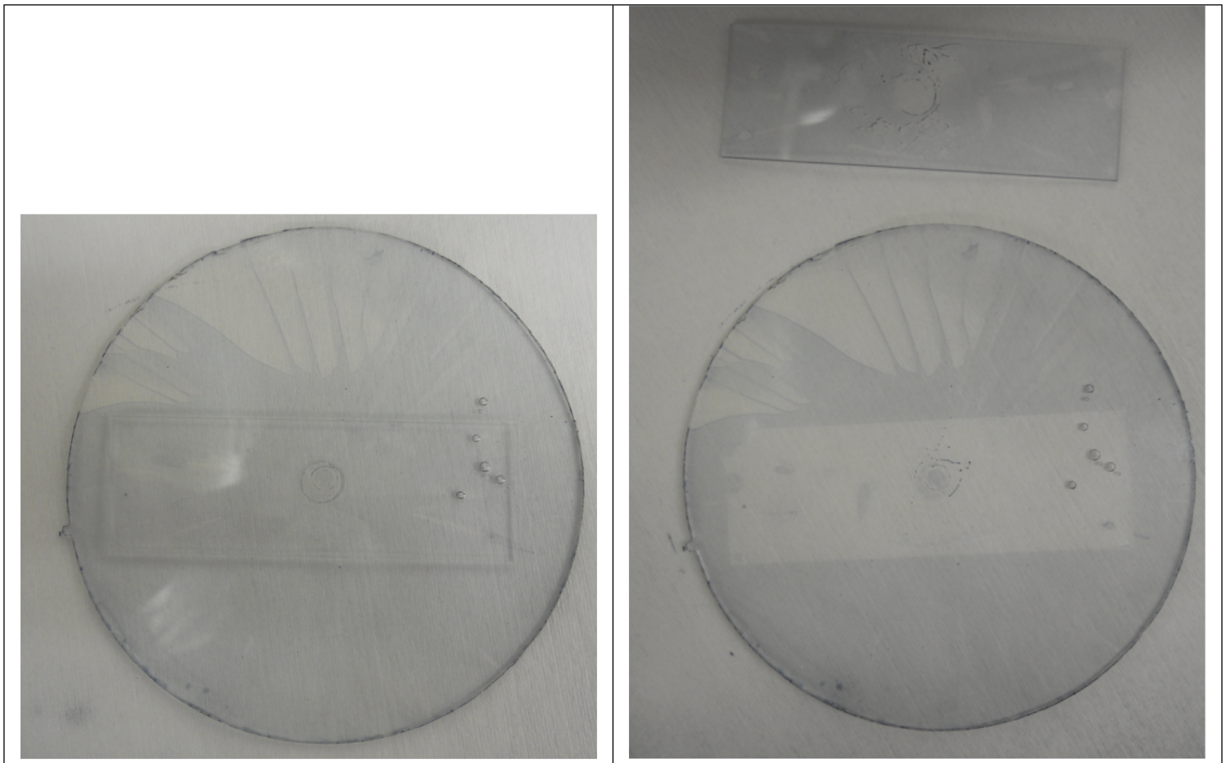

a) before peeling

b) after separation

Figure D-7: PEDOT transferred from PDMS to glass slide by hand, no pressure, ink is dried prior to slide removal. Resulting pattern shows nearly complete film transfer.

Exp #	Plasma	PEDOT:glycerol	Spin	Dry	Anneal	Anneal
3	30s 250W	3:1	2000rpm 30s	1min	90C w/ 200g 4min	170C 3min
4	30s 175W	3:1	2000rpm 30s	1min	90C w/ 200g 4min	170C 3min
5	30s 150W	2:1	2000rpm 30s	1min	90C w/ 200g 4min	170C 3min
6	30s 150W	2:1	2000rpm 30s	1min 20s	90C w/ 200g 4min	170C 3min
7	30s 150W	4:1	2000rpm 30s	1min	90C w/ 200g 4min	170C 3min
8	30s 150W	4:1	2000rpm 30s	1min	90C w/ 200g 4min	170C 3min

Table D.1: PEDOT:Glycerol ink additive ratio - Design of experiments

D.3 Experiment DOE with glycerol

Glycerol was recommended by the manufacturer as an additive for the PEDOT ink, to increase conductivity and to improve printing characteristics. To test the printing performance with glycerol additive, a PDMS stamp with 50μm lines was spincoated with inks with varying ratios of glycerol additive, and stamped onto plasma treated glass cover slips (25mm by 25mm size). The experimental parameters used are shown in Table D.1. (Variation in plasma treatment was unintentional - it can be difficult to dial in the power with the equipment available.)

Figure D-8 shows that overall view of the PEDOT:Glycerol DOE slides. It is apparent that PEDOT is definitely printed onto the glass, but the overall uniformity is poor and every glass slide has patches and voids where PEDOT did not transfer, in unpredictable locations. Figure D-9 shows a microscope image of the best results on each slide of printed 50μm lines. These selections shows that good transfer is possible, just not in a uniform manner over large areas. Unfortunately for a manufacturing study, robustness over large areas is critically important, and these results do not indicate that this process is a good candidate for high volume production.

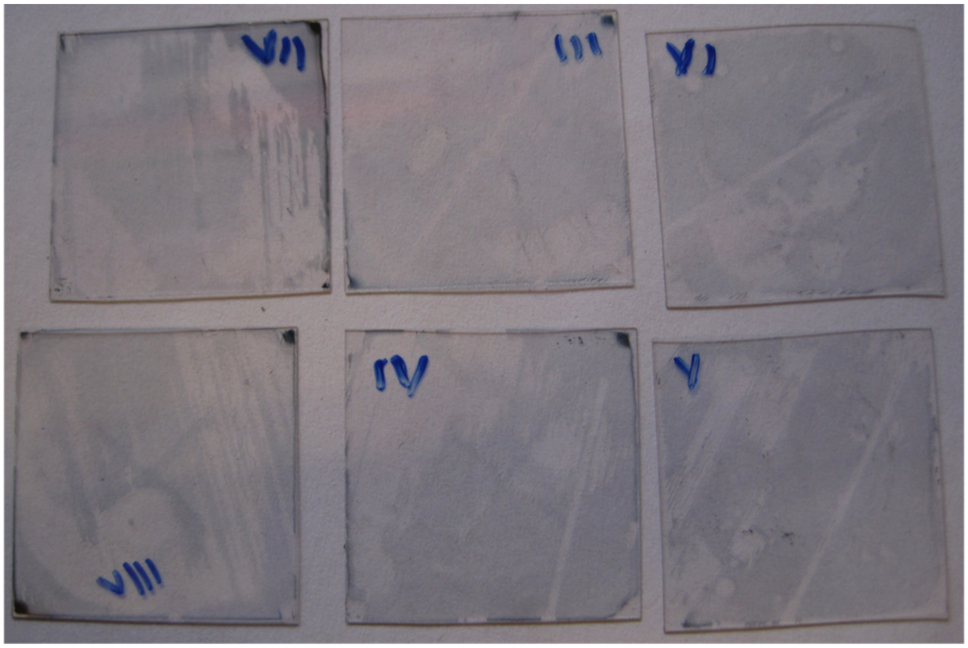
VII
III
VI
VIII
IV
V

Figure D-8: PEDOT:Glycerol design of experiments with 50μm lines, images of macro results, showing poor overall uniformity.

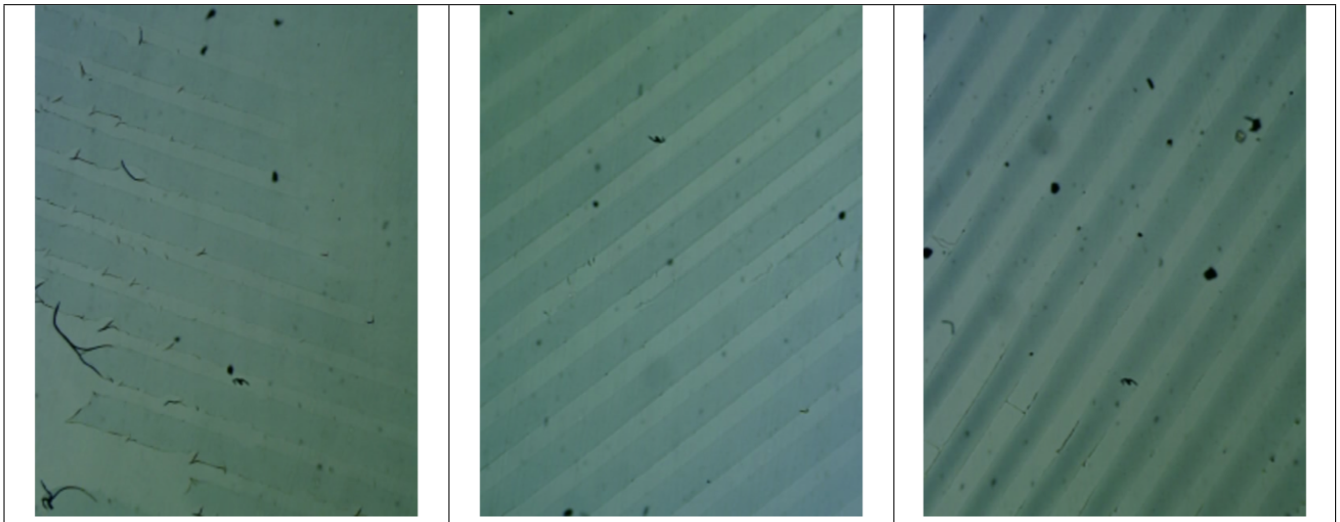

a) 4:1 PEDOT:Glycerol, exp #7 b) 3:1 PEDOT:Glycerol, exp #3 c) 2:1 PEDOT:Glycerol, exp #5

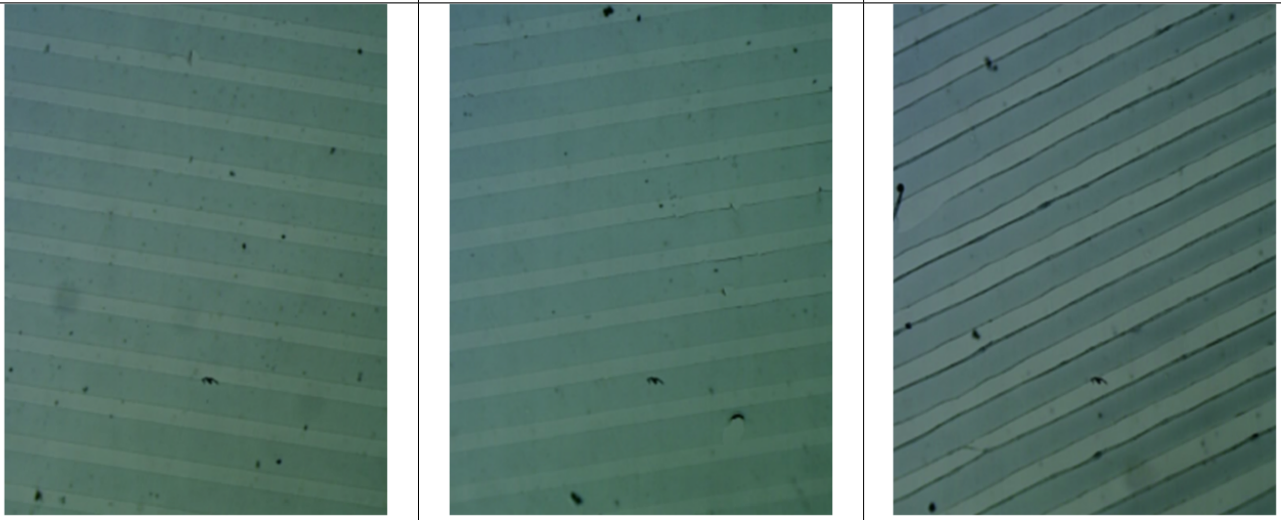

d) 4:1 PEDOT:Glycerol, exp #8 e) 3:1 PEDOT:Glycerol, exp #4 f) 2:1 PEDOT:Glycerol, exp #6

Figure D-9: PEDOT:Glycerol design of experiments with 50μm lines, images of micro results, choosing the best section to image from each experimental run. Shows that printing is possible for small areas, although not uniform over large areas.

Appendix E

Stamping Apparatus with Flexure, Designed for Incorporation with Spincoater

The idea of using a single-part stamping apparatus as an alternative to a printing roll was explored, because the initial motivation for this thesis was to print individual microfluidic devices (as opposed to continuous webs of material, as is more common in flexible electronics). It was ultimately decided that a printing roller would be more easily adapted to industrial manufacturing.

The alternate stamping design is presented in this appendix. In this configuration, a commercial spincoater (Figure E-1) is used to directly coat a PDMS stamp with ink (as opposed to coating an inkpad with ink, as in the thesis protocol, with a transfer step to the stamp). Then the substrate is held in a vacuum chuck, turned upside down, and placed in a kinematic coupling connected to a flexure. The flexure restricts the motion of the substrate to the vertical z-direction only, and allows tip and tilt to account for variations in the stamp and substrate. The x- and y-axis movements are constrained, so that alignment between substrate and stamp is maintained.

The stamping mechanism itself was envisioned as a “bubble pressure” transfer instead of rolling transfer. The substrate chuck is pressed down so that an integrated ring seals onto the outer edges of the PDMS stamp. Then positive air pressure is applied to the backside of the stamp through a hole in the middle of the spincoater chuck. This positive pressure

SCS
SPECIALTY COATING SYSTEMS™
SCS 6800 Spin Coater Series

Figure E-1: Commercial spincoater equipment used, Model SCS6800 from Specialty Coating Systems

creates a bubble behind the stamp, pressing the stamp into contact with the substrate with a radially propagating contact line. This back pressure is then released, the substrate is removed, and the transferred pattern is annealed with an integrated heater in the substrate chuck.

E.1 Design of flexure for stamping apparatus

The flexure design for this apparatus is shown in Figure E-2. This flexure is grounded to the spincoater, and an independent substrate chuck sits on kinematic couplings through the center of the flexure. The flexure integrated into the overall equipment is shown in Figure E-3, with the flexure bolted into a spacer assembly and then grounded to the spincoater base.

E.2 Design of substrate holder for stamping apparatus

The substrate to be printed is held in a substrate chuck, with integrated vacuum line and heater. The vacuum is used to hold the substrate in place while inverted during printing. The integrated heater is used to anneal the printed pattern after transfer (or potentially

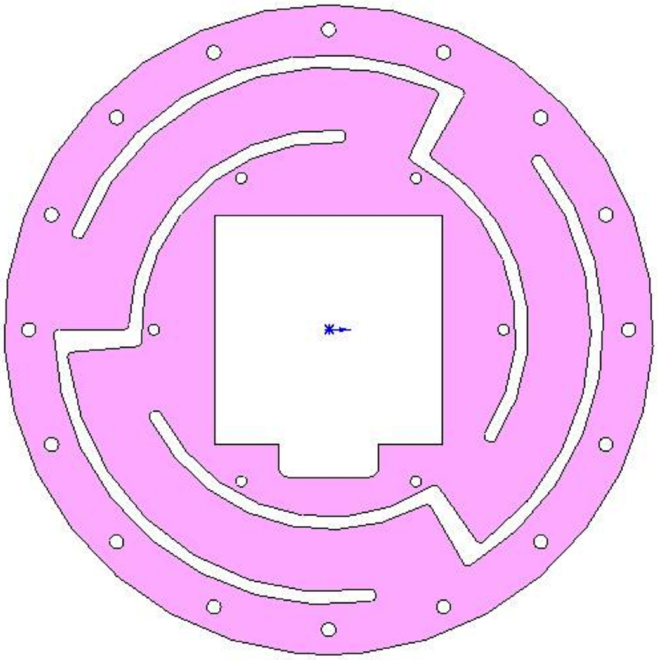

Figure E-2: Flexure design for stamping apparatus allowing motion in the vertical z-direction, tip, and tilt; constraining movement in the x, y, and θ_z directions.

even during printing). The heater element would also allow exploration of the effect of temperature on the transfer process itself.

A CAD model of the substrate chuck is shown in Figure E-4. The assembly consists of i) a substrate holder (two designs were made, for a 1x3" microscope slide size and for a 1x1" substrate size) with alignment ridges for substrate placement, an outer ring for sealing against the PDMS stamp, and integrated vacuum line, ii) aluminum plate with pocket to hold ceramic heater, iii) thermal insulator block to prevent excessive heat transfer through the backplate, and iv) backplate with kinematic half-spheres, for repeatable mating to the flexure assembly.

Detailed drawings for the critical piece - the substrate holder - are shown in Figures E-5 and E-6, for the 1x3" and the 1x1" size respectively. The detailed drawing for the heater holder is shown in Figure

E.3 Assembled stamping apparatus

The fabricated equipment is shown in Figure E-8. Note that for safety reasons, the equipment should be operated with a cover during use. Shown without cover for illustrative purposes.

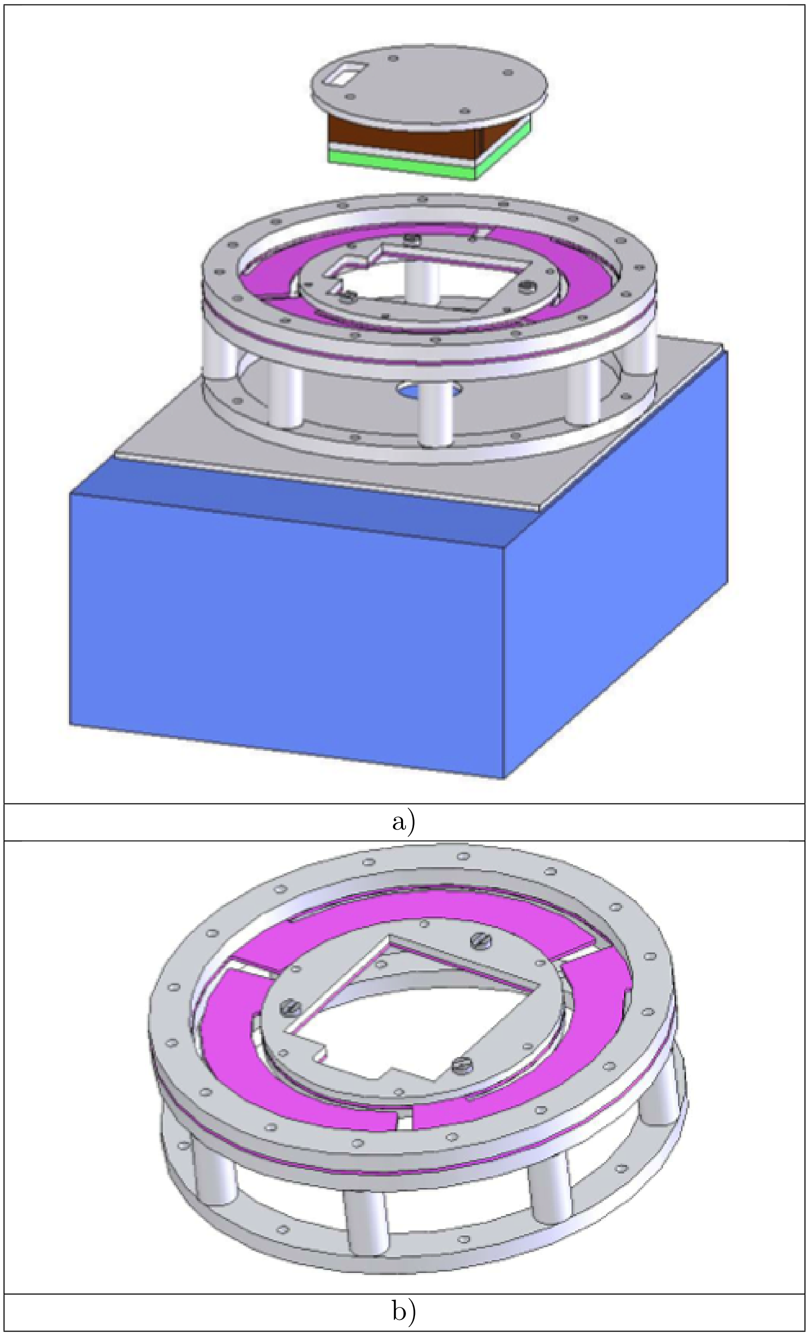

a)

b)

Figure E-3: Spincoater with integrated flexure design. a) spincoater base with flexure assembly grounded to equipment. b) flexure assembly, with flexure attached to spacers to hold flexure at specific distance above spincoater chuck.

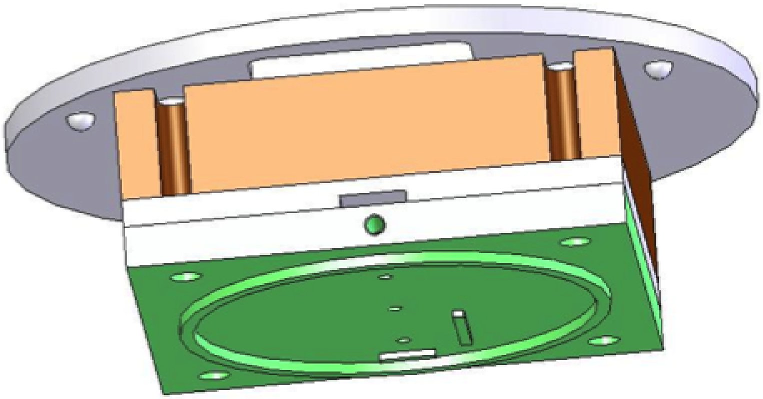

Figure E-4: CAD model of substrate chuck, showing (from bottom to top), substrate holder with alignment ridges and sealing ring, heater, insulation block, and backing plate with kinematic coupling half-spheres.

The critical assembly criteria is the gap between the substrate holder and the spincoater chuck, when the substrate chuck is placed into the flexure (show in Figure E-9). The gap needs to be small enough to be within the flexure range of travel (∼2mm), so that the when pressed down the outer ring on the substrate holder will form a tight seal with the edges of the PDMS stamp. This holds the alignment between the stamp and the substrate, and allows the stamp to be pressurized from the backside without leakage. Positive pressure is applied through the same port that normally provides vacuum to the spincoater chuck during operation (the spincoater was modified with an additional valve for this purpose).

This fabricated apparatus was briefly tested with printing of PEDOT, but no protocol was able to achieve successful printing. Further investigation into surface energy revealed that it was not an equipment failure, but rather a fundamental problem with the materials being used. By the time research investigation shifted to microcontact printing of silver, a suitable printing roll had been developed by Joe Petrzelka [10]. Because a printing roll can be extended directly into industry (by simple substitution into existing roll-to-roll printing equipment), and because the printing roll was developed specifically with careful process control in mind (even in general a rolling motion was hypothesized to be easier to control in a precise manner than bubble pressure), this stamping apparatus was abandoned in favor of using a rolling motion.

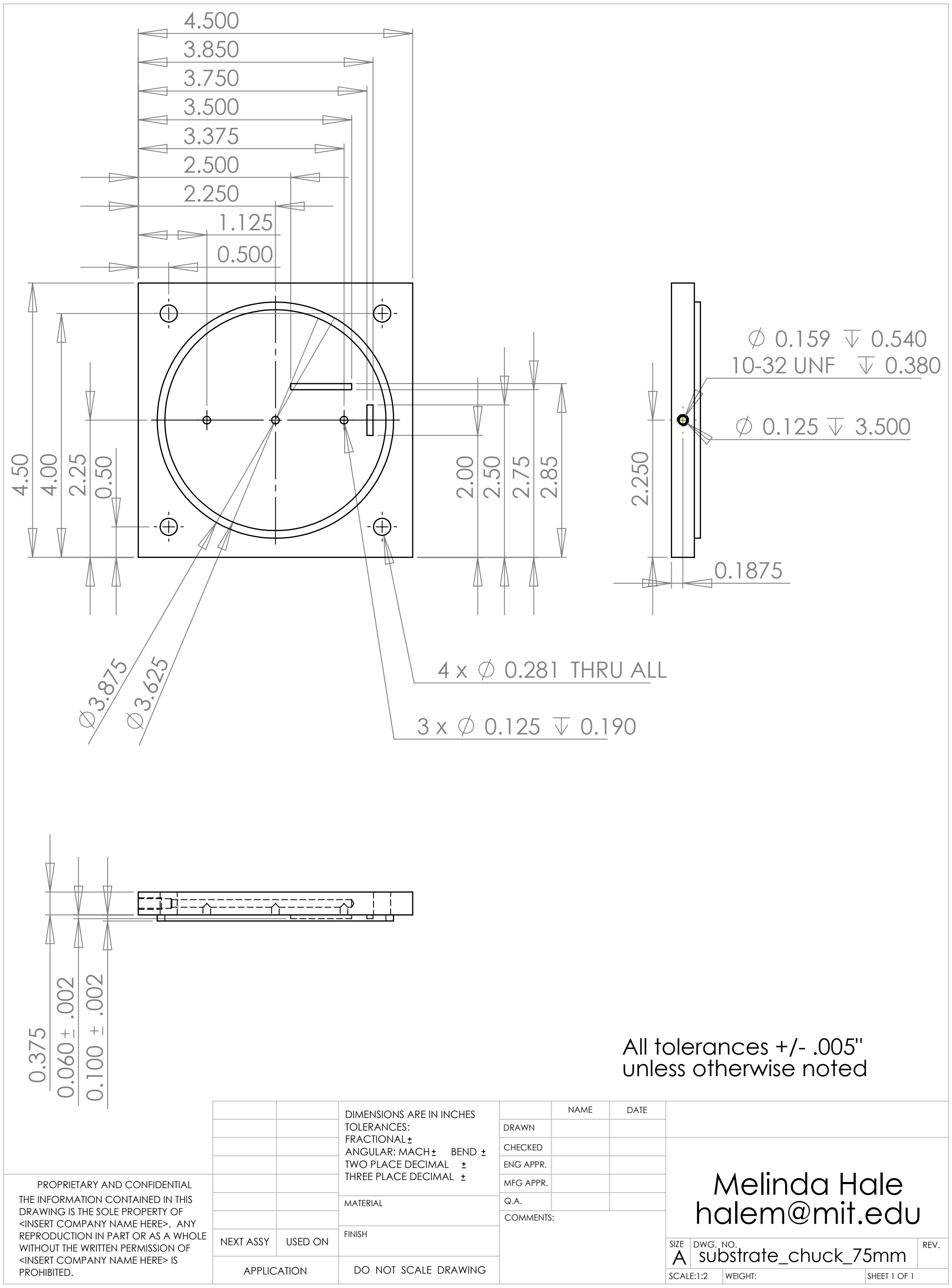
4.500
3.850
3.750
3.500
3.375
2.500
2.250
1.125
0.500
4.50
4.00
2.25
0.50
2.00
2.50
2.75
2.85
∅ 0.159 ↧ 0.540
10-32 UNF ↧ 0.380
∅ 0.125 ↧ 3.500
2.250
0.1875
∅3.875
∅3.625
4 x ∅ 0.281 THRU ALL
3 x ∅ 0.125 ↧ 0.190
0.375
0.060 ± .002
0.100 ± .002
All tolerances +/- .005"
unless otherwise noted
DIMENSIONS ARE IN INCHES
TOLERANCES:
FRACTIONAL±
ANGULAR: MACH± BEND ±
TWO PLACE DECIMAL ±
THREE PLACE DECIMAL ±
NAME
DATE
DRAWN
CHECKED
ENG APPR.
MFG APPR.
Q.A.
COMMENTS:
MATERIAL
FINISH
NEXT ASSY
USED ON
APPLICATION
DO NOT SCALE DRAWING
PROPRIETARY AND CONFIDENTIAL
THE INFORMATION CONTAINED IN THIS DRAWING IS THE SOLE PROPERTY OF <INSERT COMPANY NAME HERE>. ANY REPRODUCTION IN PART OR AS A WHOLE WITHOUT THE WRITTEN PERMISSION OF <INSERT COMPANY NAME HERE> IS PROHIBITED.
Melinda Hale
halem@mit.edu
SIZE
A
DWG. NO.
substrate_chuck_75mm
REV.
SCALE:1:2
WEIGHT:
SHEET 1 OF 1

Figure E-5: Detailed drawing of 1x3" slide holder, part of substrate chuck assembly

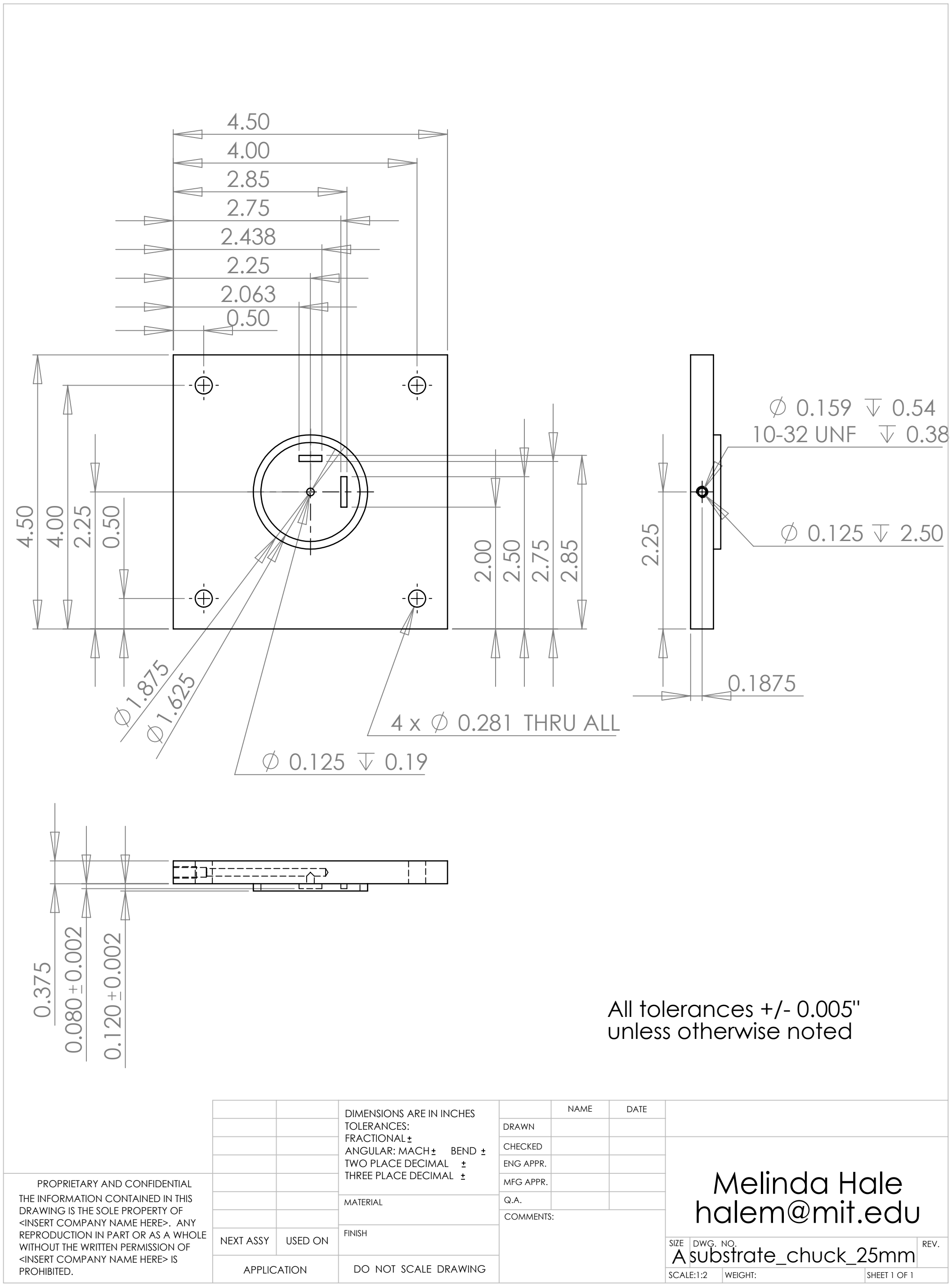
4.50
4.00
2.85
2.75
2.438
2.25
2.063
0.50
∅ 0.159 ↧ 0.54
10-32 UNF ↧ 0.38
∅ 0.125 ↧ 2.50
2.00
2.50
2.75
2.85
2.25
0.1875
∅1.875
∅1.625
4 x ∅ 0.281 THRU ALL
∅ 0.125 ↧ 0.19
0.375
0.080±0.002
0.120±0.002
All tolerances +/- 0.005"
unless otherwise noted
DIMENSIONS ARE IN INCHES
TOLERANCES:
FRACTIONAL±
ANGULAR: MACH± BEND ±
TWO PLACE DECIMAL ±
THREE PLACE DECIMAL ±
NAME
DATE
DRAWN
CHECKED
ENG APPR.
MFG APPR.
Q.A.
COMMENTS:
MATERIAL
FINISH
NEXT ASSY
USED ON
APPLICATION
DO NOT SCALE DRAWING
PROPRIETARY AND CONFIDENTIAL
THE INFORMATION CONTAINED IN THIS DRAWING IS THE SOLE PROPERTY OF <INSERT COMPANY NAME HERE>. ANY REPRODUCTION IN PART OR AS A WHOLE WITHOUT THE WRITTEN PERMISSION OF <INSERT COMPANY NAME HERE> IS PROHIBITED.
Melinda Hale
halem@mit.edu
SIZE
DWG. NO.
REV.
A
substrate_chuck_25mm
SCALE:1:2
WEIGHT:
SHEET 1 OF 1

Figure E-6: Detailed drawing of 1x1" slide holder, part of substrate chuck assembly

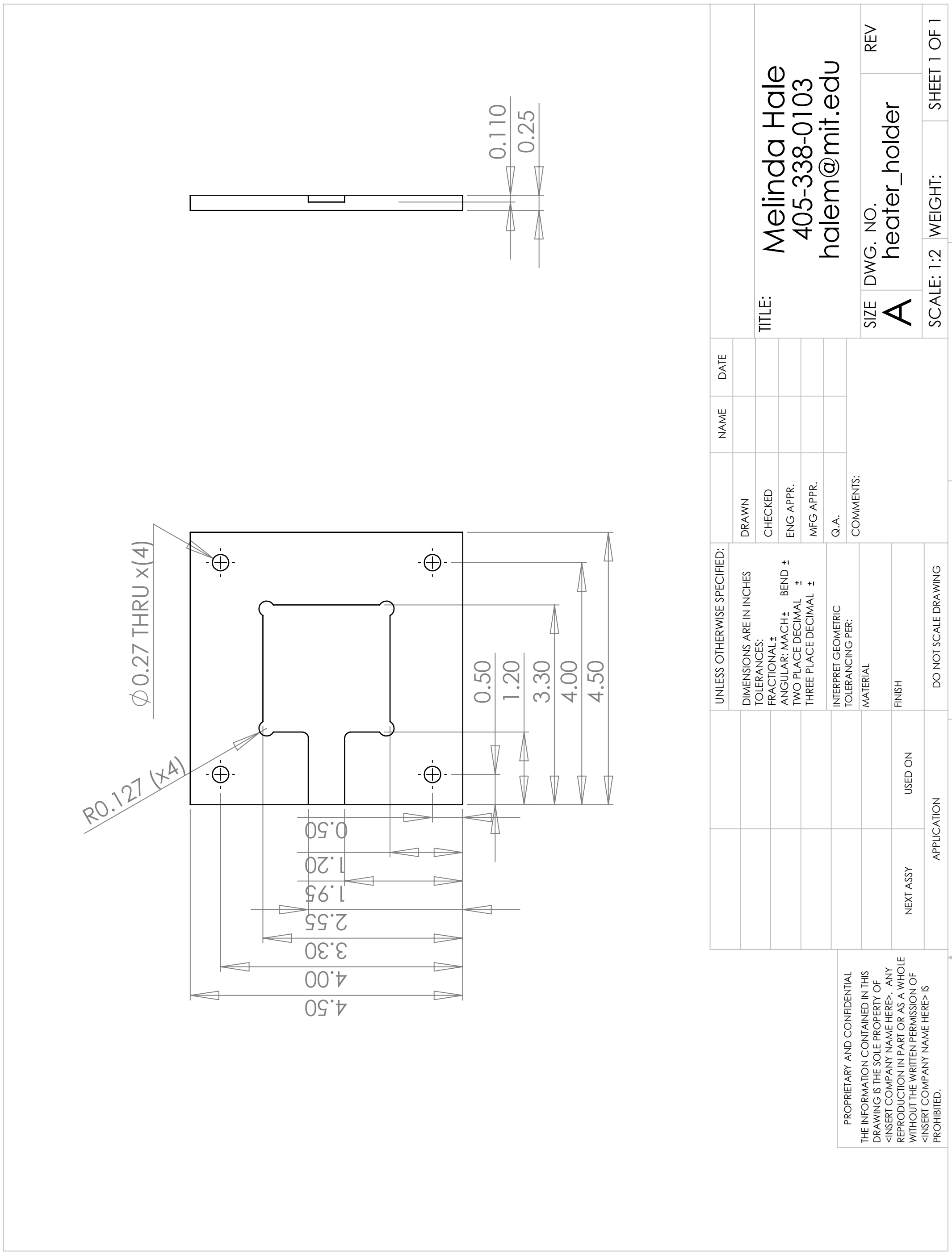
0.110
0.25
∅0.27 THRU x(4)
R0.127 (x4)
0.50
1.20
3.30
4.00
4.50
0.50
1.20
1.95
2.55
3.30
4.00
4.50
UNLESS OTHERWISE SPECIFIED:
DIMENSIONS ARE IN INCHES
TOLERANCES:
FRACTIONAL ±
ANGULAR: MACH ± BEND ±
TWO PLACE DECIMAL ±
THREE PLACE DECIMAL ±
INTERPRET GEOMETRIC TOLERANCING PER:
MATERIAL
FINISH
DO NOT SCALE DRAWING
NAME
DATE
DRAWN
CHECKED
ENG APPR.
MFG APPR.
Q.A.
COMMENTS:
NEXT ASSY
USED ON
APPLICATION
PROPRIETARY AND CONFIDENTIAL
THE INFORMATION CONTAINED IN THIS DRAWING IS THE SOLE PROPERTY OF <INSERT COMPANY NAME HERE>. ANY REPRODUCTION IN PART OR AS A WHOLE WITHOUT THE WRITTEN PERMISSION OF <INSERT COMPANY NAME HERE> IS PROHIBITED.
TITLE:
Melinda Hale
405-338-0103
halem@mit.edu
SIZE
A
DWG. NO.
heater_holder
REV
SCALE: 1:2
WEIGHT:
SHEET 1 OF 1
1
2
3
4
5

Figure E-7: Detailed drawing of heater holder, part of substrate chuck assembly

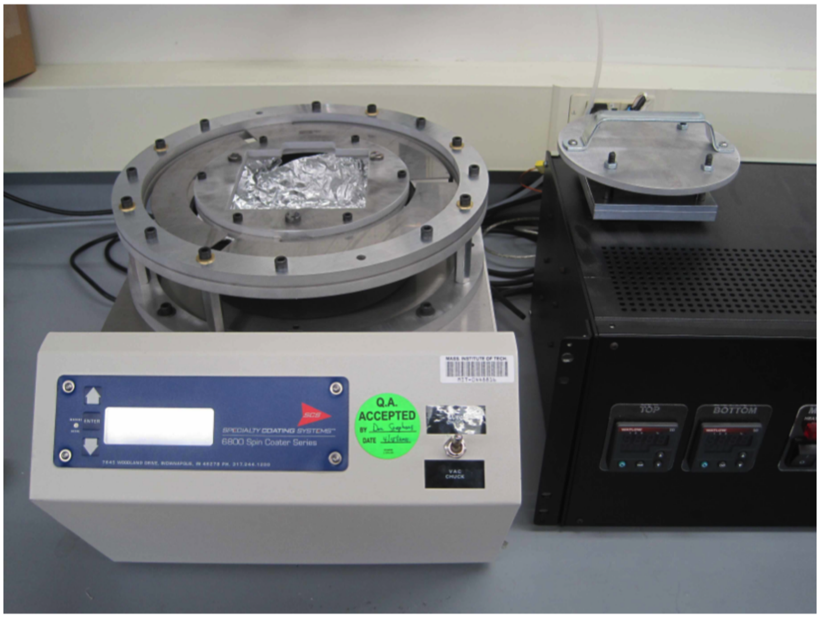

Figure E-8: Fabricated stamping apparatus, with integrated flexure and independent substrate chuck.

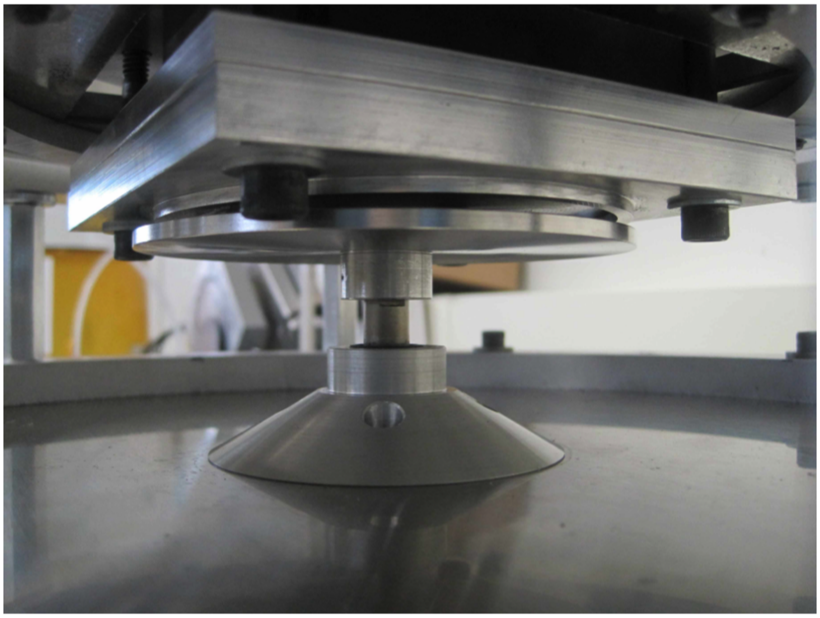

Figure E-9: Detailed view of gap between substrate holder and spincoater chuck. This is a critical assembly tolerance, as the gap must be less than the flexure range of travel. During printing the substrate holder is pressed down so that outer ring tightly contacts the outer edges of the PDMS stamp, holding alignment and maintaining seal as positive pressure is applied to the back of the stamp for "bubble transfer."

Appendix F

Taguchi L18 DOE for Exploring μCP of Ag ink - Detailed DOE Parameters and Results

So that future researchers will be able to replicate the experiments and the analysis in this thesis, here presented are the exact experimental parameters used in the Taguchi L18 DOE for exploring μCP of Ag ink, and the measured results from those experiments.

F.1 Taguchi L18 DOE for exploring μCP of Ag ink - List of runs with specific parameters used

See Table F.1.

F.2 Taguchi L18 DOE for exploring μCP of Ag ink - Thickness and geometry coverage measurements

See Table F.2.

	Force	Substrate	Feature Size	Inkpad Thickness	Ink	Spincoating Speed	Spincoating Time	Inkpad Thickness	Force
Run	A	B	C	D	E	rpm	sec	nm	N
1	1/3 pc	PET	5μm	75%t_o	MES 40	800	4	206.2	2.5N
2	1/3 pc	PET	20μm	t_o	CCI-300	6000	30	64.1	2.5N
3	1/3 pc	PET	50μm	125%t_o	CSD-66	6000	30	90.0	2.5N
4	1/3 pc	PMMA	5μm	75%t_o	CCI-300	9000	30	59.7	2.5N
5	1/3 pc	PMMA	20μm	t_o	CSD-66	7000	30	71.1	2.5N
6	1/3 pc	PMMA	50μm	125%t_o	MES 40	600	4	343.7	2.5N
7	1/3 pc	Glass	5μm	t_o	MES 40	700	4	275.0	2.5N
8	1/3 pc	Glass	20μm	125%t_o	CCI-300	4800	30	90.0	2.5N
9	1/3 pc	Glass	50μm	75%t_o	CSD-66	8000	30	54.1	2.5N
10	1/2pc	PET	5μm	125%t_o	CSD-66	6000	30	90.0	3.75N
11	1/2pc	PET	20μm	75%t_o	MES 40	800	4	206.2	3.75N
12	1/2pc	PET	50μm	t_o	CCI-300	6000	30	64.1	3.75N
13	1/2pc	PMMA	5μm	t_o	CSD-66	7000	30	71.1	3.75N
14	1/2pc	PMMA	20μm	125%t_o	MES 40	600	4	343.7	3.75N
15	1/2pc	PMMA	50μm	75%t_o	CCI-300	9000	30	59.7	3.75N
16	1/2pc	Glass	5μm	125%t_o	CCI-300	4800	30	90.0	3.75N
17	1/2pc	Glass	20μm	75%t_o	CSD-66	8000	30	54.1	3.75N
18	1/2pc	Glass	50μm	t_o	MES 40	700	4	275.0	3.75N

Table F.1: L18 DOE list of runs - Specific experimental parameters

	Force	Substrate	Feature Size	Inkpad Thickness	Ink	Coverage	Thickness	Viscosity	Density	Solids Loading	Surface Energy Ink	Surface Energy Substrate	Energy Ratio	Pressure	Notes
Run	A	B	C	D	E	$\frac{Actual}{Ideal}$	(nm)	cP	g/mL	wt%	mN/m	mN/m		$\frac{N}{mm^2}$	
1	1/3 pc	PET	5μm	75%t_o	MES 40	1.286	24.13	5.35	1.44	40	27.5	35.2	0.781	0.19	Not used in thickness model
2	1/3 pc	PET	20μm	t_o	CCI-300	2.0349	27.21	13	1.235	20	31.5	35.2	0.895	0.13	
3	1/3 pc	PET	50μm	125%t_o	CSD-66	1.2971	48.85	75	2.25	60	47.5	35.2	1.349	0.10	
4	1/3 pc	PMMA	5μm	75%t_o	CCI-300	1.5748	17.3	13	1.235	20	31.5	41	0.768	0.19	
5	1/3 pc	PMMA	20μm	t_o	CSD-66	1.7626	41.96	75	2.25	60	47.5	41	1.159	0.13	
6	1/3 pc	PMMA	50μm	125%t_o	MES 40	0.844	55.86	5.35	1.44	40	27.5	41	0.671	0.10	
7	1/3 pc	Glass	5μm	t_o	MES 40	1.0616	129.28	5.35	1.44	40	27.5	69.78	0.394	0.19	Not used in thickness model
8	1/3 pc	Glass	20μm	125%t_o	CCI-300	2.2933	21.50	13	1.235	20	31.5	69.78	0.451	0.13	
9	1/3 pc	Glass	50μm	75%t_o	CSD-66	0.9941	22.82	75	2.25	60	47.5	69.78	0.681	0.10	
10	1/2pc	PET	5μm	125%t_o	CSD-66	1.8813	26.50	75	2.25	60	47.5	35.2	1.349	0.285	
11	1/2pc	PET	20μm	75%t_o	MES 40	0.5074	53.57	5.35	1.44	40	27.5	35.2	0.781	0.20	Not used in thickness model
12	1/2pc	PET	50μm	t_o	CCI-300	1.2348	46.58	13	1.235	20	31.5	35.2	0.895	0.15	
13	1/2pc	PMMA	5μm	t_o	CSD-66	1.4138	31.46	75	2.25	60	47.5	41	1.159	0.285	
14	1/2pc	PMMA	20μm	125%t_o	MES 40	1.2239	48.89	5.35	1.44	40	27.5	41	0.671	0.20	
15	1/2pc	PMMA	50μm	75%t_o	CCI-300	1.1498	23.01	13	1.235	20	31.5	41	0.768	0.15	
16	1/2pc	Glass	5μm	125%t_o	CCI-300	1.4475	12.94	13	1.235	20	31.5	69.78	0.451	0.285	
17	1/2pc	Glass	20μm	75%t_o	CSD-66	2.1508	36.03	75	2.25	60	47.5	69.78	0.681	0.20	Not used in coverage model
18	1/2pc	Glass	50μm	t_o	MES 40	0.734	101.13	5.35	1.44	40	27.5	69.78	0.394	0.15	Not used in thickness model

Table F.2: L18 DOE Results - Raw data of thickness and geometry coverage measurements

Bibliography

[1] Z. Nie and E. Kumacheva, "Patterning surfaces with functional polymers," *Nature Materials*, vol. 7, no. 4, pp. 277–290, 2008.

[2] J. E. Petrzelka, "Contact region fidelity, sensitivity, and control in roll-based soft lithography," *mit.dspace.org*, pp. 1–349, Oct. 2012.

[3] R. Parashkov, E. Becker, and T. R. ldots, "Large area electronics using printing methods," *Proceedings of the ...*, Jan. 2005.

[4] C. Tsao, L. Hromada, J. Liu, P. Kumar, and D. L. DeVoe, "Low temperature bonding of PMMA and COC microfluidic substrates using UV/ozone surface treatment," *Lab on a Chip*, pp. 499–505, Jan. 2007.

[5] A. Kaminska, H. Kaczmarek, and J. Kowalonek, "The influence of side groups and polarity of polymers on the kind and effectiveness of their surface modification by air plasma action," *European Polymer Journal*, vol. 38, pp. 1915–1919, Jan. 2002.

[6] W. Cheng, N. Park, M. T. Walter, M. R. Hartman, and D. Luo, "Nanopatterning self-assembled nanoparticle superlattices by moulding microdroplets," *Nature Nanotechnology*, vol. 3, pp. 682–690, Sept. 2008.

[7] B. Derby, "Inkjet Printing of Functional and Structural Materials: Fluid Property Requirements, Feature Stability, and Resolution," *Annual Review of Materials Research*, vol. 40, pp. 395–414, June 2010.

[8] M. K. Kwak, K. H. Shin, E. Y. Yoon, and K. Y. Suh, "Fabrication of conductive metal lines by plate-to-roll pattern transfer utilizing edge dewetting and flexographic printing," *Journal of Colloid and Interface Science*, vol. 343, pp. 301–305, Mar. 2010.

[9] A. Takakuwa and T. S. ldots, "Electrode micropatterning by microcontact printing method to large area substrates using nickel mold," *Proceedings of SPIE*, Jan. 2010.

[10] J. E. Petrzelka and D. E. Hardt, "Design, characterization, and control of a parallel kinematic stage for precision roll based manufacturing," *Submitted to Precision Engineering*, pp. 1–41, Apr. 2012.

[11] D. H. Ahmed, H. J. Sung, and D. S. Kim, "ScienceDirect.com - International Journal of Heat and Fluid Flow - Simulation of non-Newtonian ink transfer between two separating plates for gravure-offset printing," *International Journal of Heat and Fluid Flow*, 2011.

[12] K. Y. Suh, J. Park, and H. H. Lee, "Controlled polymer dewetting by physical confinement," *The Journal of Chemical Physics*, vol. 116, p. 7714, Apr. 2012.

[13] P. G. Jung, I. D. Jung, S. M. Lee, and J. S. Ko, "A micropatterned metal embedding process for the formation of metal lines in flexible electronics," *Journal of Micromechanics and Microengineering*, vol. 18, p. 035017, 2008.

[14] J. Yeom and M. A. Shannon, "Detachment Lithography of Photosensitive Polymers: A Route to Fabricating Three-Dimensional Structures," *Advanced Functional Materials*, vol. 20, pp. 289–295, Jan. 2010.

[15] J. E. Petrzelka, "Modeling and Control of Elastomeric Stamps in Roll-based Micro Contact Printing," *Unpublished Doctoral Proposal*, pp. 1–26, Jan. 2011.

[16] J. E. Petrzelka and D. E. Hardt, "Static load-displacement behavior of PDMS microfeatures for soft lithography," pp. 1–13, June 2012.

[17] A. MANZ, N. GRABER, and H. M. Widmer, "Miniaturized Total Chemical Analysis Systems: a Novel Concept for Chemical Sensing," *Sensors and Actuators*, vol. B1, pp. 244–248, 1990.

[18] P. Gravesen, J. Branebjerg, and O. Jensen, "Microfluidics-a review," *Journal of Micromechanics and Microengineering*, Jan. 1993.

[19] H. Becker and L. Locascio, "Review: Polymer microfluidic devices," *Talanta*, vol. 56, pp. 267–287, Jan. 2002.

[20] A. de Mello, “Plastic fantastic?,” *Lab on a Chip*, 2002.

[21] M. Heckele and W. Schomburg, “Review on micro molding of thermoplastic polymers,” *Journal of Micromechanics and Microengineering*, Jan. 2004.

[22] J. Ouellette, “A new wave of microfluidic devices,” *The Industrial Physicist*, 2003.

[23] Y. Xia and G. Whitesides, “Soft Lithography,” *Annual Reviews in Materials Science*, pp. 153–184, Jan. 1998.

[24] M. Heckele, W. Bacher, and K. Müller, “Hot embossing-The molding technique for plastic microstructures,” *Microsystem Technologies*, Jan. 1998.

[25] H. Becker and C. Gartner, “Polymer microfabrication technologies for microfluidic systems,” *Analytical and Bioanalytical Chemistry*, vol. 390, no. 1, pp. 89–111, 2008.

[26] A. K. Agarwal, S. S. Sridharamurthy, D. J. Beebe, and H. Jiang, “Programmable autonomous micromixers and micropumps,” *J. Microelectromech. Syst*, vol. 14, no. 6, pp. 1409–1421, 2005.

[27] A. Ranzoni, X. J. A. Janssen, M. Ovsyanko, L. J. Van Ijzendoorn, and M. W. J. Prins, “Magnetically controlled rotation and torque of uniaxial microactuators for lab-on-a-chip applications,” *Lab on a Chip*, vol. 10, p. 179, Jan. 2010.

[28] F. C. Leinweber, J. Eijkel, J. G. Bomer, and A. Van Den Berg, “Continuous flow microfluidic demixing of electrolytes by induced charge electrokinetics in structured electrode arrays,” *Analytical chemistry(Washington, DC)*, vol. 78, no. 5, pp. 1425–1434, 2006.

[29] D. Bhusari, H. A. Reed, M. Wedlake, A. M. Padovani, S. Allen, and P. A. Kohl, “Fabrication of air-channel structures for microfluidic, microelectromechanical, and microelectronic applications,” *JOURNAL OF MICROELECTROMECHANICAL SYSTEMS*, vol. 10, no. 3, pp. 400–408, 2001.

[30] S. Baek, J. Min, and J. H. Park, “Wireless induction heating in a microfluidic device for cell lysis,” *Lab on a Chip*, vol. 10, no. 7, pp. 909–917, 2010.

[31] R. Martinez-Duarte, R, III, and K. A.-S. ldots, “The integration of 3D carbon-electrode dielectrophoresis on a CD-like centrifugal microfluidic platform,” *Lab on a Chip*, Jan. 2010.

[32] D. Sinton, P. Wood, C. Escobedo, and F. E. ldots, “Microfluidic and nanofluidic integration of plasmonic substrates for biosensing,” *Proceedings of . . .* , Jan. 2009.

[33] D. Daniel and I. Gutz, “Microfluidic cell with a TiO2-modified gold electrode irradiated by an UV-LED for in situ photocatalytic decomposition of organic matter and its potentiality for voltammetric analysis of metal ions,” *Electrochemistry communications*, vol. 9, no. 3, pp. 522–528, 2007.

[34] X. Zhu, C. Gao, J. W. Choi, P. L. Bishop, and C. H. Ahn, “On-chip generated mercury microelectrode for heavy metal ion detection,” *Lab on a Chip*, vol. 5, no. 2, pp. 212–217, 2005.

[35] A. T. Maghasi, S. D. Conklin, T. Shtoyko, A. Piruska, J. N. Richardson, C. J. Seliskar, and W. R. Heineman, “Spectroelectrochemical sensing based on attenuated total internal reflectance stripping voltammetry. 2. Determination of mercury and lead,” *Analytical chemistry(Washington, DC)*, vol. 76, no. 5, pp. 1458–1465, 2004.

[36] C. Chen, J. Zhang, Y. Du, X. Yang, and E. Wang, “Microfabricated on-chip integrated Au–Ag–Au three-electrode system for in situ mercury ion determination,” *The Analyst*, vol. 135, no. 5, pp. 1010–1014, 2010.

[37] Y. Lin, R. Zhao, K. D. Thrall, C. A. Timchalk, W. D. Bennett, and D. W. Matson, “Integration of microfluidics/electrochemical system for trace metal analysis by stripping voltammetry,” *Proceedings of SPIE*, vol. 3877, p. 248, 1999.

[38] S. S. Sridharamurthy, L. Dong, and H. Jiang, “A microfluidic chemical/biological sensing system based on membrane dissolution and optical absorption,” *Measurement Science and Technology*, vol. 18, pp. 201–207, 2007.

[39] P. B. Allen, I. Rodriguez, C. L. Kuyper, R. M. Lorenz, P. Spicar-Mihalic, J. S. Kuo, and D. T. Chiu, “Selective electroless and electrolytic deposition of metal for applications in microfluidics: Fabrication of a microthermocouple,” *Anal. Chem*, vol. 75, no. 7, pp. 1578–1583, 2003.

[40] N. Srivastava and M. A. Burns, “Electronic drop sensing in microfluidic devices: automated operation of a nanoliter viscometer,” *Lab on a Chip*, vol. 6, no. 6, p. 744, 2006.

[41] B. Lee, S. Seo, D. Lee, M. Lee, J. LEE, and J. C. ldots, “Biosensor system-on-a-chip including CMOS-based signal processing circuits and 64 carbon nanotube-based sensors for the detection of a neurotransmitter,” *Lab on a Chip*, Jan. 2010.

[42] J.-K. Shin, D. Kim, and J. Park, “Detection of streptavidin-biotin protein complexes using a MOSFET-type biosensor . . . ,” *Proceedings of SPIE*, Jan. 2005.

[43] S. Vengasandra, Y. Cai, D. Grewell, J. Shinar, and R. Shinar, “Polypropylene CD-organic light-emitting diode biosensing platform,” *Lab on a Chip*, vol. 10, no. 8, pp. 1051–1056, 2010.

[44] V. Adam, D. Huska, J. Hubalek, and R. Kizek, “Easy to use and rapid isolation and detection of a viral nucleic acid by using paramagnetic microparticles and carbon nanotubes-based screen-printed electrodes,” *Microfluidics and Nanofluidics*, vol. 8, pp. 329–339, Mar. 2010.

[45] H. Wang, X. Luo, H. Yao, C. Du, Z. Zhao, and S. Zhu, “Key technologies for LSPR-sensing microfluidic biochip,” *Proceedings of SPIE*, Jan. 2007.

[46] K. Tetz, L. Pang, M. Nezhad, and Y. Fainman, “Optofluidic plasmonics,” *Proceedings of SPIE*, Jan. 2006.

[47] H. Hiep, T. Endo, D. Kim, and E. Tamiya, “Nanostructure and molecular interface for biosensing devices,” *Proceedings of SPIE*, Jan. 2007.

[48] Z. Geng, Q. Li, W. Wang, and Z. Li, “Theoretical Analysis and Fabrication of PDMS-Based Surface Plasmon Resonance Sensor Chips,” *Proceedings of the 5th IEEE International Conference on Nano/Micro Engineered and Molecular Systems*, p. 51, Jan. 2009.

[49] D. Amarie, A. Alileche, B. Dragnea, and J. A. Glazier, “Microfluidic Devices Integrating Microcavity Surface-Plasmon-Resonance Sensors: Glucose Oxidase Binding-Activity Detection,” *Analytical Chemistry*, vol. 82, no. 1, pp. 343–352, 2009.

[50] P. Steinvurzel, T. Yang, and K. B. Crozier, “Experimental characterization of dispersion in plasmonic nanostripes for integrated DNA sensing,” *Proceedings of SPIE*, vol. 7604, pp. 760417–760417–11, Jan. 2010.

[51] A. Piruska, S. P. Branagan, A. B. Minnis, Z. Wang, D. M. Cropek, J. V. Sweedler, and P. W. Bohn, “Electrokinetic control of fluid transport in gold-coated nanocapillary array membranes in hybrid nanofluidic–microfluidic devices,” *Lab on a Chip*, vol. 10, no. 10, pp. 1237–1244, 2010.

[52] A. Plecis, J. Tazid, A. Pallandre, P. Martinhon, C. Deslouis, Y. Chen, and A. M. Haghiri-Gosnet, “Flow field effect transistors with polarisable interface for EOF tunable microfluidic separation devices,” *Lab on a Chip*, vol. 10, no. 10, pp. 1245–1253, 2010.

[53] J. W. Choi, S. Rosset, M. Niklaus, J. R. Adleman, H. Shea, and D. Psaltis, “3-dimensional electrode patterning within a microfluidic channel using metal ion implantation,” *Lab on a Chip*, vol. 10, no. 6, pp. 783–788, 2010.

[54] W. André, Z. Lu, B. Moufarrej, and S. Martel, “Micro-electro-fluidic module to control magnetotactic bacteria for micromanipulation tasks under an optical microscope,” *Society of Photo-Optical Instrumentation Engineers (SPIE) Conference Series*, vol. 6717, p. 20, 2007.

[55] A. C. Siegel, S. S. Shevkoplyas, D. B. Weibel, D. A. Bruzewicz, A. W. Martinez, and G. M. Whitesides, “Cofabrication of electromagnets and microfluidic systems in poly (dimethylsiloxane),” *ANGEWANDTE CHEMIE-INTERNATIONAL EDITION IN ENGLISH-*, vol. 45, no. 41, p. 6877, 2006.

[56] M. Z. Bazant and T. M. Squires, “Induced-charge electrokinetic phenomena: theory and microfluidic applications,” *Physical Review Letters*, vol. 92, no. 6, p. 66101, 2004.

[57] B. H. Timmer, K. M. Van Delft, W. W. Koelmans, W. Olthuis, and A. Van Den Berg, “Selective low concentration ammonia sensing in a microfluidic lab-on-a-chip,” *IEEE Sensors Journal*, vol. 6, no. 3, p. 829, 2006.

[58] W. Sparreboom, J. Eijkel, J. Bomer, and A. Berg, "Rapid sacrificial layer etching for the fabrication of nanochannels with integrated metal electrodes," *Lab on a Chip*, vol. 8, no. 3, pp. 402–407, 2008.

[59] A. D. Goater, J. Burt, D. J. Morris, A. Menachery, N. H. Rizvi, D. R. Matthews, and H. D. Summers, "Laser micromachining of optical biochips," *Society of Photo-Optical Instrumentation Engineers (SPIE) Conference Series*, vol. 6459, p. 9, 2007.

[60] M. A. Lee and D. Leslie, "Reaction vessels," 1999.

[61] D. Issadore, K. J. Humphry, K. A. Brown, L. Sandberg, D. A. Weitz, and R. M. Westervelt, "Microwave dielectric heating of drops in microfluidic devices," *Lab on a Chip*, vol. 9, no. 12, pp. 1701–1706, 2009.

[62] Y. Fu, J. Luo, X. Du, A. Flewitt, and Y. Li, "Recent developments on ZnO films for acoustic wave based bio-sensing and microfluidic applications: a review," *Sensors & Actuators: B. . . .*, Jan. 2009.

[63] J. Yoon, B. Heinze, and J. G. ldots, "Detection of avian influenza antigens in proximity fiber, droplet, and optical waveguide microfluidics," *Proceedings of SPIE*, Jan. 2009.

[64] N. Inomata, T. Mizunuma, Y. Yamanishi, S. Kudo, and F. Arai, "On-chip magnetically driven micro-robot for enucleation of oocyte," *Micro-NanoMechatronics and Human Science, 2009. MHS 2009. International Symposium on*, pp. 493–498, 2009.

[65] M. Gersborg-Hansen, S. Balslev, N. A. Mortensen, and A. Kristensen, "A coupled cavity micro-fluidic dye ring laser," *Microelectronic Engineering*, vol. 78, pp. 185–189, 2005.

[66] X. Heng, D. Erickson, L. R. Baugh, Z. Yaqoob, P. W. Sternberg, D. Psaltis, and C. Yang, "Optofluidic microscopy—a method for implementing a high resolution optical microscope on a chip," *Lab on a Chip*, vol. 6, no. 10, pp. 1274–1276, 2006.

[67] G. L. Liu and L. P. Lee, "Nanowell surface enhanced Raman scattering arrays fabricated by soft-lithography for label-free biomolecular detections in integrated microfluidics," *Applied Physics Letters*, vol. 87, p. 074101, 2005.

[68] R. M. Connatser, L. A. Riddle, and M. J. Sepaniak, "Metal-polymer nanocomposites for integrated microfluidic separations and surface enhanced Raman spectroscopic detection," *Journal of Separation Science*, vol. 27, no. 17-18, pp. 1545–1550, 2004.

[69] E. T. Castellana, S. Kataoka, F. Albertorio, and P. S. Cremer, "Direct writing of metal nanoparticle films inside sealed microfluidic channels," *Anal. Chem*, vol. 78, no. 1, pp. 107–112, 2006.

[70] J.-H. So, J. Thelen, A. Qusba, G. J. Hayes, G. Lazzi, and M. D. Dickey, "Reversibly Deformable and Mechanically Tunable Fluidic Antennas," *Advanced Functional Materials*, vol. 19, pp. 3632–3637, Nov. 2009.

[71] A. Pepin and Y. Chen, "Soft lithography and imprint-based techniques for microfluidics and biological analysis," *Alternative lithography: unleashing the potentials of nanotechnology*, Jan. 2003.

[72] M. Hale, "Development of a low-cost, rapid-cycle hot embossing system for microscale parts," *dspace.mit.edu*, 2009.

[73] S. V. Pereira, G. A. Messina, and J. Raba, "Integrated microfluidic magnetic immunosensor for quantification of human serum IgG antibodies to Helicobacter pylori," *Journal of Chromatography B*, 2009.

[74] M. Arundell, A. Diego, and O. C. ldots, "Chips & Tips: Rapid prototyping of a PMMA microfluidic chip with integrated platinum electrodes," *Lab on a Chip*, Jan. 2008.

[75] T. Wang, M. Quaglio, F. Pirri, and Y. C. ldots, "Patterning of SU-8 resist with digital micromirror device (DMD) maskless lithography," *Proceedings of . . .* , Jan. 2009.

[76] Y. Ito, Y. Onodera, R. Tanabe, and M. Ichihara, "Fabrication of OLED display by an ultrashort laser: selective patterning of thin metal electrode," *Proceedings of SPIE*, Jan. 2007.

[77] R. Veenhuis, E. van der Wouden, and J. van ldots, "Field-effect based attomole titrations in nanoconfinement," *rsc.org*.

[78] K. Sugioka, Y. Cheng, M. Masuda, K. Midorikawa, and K. Shihoyama, "Fabrication of microreactors in photostructurable glass by 3D femtosecond laser direct write," *Proceedings of SPIE*, vol. 5339, p. 205, 2004.

[79] C. D. Chin, V. Linder, and S. K. Sia, "Commercialization of microfluidic point-of-care diagnostic devices," *Lab on a Chip*, vol. 12, no. 12, p. 2118, 2012.

[80] "U.S. Microfluidics/Lab-on-a-chip Markets," *Frost and Sullivan*, May 2006.

[81] "World Microfluidics/Lab-on-a-chip Markets," *Frost and Sullivan*, Jan. 2003.

[82] R. Zengerle and J. Ducrée, "The Future of Microfluidics: Low-Cost Technologies and Microfluidic Platforms," *Microsystems & Nanotechnology*, pp. 806–813, Jan. 2007.

[83] G. M. Whitesides, "The origins and the future of microfluidics," *Nature*, vol. 442, pp. 368–373, July 2006.

[84] D. Qin, Y. Xia, and G. Whitesides, "Soft lithography for micro-and nanoscale patterning," *Nature Protocols*, vol. 5, p. 491, Jan. 2010.

[85] Y. Xia and G. M. Whitesides, "Soft Lithography," *Angewandte Chemie International Edition*, vol. 37, no. 5, pp. 550–575, 1998.

[86] X. Zhao and Y. X. ldots, "Soft lithographic methods for nano-fabrication," *Journal of Materials Chemistry*, Jan. 1997.

[87] K. M. Choi and J. A. Rogers, "A photocurable poly (dimethylsiloxane) chemistry designed for soft lithographic molding and printing in the nanometer regime," *J. Am. Chem. Soc*, vol. 125, pp. 4060–4061, Jan. 2003.

[88] A. Kumar, H. Biebuyck, N. L. Abbott, and G. M. Whitesides, "The use of self-assembled monolayers and a selective etch to generate patterned gold features," *J. Am. Chem. Soc*, pp. 9189–9191, Jan. 1992.

[89] A. Kumar and G. M. Whitesides, "Features of gold having micrometer to centimeter dimensions can be formed through a combination of stamping with an elastomeric stamp and an alkanethiol "ink" followed by chemical etching," *Applied Physics Letters*, vol. 63, pp. 2002–2004, Jan. 1993.

[90] B. Michel, A. Bernard, A. Bietsch, E. Delamarche, M. Geissler, D. Juncker, H. Kind, J. P. Renault, H. Rothuizen, and H. Schmid, "Printing meets lithography: Soft approaches to high-resolution patterning," *CHIMIA International Journal for Chemistry*, vol. 56, no. 10, pp. 527–542, 2002.

[91] L. Bao, L. Tan, X. Huang, Y. Kong, L. Guo, and S. Pang, "Polymer inking as a micro-and nanopatterning technique," *Journal of Vacuum Science & Technology B: Microelectronics . . .*, Jan. 2003.

[92] R. J. Jackman, S. T. Brittain, A. Adams, H. Wu, M. G. Prentiss, S. Whitesides, and G. M. Whitesides, "Three-dimensional metallic microstructures fabricated by soft lithography and microelectrodeposition," *Langmuir*, vol. 15, no. 3, pp. 826–836, 1999.

[93] J. C. Love, L. A. Estroff, J. K. Kriebel, R. G. Nuzzo, and G. M. Whitesides, "Self-assembled monolayers of thiolates on metals as a form of nanotechnology," *Chem. Rev*, vol. 105, no. 4, pp. 1103–1170, 2005.

[94] H. A. Biebuyck, N. B. Larsen, E. Delamarche, and B. Michel, "Lithography beyond light: Microcontact printing with monolayer resists," *IBM Journal of Research and Development*, vol. 41, Jan. 1997.

[95] E. Delamarche, H. Schmid, B. Michel, and H. Biebuyck, "Stability of molded polydimethylsiloxane microstructures," *Advanced Materials*, vol. 9, no. 9, pp. 741–746, 1997.

[96] A. Bietsch and B. Michel, "Conformal contact and pattern stability of stamps used for soft lithography," *Journal of Applied Physics*, vol. 88, no. 7, p. 4310, 2000.

[97] M. Geissler, A. Bernard, and A. Bietsch, "Microcontact-printing chemical patterns with flat stamps," *. . . CHEMICAL . . .*, 2000.

[98] M. Geissler, H. Schmid, A. Bietsch, B. Michel, and E. Delamarche, "Defect-Tolerant and Directional Wet-Etch Systems for Using Monolayers as Resists," *Langmuir*, vol. 18, pp. 2374–2377, Mar. 2002.

[99] M. Geissler, H. Wolf, R. Stutz, E. Delamarche, U. W. Grummt, B. Michel, and A. Bietsch, "Fabrication of metal nanowires using microcontact printing," *Langmuir*, vol. 19, no. 15, pp. 6301–6311, 2003.

[100] L. Libioulle, A. Bietsch, H. Schmid, B. Michel, and E. Delamarche, “Contact-Inking Stamps for Microcontact Printing of Alkanethiols on Gold,” *Langmuir*, vol. 15, pp. 300–304, Jan. 1999.

[101] T. E. Balmer, H. Schmid, R. Stutz, E. Delamarche, B. Michel, N. D. Spencer, and H. Wolf, “Diffusion of Alkanethiols in PDMS and Its Implications on Microcontact Printing (ÎŒCP),” *Langmuir*, vol. 21, pp. 622–632, Jan. 2005.

[102] A. P. Quist, E. Pavlovic, and S. Oscarsson, “Recent advances in microcontact printing,” *Analytical and Bioanalytical Chemistry*, vol. 381, no. 3, pp. 591–600, 2005.

[103] E. Delamarche, “Microcontact Processing for Microtechnology and Biology,” *CHIMIA International Journal for Chemistry*, Jan. 2007.

[104] A. Perl, D. N. Reinhoudt, and J. Huskens, “Microcontact Printing: Limitations and Achievements,” *Advanced Materials*, vol. 21, pp. 2257–2268, June 2009.

[105] I. Elloumi-Hannachi, M. Maeda, and M. Y. ldots, “Portable microcontact printing device for cell culture,” *Biomaterials*, Jan. 2010.

[106] R. Cracauer, R. Ganske, and M. G. ldots, “Method and apparatus for micro-contact printing,” *US Patent App. 10/ . . .*, Jan. 2003.

[107] A. M. Kendale, “Automation of Soft Lithographic Microcontact Printing,” *Unpublished Master’s thesis, Massachusetts Insitute of Technology*, 2002.

[108] A. Kendale, “System and process for automated microcontact printing,” *US Patent 7,338,613*, Jan. 2008.

[109] A. K. ldots, “Microcontact printing,” *US Patent 7,665,983*, Jan. 2010.

[110] B. CHAKRA and B. E. ldots, “A new instrument for automated microcontact printing with applications to mems and biochips fabrication,” *documents.irevues.inist.fr*, Jan. 2007.

[111] C. Ho, C. Chieng, and M. C. ldots, “Micro-Stamp Systems for Batch-Filling, Parallel-Spotting, and Continuously Printing of Multiple Biosample Fluids,” *. . . for Laboratory Automation*, Jan. 2008.

[112] A. Stagnaro, “Design and development of a roll-to-roll machine for continuous high-speed microcontact printing,” *dspace.mit.edu*, Jan. 2008.

[113] Y. Xia, D. Qin, and G. M. Whitesides, “Microcontact printing with a cylindrical rolling stamp: A practical step toward automatic manufacturing of patterns with submicrometer-sized features,” *Advanced Materials*, vol. 8, pp. 1015–1017, Dec. 1996.

[114] J. A. Rogers, Z. Bao, and A. Makhija, “Printing process suitable for reel-to-reel production of high-performance organic transistors and circuits,” *Advanced . . .*, 1999.

[115] P. Baldesi, “Design and development of high precision five-axis positioning system for roll-to-roll multi-layer microcontact printing,” *dspace.mit.edu*, Jan. 2009.

[116] C. Datar and D. Hardt, “Design and development of high precision elastomeric-stamp wrapping system for roll-to-roll multi-layer microcontact printing,” *dspace.mit.edu*, Jan. 2009.

[117] K. Khanna, “Analysis of the capabilities of continuous high-speed microcontact printing,” *dspace.mit.edu*, Jan. 2008.

[118] X. Shen, “Design and Analysis of High-Speed Continuous Micro-contact Printing,” *Unpublished Master’s thesis, Massachusetts Insitute of Technologyhesis, Massachusetts Insitute of Technology*, 2008.

[119] W. Yang and D. E. Hardt, “Design and manufacturing of high precision roll-to-roll multi-layer printing machine: measurement and experiment,” *dspace.mit.edu*, Jan. 2009.

[120] H. Kim, “Automation of soft lithography,” *dspace.mit.edu*, Jan. 2006.

[121] K. Chauhan, “Design and prototype of an automated system for commercially viable production using micro contact printing,” *mit.dspace.org*, Jan. 2007.

[122] A. Goel, S. L. ldots, Y. XIa, and D. Hardt, “Understanding and developing capabilities for large area and continuous micro contact printing,” *dspace.mit.edu*, Jan. 2007.

[123] T. Kololuoma, M. Tuomikoski, T. Makela, and J. Heilmann, “Towards roll-to-roll fabrication of electronics, optics, and optoelectronics for smart and . . . ,” *Proceedings of SPIE*, Jan. 2004.

[124] J. A. Rogers and Z. Bao, “Printed plastic electronics and paperlike displays,” *Journal of Polymer Science Part A: . . .*, vol. 40, pp. 3327–3334, Jan. 2002.

[125] M. Scholles, L. Kroker, U. Vogel, and J. K. ldots, “LABONFOIL: investigations regarding microfluidic skin patches for drug detection using flexible OLEDs,” *Proceedings of . . .*, Jan. 2010.

[126] “Singapore-MIT Alliance Annual Report 07/08,” 2008.

[127] D. Lee, K. Chung, H. Yang, S. Park, and S. KIM, “Plastic thermally controllable platform with integrated thin film microcomponents,” *Proceedings of SPIE*, vol. 5650, p. 429, Jan. 2005.

[128] C. Gartner, S. Kirsch, B. Anton, and H. Becker, “Hybrid microfluidic systems: combining a polymer microfluidic toolbox with biosensors,” *Proceedings of SPIE*, vol. 6465, p. 64650F, 2007.

[129] H. Lee, Y. Liu, D. Ham, and R. M. Westervelt, “Integrated cell manipulation system—CMOS/microfluidic hybrid,” *Lab on a Chip*, vol. 7, no. 3, pp. 331–337, 2007.

[130] P. Abgrall and A. Gué, “TOPICAL REVIEW: Lab-on-chip technologies: making a microfluidic network and coupling it into a complete microsystem - a review,” *Journal of Micromechanics and Microengineering*, Jan. 2007.

[131] S. Chemnitz, H. Schafer, S. Schumacher, V. Koziy, A. Fischer, A. J. Meixner, D. Ehrhardt, and M. Bohm, “Monolithical integration of polymer-based microfluidic structures on application-specific integrated circuits,” *Proceedings of SPIE*, vol. 5116, p. 782, 2003.

[132] P. Van Zant, “Microchip fabrication,” p. 642, Jan. 2004.

[133] D. Rhine and T. Smekal, “Microfluidic devices having embedded metal conductors and methods of . . .,” *US Patent 6,787,339*, Jan. 2004.

[134] X. Janssen, A. J. Schellekens, K. van Ommering, L. J. van Ijzendoorn, and M. Prins, “Controlled torque on superparamagnetic beads for functional biosensors,” *Biosensors and Bioelectronics*, vol. 24, no. 7, pp. 1937–1941, 2009.

[135] R. B. Fair, V. Srinivasan, H. Ren, P. Paik, V. K. Pamula, and M. G. Pollack, "Electrowetting-based on-chip sample processing for integrated microfluidics," *INTERNATIONAL ELECTRON DEVICES MEETING*, pp. 779–782, 2003.

[136] K. B. Kim, H. Chun, H. C. Kim, and T. D. Chung, "Microfluidic chip based hematoanalyzer using polyelectrolytic gel electrodes," *Proceedings of SPIE*, vol. 7207, p. 72070S, 2009.

[137] W. Ebina, A. C. Rowat, and D. A. Weitz, "Electrodes on a budget: Micropatterned electrode fabrication by wet chemical deposition," *Biomicrofluidics*, vol. 3, p. 034104, Jan. 2009.

[138] A. K. Agarwal, D. J. Beebe, and H. Jiang, "Integration of polymer and metal microstructures using liquid-phase photopolymerization," *Journal of Micromechanics and Microengineering*, vol. 16, pp. 332–340, 2006.

[139] C. E. White, T. Anderson, C. L. Henderson, H. D. Rowland, and W. P. King, "Microsystems manufacturing via embossing of photodefinable thermally sacrificial materials," *Proceedings of SPIE*, vol. 5374, p. 361, 2004.

[140] T. Velten, H. Schuck, M. Richter, G. Klink, K. Bock, C. K. Malek, S. Roth, H. Schoo, and P. J. Bolt, "Microfluidics on foil: state of the art and new developments," *Proceedings of the Institution of Mechanical Engineers, Part B: Journal of Engineering Manufacture*, vol. 222, no. 1, pp. 107–116, 2008.

[141] A. C. Siegel, S. Tang, C. A. Nijhuis, M. Hashimoto, S. T. Phillips, M. D. Dickey, and G. M. Whitesides, "Cofabrication: A Strategy for Building Multicomponent Microsystems," *Accounts of chemical research*, vol. 43, no. 4, pp. 518–528, 2010.

[142] J.-W. Choi, S. Rosset, M. Niklaus, J. R. Adleman, H. Shea, and D. Psaltis, "Tuning parameters of metal ion implantation within a microfluidic channel," *Proceedings of SPIE*, vol. 7593, pp. 75930D–75930D–7, Jan. 2010.

[143] M. Chabinyc, W. Wong, and R. Street, "Method of fabrication of electronic devices using microfluidic channels," *US Patent App. 10/ . . .*, Jan. 2002.

[144] S. H. Paek, Y. K. Choi, and D. S. Kim, "Selective microfabrication of silver electrodes inside a microchannel by multiphase laminar flow with density difference," *Microelectronic Engineering*, vol. 87, pp. 1375–1378, May 2010.

[145] E. Tekin, P. J. Smith, and U. S. Schubert, "Inkjet printing as a deposition and patterning tool for polymers and inorganic particles," *Soft Matter*, vol. 4, no. 4, pp. 703–713, 2008.

[146] B. A. Grzybowski, R. Haag, N. Bowden, and G. M. Whitesides, "Generation of micrometer-sized patterns for microanalytical applications using a laser direct-write method and microcontact printing," *Anal. Chem*, vol. 70, no. 22, pp. 4645–4652, 1998.

[147] G. M. Whitesides, "Chapter 4: Soft lithography," *Class Notes*, pp. 1–4, 2003.

[148] Y. L. Loo, R. L. Willett, K. W. Baldwin, and J. A. Rogers, "Additive, nanoscale patterning of metal films with a stamp and a surface chemistry mediated transfer process: Applications in plastic electronics," *Applied Physics Letters*, vol. 81, p. 562, 2002.

[149] K. L. Yang, K. Cadwell, and N. L. Abbott, "Contact printing of metal ions onto carboxylate-terminated self-assembled monolayers," *Advanced Materials*, vol. 15, no. 21, pp. 1819–1823, 2003.

[150] D. Li and L. Guo, "Micron-scale organic thin film transistors with conducting polymer electrodes patterned by polymer inking and stamping," *Applied Physics Letters*, vol. 88, p. 063513, 2006.

[151] A. A. Darhuber, S. M. Troian, and S. Wagner, "Physical mechanisms governing pattern fidelity in microscale offset printing," *Journal of Applied Physics*, vol. 90, p. 3602, Sept. 2001.

[152] J. E. Petrzelka and D. E. Hardt, "Fabrication of seamless micropatterned cylindrical stamps for roll based lithography," pp. 1–22, Sept. 2012.

[153] T. Sekitani, Y. Noguchi, U. Zschieschang, H. Klauk, and T. Someya, "Organic transistors manufactured using inkjet technology with subfemtoliter accuracy," *Proceedings of the National Academy of Sciences*, vol. 105, no. 13, pp. 4976–4980, 2008.

[154] A. Yakoub, M. Saadaoui, R. Cauchois, J.-M. Li, and P. Benaben, "An Improved In-line Inkjet Printing Process for 3D Multilayer Passive Devices," *MRS Proceedings*, vol. 1401, pp. 1–6, May 2012.

[155] S. C. Lim, S. H. Kim, Y. S. Yang, M. Y. Lee, S. Y. Nam, and J. B. Ko, "Organic Thin-Film Transistor Using High-Resolution Screen-Printed Electrodes," *Japanese Journal of Applied Physics*, vol. 48, p. 081503, Aug. 2009.

[156] P.-T. Pan, S.-S. Hsu, and A.-B. Wang, "Development of a capillary coating technology with on-line detecting system and its application for silver conductive circuit patterning," in *Microsystems Packaging Assembly and Circuits Technology Conference (IMPACT), 2010 5th International*, pp. 1–4, 2010.

[157] A. J. Campbell, D. Y. Chung, and J. Huang, "Gravure contact printing of flexible, high-performance polymer light emitting diodes for large-area displays and lighting," *MRS . . .* , 2011.

[158] D. Sung, A. de la Fuente Vornbrock, and V. Subramanian, "Scaling and Optimization of Gravure-Printed Silver Nanoparticle Lines for Printed Electronics," *IEEE Transactions on Components and Packaging Technologies*, vol. 33, no. 1, pp. 105–114.

[159] T.-M. Lee, J.-H. Noh, I. Kim, D.-S. Kim, and S. Chun, "Reliability of gravure offset printing under various printing conditions," *Journal of Applied Physics*, vol. 108, no. 10, p. 102802, 2010.

[160] R. Sangoi, C. G. Smith, M. D. Seymour, J. N. Venkataraman, D. M. Clark, M. L. Kleper, and B. E. Kahn, "Printing Radio Frequency Identification (RFID) Tag Antennas Using Inks Containing Silver Dispersions," *Journal of Dispersion Science and Technology*, vol. 25, pp. 513–521, Jan. 2005.

[161] R. C. Kattumenu, "Flexography Printing of Silver Based Conductive Inks on Packaging Substrates - Ramesh Chandra Kattumenu - Google Books," 2008.

[162] J. Jo, J.-S. Yu, T.-M. Lee, and D.-S. Kim, "Fabrication of Printed Organic Thin-Film Transistors Using Roll Printing," *Japanese Journal of Applied Physics*, vol. 48, p. 04C181, Apr. 2009.

[163] J. Jo, J.-S. Yu, T.-M. Lee, D.-S. Kim, and K.-Y. Kim, "Roll-Printed Organic Thin-Film Transistor Using Patterned Poly(dimethylsiloxane) (PDMS) Stamp," *Journal of Nanoscience and Nanotechnology*, vol. 10, pp. 3595–3599, May 2010.

[164] J. Jo, J.-S. Yu, T.-M. Lee, D.-S. Kim, and K.-Y. Kim, "Fabrication of Organic Thin-Film Transistors with Roll-Printed Electrodes Using Patterned Polymer Stamp," *Molecular Crystals and Liquid Crystals*, vol. 514, pp. 81/[411]–91/[421], Nov. 2009.

[165] B.-D. Chan, K.-H. Hsieh, and S.-Y. Yang, "Thin-film patterns directly fabricated using a transfer stamping technique," *Journal of Micromechanics and Microengineering*, vol. 19, p. 025010, Jan. 2009.

[166] B.-D. Chan, K.-H. Hsieh, and S.-Y. Yang, "Fabrication of organic flexible electrodes using transfer stamping process," *Microelectronic Engineering*, vol. 86, pp. 586–589, June 2009.

[167] A. A. Tracton, "Coatings Technology Handbook, Third Edition - Google Books," 2005.

[168] R. J. Good, "Contact angle, wetting, and adhesion: a critical review," *Journal of Adhesion Science and Technology*, vol. 6, no. 12, pp. 1269–1302, 1992.

[169] J. S. Moon, J. H. Park, T. Y. Lee, Y. W. Kim, J. B. Yoo, C. Y. Park, J. M. Kim, and K. W. Jin, "Transparent conductive film based on carbon nanotubes and PEDOT composites," *Diamond and Related Materials*, vol. 14, no. 11-12, pp. 1882–1887, 2005.

[170] B. D. Washo, "Rheology and modeling of the spin coating process," *IBM Journal of Research and Development*, vol. 21, no. 2, pp. 190–198, 1977.

[171] W. W. Flack, D. S. Soong, A. T. Bell, and D. W. Hess, "A mathematical model for spin coating of polymer resists," *Journal of Applied Physics*, vol. 56, no. 4, p. 1199, 1984.

[172] Z. Wang, R. Xing, X. Yu, and Y. Han, "Adhesive lithography for fabricating organic electronic and optoelectronics devices," *Nanoscale*, vol. 3, p. 2663, Jan. 2011.

[173] W. Jiang, H. Liu, Y. Ding, Y. Tang, Y. Shi, L. Yin, and B. Lu, "Investigation of ink transfer in a roller-reversal imprint process," *Journal of Micromechanics and Microengineering*, vol. 19, p. 015033, Dec. 2008.

[174] S. Im and K. Gleason, "Oxidative chemical vapor deposition of electrically conducting poly (3, 4-ethylenedioxythiophene) films," *Macromolecules*, Jan. 2006.

[175] N. V. Agfa-Gevaert, "Flexible Flat Panel Displays - Google Books," *Flexible Flat Panel Displays*, 2005.

[176] Y. Xia, K. Sun, and J. Ouyang, "Solution-Processed Metallic Conducting Polymer Films as Transparent Electrode of Optoelectronic Devices," *Advanced Materials*, vol. 24, pp. 2436–2440, Apr. 2012.

[177] S. G. Im, P. Yoo, P. Hammond, and K. Gleason, "Grafted Conducting Polymer Films for Nano-patterning onto Various Organic and Inorganic Substrates by Oxidative Chemical Vapor Deposition," *Advanced Materials Research*, pp. 2863–2867, Jan. 2007.

[178] A. Takakuwa, M. Ikawa, M. Fujita, and K. Yase, "Micropatterning of Electrodes by Microcontact Printing Method and Application to Thin Film Transistor Devices," *Japanese Journal of Applied Physics*, vol. 46, pp. 5960–5963, Sept. 2007.

[179] T. Granlund, T. Nyberg, and L. Stolz Roman, "Patterning of Polymer Light Emitting Diodes with Soft Lithography," *Advanced Materials*, 2000.

[180] Y. Yim, J. Park, and B. Park, "Solution-Processed Flexible ITO-Free Organic Light-Emitting Diodes Using Patterned Polymeric Anodes," *Journal of Display Technology*, vol. 6, no. 7, pp. 252–256.

[181] C. Piliego, M. Mazzeo, B. Cortese, R. Cingolani, and G. Gigli, "Organic light emitting diodes with highly conductive micropatterned polymer anodes," *Organic Electronics*, vol. 9, pp. 401–406, June 2008.

[182] Z. Wang, J. Yuan, J. Zhang, R. Xing, and D. Yan, "Metal Transfer Printing and Its Application in Organic Field-Effect Transistor Fabrication - Wang - 2003 - Advanced Materials - Wiley Online Library," *Advanced . . .*, 2003.

[183] P. J. Ross, *Taguchi Techniques for Quality Engineering.* Loss Function, Orthogonal Experiments, Parameter and Tolerance Design, McGraw-Hill, 1996.

[184] F. Ghadiri, D. H. Ahmed, H. J. Sung, and E. Shirani, “Non-Newtonian ink transfer in gravure–offset printing,” *International Journal of Heat and Fluid Flow*, vol. 32, pp. 308–317, Feb. 2011.

[185] A. C. Siegel, D. A. Bruzewicz, D. B. Weibel, and G. M. Whitesides, “Microsolidics: Fabrication of Three Dimensional Metallic Microstructures in Poly (dimethylsiloxane),” *Advanced Materials*, vol. 19, no. 5, pp. 727–733, 2007.

[186] H. Li, C. X. Luo, H. Ji, Q. Ouyang, and Y. Chen, “Micro-pressure sensor made of conductive PDMS for microfluidic applications,” *Microelectronic Engineering*, vol. 87, no. 5-8, pp. 1266–1269, 2010.

[187] T. Johnson and F. Amirouche, “Multiphysics modeling of an IPMC microfluidic control device,” *Microsystem Technologies*, vol. 14, no. 6, pp. 871–879, 2008.

[188] K. J. Kim and M. Shahinpoor, “A novel method of manufacturing three-dimensional ionic polymer-metal composites (IPMCs) biomimetic sensors, actuators and artificial muscles,” *Polymer*, vol. 43, no. 3, pp. 797–802, 2002.

[189] K. J. Kim and M. Shahinpoor, “Ionic polymer-metal composites: II. Manufacturing techniques,” *Smart Materials and Structures*, vol. 12, no. 1, pp. 65–79, 2003.

[190] M. Shahinpoor and K. J. Kim, “Novel ionic polymer-metal composites equipped with physically loaded particulate electrodes as biomimetic sensors, actuators and artificial muscles,” *Sensors and Actuators A: Physical*, vol. 96, no. 2-3, pp. 125–132, 2002.

[191] P. C. Hidber, P. F. Nealey, W. Helbig, and G. M. Whitesides, “New strategy for controlling the size and shape of metallic features formed by electroless deposition of copper: Microcontact printing of catalysts on oriented polymers, followed by thermal shrinkage,” *Langmuir*, vol. 12, no. 21, pp. 5209–5215, 1996.